ON THE CONTROL OF PARAPLEGIC STANDING USING FUNCTIONAL ELECTRICAL STIMULATION

A DISSERTATION

SUBMITTED TO THE DEPARTMENT OF MECHANICAL ENGINEERING

OF GLASGOW UNIVERSITY

IN COMPLETE FULFILLMENT OF THE REQUIREMENTS

FOR THE DEGREE OF

DOCTOR OF PHILOSOPHY

By

Ralf-Peter Jaime

May 2002

Abstract

Spinal cord injury results in an interruption of the neurological pathways from the brain to the muscles. However, the muscles themselves retain their ability to contract and to produce force. Thus, paralysed muscles can be stimulated artificially by applying electrical pulses to them, thereby regaining their function. This technique is known as Functional Electrical Stimulation (FES). This thesis is concerned with the restoration of upright standing after spinal cord injury (SCI) by the means of Functional Electrical Stimulation. In particular, the work presented in this thesis is concerned with unsupported standing, i.e. standing without any support by the arms for stabilisation.

Firstly, the experimental apparatus and feedback control approach is described. Secondly, the experimental work is divided into three parts. The motivation, experimental setup and procedure as well as results and conclusions are given for each of them. The feasibility of the investigated approach was usually tested on a neurologically intact subject. The results were subsequently confirmed with a paraplegic subject.

First the feasibility and fundamental limitations of unsupported standing were investigated. Assuming the subject as a single-link inverted pendulum, an improved full dynamic control approach was employed in the first step, confirming existing results. Here, the voluntary influence by the central nervous system was minimised. However, it is naturally desirable to take advantage of the residual sensory-motor abilities of the paraplegic subject to ease the task of stabilising the body. Ankle stiffness control has been proposed in the literature to accomplish this task. Hitherto, ankle stiffness was provided by artificial actuators. In the second part we investigated the feasibility and limitations of ankle stiffness control by means of FES. The same single-link approach was employed as above. Ankle stiffness control by FES was used in the third part to enable paraplegic standing. Here, the subject was required to participate actively in the task of stable standing and, while doing so, behaving like a double-link inverted pendulum.

It could be shown that FES-controlled ankle stiffness contributed crucially to the subject's ability to stand. The thesis concludes with propositions for future work.

Acknowledgements

Success has many fathers! Therefore I would like to thank everybody who contributed to it in some way or the other. Notably, my supervisor Ken Hunt for giving me the opportunity to work on this project and his ongoing interest in the progress of my work. Henrik Gollee for his collaboration and his comments on my thesis. Zlatko Matjačić for his collaboration and contribution to making the stay at Aalborg University a great success.

Furthermore, all members of staff at the Department of Mechanical Engineering as there are the secretary staff, the computing staff, and the workshop people for giving birth to the MRF.

Moreover, I would like to thank my colleagues for keeping a good spirit within the research group, in particular Thomas Schauer for friendship and fruitful discussions. I do not want to forget anyone who came and left and shared their spell with me during my time at Glasgow University. There are too many to name here. Thanks also to Karsten Bubke who is the better chess player of us two.

To keep going during a three years project needs some encouragement from time to time. Therefore I need to thank everyone who contributed to this. Foremost Christiane for coming to Glasgow with me and her support at all times not to mention her tireless proofreading of virtually everything I ever wrote in English (including these acknowledgements). Thank you Mozart for not letting me sleep at night. My family and all friends in Dresden and elsewhere in Germany who did not forget us "foreigners" and took all the effort to come up to the very edge of Europe and visit us or, at least, stayed in touch with us. In particular my wee sister Elke who spent six months in Scotland herself for keeping the family ties and the "competition" alive.

Finally, I would like to thank everybody who made the three years in Glasgow for Christiane, Mozart and myself a good experience and an enjoyable time. Goodbye Glasgow, Goodbye Scotland!

Klimme klimb,
zum Olymp.
Stell dir vor: dort oben winken
Schnäpse und Schinken.

Ringelnatz

Contents

List of Tables

List of Figures

List of Abbreviations

ARX	Auto Regressive with an Exogenous Input
CNS	Central Nervous System
CoM	Centre of Mass
DC	Direct Current
EPC	External Posture Control
FES	Functional Electrical Stimulation
IEEE	Institute of Electrical and Electronics Engineers
IFESS	International Functional Electrical Stimulation Society
LQG	Linear Quadratic Gaussian
MRF	Multipurpose Rehabilitation Frame
PD	Proportional Derivative
PID	Proportional Integral Derivative
PRBS	Pseudo Random Binary Sequence
SCI	Spinal Cord Injury
SISO	Single Input Single Output
SNR	Signal to Noise Ratio
T5	Thoracic Vertebra No. 5
T8	Thoracic Vertebra No. 8

Chapter 1

Introduction

We usually take upright standing for granted. It is only when we fail to manage this task, due to illness or injury, that we realise how complex and difficult it is. This thesis is concerned with the restoration of upright standing after spinal cord injury (SCI) by the means of Functional Electrical Stimulation (FES). Its feasibility and fundamental limitations are studied. A strategy to incorporate the residual sensory-motor function is investigated. Finally, a path for further development is proposed.

This introductory chapter provides background information about spinal cord injury and FES and gives an overview of the thesis.

1.1 Spinal Cord Injury and Functional Electrical Stimulation

Spinal cord injury results in an interruption of the neurological pathways from the brain to the muscles. Depending on the level of injury, this causes a loss of motor and sensory functions and results in immobilisation of the patient. Figure 1.1 shows the impairment resulting from an injury at a particular spinal level.

However, the muscles themselves retain their ability to contract and produce force. Furthermore, paralysed muscles can be stimulated artificially by applying electrical pulses to them, thereby regaining their function. This technique is known as Functional Electrical Stimulation. Figure 1.2 compares the principle of motor function control in a physiologically intact person and a paraplegic.

Applications of FES include bowel and bladder control after SCI [Creasey, 1999], foot drop correction in stroke patients and hemiplegics [Haugland *et al.*, 2000; Hansen *et al.*, 2000], hand grasp for tetraplegics [Inmann and Haugland, 2000; Kilgore, 2000], cardiac support using skeletal muscle ventricles [Salmons and Jarvis, 1992], ventilatory assistance for patients with a cervical level injury [Miller and Mortimer, 2001], standing, standing-up and sitting down [Donaldson and Yu, 1996; Riener and Fuhr, 1998], and cycling [Hunt *et*

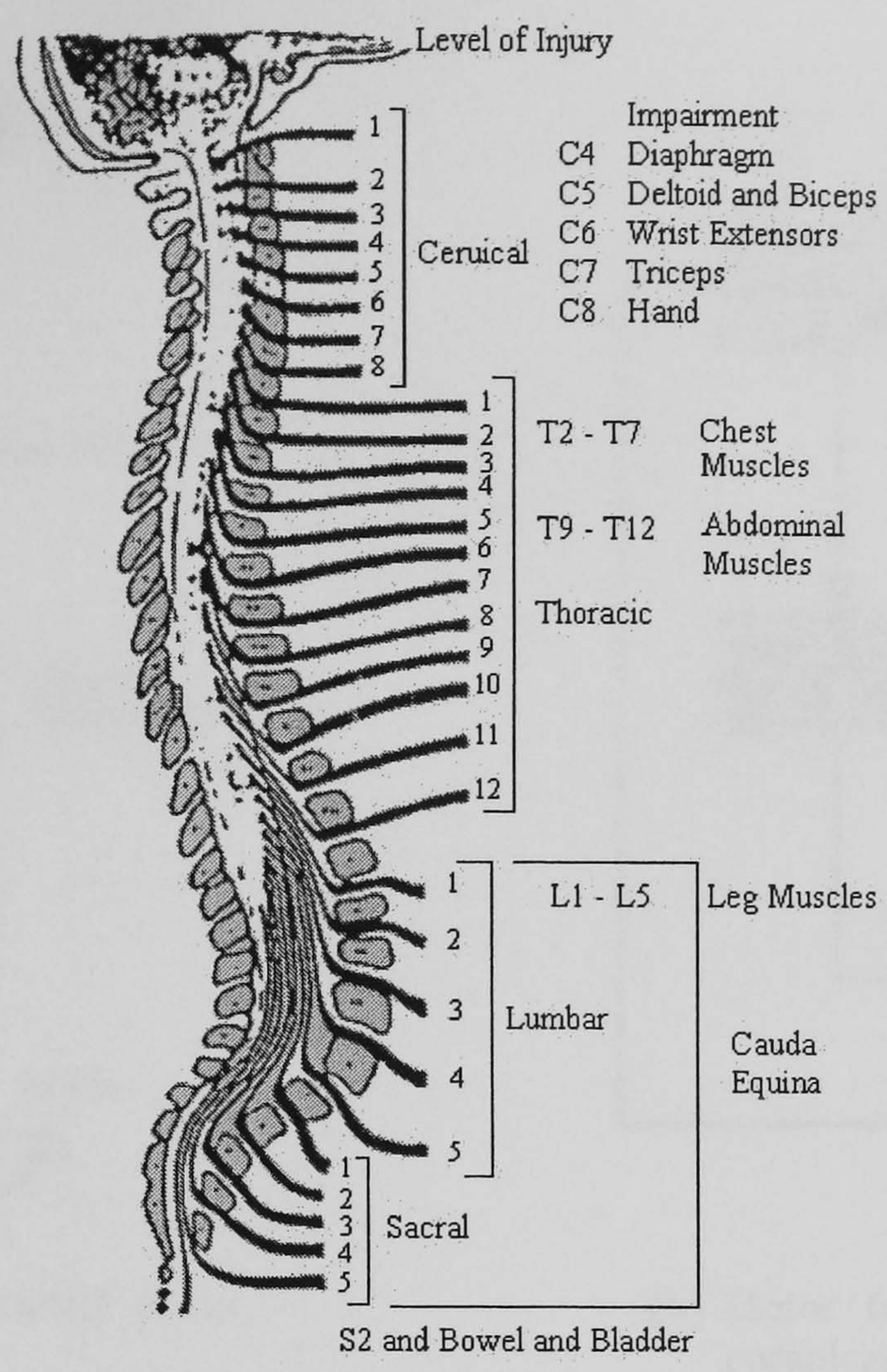

Figure 1.1: Spinal column with spinal cord and impairment resulting from an injury at a particular level. Source: Canadian Paraplegic Association, http://www.nsnet.org.

al., 2001]. For some of these applications commercial systems are already available (e.g. FREEHAND®, VOCARE™, LifeSTIM™ by NeuroControl™).

Prolonged immobilisation causes several physiological problems such as bladder infections, pressure sores, demineralisation of bones, muscular atrophy, spasticity and hypotension due to damage to the sympathetic nervous system, leading to vasodilation. Joint contractures limit the range of motion which impairs the patient's mobility and independence. Beyond the direct functional motor effects, some therapeutical side effects of FES on these difficulties have been reported [Daly *et al.*, 1996]. Stefanovska *et al.* [1989] reported a decrease in tonic spasticity after a long-term use of FES in hemiplegia in both ankle joint antagonist/agonist muscle groups as well as an improvement in voluntary strength.

Passive standing using special standing frames is a widely employed procedure in physiotherapy after SCI to overcome some of these physiological problems [Hammel, 1995; Grundy and Swain, 1996]. While standing, the leg bones are subject to normal weight loading. This reduces the risk of osteoporosis and associated fractures. The patient's knee and hip joints will be locked by a belt attached to the frame. Braced in this way, the patient is mechanically stable. Such a standing session will typically last 30 minutes. Alternatively,

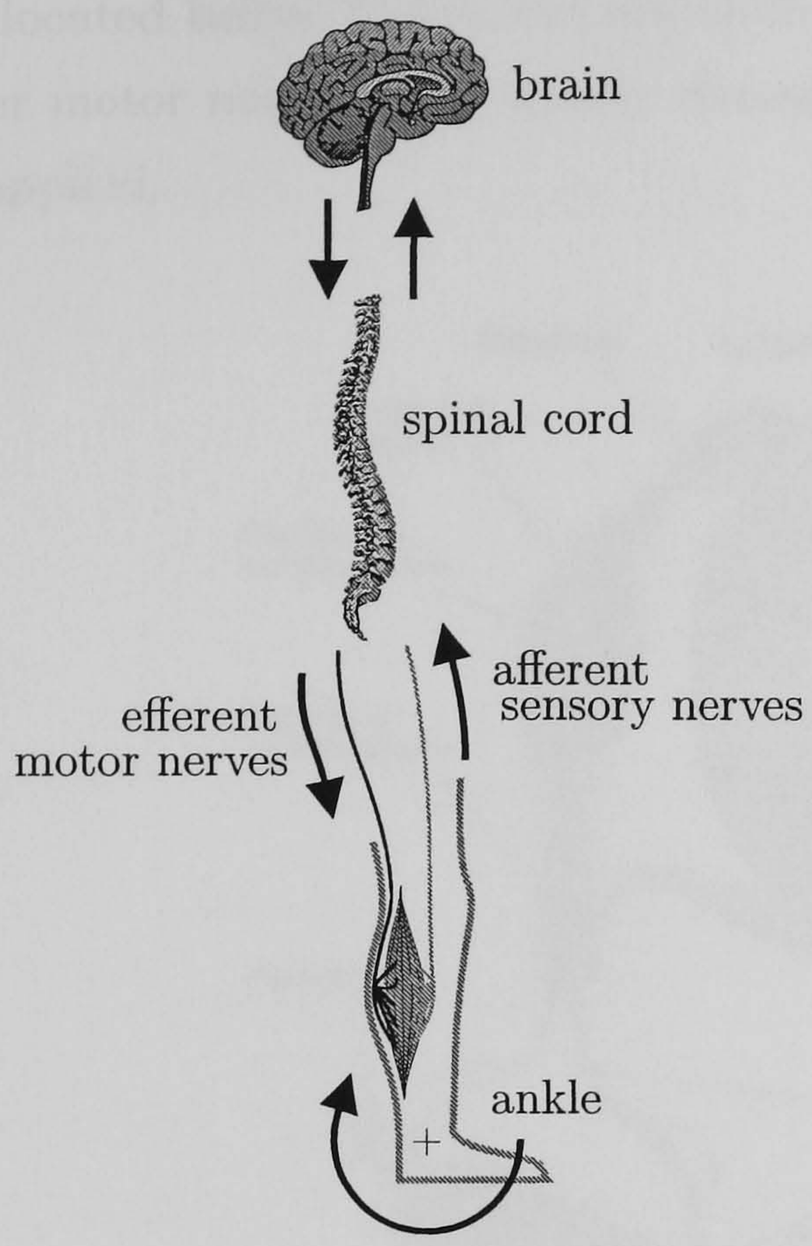

(a) Motor function control in an intact individual.

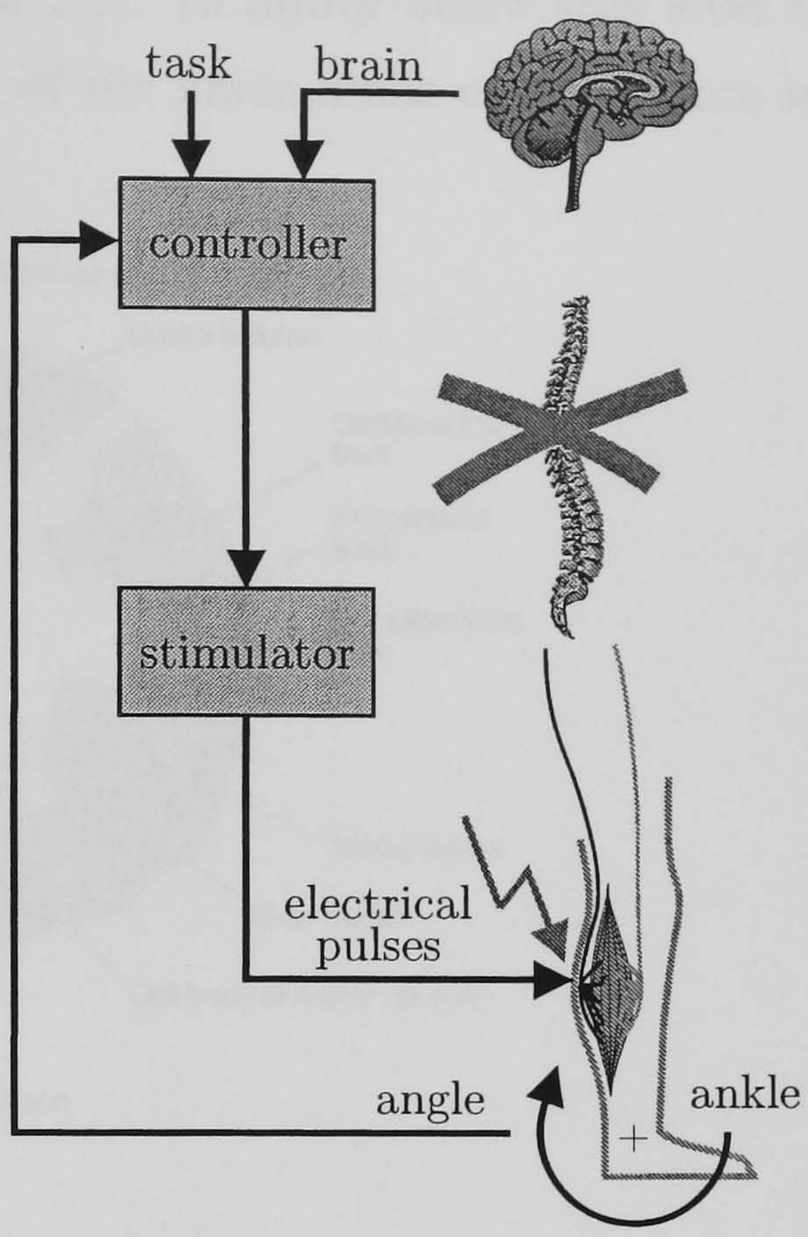

(b) Motor function control in a paraplegic using FES.

Figure 1.2: The principle of FES to restore motor function control in paraplegia exemplary for plantarflexor stimulation.

long leg braces can be used. These also allow ambulation over short distances. However, the patient will typically be positioned between parallel bars and be required to hold on to the bars for postural stability.

The SCI population consists of 50,000 people in the U.K. 700 people injure their spinal cord each year in the U.K. In Europe the SCI population comprises 600,000 people, in North America 200,000 people. 80% of the injuries are sustained at an age of 16–45. The main causes within the U.K. are road traffic accidents (37%), domestic and industrial accidents (36%), sport accidents (20%), and acts of violence (7%) [Grundy and Swain, 1996].

These numbers show that the SCI population is a considerable target population with SCI being a dramatic turning point in the life of the person concerned. Hence, research activities are justified which aim to improve some of the circumstances accompanying spinal cord injury. This thesis focusses on the restoration of "functional" standing, i.e. standing without use of the arms for stability. These would then be free to perform tasks.

A pre-requisite for the application of FES are intact lower motor neurons. Figure 1.3 shows the spinal control circuit comprising the afferent (sensory) nerve, the efferent nerve (lower motor neuron) and the muscle as the actuator. If either the afferent or efferent nerve was damaged, the nerve cell would die. For the lower limbs the lower motor neurons

are located below T12 in the spinal cord (cf. Figure 1.1). In injury below this level the lower motor neurons are usually damaged and FES of the lower limbs can therefore not be applied.

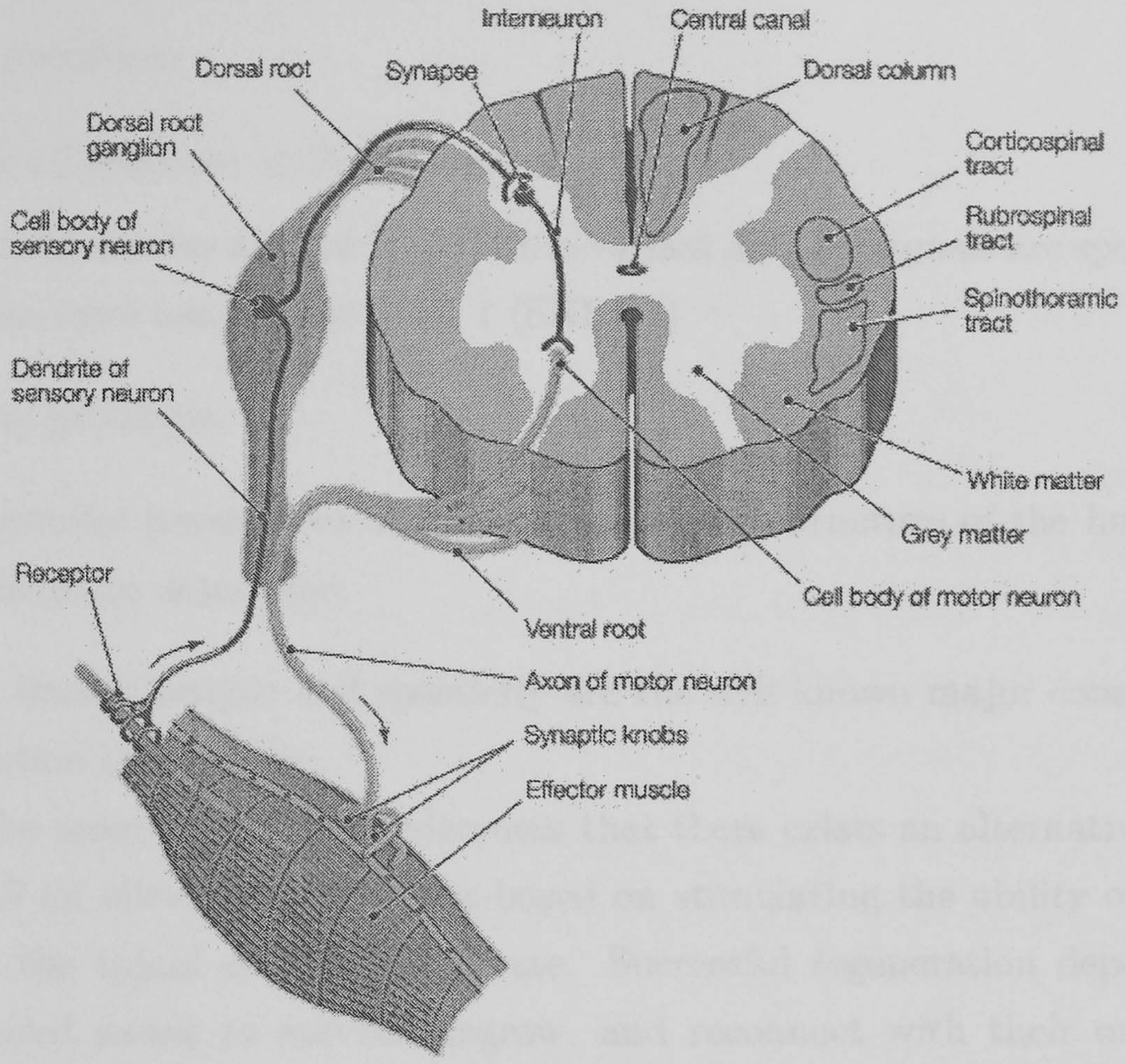

Figure 1.3: Spinal cord cross section with lower motor neuron, afferent and efferent nerves and muscle. Source: Venes *et al.* [1997].

Patients with a cervical lesion will have a lack of trunk stability as their trunk muscles will be paralysed. This limits the potential candidates for FES supported standing to people with a thoracic injury level (41% of the SCI population [Grundy and Swain, 1996]).

The main difficulties with the application of FES for the control of standing are as follows:

- problems associated with the muscles:
  - highly nonlinear and time-variant
  - synchronous and inverse recruitment pattern results in fast muscle fatigue when artificially stimulated
  - spasticity (in paralysed muscles), hyperexcitability of reflex nerves in SCI
  - paralysed muscle and nerve fibres degenerate when not used.
- problems associated with targeting of the stimulation:
  - diffuse stimulation pattern when using surface electrodes

  - difficulties catching shorter muscles and muscles located deeper below the skin when using surface electrodes
  - number of channels when using implanted electrodes

- sensory problems:
  - lack of practical artificial sensors
  - natural sensors are nonlinear, time-variant and the signals are spoilt by a signal-noise-ratio usually less than 1 (SNR<1)

- modelling problems:
  - kinematic parameters of the bio-mechanical structure of the human body are difficult to determine

Among these, muscle fatigue and spasticity are the well known major constraints of FES for the restoration of standing.

It should be mentioned for completeness that there exists an alternative research approach to FES on alleviating SCI. It is based on stimulating the ability of the damaged nerve cells in the spinal cord to regenerate. Successful regeneration depends upon the ability of injured axons to survive, regrow, and reconnect with their original targets. Unfortunately, the central nervous system (CNS) cannot regenerate injured nerve fibres. Normally, injured neurons die and a scar forms. Achieving axonal growth, though, is not sufficient; retrieval of the appropriate pathways, target recognition, orderly reinnervation and reestablishment of functioning synapses are also essential. Although progress has been made in various fields including genetics, biochemistry, molecular and cellular biology and physiology, embryonic and adult stem cell biology, the issue remains and there are still a number of scientific challenges to be met before it is time to initiate clinical therapies [Behar *et al.*, 2000; Frey, 2001; Ramer *et al.*, 2000].

In current clinical therapy, FES supported standing is still being achieved by stimulation of the knee extensor muscles while the ankle joints are braced by an orthosis and stability has to be achieved by arm support [Kobetic *et al.*, 1999; Cleveland FES Center, Ohio; Salisbury District Hospital, U.K.]. Simple feedback algorithms such as standard proportional-integral-derivative control (PID) may be implemented to regulate knee extension [Wood *et al.*, 1998]. Therefore, it can be said that little progress has been made in terms of control techniques since the beginning of clinical FES assisted standing programmes in the 70's [Kralj and Bajd, 1989]. Stable standing still relies on arm support. Here, the upper extremities support an average of 25% of the body's weight [Kobetic *et al.*, 1999]. Moreover, the arms provide all of the posture stabilisation. Consequently, paraplegic standing is still functionally limited. Progress has been made, however, in terms of surgical and stimulation techniques with implanted systems now experimentally

available [Kobetic *et al.*, 1999; Wood *et al.*, 2001]. This thesis is concerned with achieving standing without arm support by applying feedback methods to facilitate stability in order to increase the functional potential of standing in paraplegia.

1.2 Outline of the Thesis

The work presented in this thesis is subdivided into three partial objectives. The motivation is given for each of them, followed by a description of the experimental setup. The results are presented, discussed and finally, conclusions are drawn.

- **Chapter 2** describes the experimental methods employed throughout the thesis. This chapter precedes the presentation of the individual studies because these methods were repeatedly utilised throughout the different parts of the work. The experimental apparatus used is described. The generic control approach is outlined and a scheduling strategy is developed to control agonist/antagonist muscle groups.

- **Chapter 3** investigates the feasibility of unsupported standing in paraplegia. The subject is assumed as a single-link inverted pendulum. This configuration is realised by a custom-made body brace attached to the subject's back in such a way that movement is possible only around the ankle joints while the plantarflexor muscles are being stimulated. In this way, the influence of any voluntary control effort by the CNS is minimised. Standing then completely relies on the artificial control system, and the stabilising moment has to be provided by the plantarflexor muscles only while they are being stimulated. The effect of a number of control design options is investigated in experiments with an intact subject. The experiments are repeated with a paraplegic subject employing the most appropriate control design options.

- **Chapter 4** evaluates the practicality of ankle joint stiffness control using FES. As in the previous chapter, voluntary CNS input is minimised by the same single-link inverted pendulum approach. The chapter investigates the achievable quality of ankle joint stiffness control and the extend to which ankle stiffness control might facilitate stable standing. The plantarflexor and dorsiflexor muscles are subjected to FES and a series of experimental tests is carried out. These tests were first performed with an intact subject and the results were later evaluated with a paraplegic subject.

- In **Chapter 5** ankle joint stiffness control is employed to facilitate paraplegic standing. The subject is required to actively participate in the task of stable standing. However, stability is not provided by arm support but by upper body movement, potentially leaving the arms free for functional tasks. In contrast to the previous chapters the subject behaves like a double-link inverted pendulum. Voluntary upper

body input is essential and necessary. A number of successful standing tests were performed with a paraplegic subject.

- Finally, conclusions and recommendations for future work are addressed in **Chapter 6**.

1.3 Contribution of the Thesis

Control of Isometric Muscle Moment. A control method for isometrically contracting antagonist/agonist muscle groups is developed. The design is based on empirically determined models of each muscle group. The models are estimated from measured input/output data. The design approach consists of separate controllers for each muscle group with common states and a suitable scheduling strategy. It also includes an anti-windup which is not only a performance feature of the presented approach but an essential component of the scheduling scheme.

Antagonist/agonist muscles consist of two systems which are well separated and produce an opposite output from the same input signal. This represents the main difficulty in control of antagonist muscles. The presented method is an integral component in higher level experiments which demonstrate its feasibility.

Control of Unsupported Standing. Previous results on the feasibility of unsupported standing and its fundamental limitations are verified to make those results more significant. An improved control system design for paraplegic standing is developed which deals with the left/right asymmetry in muscle strength and significantly prolongs the period of standing in paraplegic subjects. The influence of various design aspects is discussed in order to provide a transparent methodology for the design of feedback controllers for standing. These control design methods are based on polynomial methods.

Control of Ankle Stiffness while Standing. The feasibility of the control of ankle stiffness while standing is demonstrated. A control strategy is developed and the significance of various stiffness values for the task of standing is discussed as well as the limitations regarding the accuracy of ankle stiffness control. This work represents a pilot study towards a complete impedance control at the ankle joints and "integrated voluntary control" for standing. The results are presented for both an intact and a paraplegic subject.

Integrated Voluntary Control—Paraplegic Standing supported by FES-Controlled Ankle Stiffness. A new approach of combining residual upper body function and closed-loop FES is introduced. This is called "integrated voluntary control". A

closed-loop controlled ankle stiffness is provided by means of FES while the subject is balancing by means of voluntary and reflex activity. The FES system incorporates the above mentioned method to control antagonist/agonist muscle groups. The feasibility of this approach is demonstrated and the stabilising contribution of the FES system is shown. It is demonstrated that FES-controlled and externally applied stiffness can be combined. The presented method has the potential to make the task of paraplegic standing "functional" The possibility to extend the method is discussed. These results are a major novel contribution to the literature and represent the main contribution of this thesis.

1.4 Publications

The results presented in this thesis have previously been published, in part, as follows:

K. J. Hunt, H. Gollee, R.-P. Jaime, and N. Donaldson. Feedback control of unsupported standing. In *Proceedings of the International Biomechatronics Workshop*, pages 42–46, Enschede, The Netherlands, 1999.

K. J. Hunt, H. Gollee, R.-P. Jaime, and N. Donaldson. Feedback control of unsupported standing. *Technology and Health Care*, 7(6):443–447, November 1999.

K. J. Hunt, H. Gollee, R.-P. Jaime, and N. Donaldson. Design of feedback controllers for paraplegic standing. In *Proceedings of IEE Control 2000*, CD-ROM, Cambridge, U.K., 2000.

K. J. Hunt, R.-P. Jaime, H. Gollee, and N. Donaldson. Control of ankle joint stiffness while standing. In *Proceedings of the 5th Annual Conference of the International Functional Electrical Stimulation Society*, pages 462–465, Aalborg, Denmark, 2000.

K. J. Hunt, H. Gollee, R. Jaime, and N. Donaldson. Design of feedback controllers for paraplegic standing. *Proceedings of IEE on Control Theory and Applications*, 148(2):97–108, March 2001.

K. J. Hunt, H. Gollee, and R.-P. Jaime. Control of paraplegic ankle joint stiffness using FES while standing. *Medical Engineering & Physics.*, 23(8):541–555, October 2001.

K. J. Hunt, R.-P. Jaime, and H. Gollee. Robust control of electrically stimulated muscle using polynomial H_∞-design. *Control Engineering Practice*, 9(3):313–328, March 2001.

R.-P. Jaime, Z. Matjačić, and K. J. Hunt. Paraplegic standing supported by FES-controlled ankle stiffness. *IEEE Transactions on Neural Systems and Rehabilitation Engineering.* submitted.

R.-P. Jaime, K. J. Hunt, and H. Gollee. A polynomial H_∞-controller for muscle moment control. In *Proceedings of the European Control Conference ECC'99*, Karlsruhe, Germany, CD-ROM, 1999.

R.-P. Jaime, Z. Matjačić, and K. J. Hunt. Paraplegic standing supported by FES-controlled ankle stiffness. In *Proceedings of the 6th Annual Conference of the International Functional Electrical Stimulation Society*, Cleveland, Ohio, 2001. 68–70.

Chapter 2

Experimental Apparatus and Feedback Methods

This chapter describes the experimental methods which are used throughout the experimental work presented in this thesis. Most of the methods are employed in different parts of the work. Therefore, they shall be described separately preceding the presentation of the experimental work.

2.1 The Stimulator Device

The stimulator used in all experiments is known as the "Stanmore Stimulator" and is described in Phillips *et al.* [1993]. It is an eight channel programmable stimulator driven by a PC via the serial port and produces current controlled monophasic rectangular pulses up to a duration of 800 μs adjustable in steps of 2 μs with an accuracy of 0.5 μs. The amplitude of the pulses is adjustable in steps of 10 mA up to 130 mA. The stimulator was operated at a constant frequency of 20 Hz (sampling interval 50 ms).

We used round surface electrodes by PALS®, with a diameter of 2 inches, placed over the gastrocnemius muscle for plantarflexing and the tibialis anterior muscle for dorsiflexing.

2.2 The Wobbler Apparatus

The experimental apparatus utilised for the experiments on unsupported standing and on the control of ankle stiffness while standing—called the Wobbler apparatus (but not to be mistaken with the London Millenium bridge)—is described in Donaldson *et al.* [1997]. The Wobbler apparatus has been specially designed for the investigation of control algorithms for unsupported standing in the sagittal plane without interference from the CNS. In order to accomplish that requirement the subject standing in the apparatus wears a custom made

body shell which braces all joints above the ankle joint. In that configuration the subject can be regarded as a single-link inverted pendulum (cf. Figure 2.1).

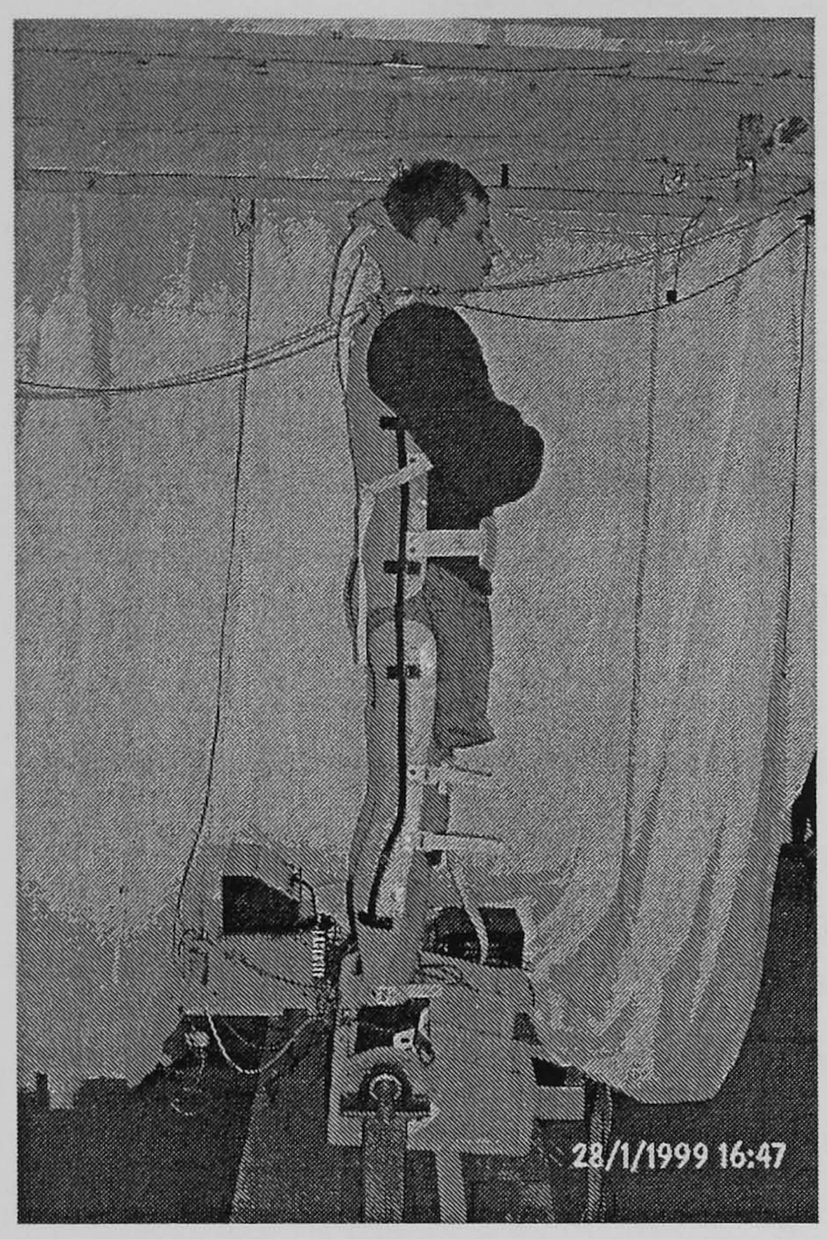

(a) Inverted pendulum configuration. Movement is only possible around the ankle joint

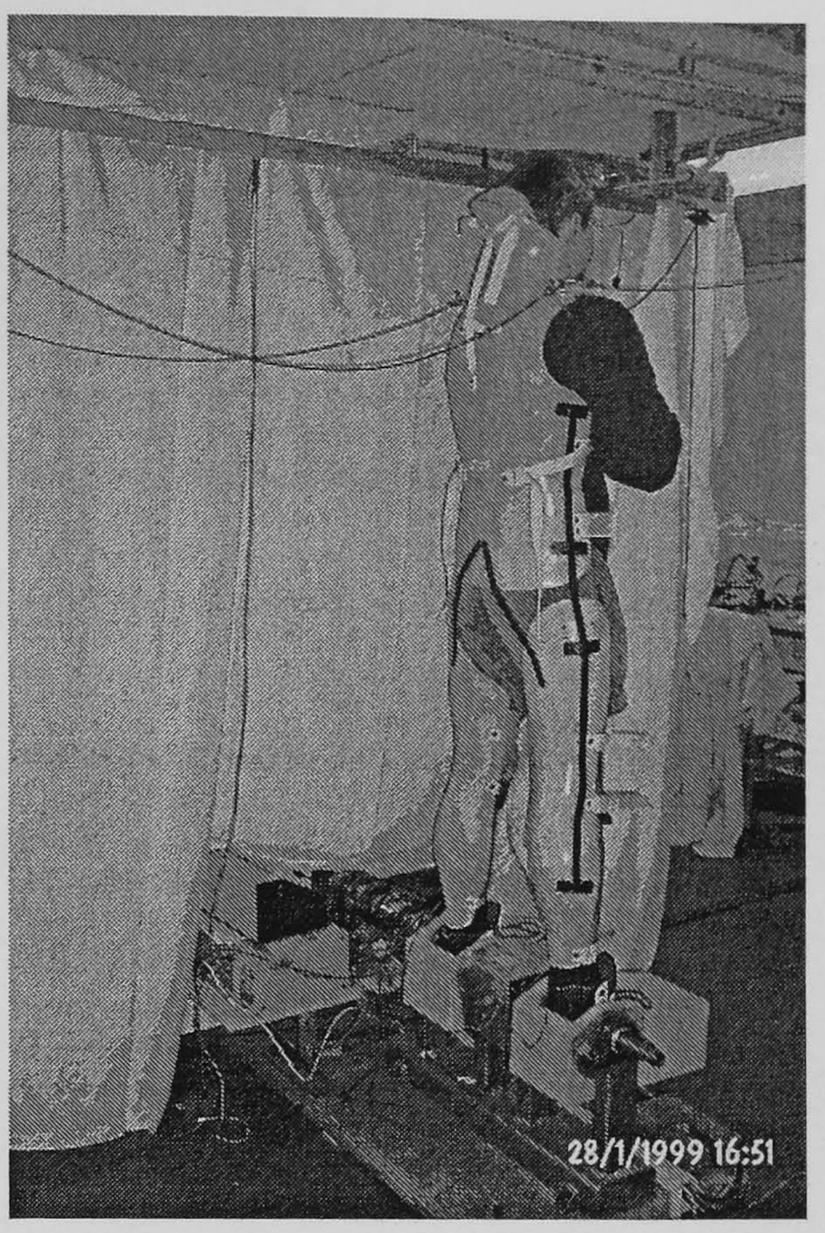

(b) Custom-made body brace.

Figure 2.1: Subject standing in the Wobbler apparatus. Safety ropes mounted to the ceiling and attached to the subject's shoulder prevent the subject from falling over.

The feet are strapped in the two footboxes as shown in Figure 2.2. The footboxes can be rocked, driven by a DC motor with a maximum "wobbling" frequency of 1 Hz or 6 Hz. The frequency range is manually adjustable. The rotational motion of the DC-motor is transformed into a sinusoidal rocking motion by a gear. The shaft angle is measured by a potentiometer. The "wobbling" mode is employed during the experiments on the control of ankle stiffness which are described later in this thesis.

A torque sensor between the footboxes measures the moment of the right ankle. Another torque sensor to the left measures the total ankle moment. A string attached to the subject's back is led over a potentiometer to measure the angle of inclination of the body.

The Wobbler can be used in three different ways:

- Footboxes in fixed position and subject in fixed position by tightening the safety ropes. This was done during the identification procedure of the muscle properties and control of the isometric muscle moment in the experiments on control of unsupported standing and on control of ankle stiffness.

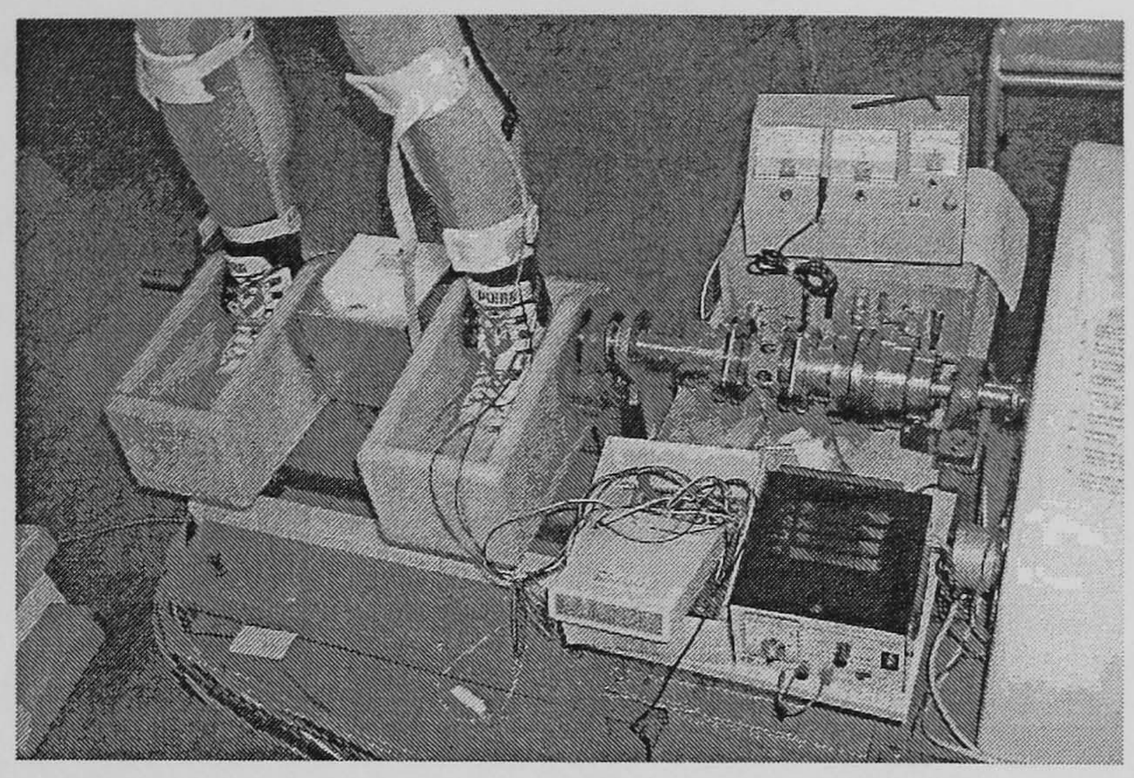

Figure 2.2: Position of feet in footboxes and moment measuring load cell.

- Footboxes in fixed position and subject free to move around the ankle joint. This was done during the actual standing test in the unsupported standing experiments as well as during different tests in the experiment of ankle stiffness control.

- Subject in fixed position and footboxes "wobbled". This was done during the experiment on ankle stiffness control in order to evaluate the stiffness control.

2.3 The Multipurpose Rehabilitation Frame—MRF

2.3.1 General Description

For the experiments on integrated voluntary control a new experimental device is employed. The apparatus is called the Multipurpose Rehabilitation Frame—MRF and is described in Matjačić [2000] and Matjačić *et al.* [2000]. A second device has been built based on Matjačić's original design within the framework of research presented in this thesis with permission by the original author but with a number of important modifications. Modifications that have been made are summarised as follows:

- An optional rotating foot platform has been built combining the features of the experimental frame presented in Matjačić and Bajd [1998b] with the device described in Matjačić [2000] and Matjačić *et al.* [2000]. This enables us to investigate artificial strategies to control standing in intact subjects.

- Absolute shaft encoders have been used instead of incremental ones. This increases the overall safety of the device since absolute shaft encoders provide a well defined angle signal at all times. With incremental shaft encoders, the frame has to undergo a special "nesting" procedure each time the device is switched on. This holds a potential source of error or malfunctioning.

- The frame's control algorithm is running on the xPC-Target for MATLAB/SIMULINK instead of on a MS-DOS based user written C-program. This increases the reliability since the control program now runs on a special real-time kernel. Moreover, this provides far greater flexibility for the experimenter if he/she wants to alter the control algorithm. The integrated environment for control design, testing and implementation of MATLAB/SIMULINK limits potential faults and enables better maintenance.

In contrast to the Wobbler the MRF has been designed in order to incorporate actively the subject's residual sensory-motor capabilities into the artificial control strategy. The MRF has two degrees-of-freedom i.e. the sagittal and the frontal plane. For safety reasons the range of motion is limited to $\pm 23°$ in both planes. This prevents the subject from falling over. It provides support around the hips but the subject is free to move his/her upper body in the lumbar/thoracic spine. In this configuration the subject can be assumed as a double-link inverted pendulum. The frame acts as an artificial ankle joint in the sagittal plane and as an artificial hip joint in the frontal plane, respectively. Figure 2.3 shows a subject standing in the MRF. There are two options: The subject can stand **(a)** on forceplates and **(b)** on a rotating foot platform.

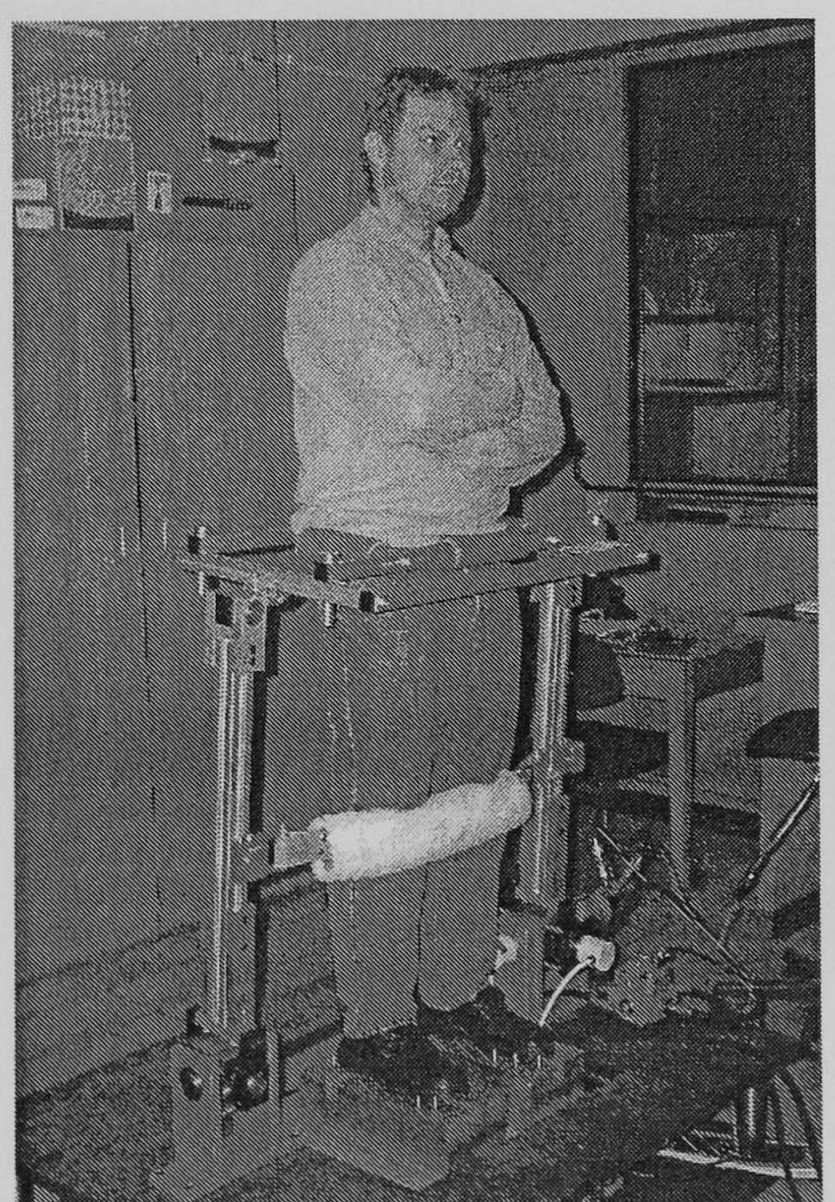

(a) Subject standing on a force platform

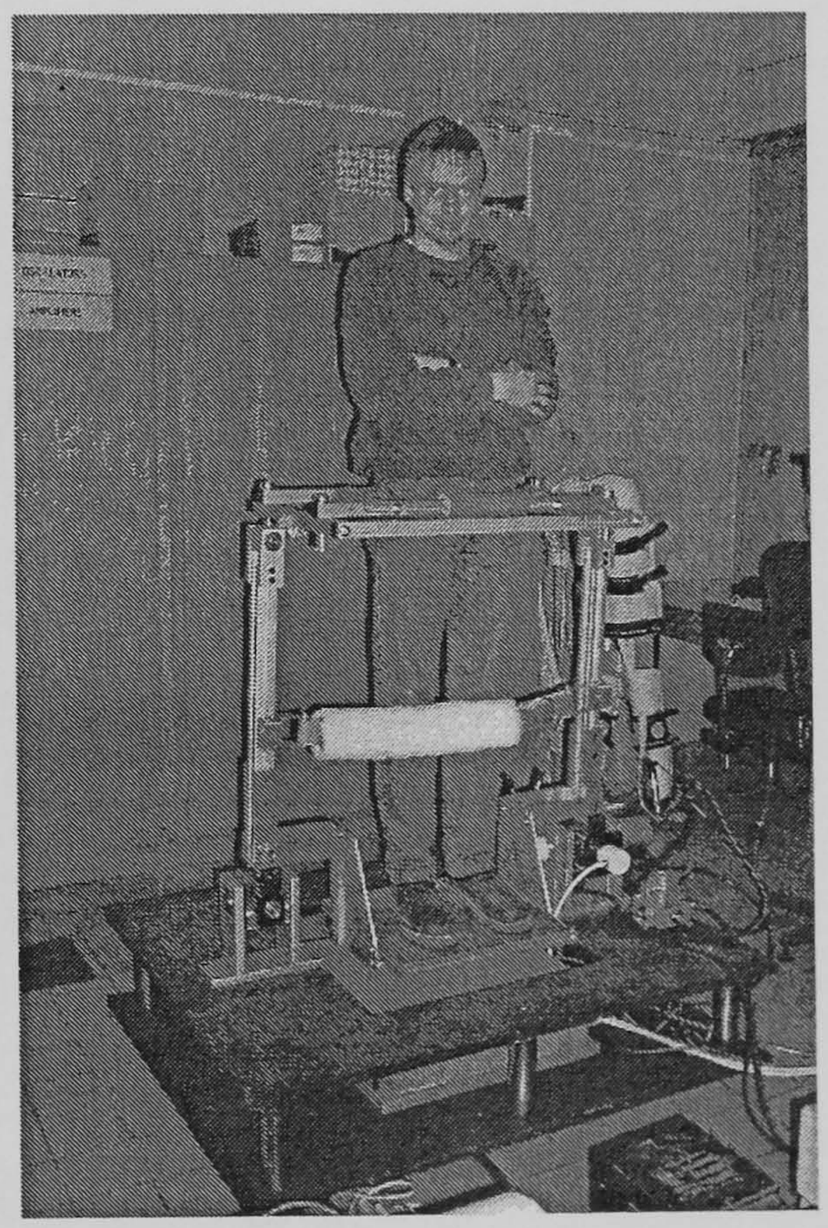

(b) Subject standing on a rotating foot platform.

Figure 2.3: Subject standing in the MRF.

The frame provides several modes of usage:

1. Intact subject standing on forceplates—enables investigation of the natural mechanism of controlling upright standing and posture.

2. Intact subject standing on a rotating foot platform—enables investigation and testing of artificial control strategies in intact subjects.

3. Impaired subject standing on forceplates:

   (a) Training of balancing skills.

   (b) Investigation and test of artificial control strategies for standing using the hydraulic actuators which power and control the frame.

   (c) Investigation and test of FES control strategies for standing.

The heart of the MRF is the two degree-of-freedom joint actively controlled by hydraulic actuators as shown in Figure 2.4. It is essential that the frame is lightweight in order to minimise the disturbance imposed by the weight of the frame. Therefore, despite their non-linear system characteristics hydraulic actuators have been chosen because one of the actuators has to be moved by the other and hydraulic drives have a much better power-weight relationship than an electrical drive.

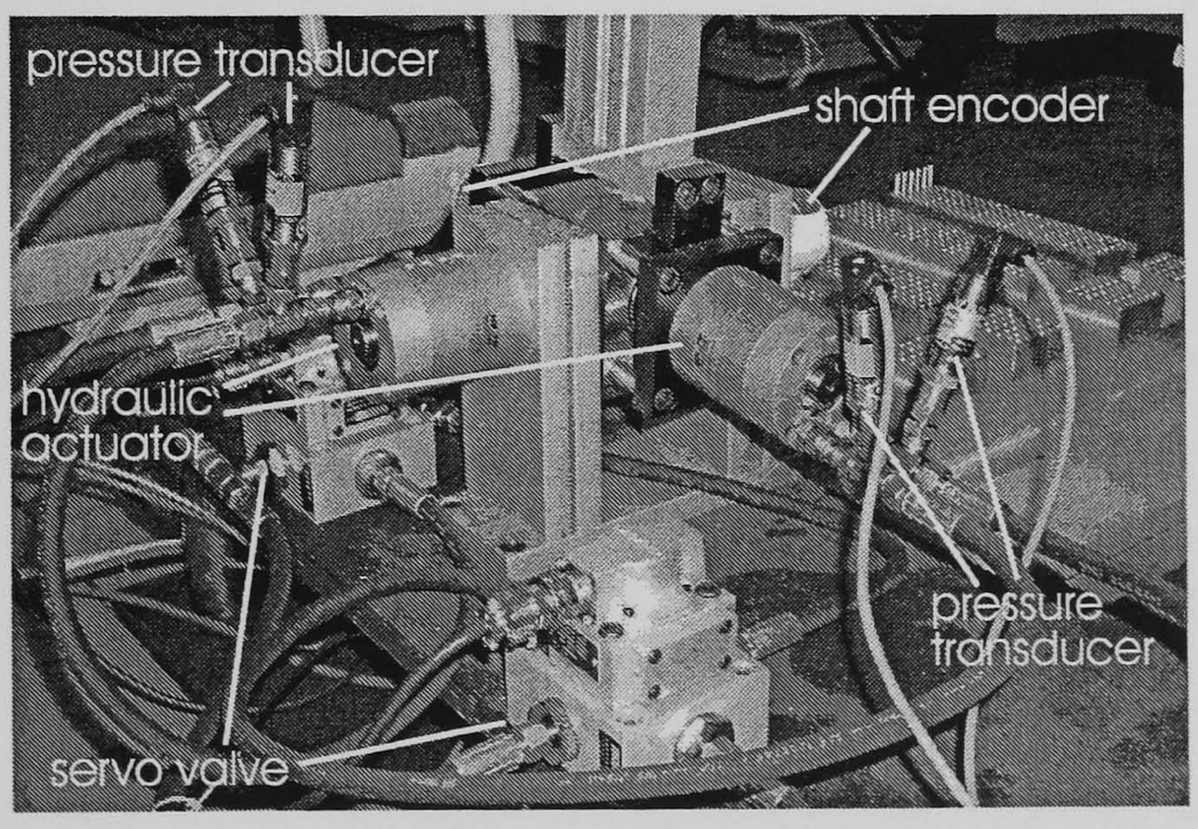

Figure 2.4: Actively controlled two degree-of-freedom joint.

Figure 2.5 shows an exploded view of the actively controlled two degree-of-freedom joint. In case the subject is standing on the rotating platform the lower joints have to bear the body weight. Therefore they are made of stainless steel which makes the rotating parts more wear resistant. The upper part of the frame is made of aluminium, partly using standard profiles and quickbuild components.

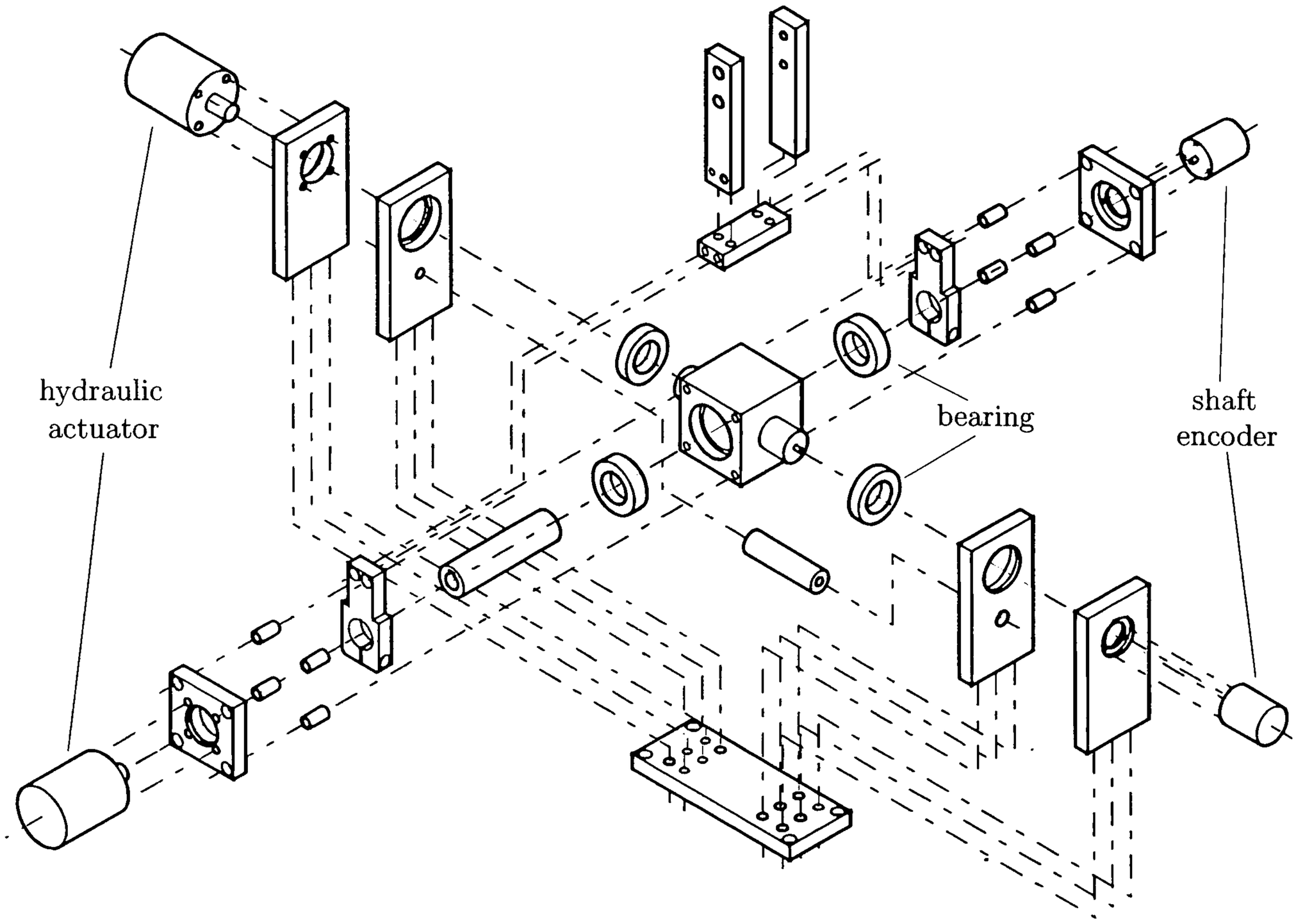

Figure 2.5: Exploded view of the actively controlled two degree-of-freedom joint.

2.3.2 The Electro-hydraulic Servo Circuit

The electro-hydraulic servo circuit is shown in Figure 2.6. There are two circuits in parallel, independently controlling the frame in the sagittal and in the frontal plane, driven by a common power unit. The power unit consists of a pump driven by a three-phase electrical motor with a power of 1.1 kW. Furthermore it consists of a suction filter, a directional valve, a pressure relief valve and a pressure gauge. In this configuration the power unit provides a constant operating pressure. A four-way servo valve controls the flow through the rotary actuator. The servo valve is driven by an electrical DC torque motor. Under no-load conditions the flow is proportional to the driving current. The torque provided by the actuator is proportional to the pressure difference across the actuator. The pressure difference across the actuator is measured by two pressure transducers. The angle of rotation and the angle of inclination of the frame are measured by an absolute shaft encoder which gives a digitally coded value of the angle. Thus, the actuator torque and the angle are available for feedback.

2.3.3 Control of the MRF

The structure of the feedback controller, running on a PC, is shown in Figure 2.7. There are two cascaded feedback loops.

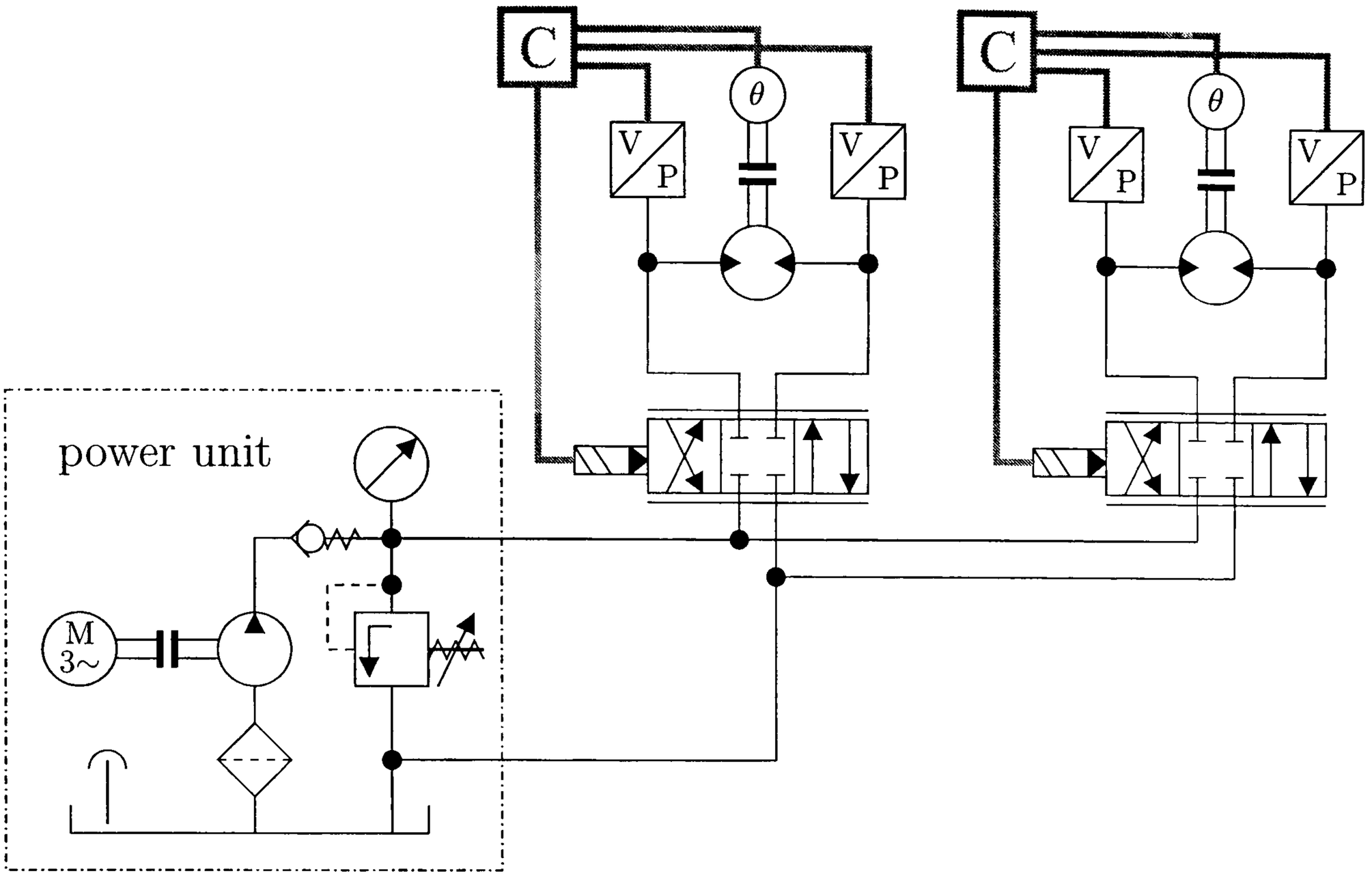

Figure 2.6: Hydraulic servo circuit of the MRF. There are two electro-hydraulic servo circuits in parallel, one of each controlling one plane of motion (sagittal plane and coronal plane), driven by a common power unit. The bold grey parts mark the electrical feedback parts of the servo mechanism. The symbol θ indicates the shaft encoder which measures the angle of inclination of the frame. The blocks labelled "C" are the feedback controllers (for details cf. Figure 2.7). For hydraulic symbols refer to Zoebl [1970]. For the specification of the hydraulic components refer to Appendix A.

The outer loop is subject to the control strategy to be investigated or employed for standing. Currently, there is a stiffness K_s and a viscosity feedback K_v implemented. The actual values for stiffness and viscosity are selectable by the experimenter. In terms of control theory this is equivalent to a PD-controller for the angle of inclination of the frame. Due to the quantisation noise, the "differentiated" angle signal is filtered by a second-order Butterworth filter with a 3 dB cut frequency of 5 Hz. This filter results in a time delay of 46 ms. The load imposed by the weight of the frame can be compensated for by a stiffness of the frame of $K_s = 2\,\mathrm{Nm/deg}$.

The moment of the hydraulic actuator m is controlled in the inner feedback loop. The sum of the angle signal, θ, multiplied by the stiffness value and the "differentiated" angle signal multiplied by the viscosity value provides the reference moment m_{ref} for the inner loop. Because of the nonlinear characteristics of the servo-hydraulic system a simple proportional control was chosen, which, taking safety and reliability of the feedback system into account, proved to be sufficient.

Additional to the outer feedback loop a perturbation moment m_p can be applied by

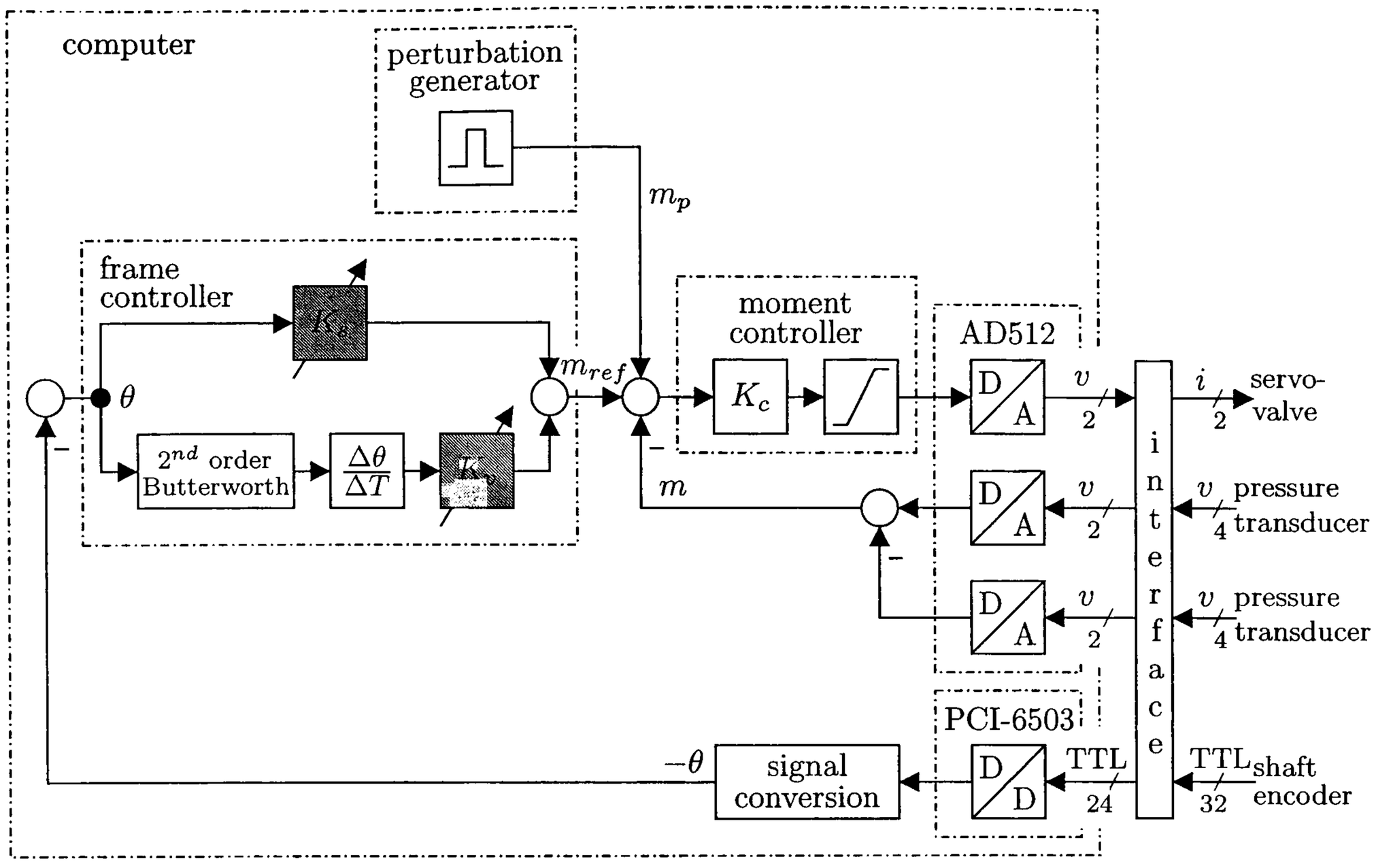

Figure 2.7: Cascaded control structure of the MRF. Each of blocks labelled "C" in Figure 2.6 is of this structure. The input/output signals are connected to the acquisition boards via an external interface. For the data acquisition boards refer to Appendix A.

the experimenter. The perturbations are of rectangular pulse-like shape and of selectable amplitude and duration. The perturbation moment can be applied in eight different predefined or randomly selected directions according to Figure 2.8.

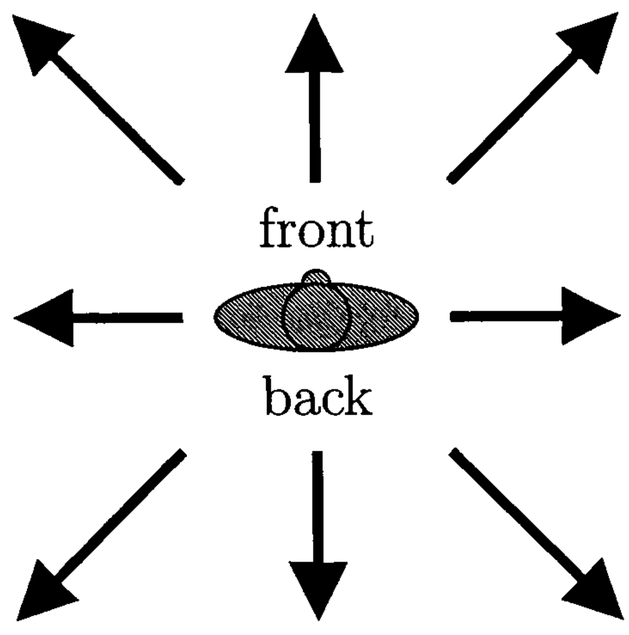

Figure 2.8: Directions of Perturbations. Top view of a standing subject along with arrows indicating the eight directions in which perturbations can be applied.

The controller according to Figure 2.7 has been implemented in MATLAB/SIMULINK and is running on the xPC-Target platform for MATLAB. While the controller is designed in MATLAB and implemented in SIMULINK, the control algorithm is translated into a C-program, compiled and downloaded onto a second PC via a serial link where it runs independently on a special real-time kernel. Parameters can be updated online via a

Graphic User Interface. This combines the safety and reliability of a real-time operating system with the open architecture of SIMULINK and provides easy access for modification of the control structure.

2.3.4 Modelling of the Hydraulic Circuit

For the purposes of controller design for the moment controller, the hydraulic servo circuit has been modelled and simulated. The purpose is to gain

1. an idea whether a simple proportional control is appropriate of performance and what performance can be expected and

2. a starting point for experimental tuning.

The basic principle of a valve-actuator combination is shown in Figure 2.9. The valve controls the flow through the actuator.

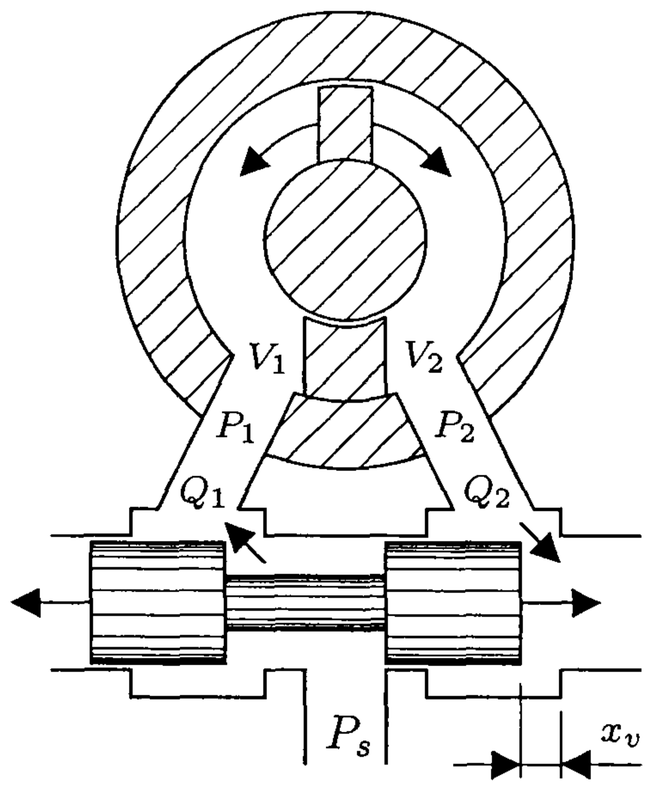

Figure 2.9: Basic principle of servo valve controlled rotary actuator. The servo valve controls the flow through the actuator. P_s is the supply pressure, x_v is the spool displacement.

The flow balance equation can be derived form the *law of the conversation of mass* [Merritt, 1967; Guillon, 1969]. The mass flow $\dot{\tilde{m}}$ within a system follows equation (2.1).

$$\sum \dot{\tilde{m}}_{in} - \sum \dot{\tilde{m}}_{out} = \frac{d\tilde{m}}{dt} \,. \tag{2.1}$$

Here, $\tilde{m}$ is the mass of the hydraulic fluid. Substituting $\dot{\tilde{m}} = \rho Q$ and $\tilde{m} = \rho V$, with ρ the density, V the volume, and Q the volume flow of the fluid, the mass flow balance equation can be expressed in terms of volume.

$$\sum Q_{in} - \sum Q_{out} = \frac{dV}{dt} + \frac{V}{\rho}\frac{d\rho}{dt} \tag{2.2}$$

This equation can be read as

sum of inlet flow - sum of outlet flow = deformation flow + compressibility flow (2.3)

Hydraulic fluids are are only approximately incompressible. Although the density changes are sufficiently small, they occur so fast that the compressibility flow is by no means negligible. The compressibility of a fluid is characterised by the variation of its density with pressure. It is usually approximated by the expression

$$\frac{\Delta\rho}{\rho} = \frac{\Delta P}{B}\,, \tag{2.4}$$

with B the bulk modulus of the fluid. The bulk modulus is closely related to the "stiffness" of the fluid. The bulk modulus is often referred to as the effective bulk modulus β_e accommodating a mathematically similar component of the deformation flow. With (2.4) and eliminating ρ in the term for the compressibility flow, (2.2) becomes

$$\sum Q_{in} - \sum Q_{out} = \frac{dV}{dt} + \frac{V}{\beta_e}\frac{dP}{dt}\,. \tag{2.5}$$

Applying (2.5) to each motor chamber yields

$$Q_1 - C_i(P_1 - P_2) - C_e P_1 = \frac{dV_1}{dt} + \frac{V_1}{\beta_e}\frac{dP_1}{dt} \tag{2.6}$$

$$C_i(P_1 - P_2) - C_e P_2 - Q_2 = \frac{dV_2}{dt} + \frac{V_2}{\beta_e}\frac{dP_2}{dt}\,, \tag{2.7}$$

where C_i is the internal or cross-port leakage and C_e is the external leakage coefficient. The volume of each motor chamber varies with shaft rotation and can be expressed as

$$V_1 = V_0 + f(\theta) \tag{2.8}$$

$$V_2 = V_0 - f(\theta)\,, \tag{2.9}$$

where V_0 is the average contained volume of each motor chamber including the fluid volume contained in the servo valve, connecting hoses, and manifolds, $f(\theta)$ is the variation of volume in each motor chamber, and θ is the angle of shaft rotation.

The deformation flow is given by the derivatives of (2.8) and (2.9)

$$\frac{dV_1}{dt} = \frac{df(\theta)}{dt} = \frac{V_m}{\theta_m}\frac{d\theta}{dt} = -\frac{dV_2}{dt}\,, \tag{2.10}$$

where V_m is the nominal absorption volume of the motor and θ_m is the nominal angle of rotation of the motor according to the actuator data sheet (see Appendix A). The term $\frac{V_m}{\theta_m}$ is also referred to as the volumetric motor displacement.

Adding (2.8) and (2.9) we obtain the total volume under pressure

$$V_t = V_1 + V_2 = 2V_0\,. \tag{2.11}$$

The load flow Q_l can be expressed as

$$Q_l = \frac{Q_1 + Q_2}{2}\,. \tag{2.12}$$

Equation (2.6) and (2.7) can be summarised by substituting Q_1 in (2.12). Using (2.8)–(2.10), we obtain

$$Q_l = \left(C_i + \frac{C_e}{2}\right)(P_1 - P_2) + \frac{V_m}{\theta_m}\frac{d\theta}{dt} + \frac{V_0}{2\beta_e}\frac{d(P_1 - P_2)}{dt} + \frac{f(\theta)}{2\beta_e}\left(\frac{dP_1}{dt} + \frac{dP_2}{dt}\right). \quad (2.13)$$

The pressure drop across the load P_l is defined as

$$P_l = P_1 - P_2\,. \quad (2.14)$$

Furthermore, the supply pressure P_s is given by

$$P_s = P_1 + P_2\,. \quad (2.15)$$

Therefore, the pressure in each chamber can be expressed by the load and supply pressure as

$$P_1 = \frac{P_s + P_l}{2} \quad (2.16)$$

$$P_2 = \frac{P_s - P_l}{2}\,. \quad (2.17)$$

Using (2.16) and (2.17), it can be seen that the last term in (2.13) is zero, since the supply pressure is constant. Therefore, the flow balance equation (2.13) can be reduced to

$$\frac{V_t}{4\beta_e}\frac{dP_l}{dt} = Q_l - \frac{V_m}{\theta_m}\frac{d\theta}{dt} - C_t P_l\,, \quad (2.18)$$

where C_t is the total leakage coefficient.

The block diagram of a valve controlled actuator is shown in Figure 2.10.

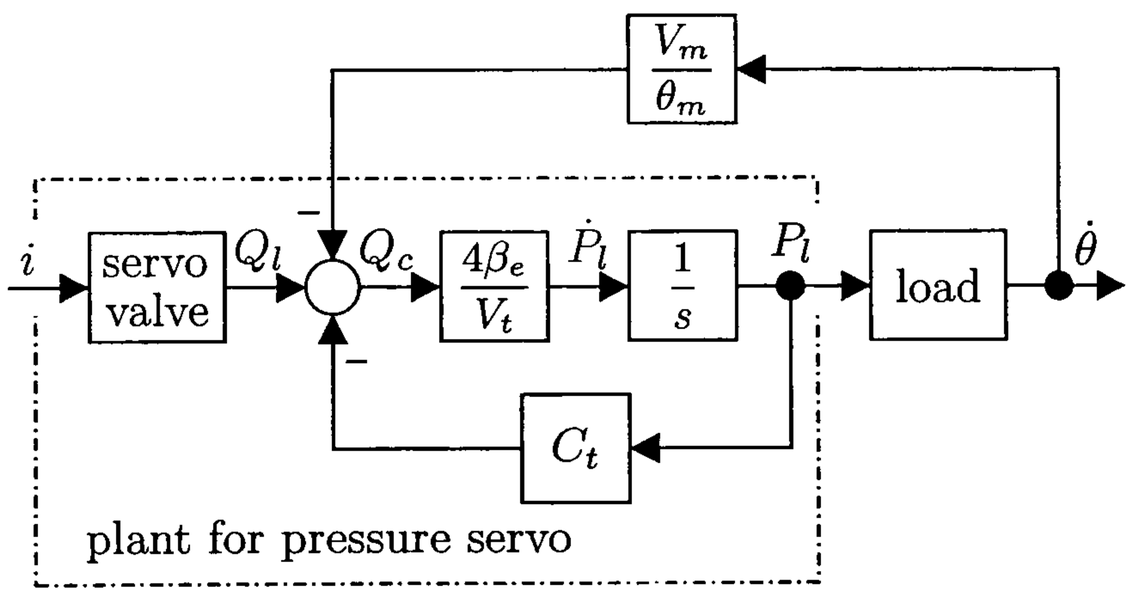

Figure 2.10: Block diagram of a valve controlled actuator. Any movement of the actuator acts as a disturbance. The effective flow is the compliance flow Q_c.

The load flow Q_l controlled by the servo valve can be derived from *Bernoulli's equation.* It is generally a function of the spool displacement and the load pressure

$$Q_l = f(x_v, P_l)\,. \quad (2.19)$$

Using the equation for turbulent hydraulic fluid flow through a sharp edged orifice, the load flow is given by

$$Q_l = C_d w x_v \sqrt{\frac{P_s - \mathrm{sgn}(x_v) P_l}{\rho}}\,, \quad (2.20)$$

where C_d is the discharge coefficient, w is the orifice area ρ is the fluid density, and x_v is the spool displacement of the valve (cf. Figure 2.9) [Merritt, 1967]. The signum function sgn is defined as

$$\text{sgn}(x_v) = \frac{x_v}{|x_v|}\,. \tag{2.21}$$

The dynamic properties of the servo valve are estimated from the step response, as taken from the data sheet. The valve is approximated by the first-order transfer function

$$G_v(s) = \frac{X_v(s)}{I(s)} = \frac{1}{T_v s + 1} = \frac{1}{0.003s + 1}\,, \tag{2.22}$$

where $X_v(s)$ and $I(s)$ are the Laplace transform of the spool displacement and the driving current, respectively.

The discharge coefficient and the orifice area are unknown quantities but they can be avoided by using the calculation equation for a servo valve. Combining the discharge coefficient, the orifice area and the fluid density into one unknown coefficient K, (2.20) can be rewritten as

$$Q_l = K x_v \sqrt{P_s - \text{sgn}(x_v) P_l}\,. \tag{2.23}$$

On the other hand, when selecting a servo valve, (2.20) can be approximated by

$$Q_l = Q_{nl} \frac{i}{i_r} \sqrt{\frac{P_v}{P_s}}\,, \tag{2.24}$$

with Q_{nl} the "no load" flow, i the driving current, i_r the rated current according to the servo valve data sheet (see Appendix A), and P_v the pressure drop across the valve [MOOG, Inc.]. Assuming the return pressure is zero, (2.24) can be written as

$$Q_l = Q_{nl} \frac{i}{i_r} \sqrt{\frac{P_s - P_l}{P_s}}\,. \tag{2.25}$$

The "no load" flow at a particular supply pressure is given by

$$Q_{nl} = Q_r \sqrt{\frac{Ps\ [\text{bar}]}{70\ [\text{bar}]}}\,, \tag{2.26}$$

with Q_r the rated flow according the servo valve data sheet (see Appendix A). Therefore, assuming the pressure in (2.23) is given in bar, the unknown coefficient K can be approximated as

$$K = \frac{Q_r}{\sqrt{70\ [\text{bar}]}\, i_r} k\,, \tag{2.27}$$

where k is a unit conversion factor with the numerical value of 1.

Thus, combining (2.18), (2.23), and (2.27), the flow balance equation (2.18) can be written as

$$\dot{P}_l = \frac{4\beta_e}{60 V_t} \left(-\frac{V_m}{\theta_m} \dot{\theta} - C_t P_l + \frac{Q_r}{\sqrt{70\ [\text{bar}]}\, i_r} k x_v \sqrt{P_s - \text{sgn}(x_v) P_l} \right)\,. \tag{2.28}$$

Equation (2.28) is valid for the pressure given in bar. Note that the flow is usually given in l/min. Therefore the factor 60 is introduced in (2.28) in order to relate the differential equation to a time scale in seconds.

Combining (2.28) with (2.22), the state space model of the pressure servo system (cf. Figure 2.10) can be written as

$$\dot{x} = \boldsymbol{A}\boldsymbol{x} + \boldsymbol{B}u \tag{2.29}$$

$$y = \boldsymbol{C}\boldsymbol{x}\,, \tag{2.30}$$

with

$$\boldsymbol{A} = \begin{pmatrix} -\alpha & \beta\sqrt{\gamma - \mathrm{sgn}(x_2)x_1} \\ 0 & -\delta \end{pmatrix}\,,\ \boldsymbol{B} = \begin{pmatrix} 0 \\ \delta \end{pmatrix}\,,\ \boldsymbol{C} = \begin{pmatrix} 1.2 & 0 \end{pmatrix}\,, \tag{2.31}$$

where

$$\alpha = \frac{4\beta_e}{60V_t}C_t \tag{2.32}$$

$$\beta = \frac{4\beta_e}{60V_t}\frac{Q_r}{\sqrt{70\ [\mathrm{bar}]\, i_r}}k \tag{2.33}$$

$$\gamma = P_s \tag{2.34}$$

$$\delta = \frac{1}{T_v}\,. \tag{2.35}$$

The states in $\boldsymbol{x}$ (2.29) are

$$\boldsymbol{x} = \begin{pmatrix} x_1 \\ x_2 \end{pmatrix}\,,$$

with

x_1 = actuator pressure differential

x_2 = valve spool position.

The output matrix $\boldsymbol{C}$ in (2.30) incorporates the pressure-moment-gain of the actuator (2.31). Note, the feedback from the load $\frac{V_m}{\theta_m}\dot{\theta}$ is considered as an unknown disturbance as $\dot{\theta}$ depends on the load. The effect of this term is discussed later in this chapter.

The bulk modulus depends on the temperature of the fluid as well as the pressure and decreases rapidly when air is entrained in the fluid. A conservative value, allowing some air entrainment is $\beta_e = 10^4\,\mathrm{bar}$ [Clark]. A conservative value for the leakage coefficient, is $C_t = 0.05Q_r/P_s$ [Neal]. The supply pressure is adjusted to $P_s = 90\,\mathrm{bar}$. T_v is the time constant of the servo valve according to (2.22). The value of the unit conversion factor is $k = 1$. With a actuator volume of $V_m = 68\,\mathrm{cm}^3$ according to the actuator data sheet (see Appendix A), hoses between the servo valve of ca. 80 cm length each, diameter $\frac{1}{4}''$, the

total volume under pressure, including a reserve for the servo valve and the manifold, is $V_t = 0.125\,\mathrm{l}$.

Figure 2.11 shows a simulation of an open loop step response of the hydraulic system described by (2.29)–(2.35). The very high moment (or pressure gain) for low input current is a typical characteristic of a servo valve.

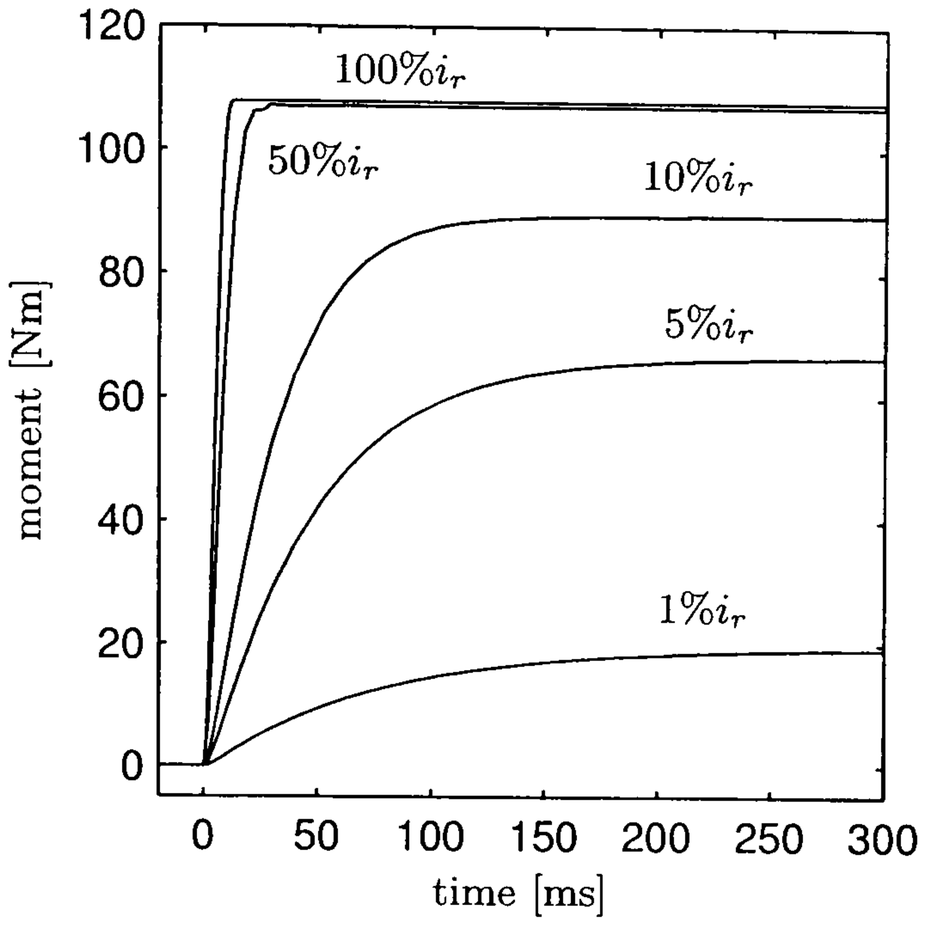

Figure 2.11: Simulation of an open-loop step response of the servo valve-actuator system described by (2.29)–(2.35) for different operating points given in % of the rated input current i_r.

2.3.5 Moment Control of the MRF

The rise-time for an input current of 100% i_r is ca. 6 ms (cf. Figure 2.11). Therefore, the controller sampling time is $T_s = 1\,\mathrm{ms}$. The resulting processor load is only 10% (CPU: Pentium III, 650 MHz). This leaves a considerable margin for extensions of the overall control scheme. The literature recommends the processor load not to exceed 30% in real time applications [Herrtwich and Hommel, 1994]. The controller gain is set to $K_c = 0.1\,\mathrm{mA/Nm}$ (cf. Figure 2.7). This value was tuned by "trial & error". The response is reasonable fast but without extensive oscillations. The moment control loops for both servo valve-actuator combination (sagittal and frontal) are identical. Experimental data of the closed loop performance are shown in Figure 2.12.

Clearly, a simple proportional control action results in a static control error. However, the measured moment at a reference signal of zero is not due to an offset of the pressure transducers. In order to achieve zero moment, control action is needed to block the fluid flow and counteract the pressure of the fluid. It is the static error of this control action that causes the measured moment at zero reference. The behaviour of the servo valve around neutral position of the spool is particularly critical. The static error at a low reference moment is ca. 2 Nm. However, maintaining balance is a *dynamic* process even

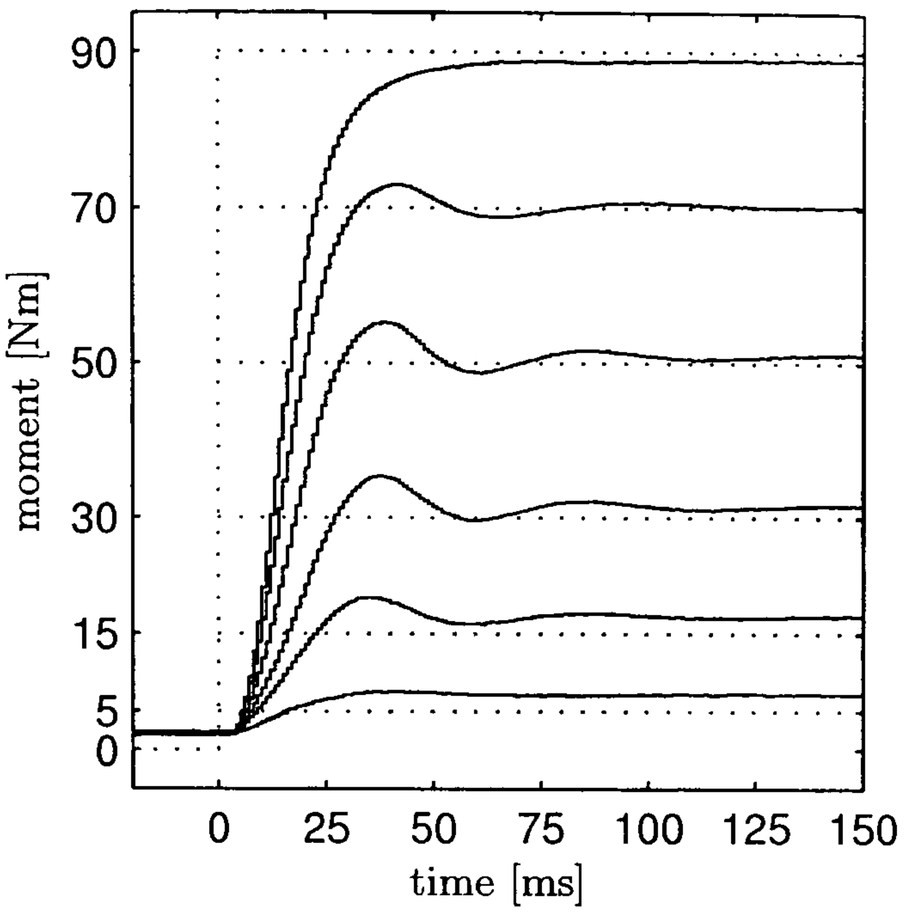

Figure 2.12: Experimental data of the closed-loop step response of the moment control loop of the MRF for various operating points. The dotted lines indicate the reference signal. The step response was measured against blocked load.

in intact subjects, therefore, a control error would be present even if integral action was employed.

The step response in Figure 2.12 was measured against blocked load, i.e. $\dot{\theta} = 0$ (cf. Figure 2.10). However, there are fundamental limitations on moment tracking control by hydraulic systems in presence of a moving load [Alleyne and Liu, 1999, 2000]. From Figure 2.10 a control-structure interaction can be identified. The actuator-load interaction is represented in Figure 2.13. The actuator and the load are represented by their transfer function $G_a(s)$ and $G_l(s)$, respectively. The load velocity occurs in an internal feedback loop. The feedback transfer function $H(s)$ can be identified as $\frac{V_m}{\theta_m}$ (cf. Figure 2.10).

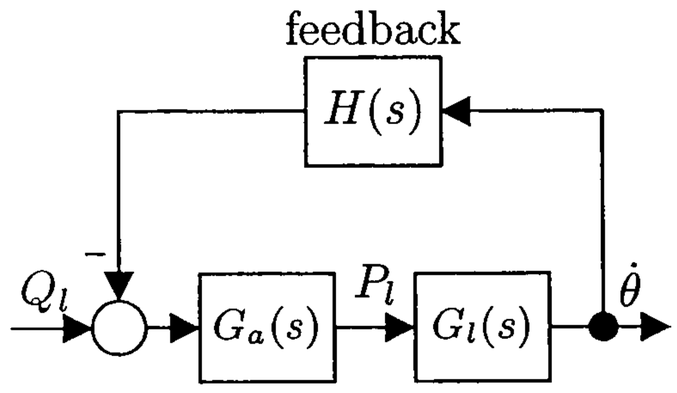

Figure 2.13: Actuator-load interaction. There is an internal feedback due to the load velocity. The feedback transfer function $H(s)$ can be identified as $\frac{V_m}{\theta_m}$ by comparison with Figure 2.10.

Defining the actuator, load, and feedback transfer function in terms of their numerator and denominator polynomials as $N_a(s)$, $N_l(s)$, $N_h(s)$, and $D_a(s)$, $D_l(s)$, $D_h(s)$, respectively, and the transfer function from the flow, to the pressure $G_{Q/P}(s)$ can be written

as

$$G_{Q/P}(s) = \frac{P_l(s)}{Q_l(s)} = \frac{N_a(s)D_l(s)D_h(s)}{D_a(s)D_l(s)D_h(s) + N_a(s)N_l(s)N_h(s)}\,. \tag{2.36}$$

The load appears in the feedback path and equation (2.36) shows that the poles of the load manifest themselves as the zeros of the flow-to-pressure transfer function $G_{Q/P}(s)$. The meaning of zeros as the frequencies blocked by the system illustrates that moment tracking control is inherently limited in its effectiveness. Moreover, these zeros can not be influenced by feedback [Alleyne and Liu, 1999]. To overcome this limitation, nonlinear control methods have been proposed in the literature especially focusing on the force tracking control of hydraulic cylinders [Alleyne and Liu, 2000]. However, experimental practice has shown that a simple control algorithm proved sufficient [Matjačić and Bajd, 1998b], although the experimenter should be aware of its limitations.

2.4 The Generic Control Algorithm

The same generic control approach has been used throughout the experiments reported in this thesis. The open-loop plant is represented by a discrete-time ARX-type model [Ljung, 1999]

$$y(k) = \frac{B(q^{-1})q^{-d_k}}{A(q^{-1})}\,u(k) + \frac{1}{\Delta(q^{-1})A(q^{-1})}\,d(k)\,. \tag{2.37}$$

Here, the signal $u(k)$ is the input sequence in discrete time, $y(k)$ is the output sequence while $d(k)$ is a disturbance term. The plant transfer function on which the control design method is based is given by

$$G_p(q^{-1}) = \frac{B(q^{-1})q^{-d_k}}{A(q^{-1})}\,. \tag{2.38}$$

$A(q^{-1})$ and $B(q^{-1})$ are polynomials in the delay operator q^{-1} as follows:

$$A(q^{-1}) = 1 + a_1 q^{-1} + \ldots + a_{na} q^{-na} \tag{2.39}$$

$$B(q^{-1}) = b_0 + b_1 q^{-1} + \ldots + b_{nb} q^{-nb}\,. \tag{2.40}$$

The delay operator is defined by

$$q^{-1} f(k) = f(k-1)\,. \tag{2.41}$$

The integer $d_k \geq 1$ is the discrete input-output time delay. The net effect of disturbances is represented at the output by the signal $d(k)$ driving the filter

$$\frac{1}{\Delta(q^{-1})A(q^{-1})}\,. \tag{2.42}$$

The polynomial $\Delta(q^{-1})$ will be defined, depending on the context, as either $\Delta(q^{-1}) = 1$ or $\Delta(q^{-1}) = 1 - q^{-1}$. In the latter case the output disturbance models the effect of stepwise-changing (piecewise constant) disturbances and offsets, which typically result from physiological and environmental factors. The choice of $\Delta(q^{-1})$ directly determines whether or not integral action should be included in the controller (see below).

The controller is designed following a polynomial pole assignment approach [Åström and Wittenmark, 1997]. The generic control structure is shown in Figure 2.14.

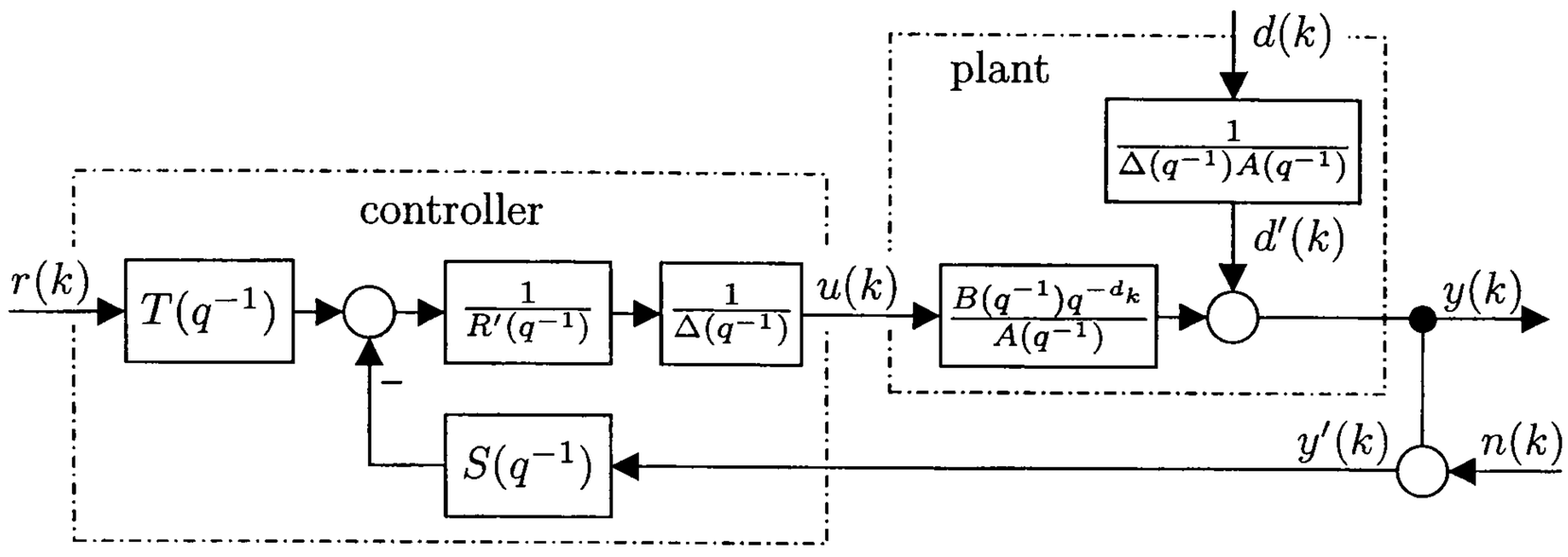

Figure 2.14: Generic control structure.

The feedback sequence $y^{'}(k)$ includes a measurement noise $n(k)$

$$y'(k) = y(k) + n(k)\,. \tag{2.43}$$

The control sequence $u(k)$ is determined by

$$u(k) = \frac{1}{R(q^{-1})}\left(T(q^{-1})r(k) - S(q^{-1})\,y'(k)\right) \tag{2.44}$$

with $R(q^{-1}) = \Delta(q^{-1})R'(q^{-1})$. The polynomials $R'(q^{-1})$, $S(q^{-1})$ and $T(q^{-1})$ are to be determined during the design procedure. The controller polynomial $\Delta(q^{-1})$ is pre-defined as either $\Delta(q^{-1}) = 1$ or $\Delta(q^{-1}) = 1-q^{-1}$ depending on whether integral action is required.

Combining (2.37) and (2.44) yields the closed-loop equation

$$y(k) = \frac{B(q^{-1})T(q^{-1})q^{-d_k}}{\Phi_{cl}(q^{-1})}\,r(k) + \frac{R'(q^{-1})}{\Phi_{cl}(q^{-1})}\,d(k) - \frac{B(q^{-1})S(q^{-1})q^{-d_k}}{\Phi_{cl}(q^{-1})}\,n(k)\,, \tag{2.45}$$

where

$$\Phi_{cl}(q^{-1}) = A(q^{-1})R(q^{-1}) + B(q^{-1})S(q^{-1})q^{-d_k} \tag{2.46}$$

is the closed-loop characteristic polynomial.

For the purposes of analysis the sensitivity function $\tilde{S}(q^{-1})$, defined as the transfer function from the output disturbance $d^{'}(k) = d(k)/\big(\Delta(q^{-1})A(q^{-1})\big)$ to the output $y(k)$, and the complementary sensitivity function $\tilde{T}(q^{-1})$, defined as the transfer function from the measurement noise $n(k)$ to the output $y(k)$, are introduced as

$$\tilde{S}(q^{-1}) = \frac{A(q^{-1})R(q^{-1})}{\Phi_{cl}(q^{-1})}\,, \quad \tilde{T}(q^{-1}) = \frac{B(q^{-1})S(q^{-1})q^{-d_k}}{\Phi_{cl}(q^{-1})}\,. \tag{2.47}$$

In analogy to the state space approach to pole assignment the desired closed-loop polynomial $\Phi_{cl}(q^{-1})$ is composed of two parts, the polynomials $\Phi_c(q^{-1})$ and $\Phi_o(q^{-1})$. $\Phi_c(q^{-1})$ specifies the the tracking response from $r(k)$ to $y(k)$ while $\Phi_o(q^{-1})$ is known as the observer polynomial and has further influence on the behaviour of the feedback system [Åström and Wittenmark, 1997]. Thus, in the standard formulation of pole assignment the Diophantine equation

$$A(q^{-1})R(q^{-1}) + B(q^{-1})S(q^{-1})q^{-d_k} = \Phi_c(q^{-1})\Phi_o(q^{-1}) \tag{2.48}$$

is solved for $R(q^{-1})$ and $S(q^{-1})$.

A further possibility, however, is to allow for cancellation of fast or oscillatory plant poles. This is known as a notch filter design since these modes will not then be excited. The plant denominator is factored as $A(q^{-1}) = A^+(q^{-1})A^-(q^{-1})$, where $A^+(q^{-1})$ includes the poles to be cancelled by the controller. In order to cancel poles of the plant, these poles must be part of the controller polynomial $S(q^{-1}) = A^+(q^{-1})S'(q^{-1})$. Therefore, the Diophantine equation (2.48) becomes

$$A^+(q^{-1})A^-(q^{-1})R(q^{-1}) + B(q^{-1})A^+(q^{-1})S'(q^{-1})q^{-d_k} = \Phi_c(q^{-1})\Phi_o(q^{-1})\,. \tag{2.49}$$

For solvability the polynomial $A^+(q^{-1})$ must also be a factor of the right hand side of (2.49). Thus, any plant poles which are cancelled will become poles of the closed-loop system. Writing $\Phi_{cl}(q^{-1}) = A^+(q^{-1})\Phi'_c(q^{-1})\Phi_o(q^{-1})$ the Diophantine equation becomes

$$A^-(q^{-1})R(q^{-1}) + B(q^{-1})S'(q^{-1})q^{-d_k} = \Phi'_c(q^{-1})\Phi_o(q^{-1})\,. \tag{2.50}$$

The structure of $R(q^{-1})$ is determined by the choice of the polynomial $\Delta(q^{-1})$ in the noise model. When $\Delta(q^{-1}) = 1 - q^{-1}$, i.e. stepwise changing constant disturbances are present, then integral action must be included in the controller to achieve zero steady-state tracking error. Substituting $R(q^{-1}) = \Delta(q^{-1})R'(q^{-1})$ in (2.50) the final design equation becomes

$$A^-(q^{-1})\Delta(q^{-1})R'(q^{-1}) + B(q^{-1})S'(q^{-1})q^{-d_k} = \Phi'_c(q^{-1})\Phi_o(q^{-1})\,. \tag{2.51}$$

The design equation is solved for $R'(q^{-1})$ and $S'(q^{-1})$ subject to the condition

$$\frac{S'(q^{-1})}{A^-(q^{-1})\Delta(q^{-1})} \quad \text{strictly proper} \tag{2.52}$$

i.e. $\deg\big(S'(q^{-1})\big) < \deg\big(A^-(q^{-1})\big) + \deg\big(\Delta(q^{-1})\big)$. If the plant described by (2.37) is completely controllable and observable, i.e. the polynomials $A(q^{-1})$ and $B(q^{-1})$ have no common factor, (2.52) will have a unique solution satisfying condition (2.52) [Kučera, 1979]. Condition (2.52) guarantees a solution with minimum degree of $S'(q^{-1})$.

Finally, the polynomial $T(q^{-1})$ has to be designed to achieve suitable reference tracking. From (2.45) the transfer function $G_{y/r}(q^{-1})$ from $r(k)$ to $y(k)$ is given by

$$G_{y/r}(q^{-1}) = \frac{B(q^{-1})T(q^{-1})q^{-d_k}}{\Phi_{cl}(q^{-1})} = \frac{B(q^{-1})T(q^{-1})q^{-d_k}}{A^+(q^{-1})\Phi'_c(q^{-1})\Phi_o(q^{-1})}. \tag{2.53}$$

In order to avoid excitation by the reference signal of system modes contained in the observer polynomial $\Phi_o(q^{-1})$, or the possibly fast or oscillatory modes in $A^+(q^{-1})$, these two factors are cancelled by appropriate definition of $T(q^{-1})$. $T(q^{-1})$ must also ensure unity steady-state gain in $G_{y/r}(q^{-1})$ and is therefore defined as

$$T(q^{-1}) = \lambda_c A^+(q^{-1})\Phi_o(q^{-1})\,, \tag{2.54}$$

where the scalar λ_c is

$$\lambda_c = \frac{\Phi'_c(1)}{B(1)}\,. \tag{2.55}$$

Assuming $B(1) \neq 0$, this results in

$$G_{y/r}(q^{-1}) = \frac{B(q^{-1})\Phi'_c(1)q^{-d_k}}{\Phi'_c(q^{-1})B(1)}\,. \tag{2.56}$$

The polynomials $\Phi'_c(q^{-1})$ and $\Phi_o(q^{-1})$ are specified by choosing rise-time t_r and damping factor ζ of the corresponding polynomials in continuous time

$$s^2 + 2\zeta\omega_n s + \omega_n^2\,, \tag{2.57}$$

with

$$\omega_n t_r = f(\zeta)\,. \tag{2.58}$$

We are left with a set of tuning knobs ($t_{r,c}$, ζ_c and $t_{r,o}$, ζ_o) with a well defined influence, where $t_{r,c}$ is the rise-time and ζ_c is the damping factor of the corresponding tracking response polynomial in continuous time and $t_{r,o}$ is the rise-time and ζ_o is the damping factor of the corresponding observer polynomial in continuous time (cf. Table 2.2).

	tracking speed	disturbance rejection	noise sensitivity
$t_{r,c}$ $\zeta_c \uparrow$	slower	worse	better
$t_{r,c}$ $\zeta_c \downarrow$	faster	better	worse
$t_{r,o}$ $\zeta_o \uparrow$	no change	worse	better
$t_{r,o}$ $\zeta_o \downarrow$	no change	better	worse

Table 2.1: Influence of tuning parameters on the closed-loop performance.

The controller given in Figure 2.14 can be extended as shown in Figure 2.15.
The design polynomials $\Phi'_c(q^{-1})$ and $\Phi_o(q^{-1})$ are of the form

$$\Phi'_c(q^{-1}) = 1+\varphi_{c,1}q^{-1} + \ldots + \varphi_{c,n\varphi_c}q^{-n\varphi_c} \tag{2.59}$$

$$\Phi_o(q^{-1}) = 1+\varphi_{o,1}q^{-1} + \ldots + \varphi_{o,n\varphi_o}q^{-n\varphi_o} \tag{2.60}$$

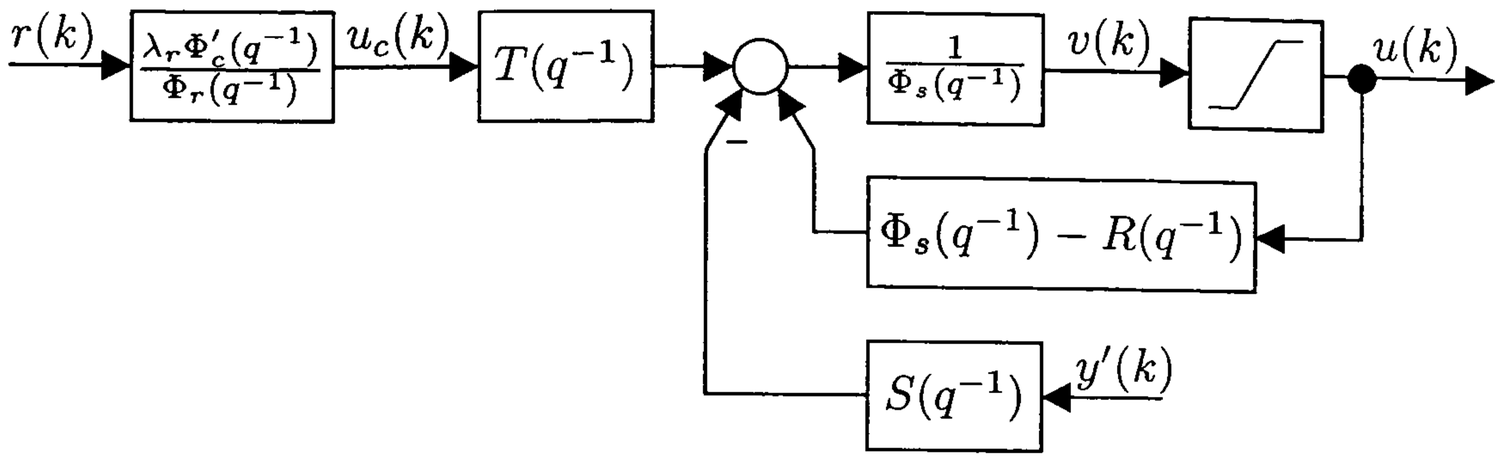

Figure 2.15: Controller structure including anti-windup and tracking pre-filter. When the control output is not in saturation the controller in Figure 2.15 has the same structure as in Figure 2.14, apart from the pre-filter.

The controller polynomials in Figure 2.15 are of the following form:

$$R(q^{-1}) = 1 + r_1 q^{-1} + \ldots + r_{nr} q^{-nr} \tag{2.61}$$

$$S(q^{-1}) = s_0 + s_1 q^{-1} + \ldots + s_{ns} q^{-ns} \tag{2.62}$$

$$T(q^{-1}) = t_0 + t_1 q^{-1} + \ldots + t_{nt} q^{-nt} \tag{2.63}$$

$$\Phi_r(q^{-1}) = 1 + \varphi_{r,1} q^{-1} + \ldots + \varphi_{r,n\varphi_r} q^{-n\varphi_r} \tag{2.64}$$

$$\Phi_s(q^{-1}) = 1 + \varphi_{s,1} q^{-1} + \ldots + \varphi_{s,n\varphi_s} q^{-n\varphi_s} . \tag{2.65}$$

The zero order polynomial coefficient of the polynomials $R(q^{-1})$, $\Phi_r(q^{-1})$, and $\Phi_s(q^{-1})$ is equal to 1. These polynomials can always be normalised in this way.

Continuing integration of the control error (if integral action included) while the controller output saturates due to the limited output range of any real actuator could cause instability. Therefore anti-windup is included (cf. Figure 2.15) [Åström and Wittenmark, 1997]. The polynomial $\Phi_s(q^{-1})$ can be considered as a saturation observer. The reference sequence $r(k)$ is pre-filtered in order to decouple the properties for reference tracking from the properties for disturbance rejection and the influence of measurement noise. The polynomial $\Phi_c'(q^{-1})$ is otherwise still part of the transfer function $G_{y/r}(q^{-1})$ (2.56) as well as of $\tilde{S}(q^{-1})$ and $\tilde{T}(q^{-1})$ (2.47).

The numerator of the pre-filter cancels the remaining part of the characteristic closed-loop polynomial, i.e. $\Phi_c'(q^{-1})$ while the denominator $\Phi_r(q^{-1})$ specifies the desired reference tracking behavior. The constant λ_r ensures a steady-state gain of 1 for reference tracking

$$\lambda_r = \frac{\Phi_r(1)}{\Phi_c'(1)} . \tag{2.66}$$

Taking the pre-filter into account, the transfer function for reference tracking (2.56) becomes

$$G_{y/r}(q^{-1}) = \frac{B(q^{-1})\Phi_r(1)q^{-d_k}}{\Phi_r(q^{-1})B(1)} . \tag{2.67}$$

The polynomials $\Phi_r(q^{-1})$ is specified by choosing rise-time $t_{r,r}$ and damping factor ζ_r of the corresponding polynomial in continuous time.

Taking the pre-filter into account table 2.2 showing the influence of the design parameters can be extended as follows:

	tracking speed	disturbance rejection	noise sensitivity
$t_{r,c}$ $\zeta_c \uparrow$	no change	worse	better
$t_{r,c}$ $\zeta_c \downarrow$	no change	better	worse
$t_{r,o}$ $\zeta_o \uparrow$	no change	worse	better
$t_{r,o}$ $\zeta_o \downarrow$	no change	better	worse
$t_{r,r}$ $\zeta_r \uparrow$	faster	no change	no change
$t_{r,r}$ $\zeta_r \downarrow$	slower	no change	no change

Table 2.2: Taking the pre-filter into account: influence of tuning parameters on the closed-loop performance.

The control design procedure can be summarised as follows:

- Given data: $A(q^{-1})$, $B(q^{-1})$, d_k
- Choose design parameter $\Delta(q^{-1})$; $t_{r,c}$, ζ_c; $t_{r,o}$, ζ_o; $t_{r,s}$, ζ_s; and $t_{r,r}$, ζ_r,
- Step 1: Compute $\Phi'_c(q^{-1})$ from $t_{r,c}$ and ζ_c; and $\Phi_o(q^{-1})$ from $t_{r,o}$ and ζ_o.
- Step 2: Solve the Diophantine equation

$$A^-(q^{-1})\Delta(q^{-1})R'(q^{-1}) + B(q^{-1})S'(q^{-1})q^{-d_k} = \Phi'_c(q^{-1})\Phi_o(q^{-1})$$

  for $R'(q^{-1})$ and $S'(q^{-1})$ subject to the condition

$$\deg\big(S'(q^{-1})\big) < \deg\big(A^-(q^{-1})\big) + \deg\big(\Delta(q^{-1})\big)$$

- Step 3: Form the polynomial $R(q^{-1})$ and $S(q^{-1})$ as

$$R(q^{-1}) = \Delta(q^{-1})R'(q^{-1})$$
$$S(q^{-1}) = A^+(q^{-1})S'(q^{-1})$$

- Step 4: Form the polynomial $T(q^{-1})$ as

$$T(q^{-1}) = \lambda_c A^+(q^{-1})\Phi_o(q^{-1})$$

  with

$$\lambda_c = \frac{\Phi'_c(1)}{B(1)}$$

- Step 5: Compute the saturation observer polynomial $\Phi_s(q^{-1})$ from $t_{r,s}$, ζ_s
- Step 6: Compute $\Phi_s(q^{-1}) - R(q^{-1})$
- Step 7: Compute the pre-filter denominator $\Phi_r(q^{-1})$ from $t_{r,r}$ and ζ_r

- Step 8: Form the pre-filter numerator polynomial as

$$\lambda_r \Phi_c'(q^{-1})$$

with

$$\lambda_r = \frac{\Phi_r(1)}{\Phi_c'(1)}$$

2.5 Scheduling Strategy

The previously outlined generic design procedure is employed for control design for individual muscle groups as well as for designing standing controllers as presented later in this thesis.

Let us assume we have designed different controllers for agonist and antagonist muscle groups using the above outlined design procedure. Neglecting the pre-filter for the moment, the control law for an individual muscle group, as shown in Figure 2.15, can be formulated as

$$\Phi_s(q^{-1})v(k) = T(q^{-1})u_c(k) - S(q^{-1})y'(k) + \big(\Phi_s(q^{-1}) - R(q^{-1})\big)u(k) \tag{2.68}$$

$$u(k) = \mathrm{sat}\big(v(k)\big) \tag{2.69}$$

Equations (2.68)–(2.69) can be rewritten in vector form as

$$u(k) = \mathrm{sat}\big(\boldsymbol{\Theta}^{\mathrm{T}}\boldsymbol{\Psi}\big)\,. \tag{2.70}$$

The parameter vector $\boldsymbol{\Theta}$ contains the coefficients of the controller polynomials:

$$\boldsymbol{\Theta} = \Big((\varphi_{s,1} - r_1) \;\ldots\; (\varphi_{s,\max(n\varphi_s,nr)} - r_{\max(n\varphi_s,nr)}) \,,\; s_0 \; s_1 \;\ldots \;\ldots\; s_{ns} \,,\; t_0 \; t_1 \;\ldots\; t_{nt} \,,\; \varphi_{s,1} \;\ldots\; \varphi_{s,n\varphi_s} \Big)^{\mathrm{T}}\,. \tag{2.71}$$

Thus, the state vector is defined as

$$\boldsymbol{\Psi} = \Big(u(k-1) \;\ldots\; u(k-\max(n\varphi_s,nr)) \,,\; -y(k) \;-y(k-1) \;\ldots \;\ldots\; -y(k-ns) \,,\; u_c(k) \; u_c(k-1) \;\ldots \;\ldots\; u_c(k-nt) \,,\; v(k-1) \;\ldots\; v(k-n\varphi_s) \Big)^{\mathrm{T}}\,. \tag{2.72}$$

If a pre-filter is employed, the value $u_c(k)$ is determined by

$$u_c(k) = \boldsymbol{\Xi}^{\mathrm{T}}\boldsymbol{\Gamma}\,. \tag{2.73}$$

The parameter vector $\boldsymbol{\Xi}$ is of the form

$$\boldsymbol{\Xi} = \Big(\varphi_{r,1} \;\ldots\; \varphi_{r,n\varphi_r} \,,\; \lambda_r \; \lambda_r\varphi_{c,1} \;\ldots\; \lambda_r\varphi_{r,n\varphi_r} \Big)^{\mathrm{T}}\,, \tag{2.74}$$

and the state vector is defined as

$$\mathbf{\Gamma} = \Big(u_c(k-1) \ \ldots \ u_c(k-n\varphi_r)\,,\ r(k)\ r(k-1) \ \ldots \ r(k-n\varphi_c) \Big)^{\mathrm{T}}. \tag{2.75}$$

The scheduling strategy is shown in Figure. 2.16 and can be described as follows:

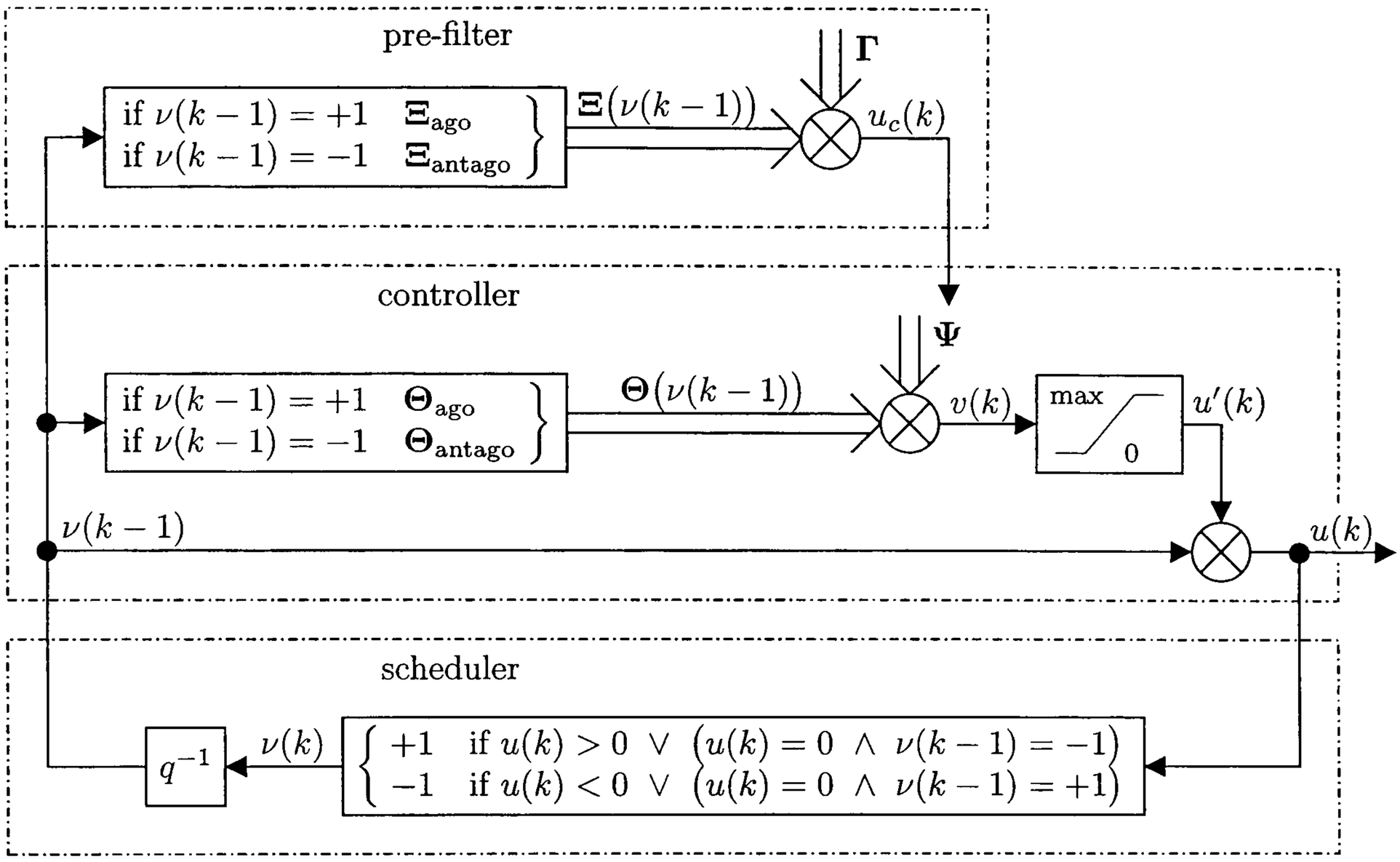

Figure 2.16: Complete structure of the controller with common states and the scheduling strategy for control of agonist/antagonist muscles.

Designing a controller individually for the agonist and antagonist muscles results in different parameter vectors $\mathbf{\Theta}_{\text{ago}}$ and $\mathbf{\Theta}_{\text{antago}}$ and, if a pre-filter is considered $\mathbf{\Xi}_{\text{ago}}$ and $\mathbf{\Xi}_{\text{antago}}$, respectively. Thus, there is a suitable switching strategy required between the two parameter vectors. In order to avoid excessive oscillations when switching, agonist and antagonist controllers have a common state vector $\mathbf{\Psi}$ or $\mathbf{\Gamma}$, respectively. The common state vector also results in a single control signal $u(k)$ which provides a unique criterion for switching between the different muscle groups. Depending on the sign of the control signal $u(k)$, either the agonist or antagonist muscle group will be stimulated (cf. Figure 2.17).

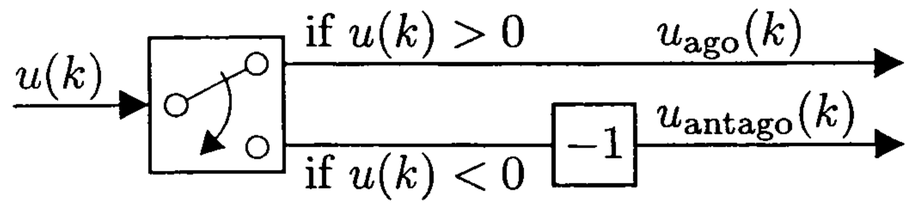

Figure 2.17: Switching strategy between agonist/antagonist muscles.

On the other hand, the common control signal $u(k)$ is used as the scheduling variable in an internal feedback loop. In the partial system labelled as "scheduler" in Figure 2.16 a decision is made whether to switch between the controllers or not. The block labelled "q^{-1}" is a unit step time delay introduced in order to keep the control law causal. Depending on

the value of the delayed indicator signal $\nu(k-1)$, which is either $+1$ or -1, it is decided whether the parameter vectors $\boldsymbol{\Xi}_{\text{ago}}$ (pre-filter) and $\boldsymbol{\Theta}_{\text{ago}}$ (controller) will be selected to calculate the preliminary control signal $v(k)$.

This preliminary non-saturated control signal $v(k)$ is limited between the maximum output and zero. Due to physiological circumstances, only non-negative values of the control signal are reasonable. A negative value of the control signal would indicate that the controllers need to be switched.

In order to respond to this situation as quickly as possible it is necessary that the saturation observer $\Phi_s(q^{-1})$ (2.65) is as fast as possible. Therefore, we set $\Phi_s(q^{-1}) = 1$. In this case $\Phi_s(q^{-1})$ can be interpreted as a dead-beat observer. If $\Phi_s(q^{-1}) = 1$ the parameter vector $\boldsymbol{\Theta}$ in (2.70) can be simplified to

$$\boldsymbol{\Theta} = \Big(r_1 \ \ldots \ r_{nr} \,,\ s_0 \ s_1 \ \ldots \ s_{ns} \,,\ t_0 \ t_1 \ \ldots \ t_{nt} \Big)^{\mathrm{T}} . \tag{2.76}$$

Thus, the state vector is defined as

$$\begin{aligned} \boldsymbol{\Psi} = \Big(& u(k-1) \ \ldots \ u(k-nr) \,,\ -y(k) \ -y(k-1) \ \ldots \\ & \ldots \ -y(k-ns) \,,\ u_c(k) \ u_c(k-1) \ \ldots \ u_c(k-nt) \Big)^{\mathrm{T}} . \end{aligned} \tag{2.77}$$

Finally, in order to achieve a control output with alternating sign as assumed above the saturated output $u'(k)$ is multiplied by the indicator signal $\nu(k-1)$. This results in a control signal $u(k)$ which is positive when the agonist muscles should be stimulated and negative when the antagonist muscles should be stimulated. However, since only non-negative values are reasonable for physiological reasons, the control signal for the antagonist muscle has to be multiplied by -1 after switching (cf. Figure 2.17).

The proposed scheduling strategy is similar to gain scheduling approaches [Rugh and Shamma, 2000]. However, stability issues are more related to switching systems. It is generally difficult to prove global stability for switching systems. Switching systems can become unstable due to switching even when all subsystems are stable. On the other hand, it is possible to globally stabilise a system consisting of unstable subsystems by a suitable switching law [Liberzon and Morse, 1999]. With the proposed scheduling strategy, possible unstable subsystems (cross combinations of controller and plant) are practically excluded by the saturation function. Instability due to switching between asymptotically stable subsystems is limited, however, in that the states of these systems cannot escape to infinity in finite time [Liberzon and Morse, 1999]. Simulations have given confidence that the overall control systems remains globally stable in practical situations.

2.6 Software

All experimental procedures reported in this thesis are based on MATLAB/SIMULINK®. For all experiments, data acquisition and real-time control of muscle stimulation are done using the Real-time toolbox by Humusoft®. The Polynomial toolbox by Polyx® was employed for the controller design. Real-time control of the MRF is done using the xPC-Target for MATLAB/SIMULINK.

Chapter 3

Control of Unsupported Standing

3.1 Summary

Aim: The work presented in this chapter aimed to investigate the feasibility of standing in paraplegia without any arm support. The work sought to validate and improve the results of Hunt *et al.* [1997] and Munih *et al.* [1997].

Methods: The work was carried out using the Wobbler apparatus described in section 2.2. A cascaded control structure was employed to decouple the nonlinear properties of the artificially stimulated muscle from the task of stabilising the body. The muscle moment is controlled in an inner loop while the body angle of inclination in controlled in the outer loop. A pole assignment approach was utilised for both control loops. A number of design options were investigated in experiments with an intact subject. Once these were found experiments with a paraplegic subject were carried out.

Results: Results with the intact subject showed that neglecting the inner loop dynamics in the design of the outer loop can result in instability of the overall system when the inner loop becomes slow due to muscle fatigue. Results with the paraplegic subject showed that unsupported standing is possible for several minutes.

Conclusion: We conclude that the most suitable design options are (i) no integral action in the inner loop, (ii) inclusion of the inner loop dynamics in the design of the outer loop, (iii) employing a notch filter approach for the outer loop. Muscle fatigue and general weakness remain the main limiting factors for unsupported standing in paraplegia.

Contribution: The author's contribution to this study consists of the development and implementation of the experimental software. Furthermore, the author was involved in the execution of the experiments and in the analysis and interpretation of the results. This work is published in Hunt *et al.* [2000a] and Gollee *et al.* [2001].

3.2 Motivation

This study was mainly motivated by the early work of Donaldson [Donaldson, 1993; Donaldson *et al.*, 1996].

Early approaches towards the restoration of standing were based on open-loop stimulation [Kralj and Bajd, 1989]. Since the erect human body is inherently unstable the subject has to use his/her arms for stabilisation while open-loop stimulation is being used for standing. Supporting the upper body with the arms to provide stability generates a closed kinematic chain and the stabilising moment is provided by the arms. However, this limits the functional potential of this approach. In order to free the subject's arms to perform functional tasks while standing, a stabilising moment has to be applied at the ankle joint. Jaeger was the first to investigate feedback control for paraplegic standing in simulations [Jaeger, 1986]. He modelled the body as a single-link inverted pendulum with an ideal ankle joint (i.e. without a static stiffness and viscosity in the ankle joint) which is preceded by a model of the muscle dynamics. He attempted to stabilise this configuration with a standard PID-controller. However, despite a number of further simplifications (controller in continuous time, ideal differential part), he was forced to conjure up a stabilising zero to succeed. This zero could be interpreted as the transfer function of the sensor. However, what this effectively means is that the body cannot be stabilised by a PID-controller if only angle feedback is available.

Donaldson suggested a cascaded control structure, consisting of an inner feedback loop controlling the muscle moment and an outer loop controlling the angle of the body which was represented again by a single-link inverted pendulum [Donaldson, 1993]. Since the muscle dynamics are of significantly higher bandwidth than the body dynamics, this was done in order to decouple the non-linear muscle properties from the issue of controlling the body angle of inclination. He suggested PD-control to stabilise this configuration showing simulations in continuous time using an ideal PD-controller. However, analysing a more realistic approach to PD-control shows that this strategy is not likely to succeed. Donaldson used the following model to describe the body as a single-link inverted pendulum:

$$G_b(s) = \frac{0.0133}{s^2 - 9.181}\,. \tag{3.1}$$

Figure 3.1 shows that the inverted pendulum model is unstable as it possesses one pole in the right-hand half of the complex s-plane.

Control systems are usually realised in discrete time with the control algorithm implemented on a computer platform. Therefore, the stability shall be analysed in discrete time. A discrete time representation of (3.1) is given by

$$G_b(z) = \frac{8.38 \cdot 10^{-6}(z^2 + 2z + 1)}{z^2 - 2.023z + 1}\,, \tag{3.2}$$

assuming a sampling time of 50 ms. The pole-zero configuration of (3.2) is shown in Figure 3.2.

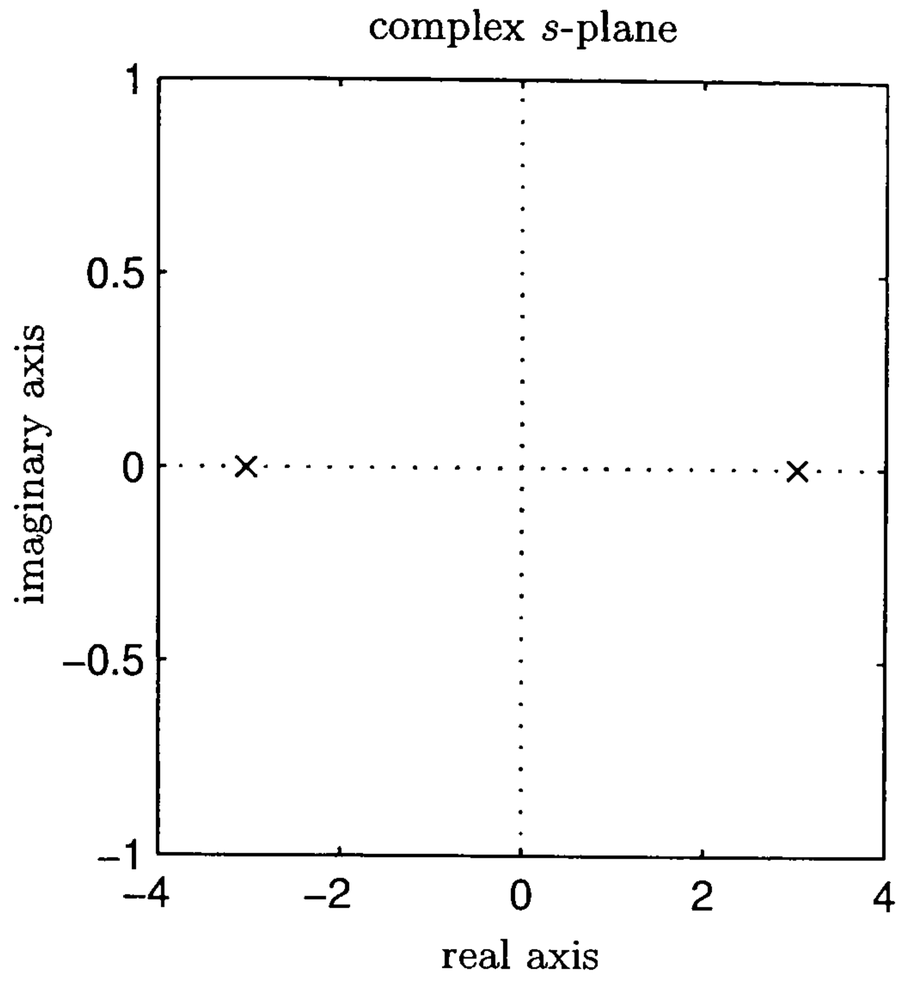

Figure 3.1: Pole configuration of the inverted pendulum model of the body following (3.1).

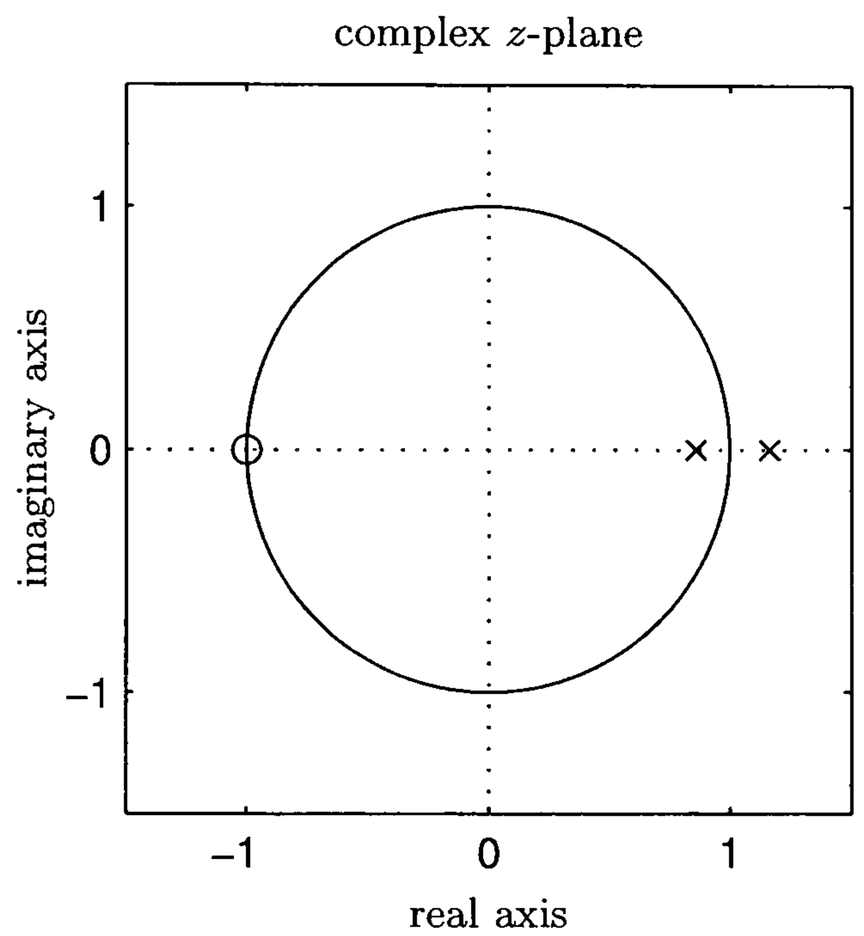

Figure 3.2: Pole-zero configuration of the inverted pendulum model (3.2). Note, there is a double zero at $z^z_{b_{1,2}} = -1$ (cf. (3.2)).

Furthermore, we assume that the muscle dynamics are described by the following transfer function in discrete time:

$$G_m(z) = \frac{0.3025z}{z^2 - 0.9z + 0.2025}\,, \tag{3.3}$$

With regard to the cascaded control structure proposed by Donaldson, equation (3.3) can be interpreted as a description of the closed-loop tracking response for the muscle moment corresponding to a rise time of $t_{r,m} = 0.2\,\mathrm{s}$ with critical damping. The pole-zero configuration of the overall system to be stabilised, $G_p(z) = G_m(z)G_b(z)$, is shown in Figure 3.3.

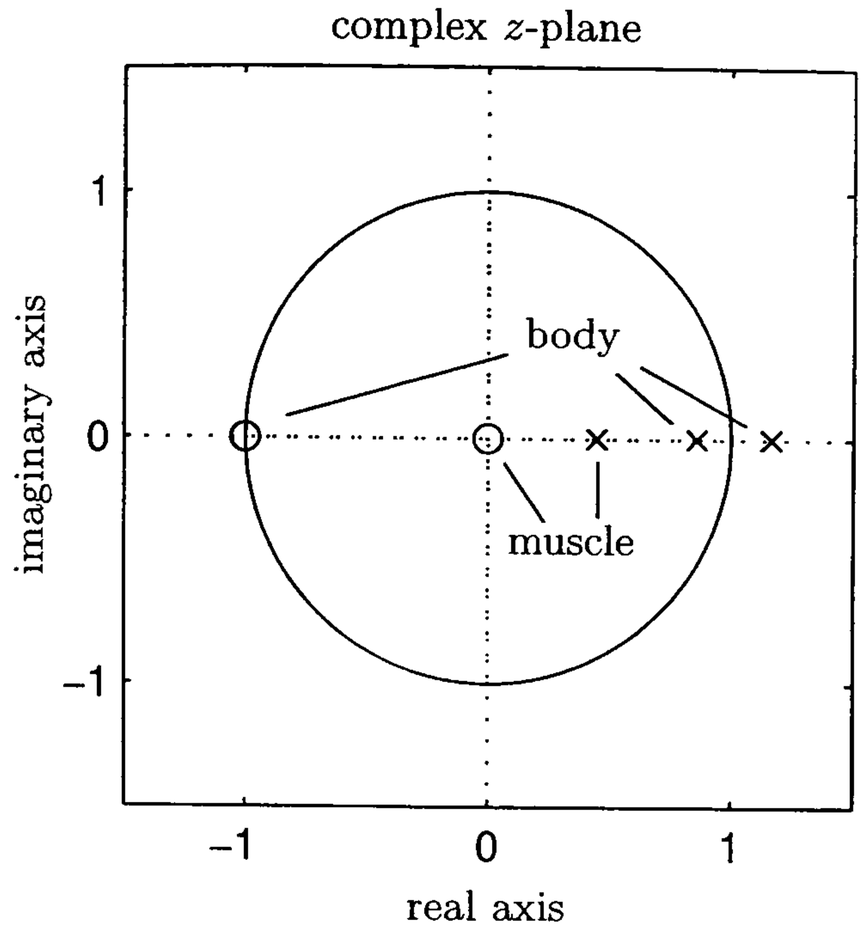

Figure 3.3: Pole-zero configuration of the overall system to be stabilised, $G_p(z) = G_m(z)G_b(z)$. The muscle dynamics are represented by a double pole at $z^p_{m_{1,2}} = 0.45$ and a zero at $z^z_m = 0$ which represents the computational time delay.

A realisable representation of a PD-controller in discrete time is

$$C_{PD}(z) = K\frac{z-b}{z}. \tag{3.4}$$

With $b = 0.85$ and K as a tunable parameter we obtain the root locus of Figure 3.4 for the feedback system $G_{cl}(z)$

$$G_{cl}(z) = \frac{C_{PD}(z)G_m(z)G_b(z)}{1 + C_{PD}(z)G_m(z)G_b(z)}. \tag{3.5}$$

Figure 3.4 shows that, theoretically, the system can be stabilised with a PD-controller. Figure 3.5 shows the normalised step response of the corresponding closed-loop system for a controller gain of $K = 5200$, which correspond to a closed-loop system with critical damping.

However, let us consider the Bode plot of the open-loop system for further analysis. The bode plot is shown for $K = 5200$ in Figure 3.6.

The phase margin indicated by the vertical line is very small (9°). The phase margin describes the robustness of the closed-loop system against an additional time delay. The overall closed-loop system becomes unstable if, for example, the rise time of the moment loop increases to 0.4 s. This can happen when high stimulation levels are required by the controller. Then more and more slower motor units will be recruited, which will result in a slower closed-loop response of the muscle loop. Fatigue and saturation of the control signal will further deteriorate the situation. Therefore, in practice, a PD-strategy is likely to fail.

A full dynamic control approach was developed and experimentally evaluated by Hunt *et al.* [1997] and Munih *et al.* [1997]. The study was intended as a feasibility study in order

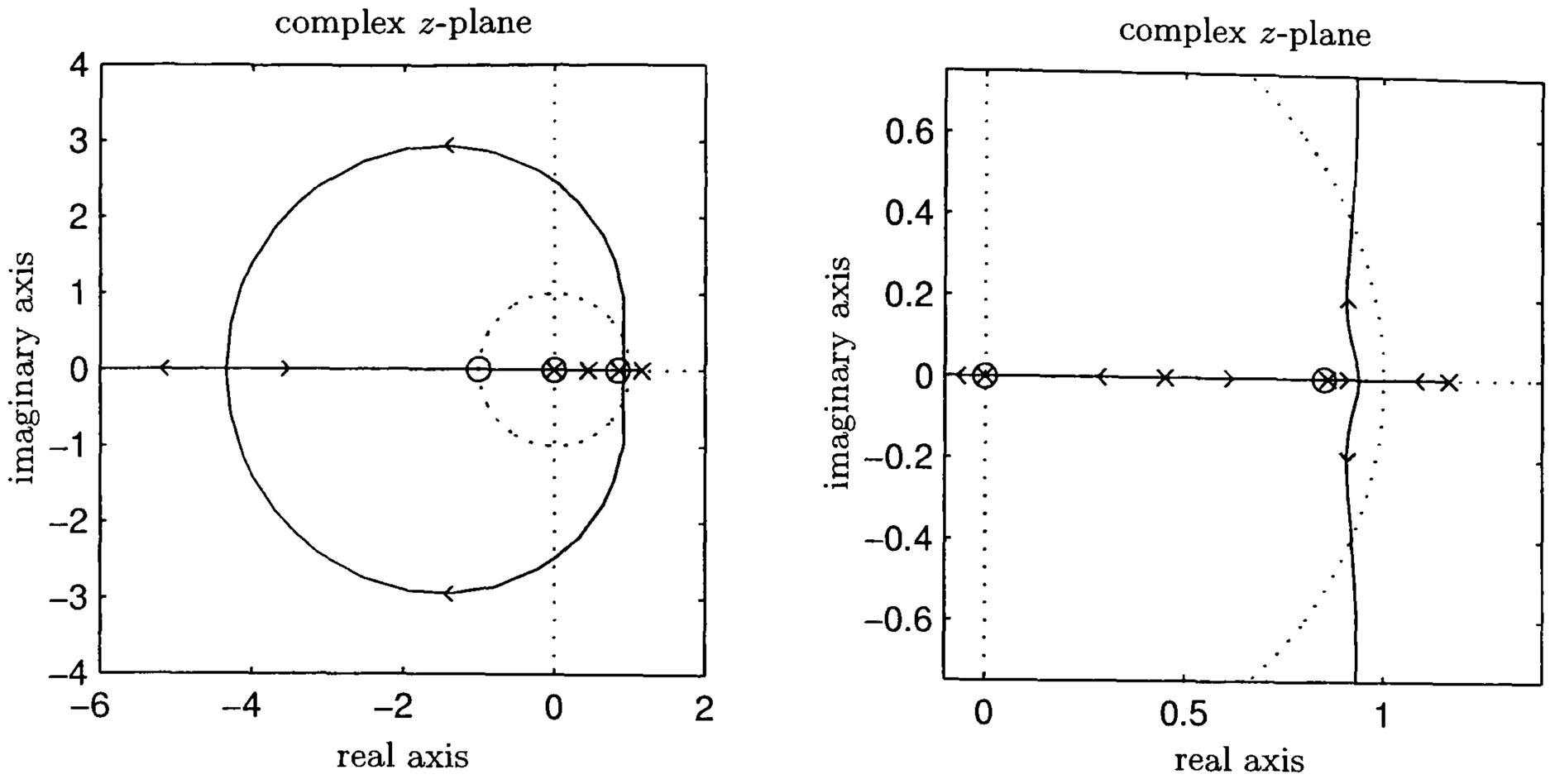

(a) Total root locus.

(b) Root locus. Detailed view of **(a)**.

Figure 3.4: Root locus of (3.5) depending on the controller gain K. The arrows indicate the evolution of the poles of (3.5) with increasing K.

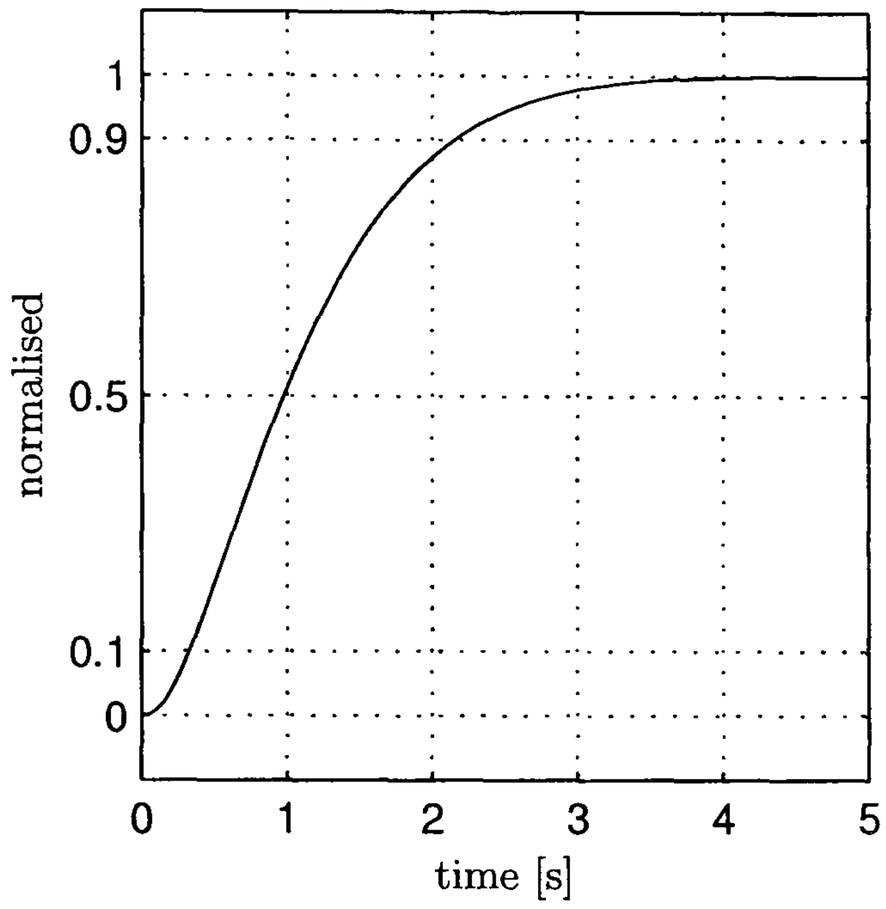

Figure 3.5: Normalised step response of the closed-loop system with a controller gain of $K = 5200$.

to investigate whether paraplegic standing is possible by artificially stimulating the calf muscles to produce the stabilising torque at the ankle joint and in order to investigate the fundamental limitations of FES induced paraplegic standing when external inputs from the CNS were excluded. They used the same single-link inverted pendulum configuration as Jaeger and Donaldson which was realised experimentally by a custom-made body-brace attached to the subject's back in such a way that all joints above the ankle joint were fixed. Independent measurement of the left and right ankle moment as well as the angle

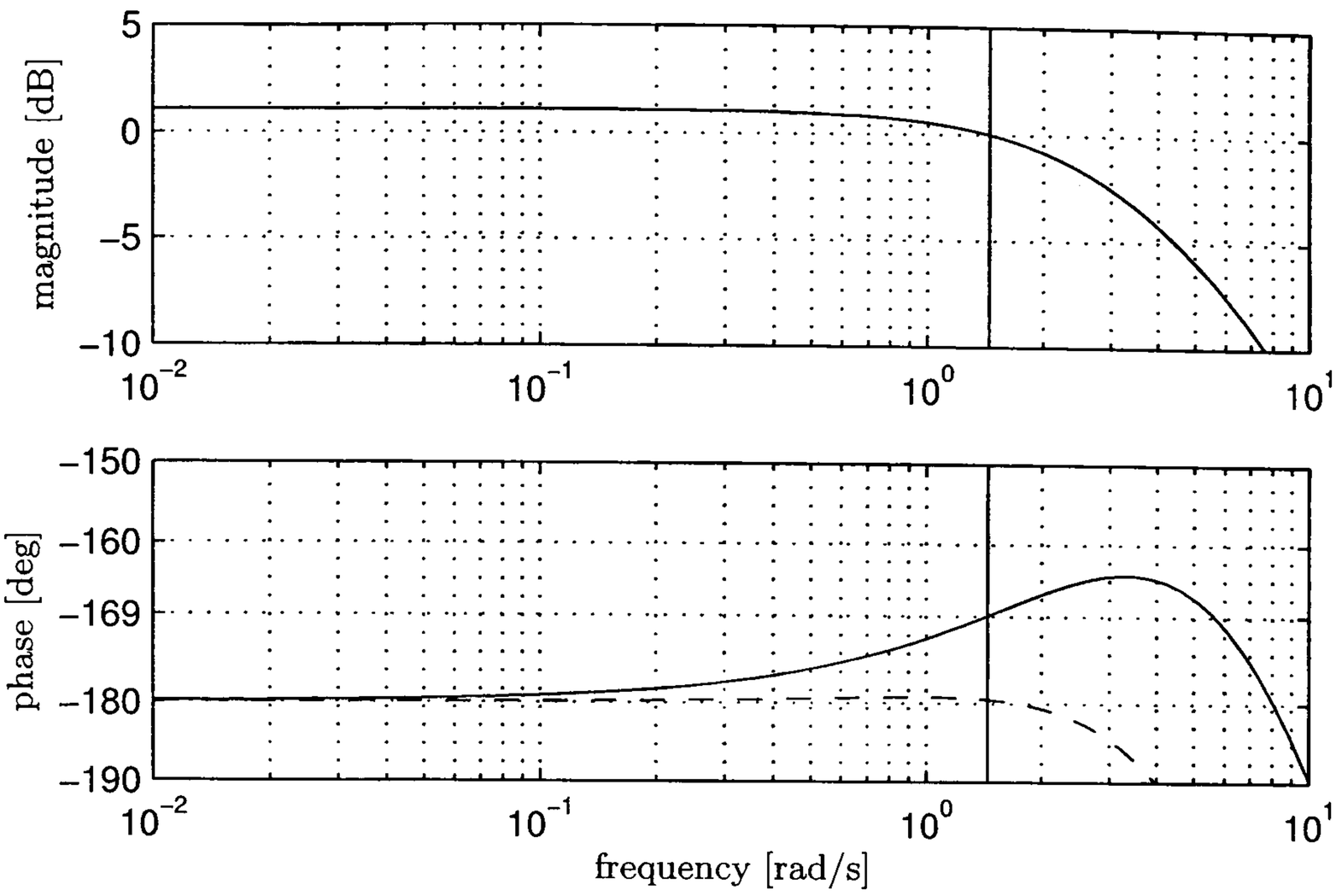

Figure 3.6: Bode plot of the open-loop system $G_{ol}(z) = C_{PD}(z)G_m(z)G_b(z)$ for a controller gain of $K = 5200$. The vertical line marks the phase margin. The dashed line shows the phase plot for a rise time of the muscle loop of $t_{r,m} = 0.4\,s$.

of inclination of the body allowed a cascade control structure regulating the left and right ankle moment in an inner control loop and the angle of inclination in an outer control loop using a multi-rate sampling strategy. Since the muscle dynamics are of significantly higher bandwidth than the body dynamics, this was done in order to decouple the non-linear muscle properties from the issue of controlling the body's angle of inclination. The angle controller provided a reference moment which was equally divided between the left and right legs. An LQG approach was employed for the controller design of both the moment control loop and angle control loop. The calf muscles were assumed to contract under quasi-isometric conditions while standing. Following the Hammerstein hypothesis, the muscle dynamics were modelled as a static non-linearity followed by second order dynamics, and both were experimentally identified. The static non-linearity was cancelled in the inner control loop. During the experiment the subject was leaning forward slightly and only plantarflexor stimulation was applied because these muscles are significantly stronger than the dorsiflexor muscles. This would also avoid any non-linear properties around the neutral position caused by the necessary switching of the stimulation between both muscle groups.

Experiments were carried out with one intact 43 year old subject, and one 35 year old paraplegic subject with a complete T5 lesion, 13 years post injury. They found that while an intact subject was able to stand for a considerable time, results for the paraplegic subject were dominated by the effects of muscle weakness, fatigue and spasticity. Standing

was limited to around $10 - 20$ s. Furthermore, the results revealed a strong asymmetry between the left and right legs of the paraplegic subject, less stable responses with a tendency to oscillate and a rapid saturation of the stimulation signal.

The study presented in this chapter aims for validation and improvement of the results from [Hunt *et al.*, 1997; Munih *et al.*, 1997], further development of the approach presented above and to deepen the insight of the effects of different design decisions. Several important changes in the control design method have been made which resulted in considerably prolonged periods of standing in paraplegic subjects. The key design changes can be summarised as follows:

- **Pole assignment** design is employed instead of LQG. The observer and control poles of the desired closed-loop response were specified indirectly within the time domain via rise-time and damping of an equivalent continuous-time linear second-order transfer function. The advantage of a pole assignment approach is that the nominal closed-loop response does not depend on the nominal plant model whereas in LQG the closed-loop response is a function of the plant model. This is important because the dynamics of the artificially stimulated muscle may significantly differ between individuals.

- The **inner moment control loop** is considered a **SISO** system. This means that the same stimulation signal is applied to the left and right legs. The feedback signal is the accumulated total ankle moment. Previously, separate controllers were designed for the left and right moments, and the legs were individually stimulated. The total reference moment was equally divided between both sides. The new approach deals with the left/right asymmetry observable in paraplegic subjects. The presence of that asymmetry means it is not reasonable to demand the same moment from both sides. The total moment is balanced between both legs in a natural manner, depending on the ability of each leg to deliver force for a given stimulation level.

- The **moment control loop** is now designed **without integral action** which means that a higher bandwidth can be achieved for this loop.

- The closed-loop characteristics of the **inner moment loop** are now treated as **part of the plant for the outer angle loop** design. It is shown that this allows achievement of stability even when the inner loop is relatively slow. Previously, the inner loop was neglected under the assumption that it is of a relatively high bandwidth. Often, however, the muscle loop can become slow (due, for example, to fatigue or general muscle weakness) resulting in system instability.

- A new **notch filter design** approach for the outer loop is implemented. The inner loop is relatively fast compared to the outer loop, and having a notch filter design

can avoid certain problems of numerical and measurement noise sensitivity in the design by cancellation of the inner closed-loop poles which could otherwise be excited to oscillation and cause instability.

These various design options provided considerable flexibility and the effect of the individual design choices could be evaluated experimentally. The aim was to have a set of design parameters with a clear physical interpretation. This is important because use of the control system in the rehabilitation laboratory involves people who do not necessarily have expertise in control engineering (e.g. bioengineers, clinicians and physiotherapists). This is also important because system identification and control design must be done during experimental sessions **while the subject is standing in the apparatus** - the design procedure must therefore be carried out quickly.

3.3 Experimental Setup

The experimental apparatus used in this experiment has been described in section 2.2. The subject is assumed to be a single-link inverted pendulum. This configuration is secured by a custom made body shell attached to the subject's back which allows movement only around the ankle joint (cf. Figure 2.1 on page 11). During the standing experiment, the subject was leaning slightly forward in order to avoid the non-linearity around the neutral position and the plantarflexor muscles are stimulated to generate the stabilising moment for the body.

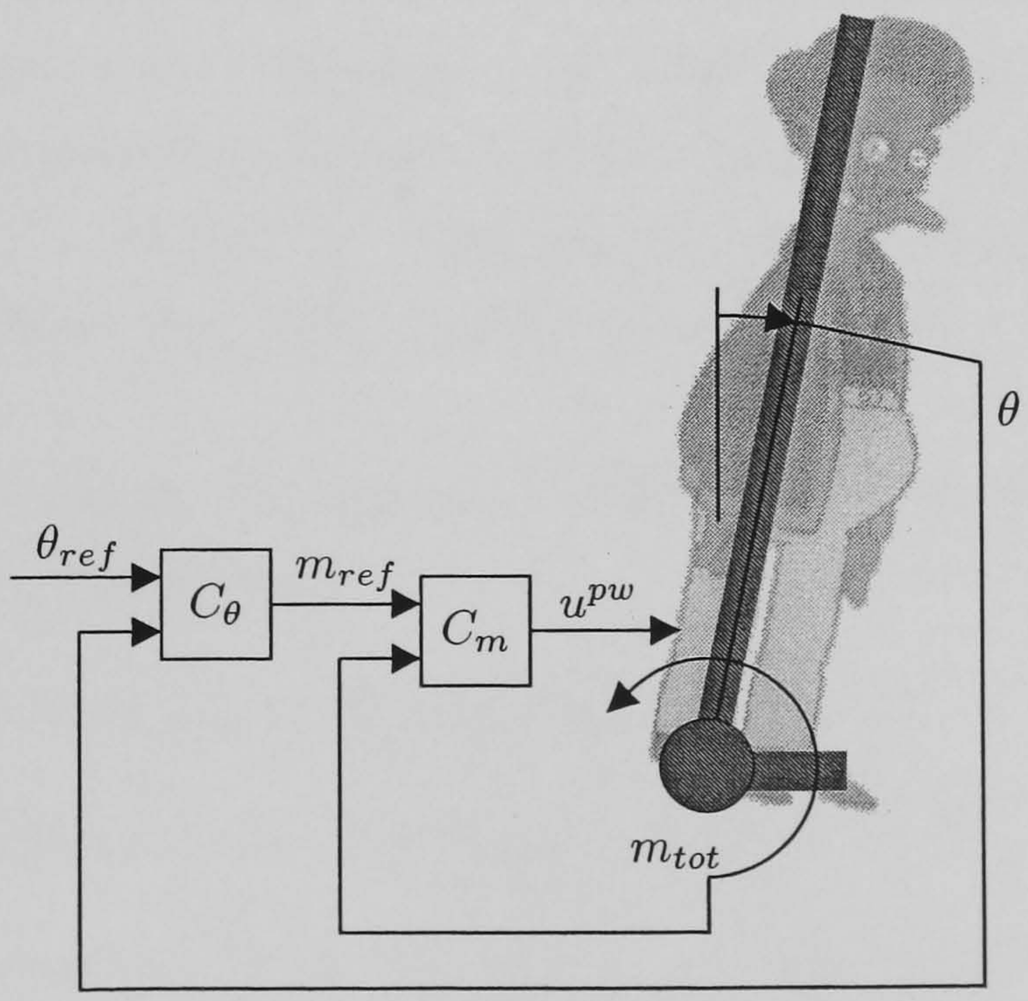

Figure 3.7: Experimental control structure. θ is the inclination angle of the body, m_{tot} is the total ankle moment, u^{pw} is the pulsewidth of stimulation. C_θ is the angle controller and C_m is the moment controller. Desired values for the inclination angle and ankle moment are θ_{ref} and m_{ref}, respectively.

A cascaded control structure has been employed in order to de-couple the non-linear properties of the muscle from the task of body angle control (cf. Figure 3.7). A reference angle for the body θ_{ref} is specified by the experimenter. The angle of inclination of the body θ is measured and controlled by the angle controller C_θ. The angle controller provides a reference moment m_{ref} for the moment controller C_m. The moment controller calculates the pulsewidth of the stimulation signal u^{pw}.

3.3.1 Ankle Moment Control

The left and right legs are lumped together into a SISO-system. The same stimulation signal is applied to both legs and the total moment is measured and available for feedback (cf. Figure 3.8).

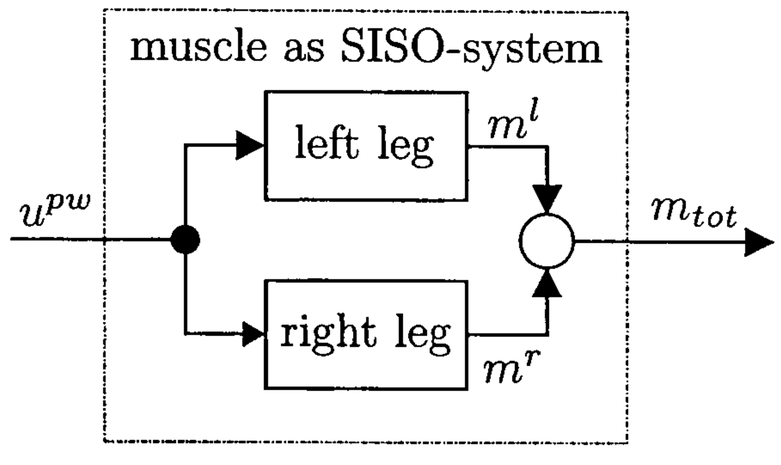

Figure 3.8: Left and right legs are considered as a SISO system. Common stimulation pulsewidth u^{pw} is applied to both sides, resulting in left and right moments m^l and m^r. The total moment is then $m_{tot} = m^l + m^r$.

A dynamic model of the muscle is identified between the stimulation signal u^{pw} and the total moment of left and right legs m_{tot}. The muscles are stimulated by a PRBS signal and the total moment is measured. An ARX-type model is estimated from the input/output data using the least square criterion. The identification procedure provides the polynomials $A(q^{-1})$ and $B(q^{-1})$. Typically, the muscle dynamics are stable and of second order with no zeros and, using a sampling time of 50 ms, a unit step input/output time delay.

The generic control design procedure of section 2.4 is then applied to the muscle model, subject to the following definitions:

- The controlled output $y(k)$ is the total moment $m_{tot}(k)$.
- The control signal $u(k)$ is the simulation pulsewidth $u^{pw}(k)$.
- The reference signal $r(k)$ is the desired total moment $m_{ref}(k)$.

Experimental results are shown below with and without integral action, i.e. for $\Delta(q^{-1}) = 1$ and $\Delta(q^{-1}) = 1 - q^{-1}$. The notch filter design option has not been employed for moment control, i.e. $A^+(q^{-1}) = 1$. No pre-filter for reference tracking is employed.

3.3.2 Body Angle Control

A model of the body dynamics is gained by approximating it as an ideal single-link inverted pendulum with an ideal joint. Thus, terms of stiffness and damping are neglected (cf. Figure 3.9). The biomechanical system can be described using the equation of motion

$$m_{tot} - \tilde{m}gl\sin\theta = -J\frac{d^2\theta}{dt^2}\,, \tag{3.6}$$

where J is the moment of inertia. For small angles we can approximate $\sin\theta \approx \theta$, and the linearised transfer function of the body dynamics $G_b(s)$ becomes

$$G_b(s) = \frac{\Theta(s)}{M_{tot}(s)} = \frac{-\frac{1}{J}}{s^2 - \frac{\tilde{m}gl}{J}}\,, \tag{3.7}$$

where s is the complex variable of the Laplace transformation and capitals indicate transformed signals. The biomechanical parameters $\tilde{m}$, J, and l are estimated following Winter [1990].

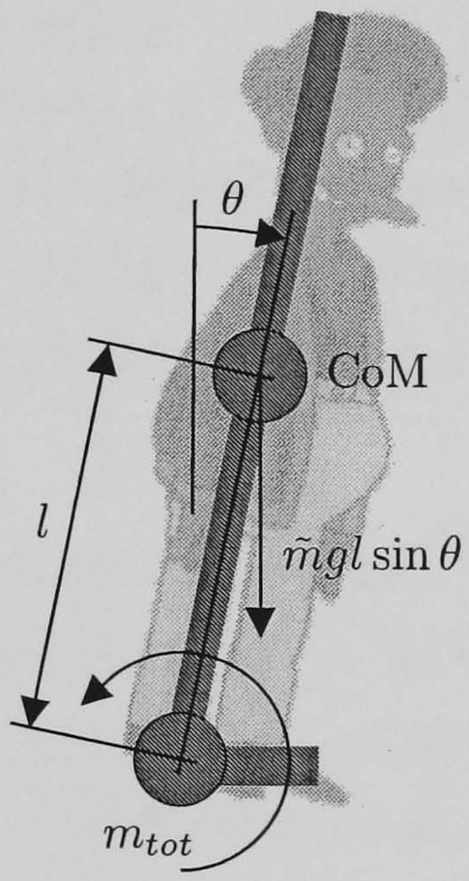

Figure 3.9: Biomechanical system approximated by an ideal single-link inverted pendulum. CoM is the Center of Mass. $\tilde{m}$ is the body mass and $\tilde{m}gl\sin\theta$ is the moment acting around the joint caused by gravity. θ is the angle of inclination measured from the vertical axis, l is the distance of the CoM from the joint of rotation and m_{tot} is the stabilising moment.

The transfer function (3.7) in continuous time is transformed into discrete time and represented in the delay operator q^{-1} for control design. The application of the generic control design procedure of section 2.4 is subject to the following definitions:

- The controlled output $y(k)$ is the angle $\theta(k)$.
- The control signal $u(k)$ is the desired moment moment $m_{ref}(k)$ for the inner loop.
- The reference signal $r(k)$ is the desired angle $\theta_{ref}(k)$.

There are two options which have been followed to determine the plant for the angle controller (the transfer function from $m_{ref}(k)$ to $\theta(k)$):

1. The first option is to neglect the dynamics of the ankle moment loop, and base the design only on the biomechanical model. Using this option can be justified by the relatively high bandwidth of the inner moment control loop. In this case the closed-loop transfer function of the inner loop $G_{y/r}$ (according to equation (2.56) on page 28) from the reference moment to the controlled moment is assumed to be 1 and the design plant $G_p(q^{-1}) = \frac{B(q^{-1})q^{-d_k}}{A(q^{-1})}$ in equation (2.38) on page 25 is obtained simply by discretising the body dynamics of equation (3.7).

2. The second option is to take the inner loop dynamics into account for the design plant. In this case the plant $G_p(q^{-1}) = \frac{B(q^{-1})q^{-d_k}}{A(q^{-1})}$ is obtained by cascading the discrete time body dynamics of equation (3.7) with the nominal closed-loop dynamics of the inner loop given by equation (2.56). This approach assumes that both loops are operated at the same sampling time. Alternatively, a multirate sampling approach can be employed. This requires transformation of the closed-loop dynamics of the inner loop (2.56) into continuous time, cascading it with the body dynamics of (3.7) in continuous time and transforming the cascaded model back into discrete time with the sampling time at which the outer loop is operated. However, in the experiments reported in this thesis, both loops are operated at the same sampling frequency of 20 Hz.

Results for both options are reported in this chapter. Regarding the further design option established in section 2.4, the angle controller is always designed to have integral action, i.e. $\Delta(q^{-1}) = 1 - q^{-1}$. When the moment loop is included into the angle controller design plant, i.e. option 2 is chosen, then a notch filter design is usually adopted for the angle controller. However, experimental results are reported for tests with and without notch filter design. When used, the purpose of the notch filter design is to cancel the relatively fast dynamics of the moment loop. In this case we set $A^+(q^{-1}) = \Phi_c'^{moment}(q^{-1})$, where $\Phi_c'^{moment}(q^{-1})$ is the closed-loop design polynomial $\Phi_c'(q^{-1})$ as specified for the moment loop. Then, $A^-(q^{-1}) = A^{body}(q^{-1})$, where $A^{body}(q^{-1})$ is the denominator of the body dynamics (3.7) in discrete time.

3.4 Experimental Procedure

During each experimental session the subject is first secured in the apparatus and then a set of five principal tests is carried out:

1. **Identification.** During the identification procedure the safety ropes (cf. Figure 2.1, page 11) are taut such that the subject is in a fixed position and no movement is possible around the ankle joints.

   (a) **Test C.** The purpose of this test is to establish a suitable amplitude of the stimulation pulses, since we use pulses with a constant amplitude and a varying pulsewidth. Starting with an appropriate value of Current the pulsewidth is ramped up from $50 - 500\,\mu$s in 5 s and the moment produced is measured. The current is then incremented by 10 mA and the stimulation pattern is repeated. This procedure is repeated until the muscles saturate at high pulsewidths while the subject still feels comfortable. The current is then fixed at the appropriate level.

   (b) **Test PRBS.** This test is an open-loop test using a stimulation signal where the pulsewidth has a **PRBS** form. The same pulsewidth is applied to both legs and the total moment produced is measured. The mean pulsewidth is then incremented and the stimulation pattern is repeated until the muscles saturate while the subject still feels comfortable. In this way we obtain a set of input/output data around different operating points. The amplitude of the PRBS signal was set at $35\,\mu$s. The PRBS signal was designed off-line to excite the major dynamic properties of the muscle. It has a period of 155 samples and is constant for at least 5 samples after each transition.

The input/output data gained from the PRBS test are used to identify local linear transfer functions around the stimulated operation points using the least square criterion. This step also involves model validation. Then, the feedback control system is designed based on the experimentally obtained model for the muscle and the pendulum model of the body equation (3.7).

2. **Control system design.** The cascaded control structure (cf. Figure 3.10) allows the overall feedback system to be designed and tested in several steps following the generic design algorithm of section 2.4:

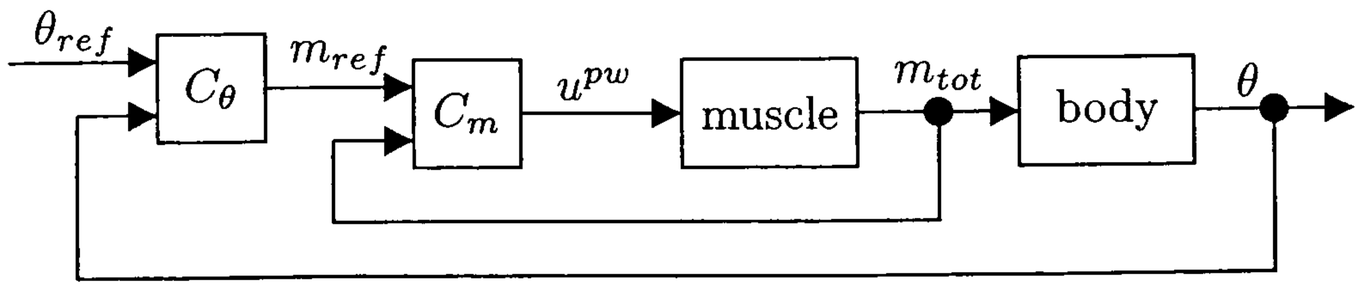

Figure 3.10: Cascaded loop structure for unsupported standing.

   (a) **Ankle moment controller.** First the ankle moment controller is designed. The muscle model with the highest DC gain is usually chosen for the control

design. This provides a design which is robust against the static recruitment non-linearities. This step establishes the desired closed-loop response between the reference moment m_{ref} and the measured total ankle moment m_{tot}. Following the controller synthesis, the moment loop is verified by inspection of the closed-loop frequency responses and tested separately (cf. test M below).

(b) **Body angle controller.** The transfer function between the reference moment m_{ref} and the body angle θ, i.e. the combination of the ankle moment loop and the open loop body dynamics, is taken as the plant to design the angle controller. The closed-loop dynamics of the ankle moment loop can either be described by equation (2.56), page 28, or approximated to be 1 (see above). The angle controller design establishes the desired closed-loop response between the reference angle θ_{ref} and the measured body angle θ. The control design is verified by inspection of the closed-loop frequency responses and the overall system is tested (tests T and D below).

3. **Test M.** Following the design of the moment loop, test M is carried out. This is a test of closed-loop **M**oment tracking. Typically a square-wave reference moment of a given amplitude and frequency is applied. The safety ropes are taut during this test.

Following analysis of the moment control system, the design parameters are sometimes changed and Test M is repeated. This process in continued until satisfactory results are obtained (usually only one or two iterations are required). The design parameters for the angle control loop are then selected, the angle controller is designed, and two kinds of closed-loop angle control tests are carried out. The safety ropes are loosened for these tests to allow movement around the ankle joint.

4. **Test T.** This is a test of closed-loop angle **T**racking. Typically, a square-wave reference angle of a given amplitude and frequency is applied. Sometimes, in a procedure known as "quiet standing", the reference angle is kept constant.

5. **Test D.** This a test of closed-loop **D**isturbance rejection. Here, the reference angle is kept constant and disturbances are applied to the body. We applied disturbances by repeatedly pulling the subject forwards or pushing him back.

6. **Test F.** For this test a constant reference angle but no external disturbances are applied. The subject is left standing until the muscles are to **F**atigued to keep the body upright. This test is carried out only with the paraplegic subject in order to explore the maximally possible duration of standing.

3.5 Subjects

Experiments reported in this thesis were carried out with intact subjects as well as with one paraplegic subject. Initially, it is important to work with intact subjects in order to study different design options and to evaluate and verify the control approach. Working with intact subjects naturally raises the question of whether voluntary postural control inputs can affect the observed results, but the experiments have been designed to ensure that such effects are minimised. During an experiment the subject stands quietly with arms folded across the chest and eyes closed. Thus the subject receives no cognitive feedback regarding the moment and angle setpoints, or of the current inclination angle. The subject also loses proprioception from the ankles and exteroception from the soles of the feet. Indeed, most intact subjects report that the electrical stimulation of the calf muscles causes a loss of normal sensation in their lower limbs, and that they found it easy to "submit" themselves to the artificial control system. In these circumstances it is clearly impossible for subjects to voluntarily achieve accurate tracking of the inclination angle setpoint. The results with an intact subject presented in this thesis are gained with one 28 year old male.

Once the most appropriate configuration was found, experiments were carried out with one male 44 year old paraplegic subject with a complete lesion at level T7/T8, 4 years post-injury. Prior to the experimental study, he underwent muscle training for 12 weeks. Initially, the muscle training involved alternated stimulation of the plantarflexor and dorsiflexor muscles for 30 minutes a day, later increased to one hour a day. The muscle training continued throughout the experimental study.

3.6 Experimental Results with Intact Subjects

Experimental results with intact subjects are presented in this section following the previously outlined procedure. The aim is to investigate the influence of different design choices, in particular:

- The effect of inclusion of integral action into the moment loop.
- The effect of the bandwidth of the moment control loop on the stability of the overall system.
- The effect of, and potential improvements resulting from, inclusion of the inner loop dynamics into the plant for the angle loop design.
- The effect and need for a notch filter design approach for angle control design.

All results are from the same experimental session. However, further series with other intact subjects were conducted which revealed similar results.

3.6.1 Results of Test C

Typical results of test C are shown in Figure 3.11. Test C was carried out separately for the left and right leg. It can clearly be seen that the produced moment starts rising once a certain threshold is passed. However, for a current of 40 mA, the muscle response is very weak, whereas when stimulated with a current of 60 mA the muscle output saturates for relatively small values of pulsewidth. Choosing a stimulation current of 50 mA enabled us to use the full range of the pulsewidth, and this value was used for the remainder of the experiment.

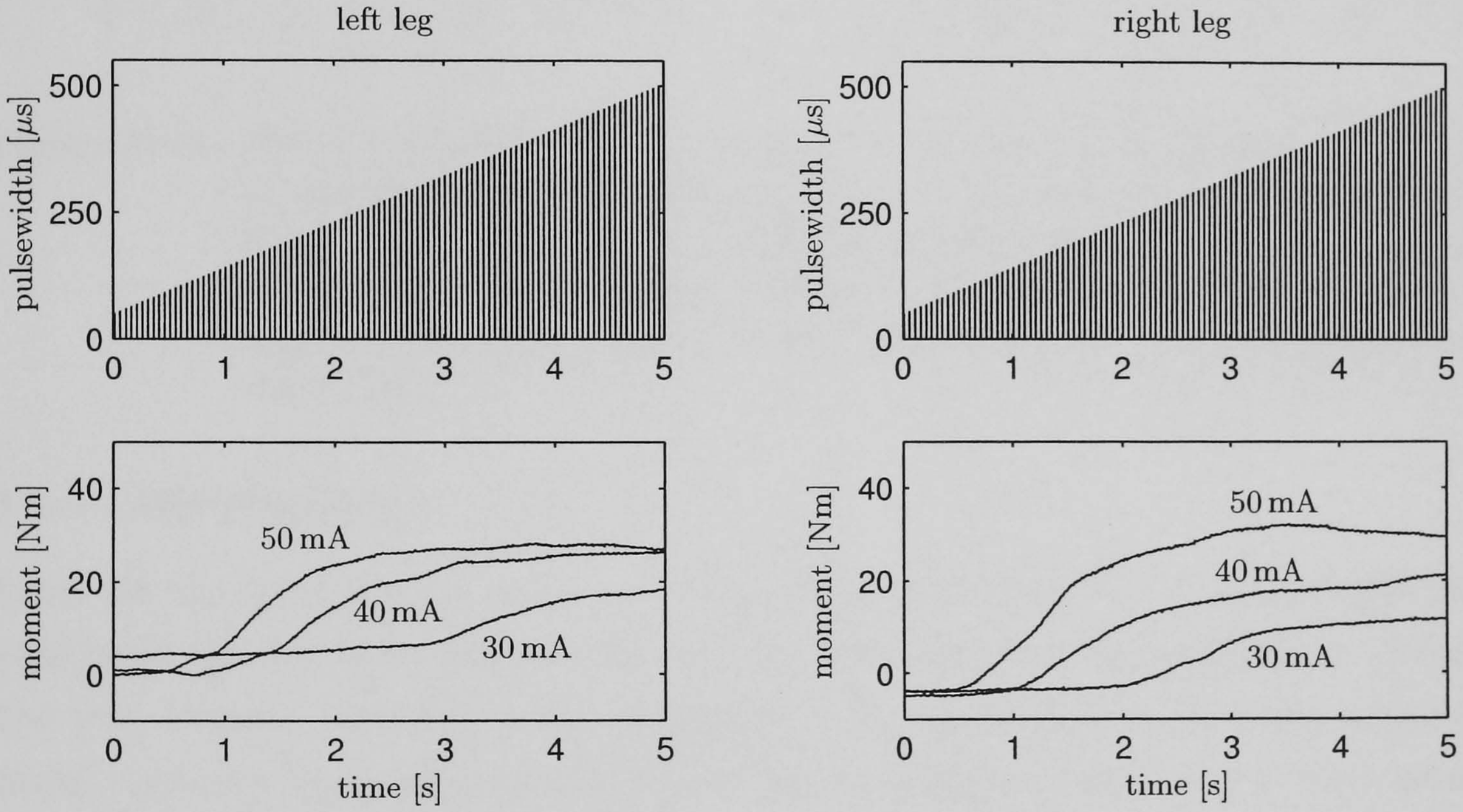

Figure 3.11: Results of test C (intact subject). The upper plot shows the sequence of impulses with ramping pulsewidth, applied to the muscle. The bottom plot shows the measured response of the muscles for three different current levels 30, 40 and 50 mA.

3.6.2 Results of Test PRBS

Results of test PRBS are shown in Figure 3.12. The bold line in the pulsewidth plot corresponds to the bold line in the moment plot underneath. Four sets of input/output data were collected around mean pulsewidths of 100, 150, 200, 250 μs. The amplitude of the PRB signal was $\pm 35\,\mu$s. The muscle response to a stimulation around 100 μs was very weak. The muscles saturated around the stimulation level of 250 μs. The first 5 seconds of each data set were cut off for the estimation process.

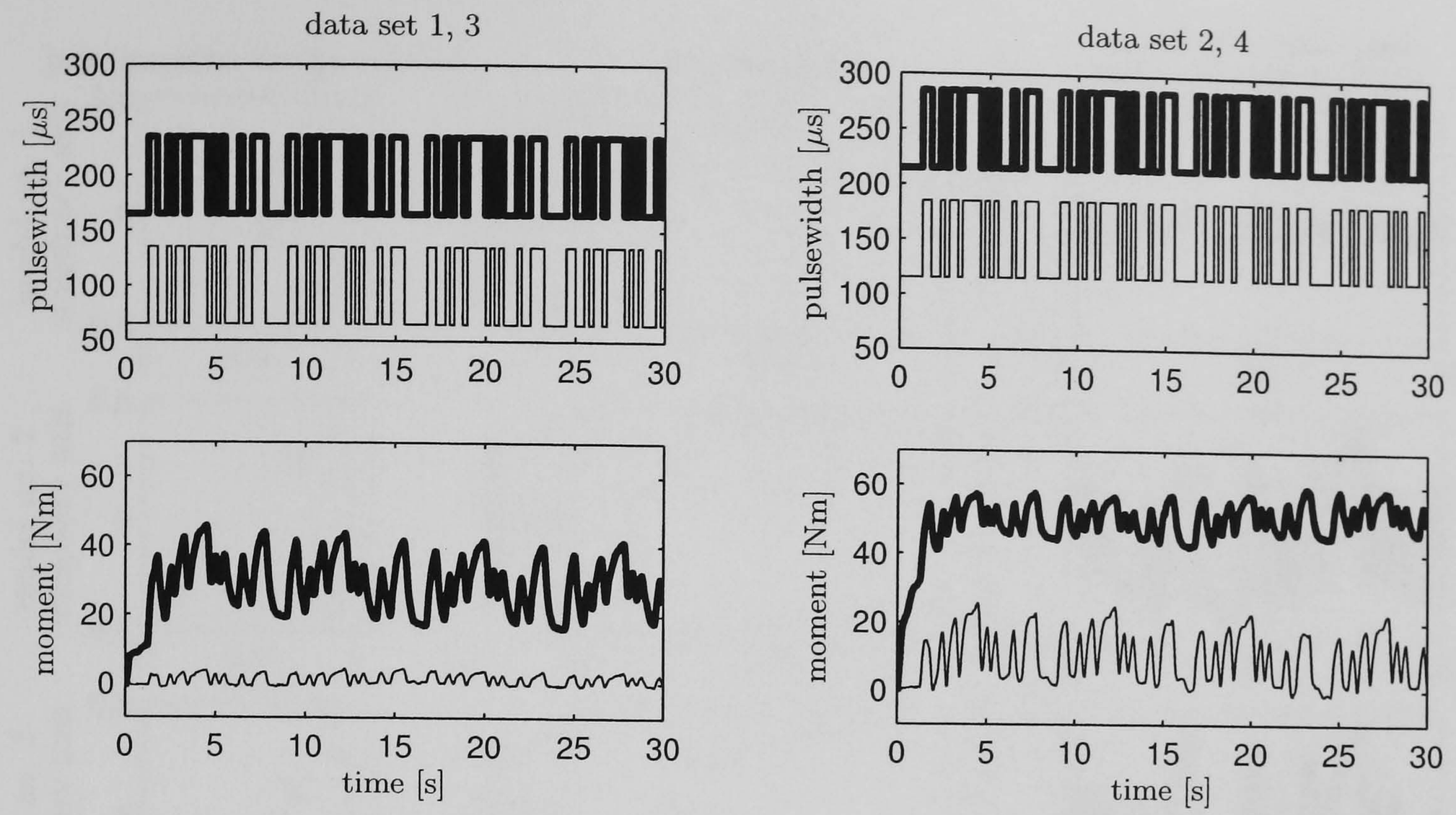

Figure 3.12: Muscle identification data for various mean levels of PRB input signal with an amplitude of 35 μs (intact subject). The upper curves show the PRBS input signals (pulsewidths) while the lower curves show the measured moments corresponding to each level of input. The bold and thin lines in the moment plots correspond to the bold and thin lines in the pulsewidth plots, respectively.

3.6.3 Identification

Based on the input/output data from Test PRBS (cf. Figure 3.12) we identified four local linear time-invariant second order transfer functions using the least square criterion. The pole location, rise time and a comparison of the simulated output of the estimated model versus the measured output of test PRBS are shown in Figure 3.13 for each model. Table 3.1 summarises the identified transfer function, the rise time and DC gain of the four identified models.

model no.	pulsewidth [μs]	transfer function $G_p(q^{-1})$	rise time [s]	DC gain [Nm/μs]
1	100	$\frac{0.936 \cdot 10^{-2} q^{-1}}{1 - 1.191 q^{-1} + 0.362 q^{-2}}$	0.29	0.06
2	150	$\frac{3.093 \cdot 10^{-2} q^{-1}}{1 - 1.486 q^{-1} + 0.597 q^{-2}}$	0.23	0.24
3	**200**	$\mathbf{\frac{2.777 \cdot 10^{-2} q^{-1}}{1 - 1.464 q^{-1} + 0.549 q^{-2}}}$	**0.42**	**0.33**
4	250	$\frac{1.921 \cdot 10^{-2} q^{-1}}{1 - 1.390 q^{-1} + 0.492 q^{-2}}$	0.39	0.19

Table 3.1: Identification results (intact subject). The transfer function, rise time and DC gain for each model. The highlighted model was selected for control design.

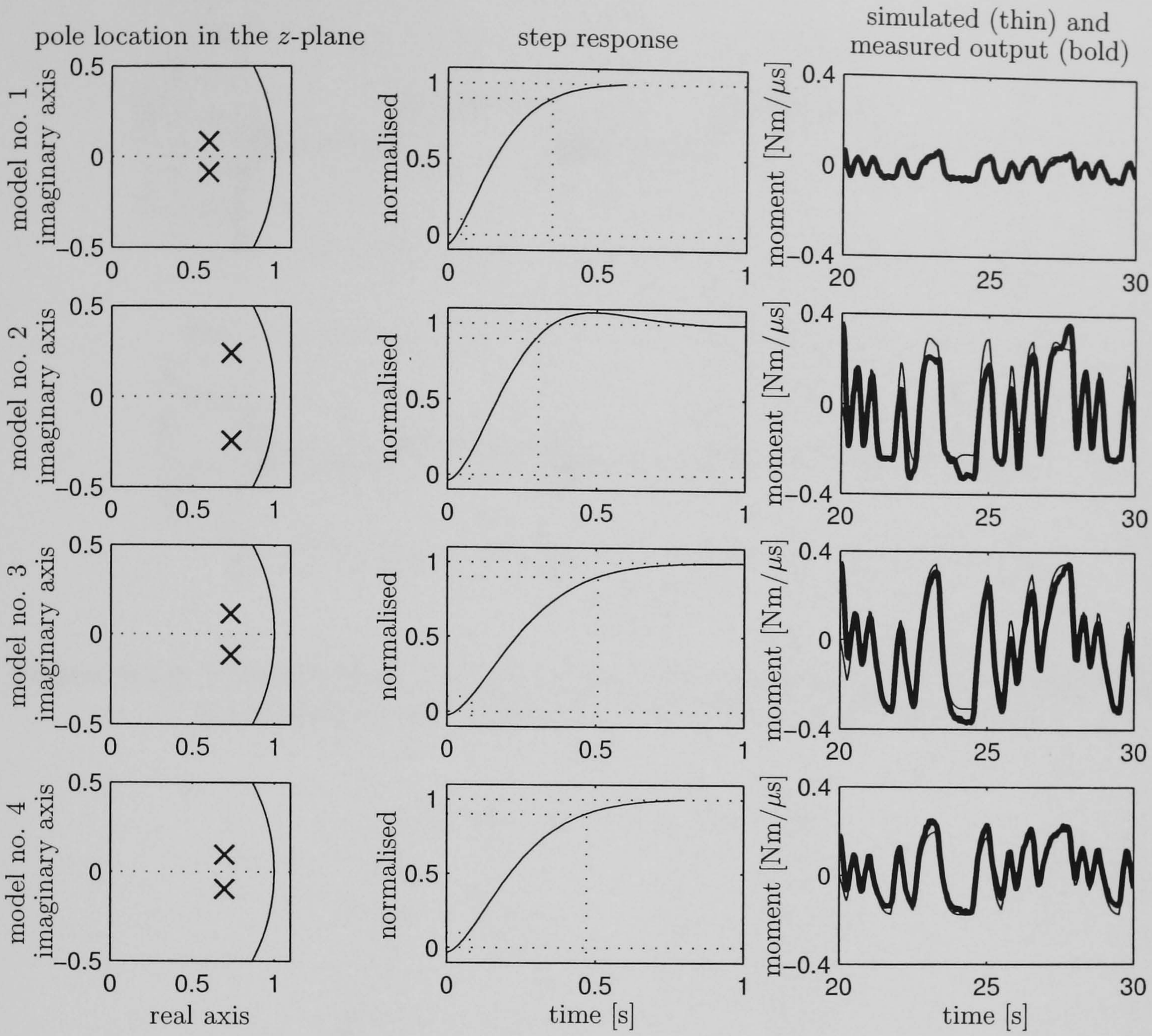

Figure 3.13: Identification results (intact subject). Each row shows the pole location in the complex z-plane, the step response and a comparison of the simulated output of the estimated model versus the measured output (mean value removed). Model no. 1 corresponds to data set 1 of test PRBS (mean pulsewidth 100 μs), model no. 2 corresponds to data set 2 (mean pulsewidth 150 μs) etc. Model no. 3 at round 200 μs was chosen for control design. The dotted lines in the step response plot indicate the $t_{10-90\%}$ rise time.

For the design of the muscle moment controller, we choose to work with the model with the highest DC gain to ensure robust stability of the moment loop for varying stimulation levels, i.e. the model identified for a mean pulsewidth of 200 μs.

3.6.4 Ankle Moment Control Test—Results Test M

Influence of integral action on the moment control loop. Results of closed-loop moment tracking are shown in Figure 3.14 and Figure 3.16. Figure 3.14 shows a design where integral action is included in the controller, i.e. $\Delta^m(q^{-1}) = 1 - q^{-1}$, whereas no integral action ($\Delta^m(q^{-1}) = 1$) was employed for the results presented in Figure 3.16.

With integral action, the closed-loop response tends to oscillate for small rise times

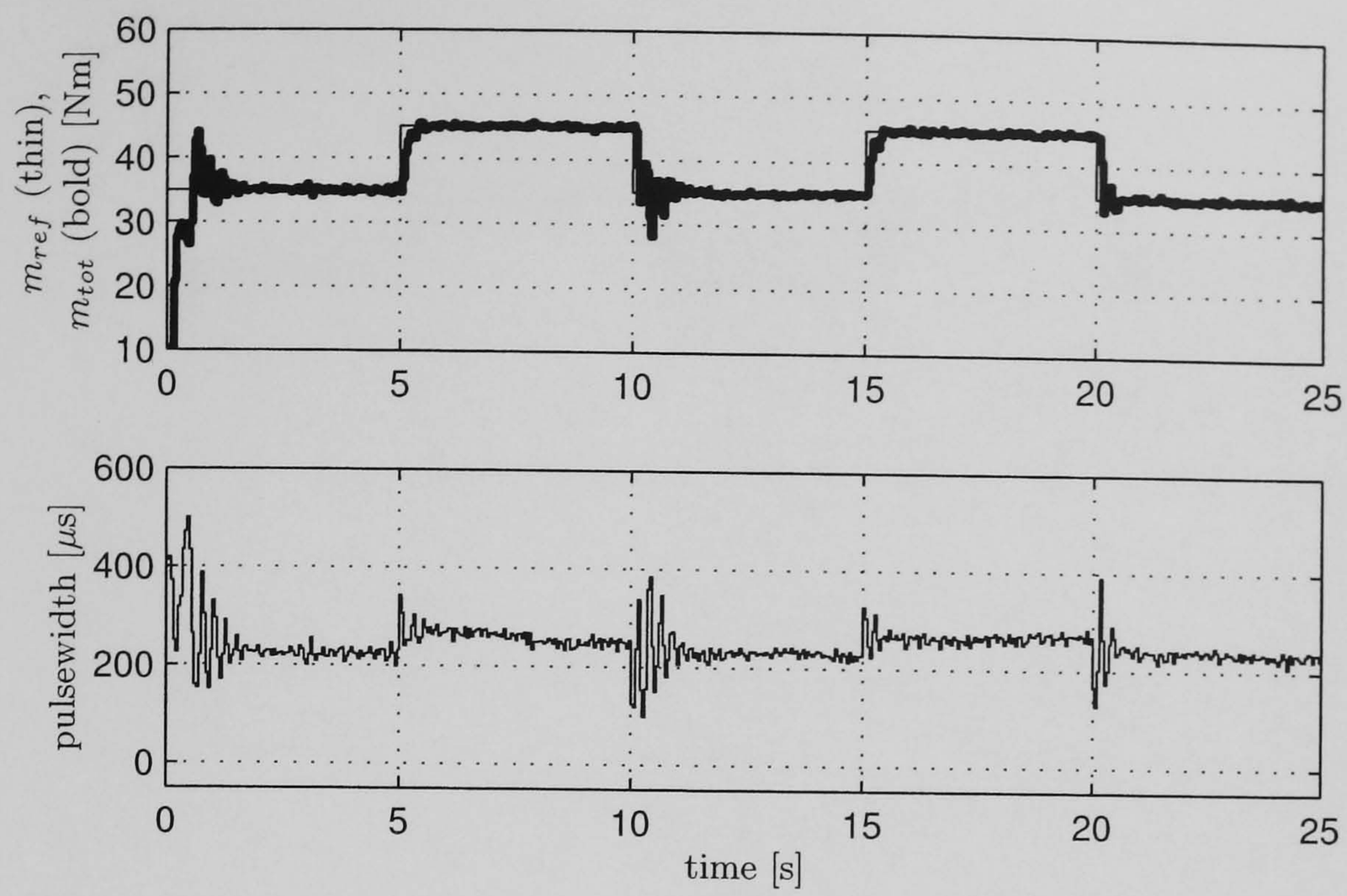

Figure 3.14: Muscle moment control with integral action (intact subject). Control design parameters are $t_{r,c}^m = 0.2\,\mathrm{s}$, $\zeta_c^m = 0.999$, $t_{r,o}^m = 0.15\,\mathrm{s}$, $\zeta_o^m = 0.999$.

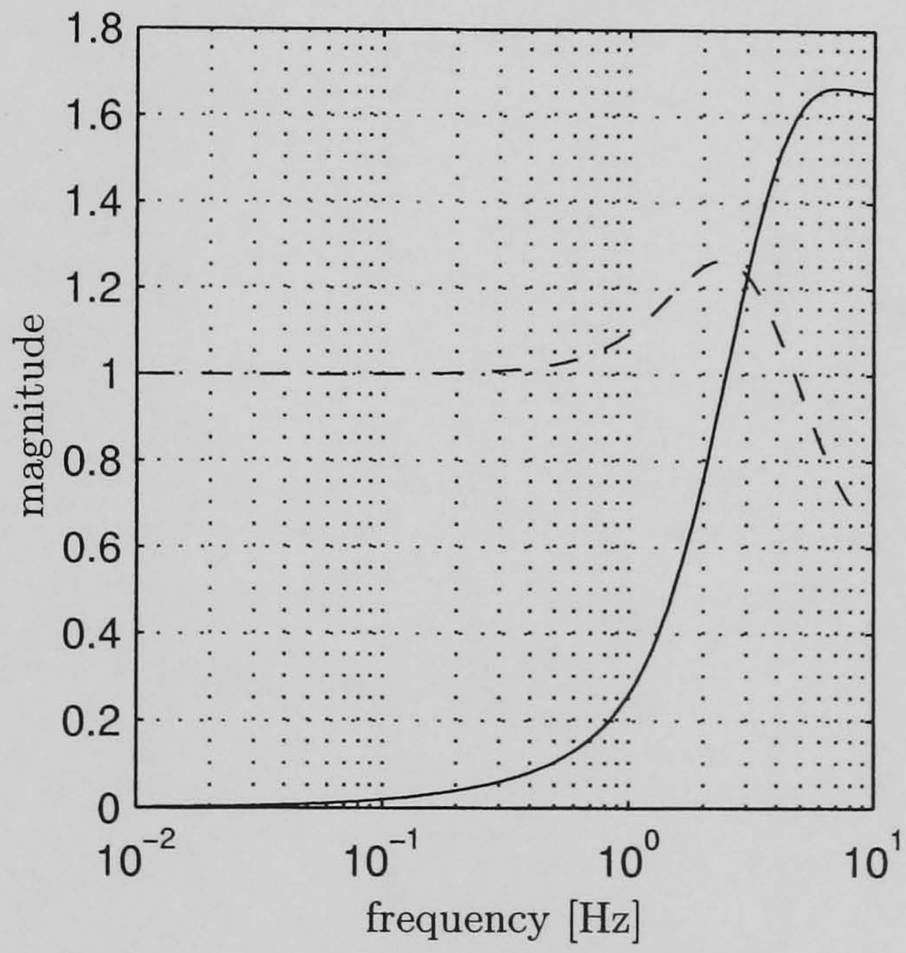

Figure 3.15: Sensitivity function $\tilde{S}$ (solid) and complementary sensitivity function $\tilde{T}$ (dashed) for moment control design corresponding to Figure 3.14.

(cf. Figure 3.14). An equivalent design without integral action remains stable and well damped (cf. Figure 3.16). This observation is supported by the shape of the corresponding closed-loop sensitivity functions $\tilde{S}$ and complementary sensitivity functions $\tilde{T}$ which are shown in Figure 3.15 and Figure 3.17. The larger peak of the sensitivity functions of the controller with integral action (cf. Figure 3.15) explains the oscillations which are present in the closed loop responses. The oscillations have a frequency of approximately 4 Hz, which is seen to lie between the peak frequencies of the sensitivity functions. Thus, a higher bandwidth can be safely achieved using a controller without integral action.

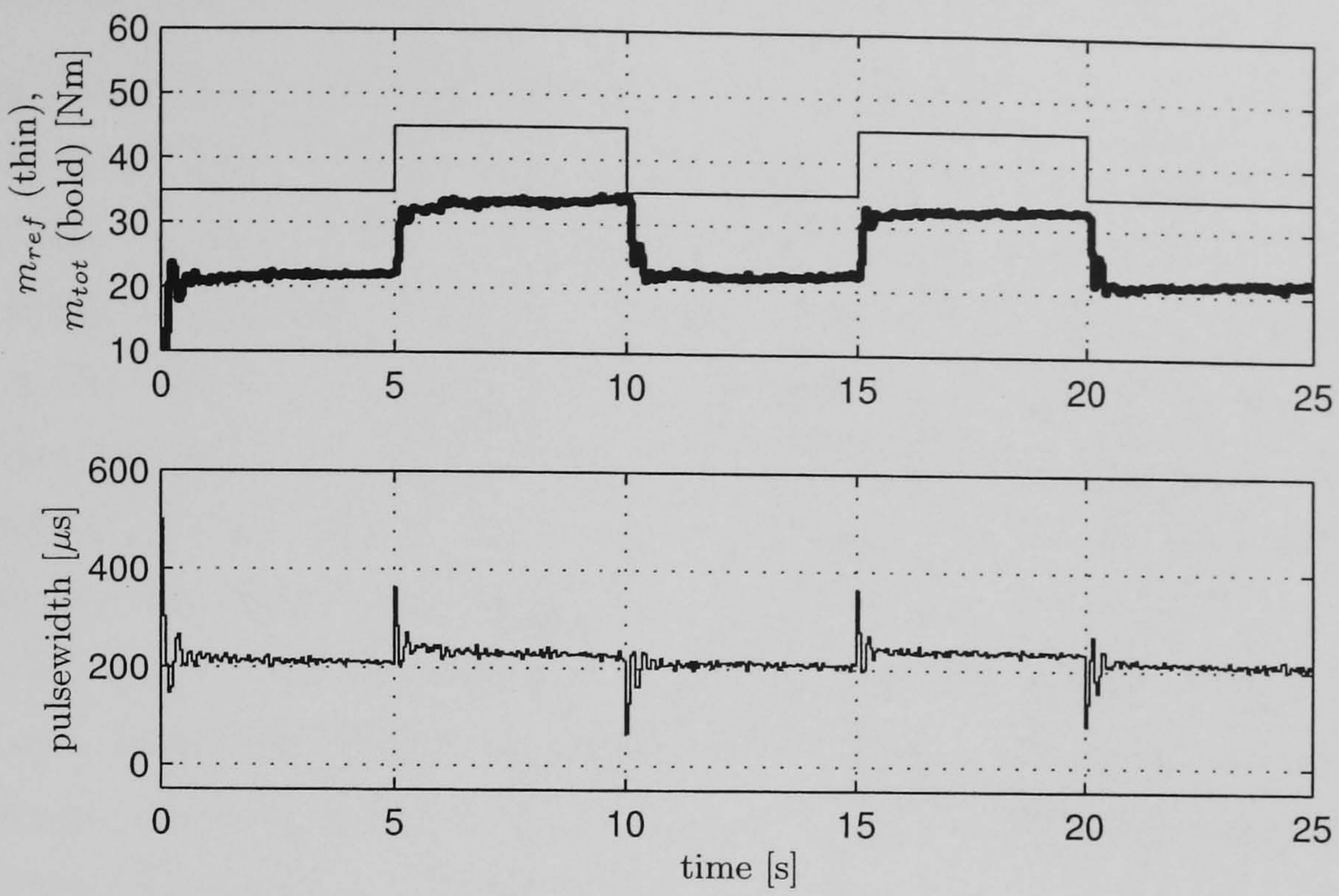

Figure 3.16: Muscle moment control without integral action. Control design parameters are $t_{r,c}^m = 0.15\,\mathrm{s}$, $\zeta_c^m = 0.999$, $t_{r,o}^m = 0.10\,\mathrm{s}$, $\zeta_o^m = 0.999$.

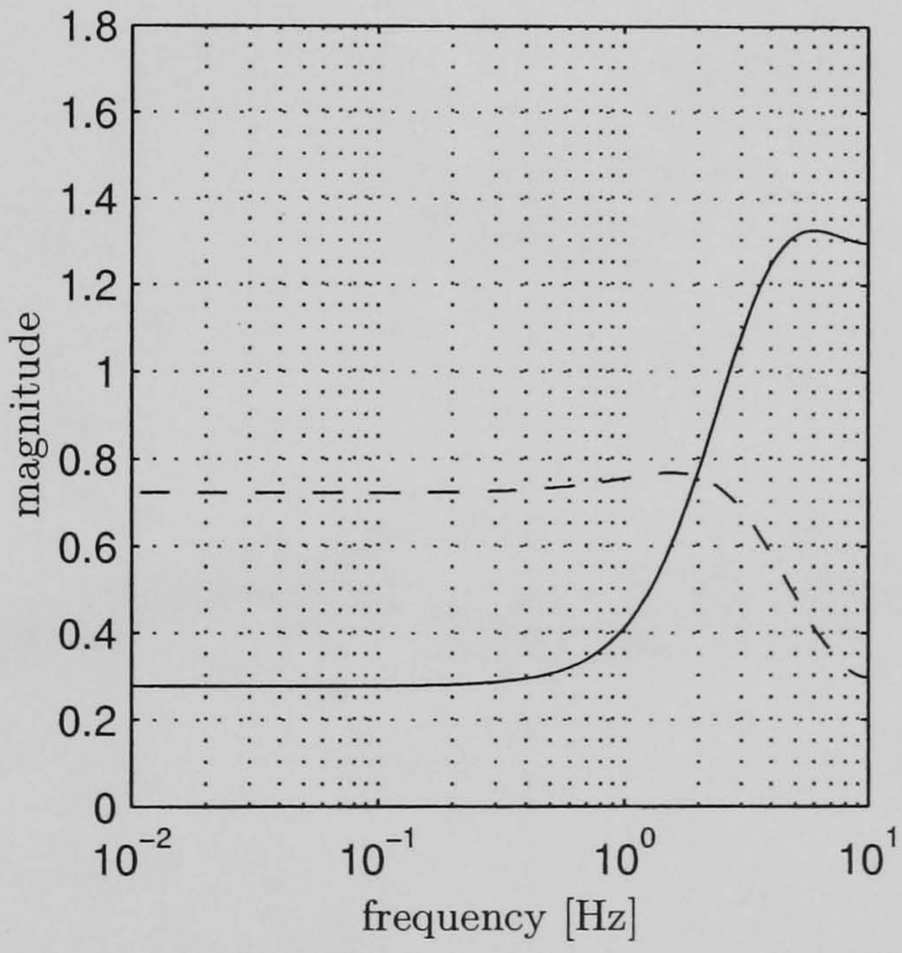

Figure 3.17: Sensitivity function $\tilde{S}$ (solid) and complementary sensitivity function $\tilde{T}$ (dashed) for moment control design corresponding to Figure 3.16.

On the other hand, no integral action results in a significant steady state error. Note that the DC gain of the reference tracking transfer function is still one. Therefore, the steady state error must be credited to equilibrium offsets, disturbances and model errors. However, the steady state error in the inner loop is of little significance for the overall system, as zero steady state angle tracking can be ensured by including integral action in the outer loop controller. The design of Figure 3.16 and Figure 3.17 was employed in the inner loop for the subsequent body angle control tests.

3.6.5 Body Angle Control Test—Results Test T and Test D

Results of closed-loop angle tracking are shown in Figures 3.18–3.24 for various design options. A square wave reference angle was specified with a mean value of 2.5°, an amplitude of 1° and a period of 20 s. For the first 20 s, no external disturbances are explicitly applied, which corresponds to 'quiet standing', (test T). During the remaining 30 s, the standing is disturbed by pulling the subject forward (at $t = 25\,\mathrm{s}$ and $t = 45\,\mathrm{s}$) and by pushing him backwards ($t = 35\,\mathrm{s}$). The physical parameters of the subject were assumed as $J = 90\,\mathrm{kgm}^2$, $\tilde{m} = 90\,\mathrm{kg}$, $l = 1\,\mathrm{m}$, (3.6)–(3.7), page 44. The design parameters for the angle loop are the same for all results shown: $t^a_{r,c} = 1\,\mathrm{s}$, $t^a_{r,o} = 0.7\,\mathrm{s}$, $\zeta^a_c = \zeta^a_o = 0.999$, $\Delta^a(q^{-1}) = 1 - q^{-1}$. The inner loop was always designed without integral action, i.e. $\Delta^m(q^{-1}) = 1$, as integral action is included in the outer loop design. The common design parameters for the inner loop are: $t^m_{r,o} = 0.10\,\mathrm{s}$, $\zeta^m_c = \zeta^m_o = 0.999$. The control rise time is varied between $t^m_{r,c} = 0.15\,\mathrm{s}$ and $t^m_{r,c} = 0.20\,\mathrm{s}$.

First, we investigated the influence of the inner loop bandwidth on the stability of the

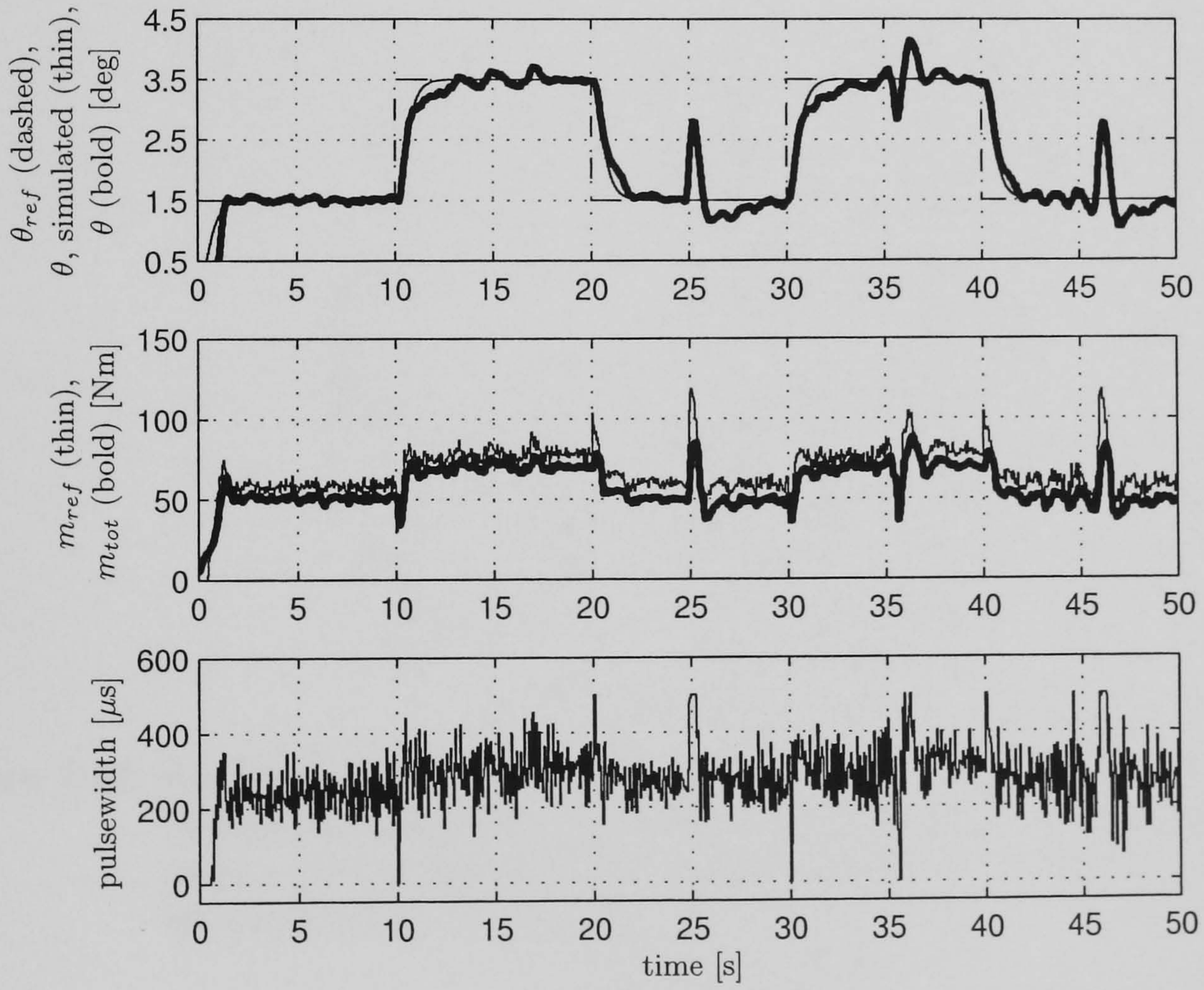

Figure 3.18: Body angle control (intact subject). Inner loop neglected for outer loop design. Fast inner loop ($t^m_{r,c} = 0.15\,\mathrm{s}$). The upper plot shows the measured (bold) and reference (dashed) body angle as well as a plot of simulated control loop (thin) which gives an impression of accuracy of the model (muscle and body). The plot in the middle shows the requested muscle moment (thin) and the measured muscle moment (bold). The lower plot shows the stimulation pulsewidth.

overall system when the inner closed-loop dynamics were neglected for the design of the outer control loop. Second, we investigate the effect of including the inner loop dynamics in the design plant for the outer loop, both for fast and slow inner loops.

The effect of the bandwidth of moment control loop on the stability of the overall system. The effect of the inner loop bandwidth on the overall stability can be seen from Figure 3.18 and Figure 3.20. A fast inner loop design was employed for the results of Figure 3.18 ($t^m_{r,c} = 0.15\,\mathrm{s}$), while a slower inner loop design was employed for the results of Figure 3.20 ($t^m_{r,c} = 0.20\,\mathrm{s}$). The inner loop dynamics were neglected in the design of the outer loop. This works well as long as the inner loop is fast enough (cf. Figure 3.18). However, for a slow inner loop, this design configuration can easily result in problems as the delay introduced by the slow inner loop response destabilises the outer loop (cf. Figure 3.20).

An analysis of the corresponding closed loop sensitivity functions $\tilde{S}$ and complementary sensitivity functions $\tilde{T}$ which are shown in Figure 3.18 and Figure 3.21 confirms this observation.

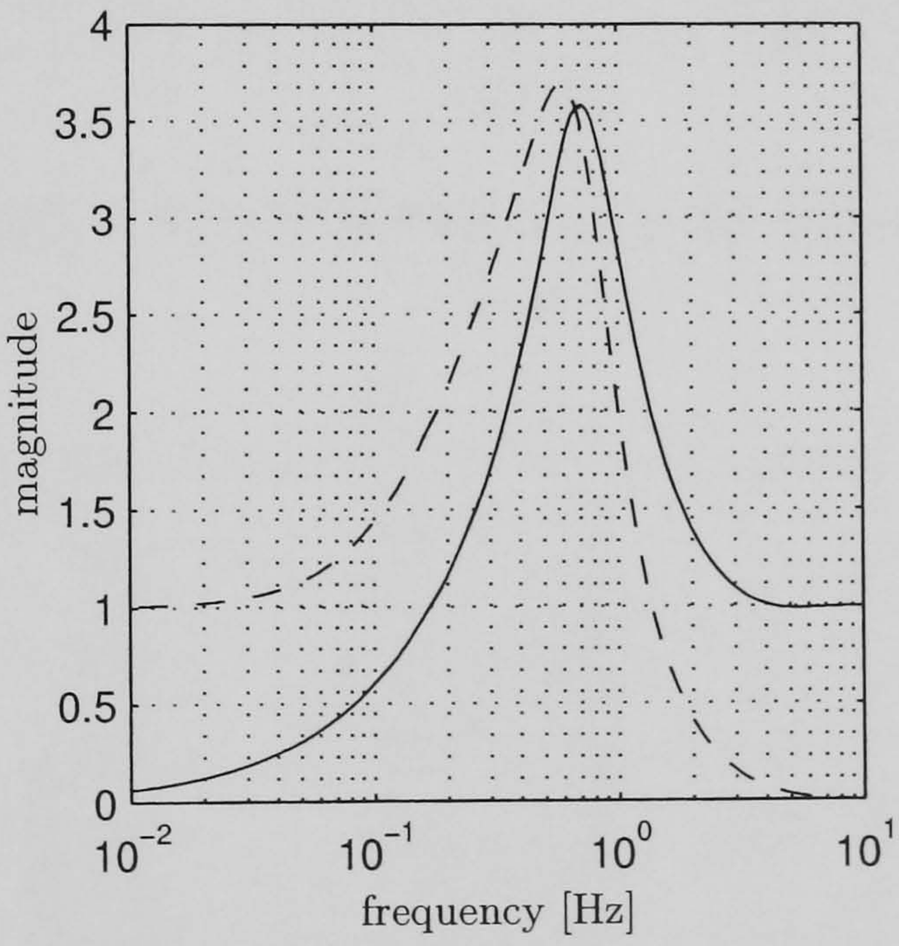

Figure 3.19: Sensitivity function $\tilde{S}$ (solid) and complementary sensitivity function $\tilde{T}$ (dashed) for controller corresponding to Figure 3.18. The inner loop dynamics were neglected in the design of the angle controller but included in the computation of $\tilde{S}$ and $\tilde{T}$.

Note that the nominal dynamics of the inner closed-loop system have been incorporated in the computation of $\tilde{S}$ and $\tilde{T}$ for the angle control loop. The peak of $\tilde{S}$ and $\tilde{T}$ occurs at a frequency of 0.72 Hz. This corresponds to a period of 1.4 s which is equivalent to the period of the oscillations observed in Figure 3.20. However, there is always a possibility that the inner loop becomes slow due to fatigue. Fatigue mainly results in the reduction of the DC gain of the muscle which then results in a reduction of the closed-loop bandwidth.

This is especially an issue when working with paraplegic subjects.

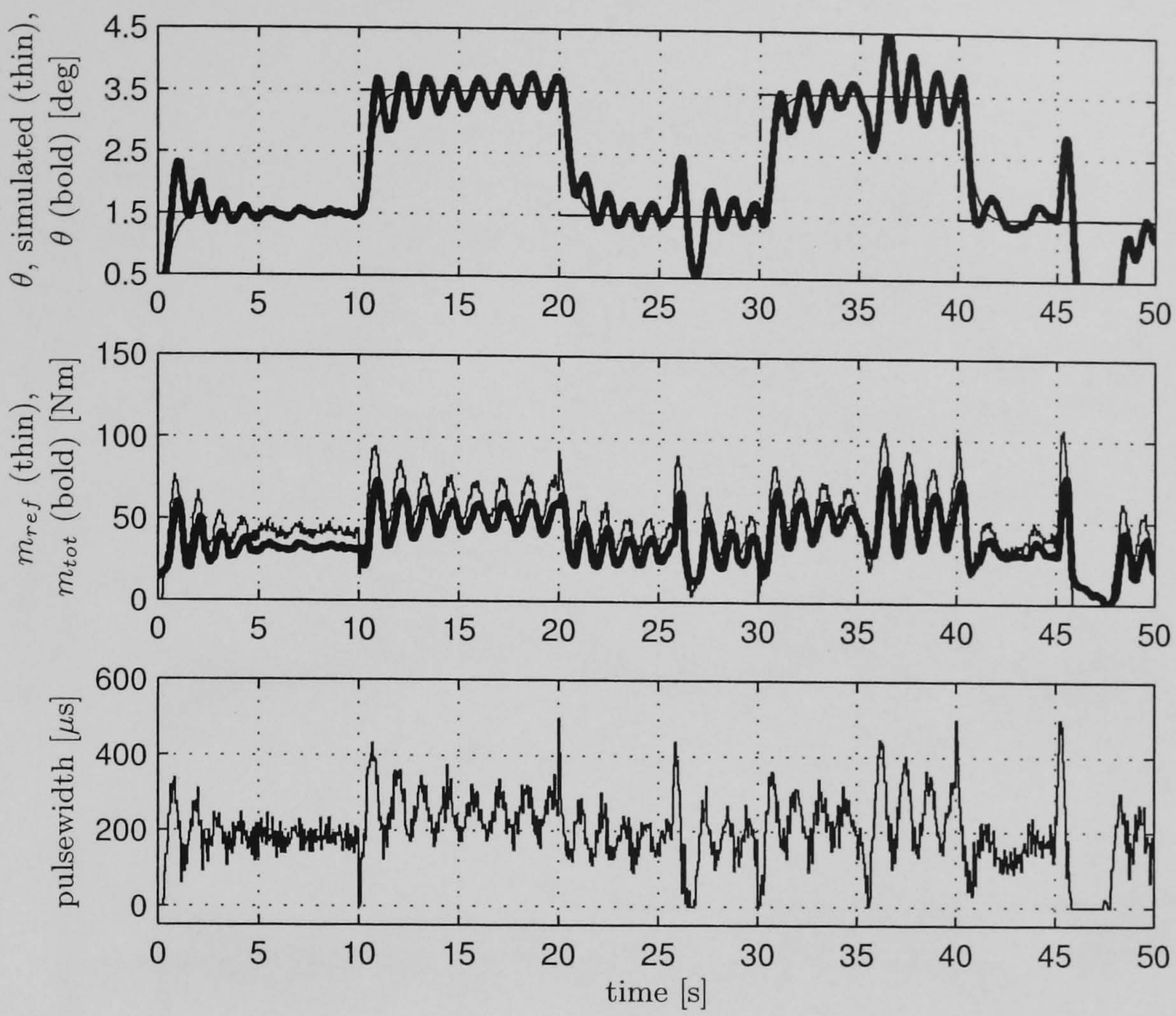

Figure 3.20: As Figure 3.18 (intact subject), but for slow inner loop ($t_{r,c}^m = 0.2\,\mathrm{s}$.)

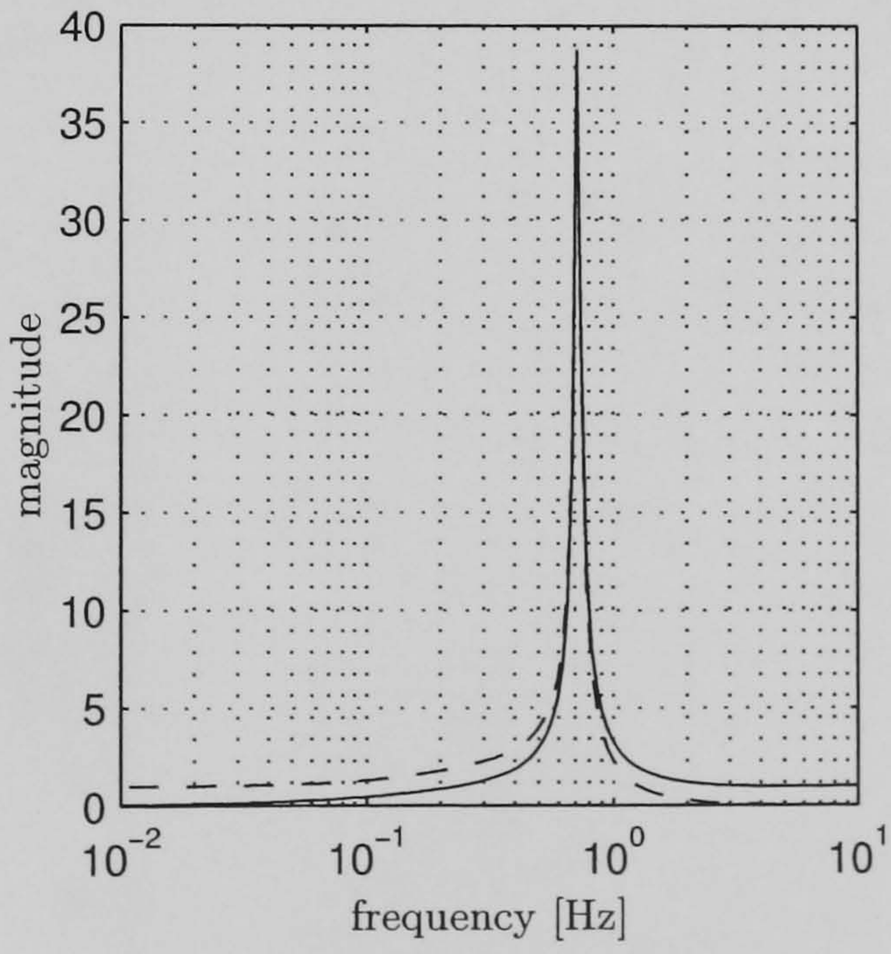

Figure 3.21: Sensitivity function $\tilde{S}$ (solid) and complementary sensitivity function $\tilde{T}$ (dashed) for controller corresponding to Figure 3.20. The inner loop dynamics were neglected in the design of the angle controller but included in the computation of $\tilde{S}$ and $\tilde{T}$.

The effect of and potential improvements resulting from inclusion of the inner closed-loop dynamics in the plant employed for the design of the angle control loop.

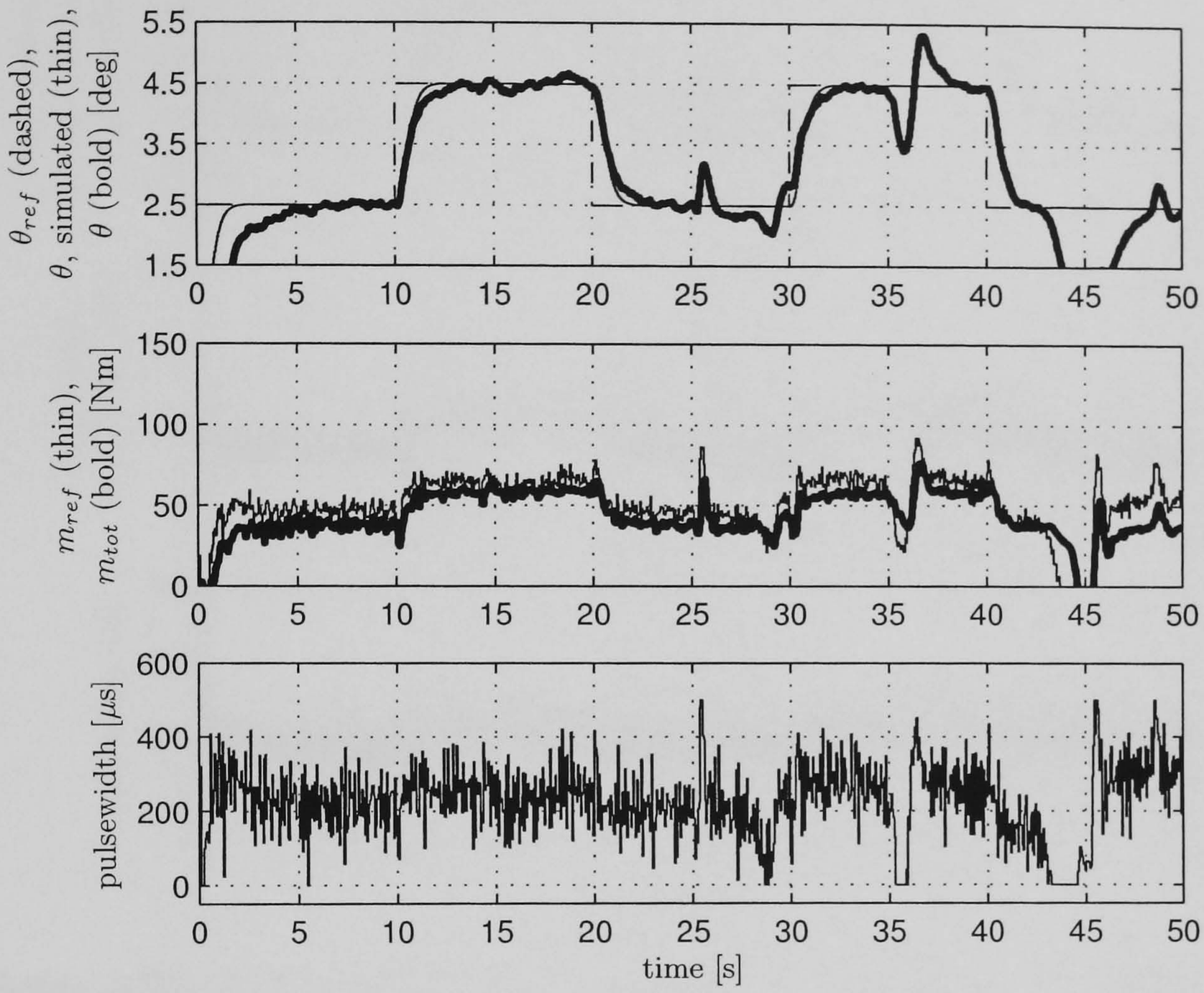

Figure 3.22: Body angle control (intact subject). Inner loop dynamics taken into account for the outer loop design. Fast inner loop ($t^m_{r,c} = 0.15\,\mathrm{s}$).

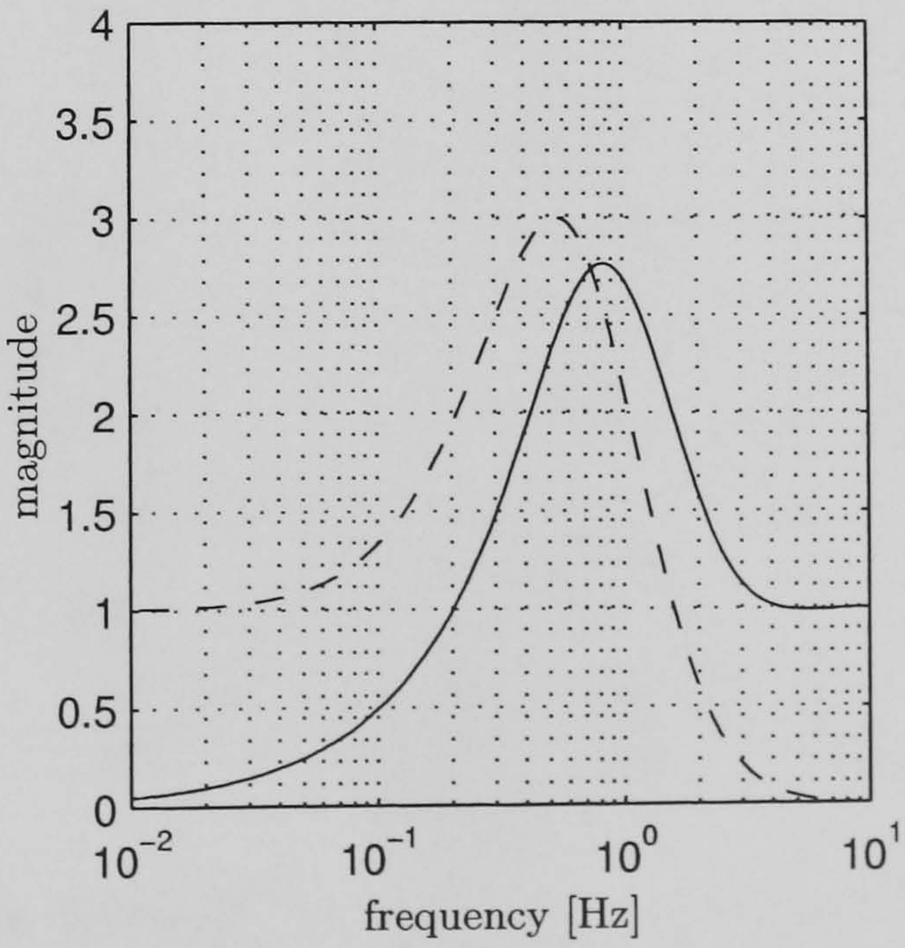

Figure 3.23: Sensitivity function $\tilde{S}$ (solid) and complementary sensitivity function $\tilde{T}$ (dashed) for controller corresponding to Figure 3.22. The inner loop dynamics are taken into account, both in the design of the angle controller and in the computation of $\tilde{S}$ and $\tilde{T}$.

For the results shown in Figure 3.22 and Figure 3.24 the inner loop dynamics were taken into account for outer loop design.

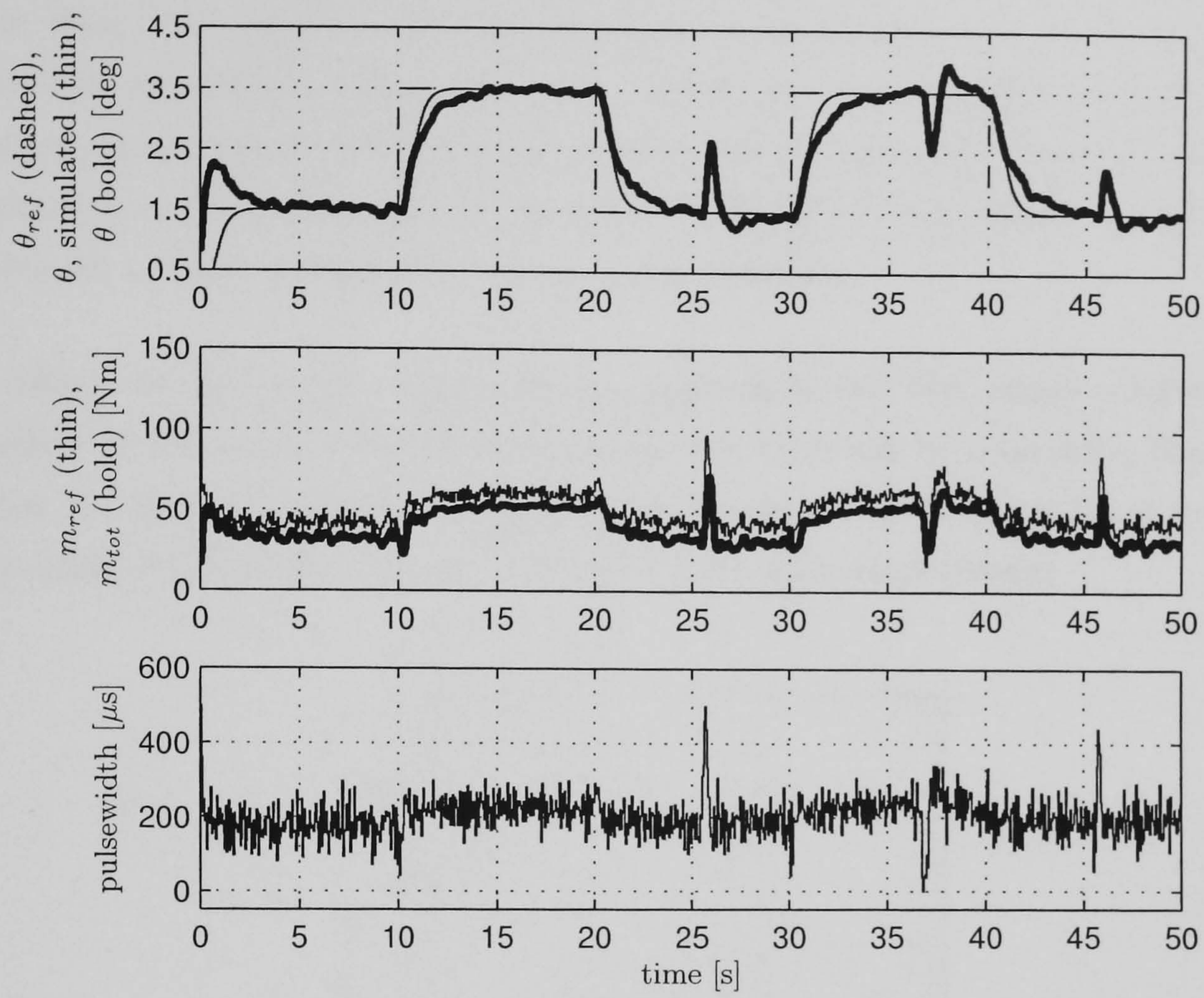

Figure 3.24: As Figure 3.22 (intact subject), but for slow inner loop ($t^m_{r,c} = 0.2\,\mathrm{s}$.)

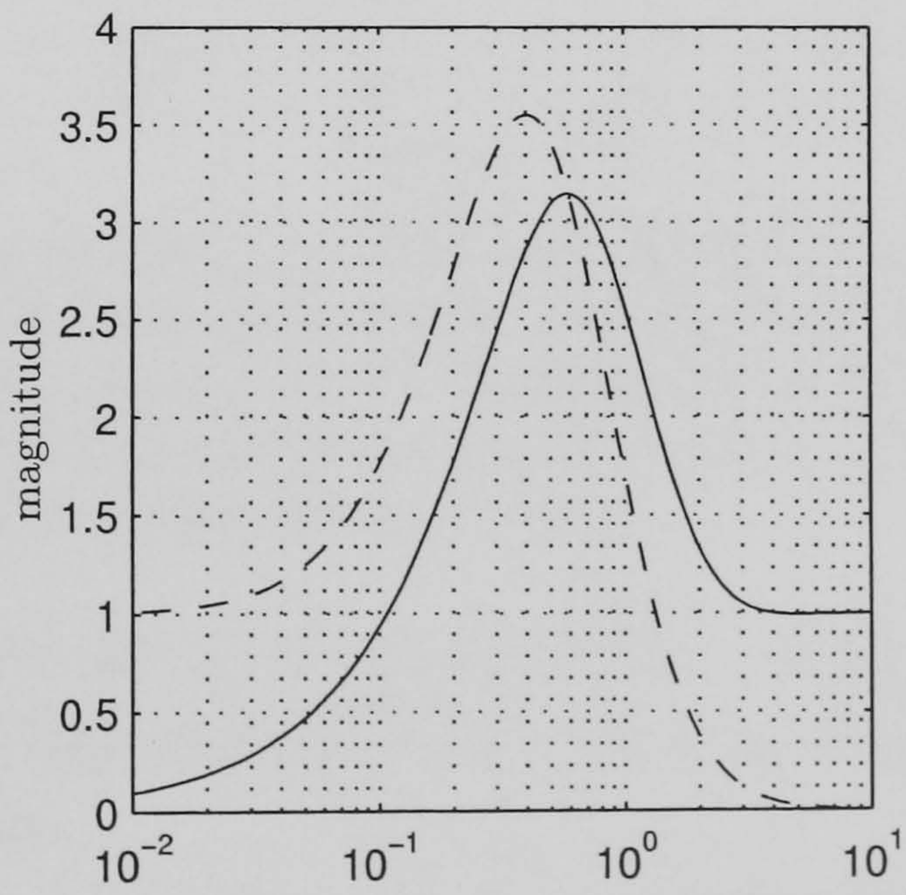

Figure 3.25: Sensitivity function $\tilde{S}$ (solid) and complementary sensitivity function $\tilde{T}$ (dashed) for controller corresponding to Figure 3.24. The inner loop dynamics are taken into account, both in the design of the angle controller and in the computation of $\tilde{S}$ and $\tilde{T}$.

A notch filter design was also employed. Figure 3.22 shows a design with a fast moment control loop ($t^m_{r,c} = 0.15\,\mathrm{s}$), whereas the inner loop is slower for the results shown in Figure 3.24 ($t^m_{r,c} = 0.20\,\mathrm{s}$).

For these two cases the corresponding sensitivity functions $\tilde{S}$ and $\tilde{T}$ are plotted in Figure 3.23 and Figure 3.25, respectively. It can be seen that the performance of the overall system is less dependent on the bandwidth of the inner loop if the inner loop is considered in the outer loop design. However, it turned out that stable standing could not be achieved without a notch filter design being included.

The effect of the notch filter design approach for the angle control design. The effect of the notch filter design approach can be found by comparing the sensitivity function $\tilde{S}$ and the complementary sensitivity function $\tilde{T}$ with and without a notch filter design being employed (cf. Figure 3.26 and Figure 3.23, respectively).

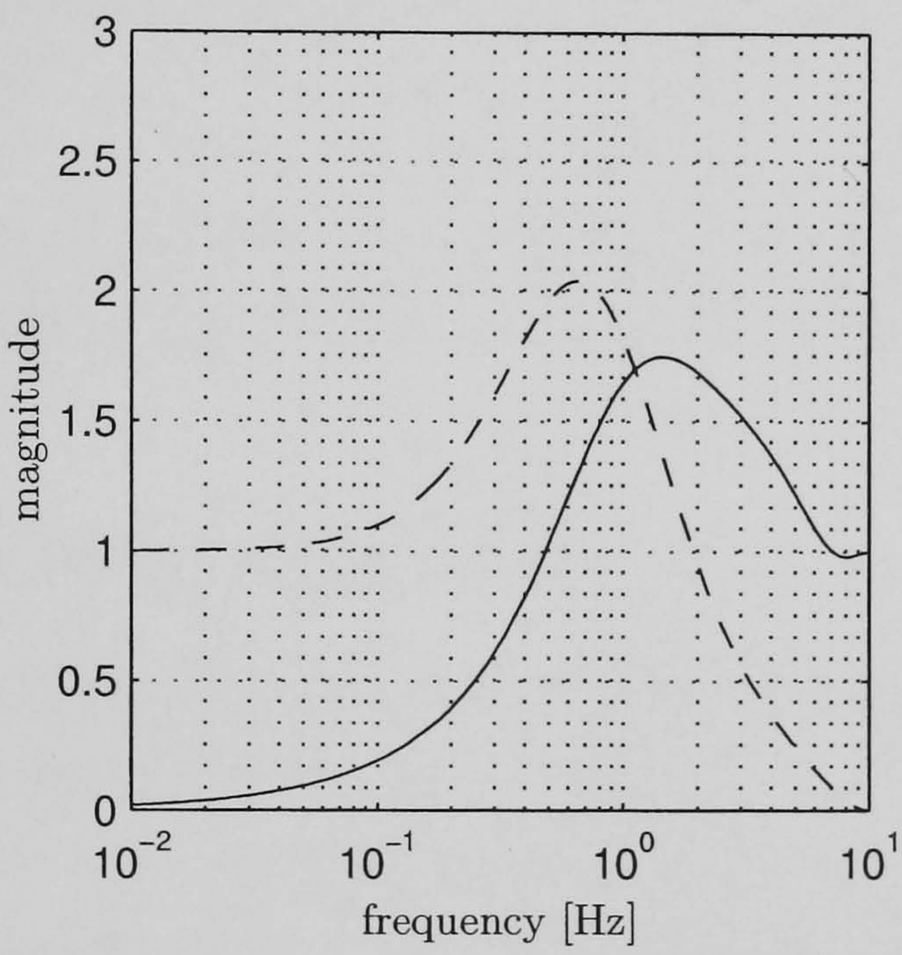

Figure 3.26: Sensitivity function $\tilde{S}$ (solid) and complementary sensitivity function $\tilde{T}$ (dashed) for body angle control when the inner loop is considered for outer loop design but no notch filter approach is employed. The additional closed-loop poles which have to be specified when no notch filter is employed are located in the origin of the z-plane.

One effect of the notch filter is that it causes the complementary sensitivity function $\tilde{T}$ to decrease faster for high frequencies, thus increasing robustness of the closed-loop against measurement noise.

The main effect, though, is seen in the input sensitivity functions for the two designs (cf. Figure 3.27). The input sensitivity function is defined as the transfer function from measurement noise to control signal. Clearly, the design without a notch filter is much more sensitive to measurement noise. Indeed, simulations show that the controllers perform equally well without measurement noise, but that the controller without the notch filter

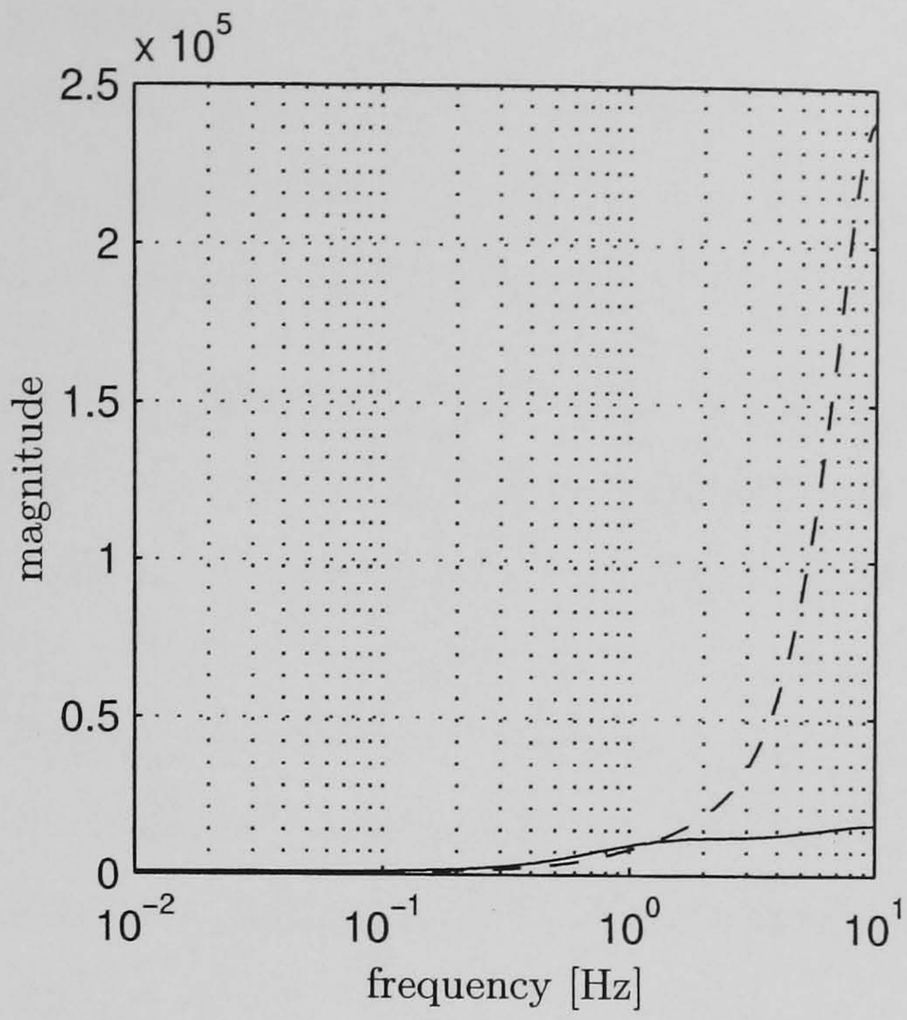

Figure 3.27: Input sensitivity function for body angle control with (solid) and without notch filter approach (dashed). The additional closed-loop poles which have to be specified when no notch filter is employed are located in the origin of the z-plane.

becomes unstable as soon as noise is added. Since measurement noise is always present during the experiments, this explains the need to use a controller design with notch filter.

3.7 Conclusions (Intact Subject)

The experimental results with intact subjects show that the proposed control approach for unsupported standing performs reliably, and according to the design formulation. A number of design options have been investigated and the influence on the system's behaviour is clear. The design parameters, such as rise-time and damping of the closed-loop response have a clear physical interpretation and allow easy tuning during an experimental session. This is important since the complete design procedure starting with identification of the muscle dynamics to the control design has to be carried out as quickly as possible while the subject stands in the apparatus. This is even more important when working with paraplegic subjects because of their limited muscle power and their proneness to fatigue.

The pole assignment approach gives a closed-loop response which is independent of the nominal plant model. Therefore, the suggested method is more generally applicable than the previously suggested LQG approach considering the variable properties of artificially stimulated muscle between individuals.

The new ankle moment control structure assumes the moment control plant as a SISO system with a common stimulation signal for both legs and the added response of the left and right leg as the single output. While we believe this is a better way to deal with the

left and right asymmetry, which is particularly present in paraplegic subjects, this also accelerates the entire identification and design procedure.

The aim of the experiments with intact subjects was to find the most suitable control design configuration with respect to the investigated design options:

- **Inner loop—as fast as possible and with no integral action.** It has been seen that a slow inner loop can potentially destabilise the overall control system. In general, it is important to maintain a bandwidth as high as possible for the inner moment control loop. This is best achieved if the inner loop is designed without integral action because an integrator is known to have destabilising effect in general. A steady state error in the moment loop is of little significance on the performance of the overall system, since integral action in the outer loop ensures a zero steady state error for the body angle.

- **Outer loop—inclusion of the inner loop dynamics in the design plant for the outer loop.** Paraplegic subjects in particular are prone to muscle fatigue which reduces the bandwidth of the moment loop. Therefore, we suggest to include the nominal inner loop dynamics in the design plant for the body angle control loop. It has been seen that this reduces the dependence of the performance of the overall system on the inner loop bandwidth.

- **Outer loop—notch filter approach for the outer control loop.** We found that when the inner loop is included in the outer loop design plant the outer control loop is to sensitive to measurement noise resulting in instability. Therefore, a notch filter design is required.

3.8 Experimental Results with Paraplegic Subjects

The results presented in this section are from different sessions. However, the results of test C, test PRBS, test M, and test T are from the same session, while the results of test D are from a different session.

3.8.1 Results of Test C

Typical results of test C for the paraplegic subject can be seen in Figure 3.28.

It can be seen that the muscles of the paraplegic subject are much weaker than those of the intact subject. A much higher current is necessary to obtain a reasonable response from the muscle. Furthermore, the saturated output of the muscles is much lower than with the intact subject as can be seen particularly in the right leg (cf. Figure 3.11). Also, there seems to be a quite significant asymmetry between the left and right leg. The currents were selected as 120 mA for the left leg and 110 mA for the right leg.

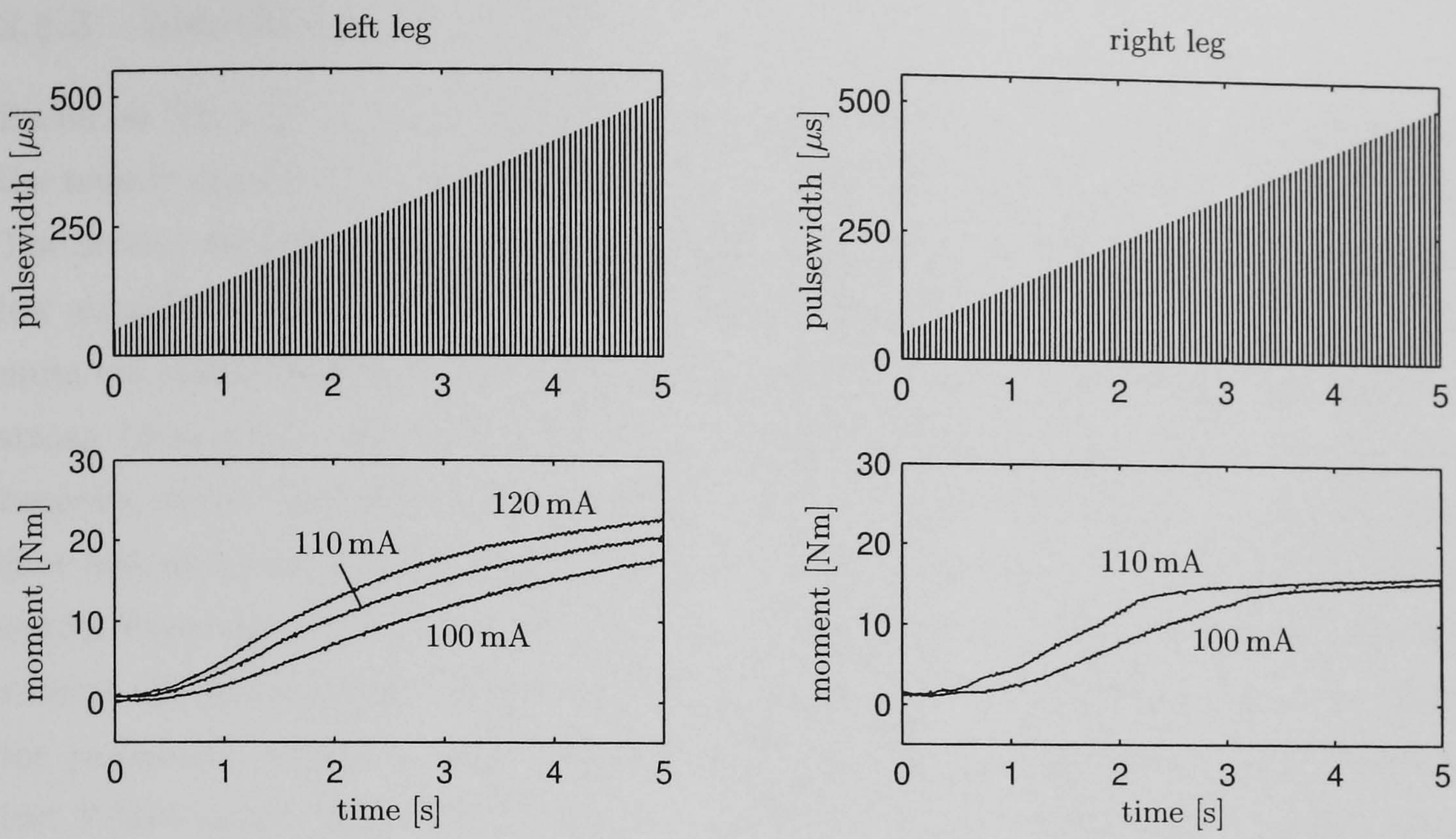

Figure 3.28: Results of test C (paraplegic subject). The upper plot shows the sequence of impulses with ramping pulsewidth, applied to the muscle. The bottom plot shows the measured response of the muscles: for the left leg for three different current levels 100, 110 and 120 mA, for the right leg for 100 and 110 mA.

3.8.2 Results of Test PRBS

Results of test PRBS are shown in Figure 3.29. Input/output data are collected around three mean values of pulsewidth of 150, 200, and 250 μs. Test PRBS was shortened to 10 seconds in order to reduce fatigue.

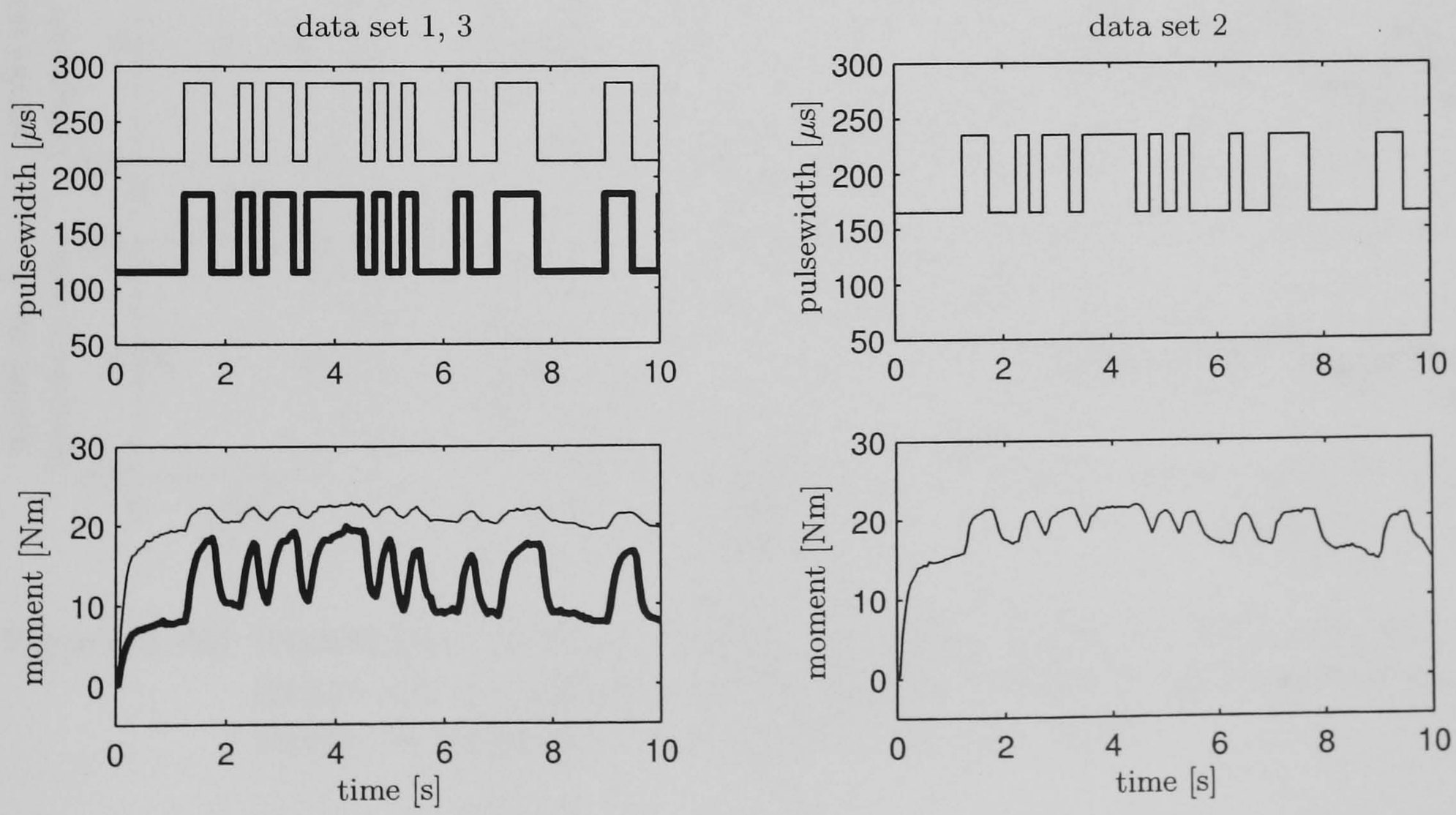

Figure 3.29: Results of test PRBS (paraplegic subject), cf. Figure 3.12. The first two seconds were cut off for the model estimation process.

3.8.3 Identification

Based on the input/output data shown in Figure 3.29 we identified three local models of the muscle dynamics as described in section 3.6.3. The results are shown in Figure 3.30. The inverse recruitment pattern of the artificial stimulation can clearly be recognised. At low stimulation levels (model no. 1) fast and strong (but susceptible to fatigue) motor units are mainly recruited. The step response is fast and the muscle response is relatively strong (first row). At higher stimulation levels the step response of the muscle model becomes slower and the muscle response weaker as more and more slower and weaker (but fatigue resistent) motor units are recruited. Furthermore, as a comparison with the results from the intact subject (cf. Figure 3.13) shows, the results with the paraplegic subject are less accurate. There are a number of explanations. First, the estimation for the paraplegic subject is based on a smaller data set. Second, the measured response of test PRBS seems to be influenced by a trend for the paraplegic subject which was not removed for the estimation process. This trend is probably due to fatigue. Finally, test PRBS might generally be more corrupted by disturbances such as spasticity.

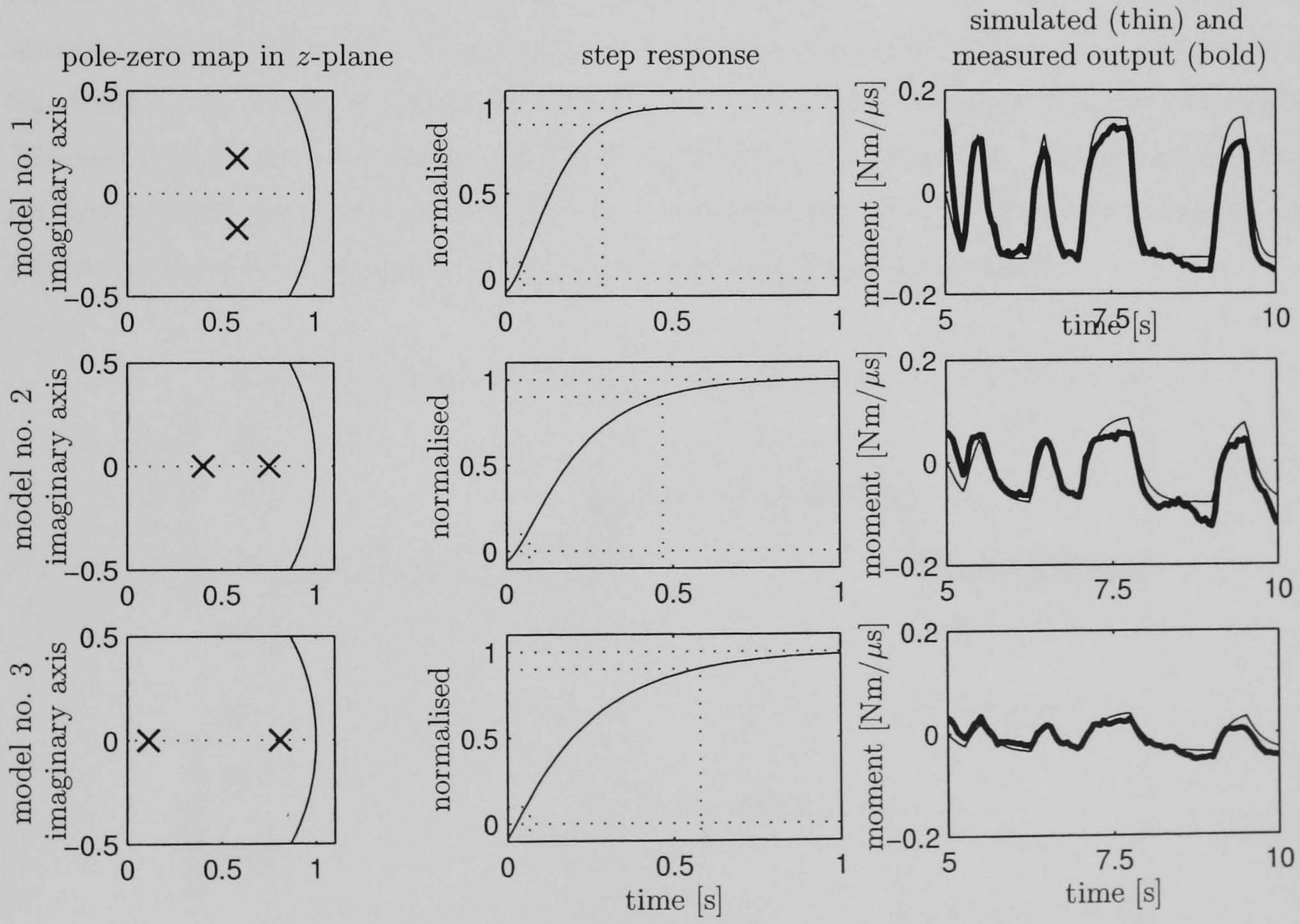

Figure 3.30: Identification results (paraplegic subject). The pole location, the step response and a comparison of the simulated output of the identified model versus the measured output is shown for each model.

The results of the identification process are summarised in Table 3.2. The model with

the highest gain was used for the control design as this choice improves robustness against recruitment nonlinearities.

model no.	pulsewidth [μs]	transfer function $G_p(q^{-1})$	rise time [s]	DC gain [Nm/μs]
1	**150**	$\mathbf{\frac{2.734 \cdot 10^{-2} q^{-1}}{1-1.173 q^{-1}+0.373 q^{-2}}}$	**0.24**	**0.14**
2	200	$\frac{1.240 \cdot 10^{-2} q^{-1}}{1-1.156 q^{-1}+0.303 q^{-2}}$	0.40	0.08
3	250	$\frac{0.669 \cdot 10^{-2} q^{-1}}{1-0.922 q^{-1}+0.091 q^{-2}}$	0.51	0.04

Table 3.2: Identification results (paraplegic subject). The transfer function, rise time and DC gain for each model. The highlighted model was selected for control design.

3.8.4 Ankle Moment Control Test—Results Test M

Results of the moment control test are shown in Figure 3.31. A square wave reference moment is provided with a mean value of 10 Nm, an amplitude of 10 Nm, and a period of 5 s. Figure 3.31 shows that the moment control loop works according to its specification. The fact that there is a calibration offset in the moment measurement is of little significance for the performance of the overall system. This happens due to small movements of the subject relative to the apparatus which are not completely preventable.

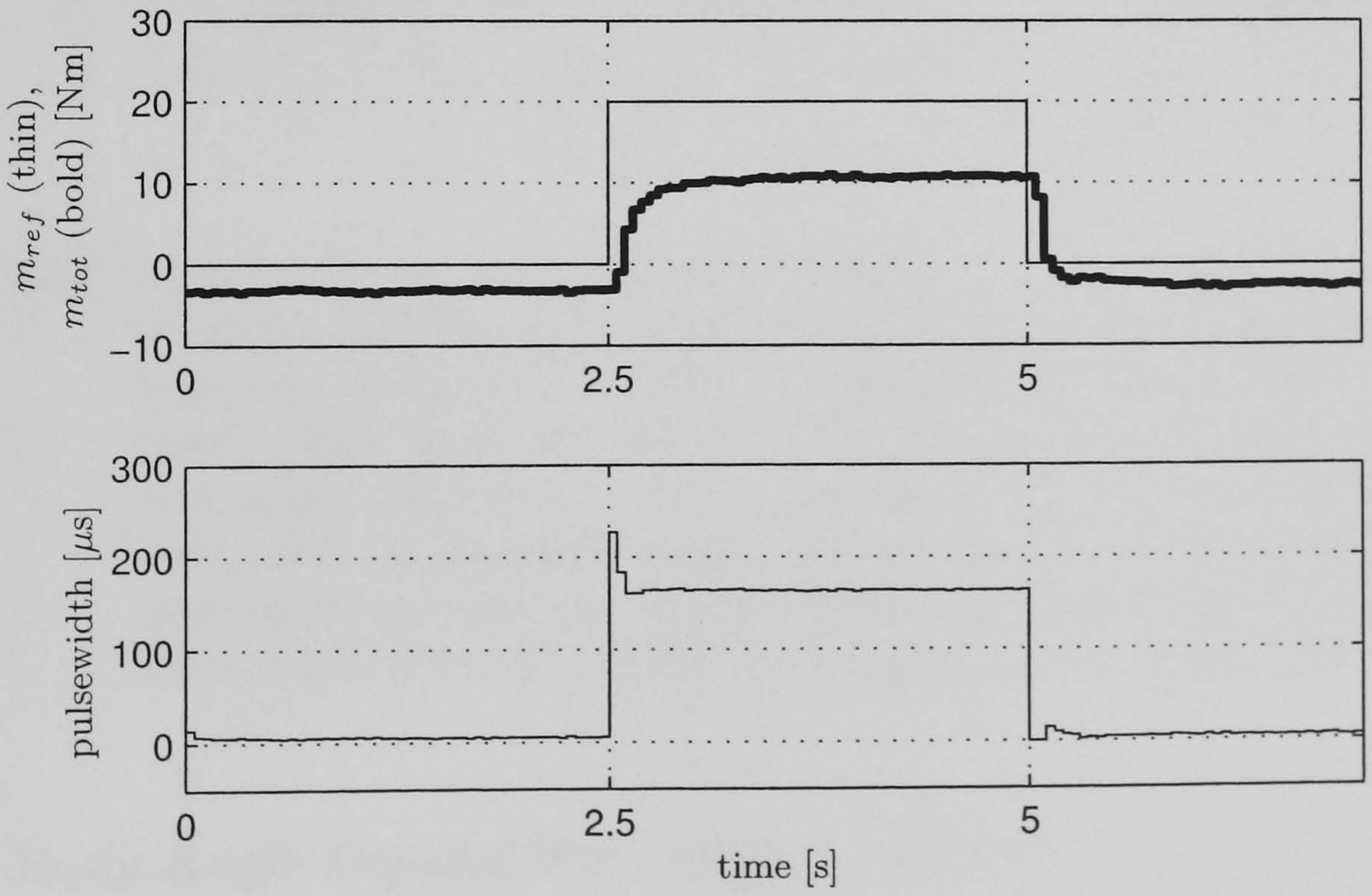

Figure 3.31: Muscle moment control (paraplegic subject). Control design parameters are $t_{r,c}^m = 0.2\,\text{s}$, $\zeta_c^m = 0.999$, $t_{r,o}^m = 0.10\,\text{s}$, $\zeta_o^m = 0.999$.

3.8.5 Body Angle Control Test—Results Test T

Results of closed-loop control of unsupported standing are shown in Figures 3.32–3.34. First, a test of undisturbed square wave reference tracking is shown (cf. Figure 3.32). The mean value of the reference signal is 0.75°, the amplitude is 0.5° and the period is 20 s. The physical parameter of the subject were assumed as $J = 110\,\mathrm{kgm}^2$, $\tilde{m} = 90\,\mathrm{kg}$, $l = 1\,\mathrm{m}$. The subject was able to stand for 50 s. The trial was then stopped. The closed-loop response is oscillatory, but the reason for this might be inaccuracy in the model of the body.

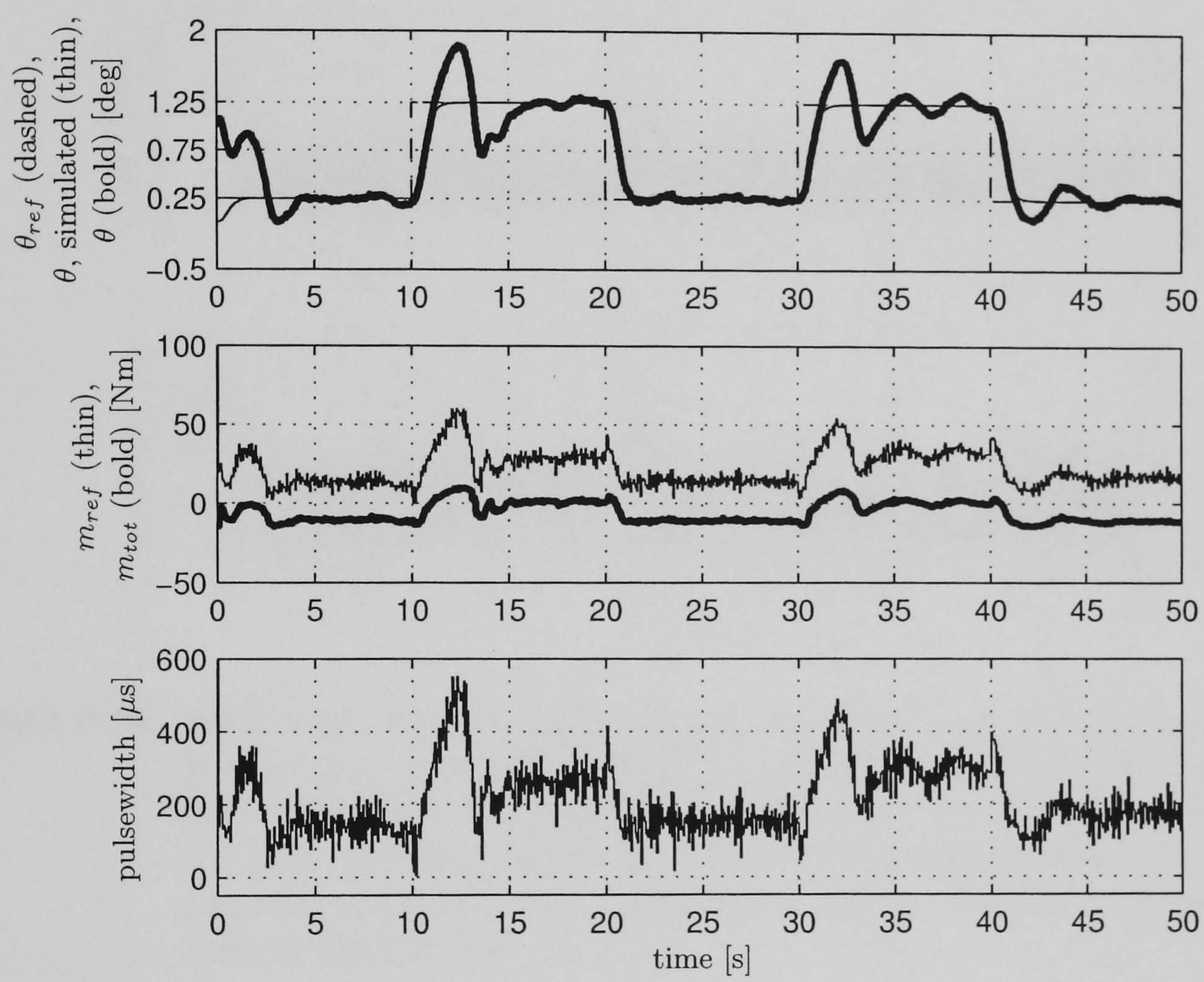

Figure 3.32: Body angle control (paraplegic subject), results of test T: Square wave reference tracking test. The upper plot shows the measured (bold) and reference (dashed) body angle as well as a plot of simulated control loop (thin) which gives an impression of the accuracy of the model (muscle and body). The plot in the middle shows the requested muscle moment (thin) and the measured muscle moment (bold). The lower plot shows the stimulation pulsewidth. Control design parameter are $t^m_{r,c} = 0.7\,\mathrm{s}$, $\zeta^m_c = 0.999$, $t^m_{r,o} = 0.7\,\mathrm{s}$, $\zeta^m_o = 0.999$, moment loop as in Figure 3.31.

3.8.6 Body Angle Control Test—Results Test D

Results of the closed-loop disturbance rejection test (test D) are shown in Figures 3.33. The results shown are not from the same session as the previous results, although the design parameters are the same as in Figure 3.32. Disturbances were applied by pulling the subject forward at chest level. The subject remained stable but the last disturbance

in Figure 3.33 at $t = 35\,\mathrm{s}$ caused the subject to fall. It was generally observed that the subject could easily be destabilised by pulling forward or pushing backward.

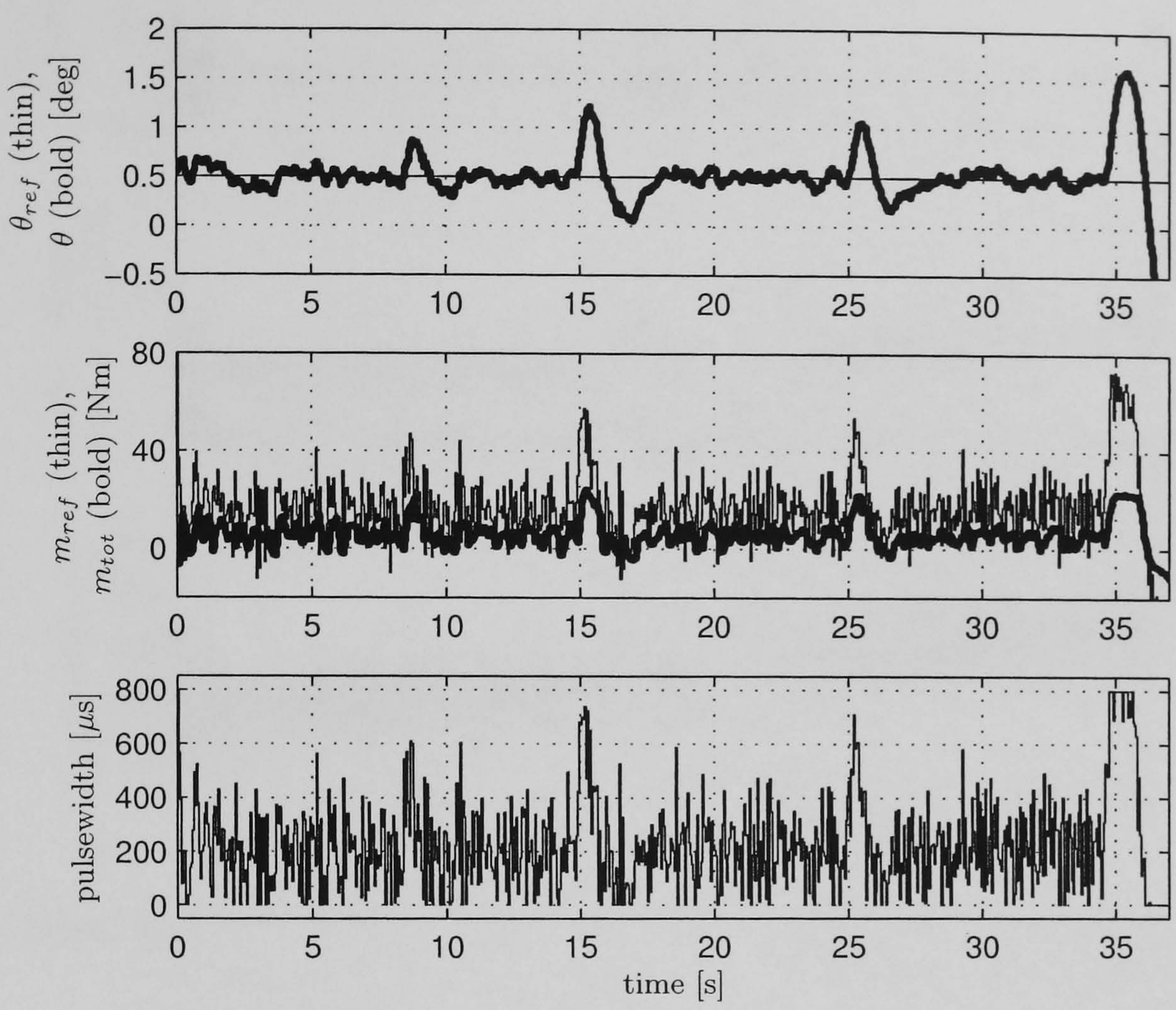

Figure 3.33: Body angle control (paraplegic subject), results of test D: Disturbance rejection test. A constant reference value is requested for the body angle at 0.5°. The subject was pulled forward at $t = 8\,\mathrm{s}$, $t = 15\,\mathrm{s}$, $t = 25\,\mathrm{s}$, and $t = 35\,\mathrm{s}$. The final disturbance caused the subject to fall. Control design parameters are the same as in Figure 3.32 but results are from a different experimental session.

3.8.7 Body Angle Control Test—Results Test F

Results of the fatigue resistance test (test F) are shown in Figure 3.34. External disturbances were also applied during the test at times $t = 90\,\mathrm{s}$ and $t = 110\,\mathrm{s}$ although this test was carried out to explore the maximal achievable period of standing. In this test fatigue caused the subject to fall after 200 s.

3.9 Conclusions (Paraplegic Subject)

The goal of this study was to verify and improve the results from Hunt *et al.* [1997] and Munih *et al.* [1997] which aimed to show that unsupported standing—without arm support—can be achieved in paraplegia by artificial stimulation of the calf muscles and by

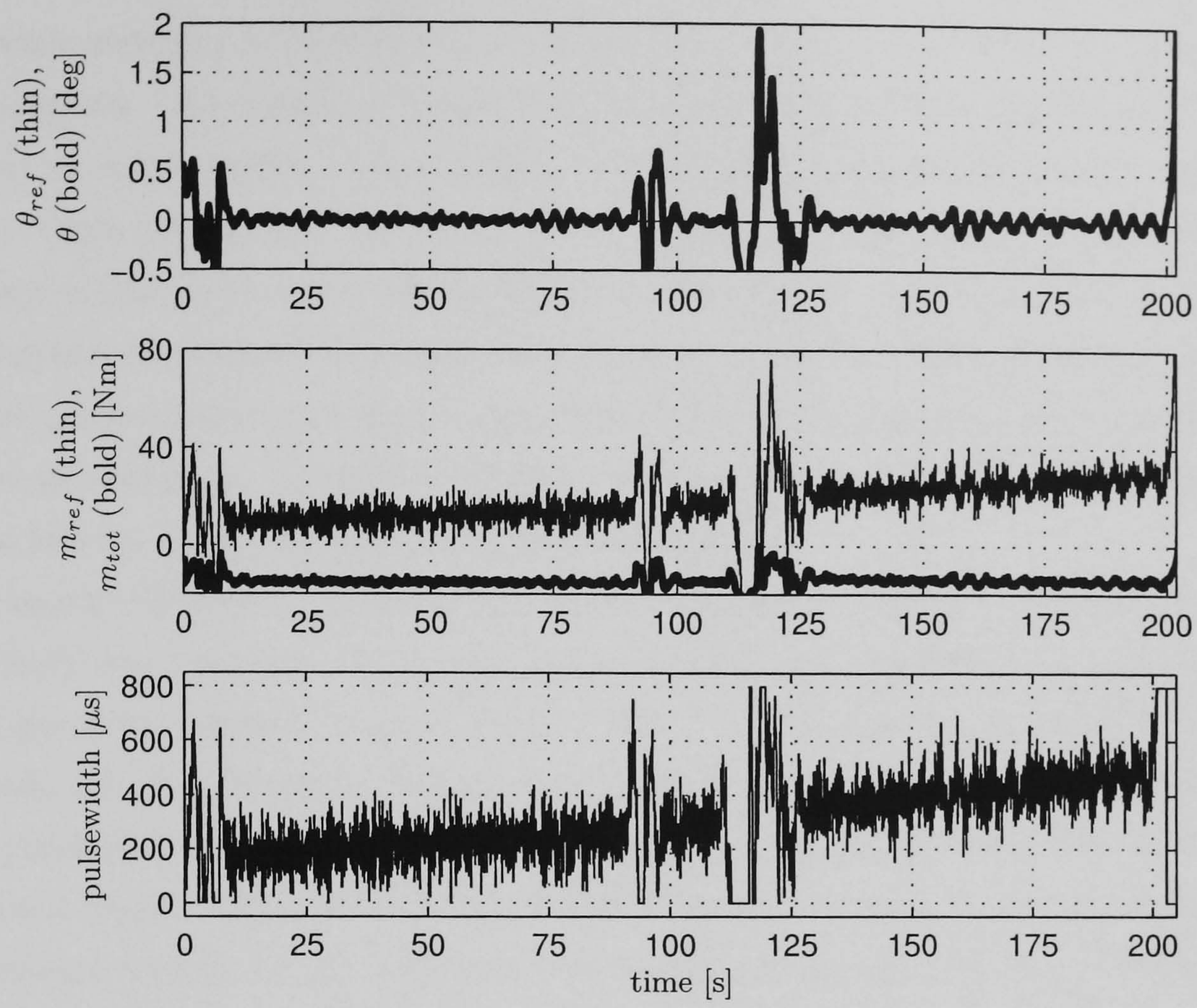

Figure 3.34: Results of test F (paraplegic subject). External disturbance applied at $t = 90\,\mathrm{s}$ and $t = 110\,\mathrm{s}$. After both disturbances the subject had to be stabilised by the experimenter and unsupported standing was resumed from 130 s onwards until fatigue caused the subject to fall after ca. 200 s. Despite the reference angle of 0°, the subject is not in the neutral position since a non-zero moment is requested by the angle controller and plantarflexor stimulation is necessary to maintain stability.

doing so using the paralysed subject's own muscle power. In Hunt *et al.* [1997] and Munih *et al.* [1997] experiments were carried out with one 35 year old subject with a complete SCI at level T5. Unsupported standing could only be achieved for ca. 20 s, mainly due to general weakness of the paralysed muscles, rapid fatigue and spasticity.

A cascaded control structure has been employed but with a number of key changes compared to Hunt *et al.* [1997]; Munih *et al.* [1997] (see section 3.2). The results have shown that unsupported standing can be achieved for considerable periods of time. The longest achieved period ever with any controller was more than seven minutes [Holderbaum and Hunt, 2001; Holderbaum *et al.*, 2002]. Small external disturbances can be rejected.

The modifications in the control design approach resulted in a faster and simpler design procedure. The control design approach proved reliable and the achievable periods of unsupported standing are significantly increased from those reported by Hunt *et al.* [1997]; Munih *et al.* [1997]. Although the properties of the muscle can vary from day to day, consistent results could be achieved with the same set of design parameters.

However, the limiting factor remains the general weakness of the muscles in the paraplegic while virtually unlimited periods of standing could be achieved with neurologically-intact subjects. Only small moments could be generated which were sufficient to stabilise the body at small angles of inclination. Larger disturbances could easily cause loss of balance. Once the muscles were fatigued, no further standing could be achieved with the paraplegic subject even after resting periods of up to 20 minutes. It is generally conceivable to strengthen the muscle by further training, e.g. using loads during muscle training but any time limited muscle training is not comparable to the every day strain on the muscles involved in standing. Therefore, muscle weakness and fatigue will remain the inherent limiting factors in unsupported standing in paraplegia.

An important feature of the study in this chapter is that any influence of the intact upper body was excluded. Practical, useful neuro-prostheses, however, will have to take advantage of the residual sensory-motor abilities of the paraplegic subject. We call this integrated voluntary control. The necessary muscle moment to hold the erect body upright can be minimised when the subject is allowed to use their upper body. On the other hand, the brain is quite a sophisticated control system, hitherto unmatched in its performance by any artificial control system, adaptive and capable of dealing with time-varying and non-linear system behaviour. Therefore it is only natural to use its capabilities for maintaining balance and to restore standing. This theme is pursued in the following chapters.

Chapter 4

Control of Ankle Joint Stiffness using FES while Standing

4.1 Summary

Aim: The aim was to investigate the feasibility of ankle stiffness control using FES and the extent to which it can contribute to the task of stabilising the body. The work was intended as a pilot study towards standing supported by FES-controlled ankle stiffness.

Methods: The work was carried out using the Wobbler apparatus described in section 2.2. Ankle stiffness was controlled by feedback control of the ankle moment involving stimulation of plantarflexor and dorsiflexor muscles and a suitable switching strategy. A series of experimental tests was carried out with one intact subject and one paraplegic subject.

Results: The results show that ankle stiffness control can be achieved by means of FES within certain limitations. When plantarflexor stimulation is required the ankle stiffness is close to the requested value. However, when dorsiflexor stimulation is required the desired ankle stiffness cannot be achieved.

Conclusion: Two factors limit the quality of stiffness control, (i) the bandwidth of the moment control loop, and (ii) the muscle strength. Ankle stiffness has the potential to facilitate the task of stabilising the body. However, an external input is required to actually achieve stability.

Contribution: The author's contribution to this study consists of the development and implementation of the experimental software. Furthermore, the author was involved in the execution of the experiments and in the analysis and interpretation of the results. This work is published in Hunt *et al.* [2000b] and Hunt *et al.* [2001b].

4.2 Motivation

The study presented in this chapter is mainly motivated by the work of Matjačić and Bajd [1998a,b]. Their work, in turn, was inspired by the strategy used by intact subjects when recovering from disturbances imposed in anterior/posterior directions. It is known that intact subjects elicit an "ankle" strategy to recover from small disturbances while they use a "hip" strategy to recover from larger disturbances, or a combination of both [Horak and Nashner, 1986]. The ankle strategy is characterised by a distal to proximal muscle activity starting in the muscles acting at the ankle joint. Balance is maintained by moving the body primarily around the ankle joint. The hip strategy, on the other hand, is characterised by muscle activation antagonist to those in the ankle strategy in the opposite proximal-to-distal sequence. The resulting movement is primarily concentrated around the hip joints.

Matjačić and Bajd [1998a,b] observed some similarities between motor resources of intact subjects employing a combined balancing strategy and the residual sensory motor abilities of paraplegic subjects with a lesion at thoracic level. An intact subject employing a mixed strategy responds to perturbations by moving the trunk around the hip joint while the knees remain extended. Increased activity of the ankle agonist and antagonist muscles results in an increased impedance of the ankle joint. A person employing this kind of balancing strategy behaves approximately like a double-link inverted pendulum.

Matjačić and Bajd thought a similar balancing activity might be elicited in a paraplegic subject. They demonstrated that a paraplegic subject with a lesion at thoracic level, after appropriate training, was able to stabilise himself using his trunk muscles if an appropriate level of stiffness around the ankle joints is present (approximately 10 Nm/deg). The subject was assumed as a double-link inverted pendulum with the knees mechanically braced by an experimental apparatus, similar to the MRF described in Section 2.3 but restricted to one degree-of-freedom in the sagittal plane only, and the trunk free to move voluntarily. These were encouraging results since stiffness is a convenient variable to regulate as it requires only measurement of the ankle joint angle (and not derivatives of the angle).

The ankle stiffness was applied by hydraulic actuators, which acted as artificial ankle joints. However, while a hydraulic system is a good experimental setup to study the feasibility of the principle, it is not useful as a practical tool. Our aim was therefore to replace the hydraulic component of the standing scheme proposed by Matjačić and Bajd [1998a,b] with an FES-controlled ankle stiffness. FES provides more flexibility and independence compared with a hydraulic system especially when it comes to an implanted system. Furthermore, FES has a greater potential to extend the system towards more functionality.

The work presented in this chapter is a pilot study towards paraplegic standing supported by FES-controlled ankle stiffness. Results of the latter are presented in the next

chapter. This chapter focusses on the feasibility and accuracy of ankle stiffness control using FES of the plantarflexor and dorsiflexor muscle groups. The work reported here was carried out in the "Wobbler" apparatus as described in Section 2.2, which allows the fundamental limitations of the approach to be studied with minimal intervention from central motor control. The presented approach involves stimulation of the ankle extensor and flexor muscles which extends our previous work on unsupported standing where only forward-leaning postures and plantarflexor stimulation were considered.

4.3 Experimental Setup

The experimental apparatus used in this experiment is described in Section 2.2. The subject is assumed as a single-link inverted pendulum. This configuration is secured by a custom made body shell attached to the subject's back which allows movement only around the ankle joint (cf. Figure 2.1 on page 11). Ankle joint movement can be induced using different modes of operation of the Wobbler:

1. The ropes are kept taut and body is fixed in an upright posture. The feet are "wobbled" and the ankle angle is measured at the shaft.
2. The feet are kept in fixed position, but the safety ropes are loosened to allow the body to move back and forth. In this case the ankle angle is inferred from the measured inclination angle.

The experimental control structure is shown in Figure 4.1. The body angle of inclination θ is measured and multiplied by the desired value of ankle stiffness K_s. This provides a reference moment m_{ref} for the ankle joint which is under closed-loop control. Depending on whether the subject is leaning forward or backward the plantarflexor muscles or dorsiflexor muscles are stimulated, respectively. In the situation shown in Figure 4.1, the subject is leaning forward and the plantarflexor muscles are stimulated. It can be seen from Figure 4.1 that a stiffness in the ankle joint corresponds to a simple proportional control (P-control) for the inverted pendulum (cf. Figure 3.7, page 42).

It was shown in the previous chapter that even a PD-control strategy is unlikely to be sufficient to stabilise the body. In the physical framework a PD-control is equivalent to a combined stiffness (P-term) and viscosity (D-term) feedback. Nevertheless, in this chapter we want to investigate the contribution of proportional feedback (ankle stiffness) to the problem of stability of the body. The reason is that a stiffness is easy to integrate into the residual sensory motor abilities of a paraplegic subject and, more importantly, easy to realise in terms of sensors (cf. Chapter 6).

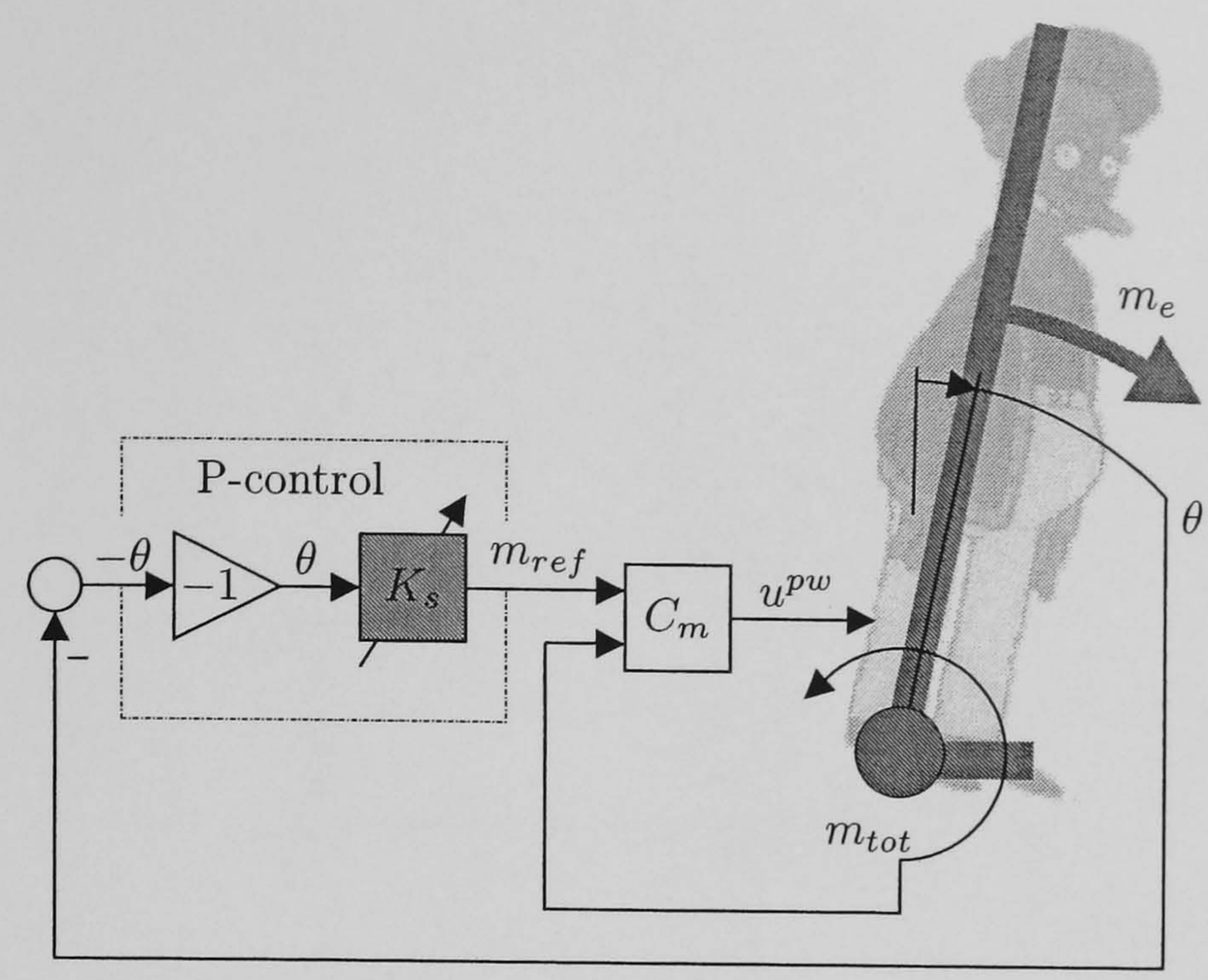

Figure 4.1: Experimental control structure. θ is the inclination angle of the body, m_{tot} is the total ankle moment, u^{pw} is the pulsewidth of stimulation. K_s is the desired stiffness value and C_m is the moment controller. m_e is the external moment applied by the experimenter to stabilise the subject. The situation shown refers to operating mode 2 of the wobbler as described above and forward leaning of the subject. When backward leaning, the dorsiflexor muscles are stimulated and the external moment is applied in the opposite direction.

A model of the body as an inverted pendulum has been derived in Section 3.3.2. Including ankle stiffness k_s[1], the model becomes

$$G_b(s) = \frac{\Theta(s)}{M(s)} = \frac{\frac{-1}{J}}{s^2 + \frac{k_s - \tilde{m}gl}{J}}, \tag{4.1}$$

where $G_b(s)$ is the linear transfer function of the body dynamics, $\Theta(s)$ and $M(s)$ are the Laplace transforms of the body angle θ and m_{tot} and s is the complex variable of the Laplace transformation. The physical parameters of the body are assumed as $\tilde{m} = 70\,\mathrm{kg}$, $J = 70\,\mathrm{kgm}^2$ and $l = 1\,\mathrm{m}$. When $k_s = 0$, the inverted pendulum model is inherently unstable with two poles on the real axis in the complex s-plane. For $0 < k_s < \tilde{m}gl$ the poles migrate towards the origin. For $k_s > \tilde{m}gl$ the poles lie on the imaginary axis (complex conjugate). Figure 4.2 shows the root locus of the inverted pendulum model (4.1) of the body depending on a static ankle stiffness k_s.

Thus, the inverted pendulum cannot be asymptotically stabilised with stiffness alone. Discretisation of the feedback loop and the phase lag due to limited dynamics of the muscle further deteriorate the situation.

Therefore, in order to stabilise the subject during the experiment, an external moment m_e (cf. Figure 4.1) has to be applied by the experimenter. With the conventions of

[1] k_s denotes the stiffness actually effective at the ankle joint which is to be distinguished from the desired stiffness K_s.

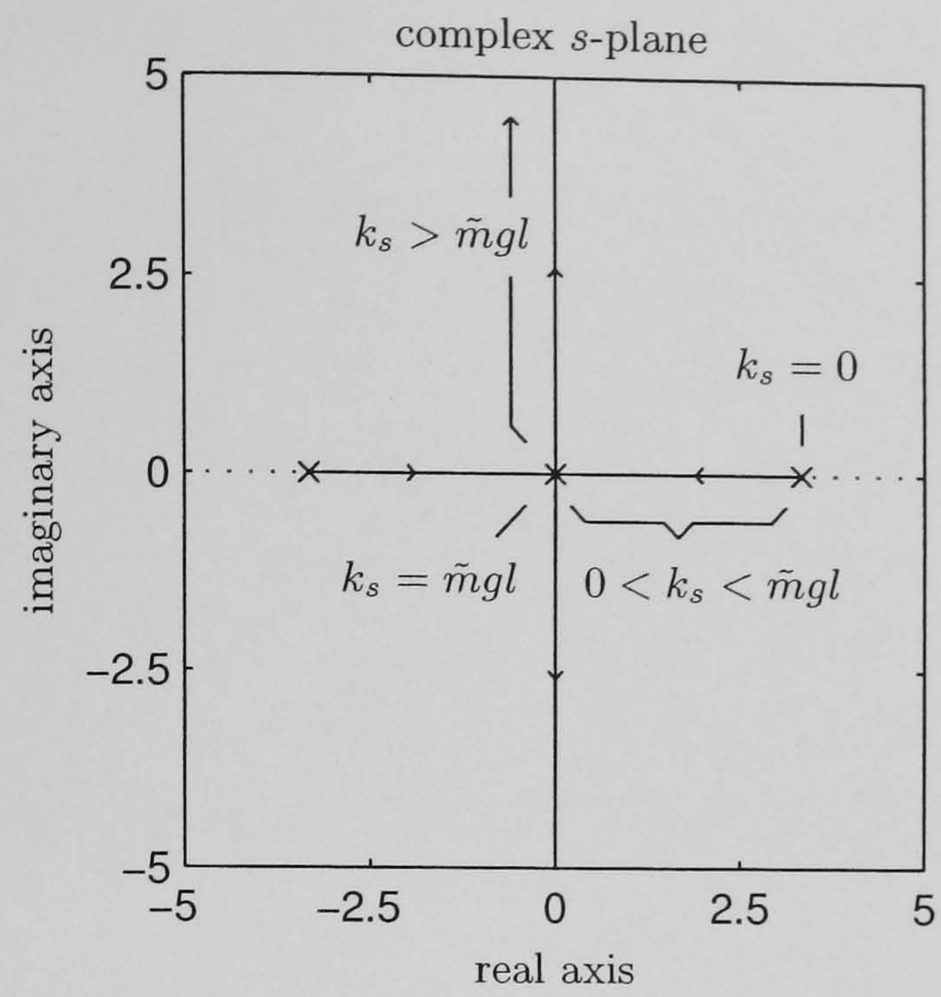

Figure 4.2: Root locus of the inverted pendulum model (4.1) depending on a static ankle stiffness k_s.

Figure 4.1, the external moment can m_e can be estimated as

$$m_e \approx m_{tot} - \tilde{m}gl\theta\,, \tag{4.2}$$

assuming that the angular acceleration of the body is sufficiently small. Here, the external moment is considered positive as the moment necessary to move the body by the experimenter manually around the ankle joint.

According to Figure 4.1, the desired stiffness K_s is given by

$$K_s = \frac{m_{ref}}{\theta}\,. \tag{4.3}$$

However, the stiffness actually acting at the ankle joint k_s is given by

$$k_s = \frac{m_{tot}}{\theta}\,. \tag{4.4}$$

On the other hand, the actually achieved moment m_{tot} and the reference moment m_{ref} are related to each other by the transfer function for reference tracking $G^m_{y/r}(q^{-1})$ as

$$m_{tot} = G^m_{y/r}(q^{-1})m_{ref}\,, \tag{4.5}$$

(cf. Figure 2.14, page 26). Substituting m_{tot} in (4.4) by (4.5) gives

$$k_s = \frac{G^m_{y/r}(q^{-1})m_{ref}}{\theta}\,. \tag{4.6}$$

With (4.3), this shows that $G_{y/r}(q^{-1})$ is indeed the transfer function from the desired, or "reference" stiffness value K_s to the actual achieved stiffness k_s as

$$\frac{k_s}{K_s} = G^m_{y/r}(q^{-1})\,. \tag{4.7}$$

With the proposed control structure, ankle stiffness control is achieved via ankle moment control.

A simple strategy for controlling the agonist/antagonist muscle group was adopted. A single ankle moment controller is designed based on the experimentally identified model of the plantarflexor muscles, where the left and right leg are combined into a SISO system (cf. Figure 3.8, page 43). However, integral action is employed for ankle moment control as we are mainly interested in accurate moment tracking. i.e. $\Delta^m(q^{-1}) = 1 - q^{-1}$ (cf. Figure 2.14). When the controller provides a positive control signal u^{pw} the plantarflexor muscles will be stimulated, while a negative control signal means the dorsiflexor muscles will be stimulated. Thus, a simple switching strategy is employed as shown in Figure 2.17, page 32.

4.4 Experimental Procedure

First a set of identification tests is carried out to establish the amplitude of the stimulation pulses and to identify the dynamic properties of the plantarflexor muscles. The ankle moment controller is based only on the model for the plantarflexor muscles. It is well known that the dorsiflexor muscles are generally weaker than the plantarflexor muscles, so this approach will provide robustness for the dorsiflexor muscles as well, although this approach is conservative and a loss of performance has to be accepted. The identification procedure follows the description in Section 3.4. Following the control design, four major experimental tests were carried out:

1. **Test M.** This is a test of ankle Moment control. In this test the body (ropes taut) and feet (shaft locked) are fixed, and ankle moment is controlled. The reference moment can be positive (plantarflexion) and negative (dorsiflexion). The "outer loop" stiffness control is not active during this test and the reference moment m_{ref} is explicitly specified by the experimenter. Usually, a square wave or a sinusoidal reference moment is specified. The purpose of this test is to evaluate the ankle moment control design and to determine whether accurate control of both positive and negative reference moments can be achieved by a single controller switching between the ankle flexor and extensor muscles.

2. **Test AS.** This is a test of Ankle Stiffness control. Here the body is fixed (ropes taut), but the feet are wobbled in order to achieve a change in ankle angle by manual adjustment of the wobbling speed. This is a test of ankle stiffness control, achieved via ankle moment control, i.e. the reference moment $m_{ref} = K_s\theta$ is determined as in Figure 4.1 by the product of the current ankle angle θ (measured by the shaft potentiometer) and the desired stiffness K_s. This test can be repeated for various values of desired stiffness and wobbling speed.

3. **Test SS.** This test is called **S**tiff **S**tanding. The feet are fixed (no wobbling) but the body is allowed to sway (loose ropes). Here the current body angle θ is measured as the angle of inclination of the body. After selecting the desired stiffness the experimenter can carry out two sub-tests:

   (a) **Test SSa.** The experimenter holds the subject in some initial position, releases the subject and observes.

   (b) **Test SSb.** The experimenter stands in front of the subject holding onto the body brace. The experimenter then moves the subject manually through a range of angles.

   Tests SSa and SSb can be repeated for various values of desired ankle stiffness.

   The external moment m_e which needs to be applied by the experimenter to move the body manually through various angles can be estimated.

4. **Test EPC.** This test is called **E**xternal **P**osture **C**ontrol. It is carried out under similar conditions to Test SS. In this case the experimenter provides **external control** (moment m_e) by standing in front of the subject and holding on to the body brace at a measured height from the ankles.

   A desired reference angle θ_{ref} is generated and displayed on a screen to the experimenter in realtime together with the measured inclination angle. The desired angle will typically be a sine wave. The task of the experimenter is to make the posture follow the reference angle as accurately as possible.

   The purpose of this test is to assess the ease or difficulty with which external **tracking control** can be achieved. This can be assessed for various desired values of ankle stiffness K_s by comparing the required external forces and the tracking errors. As in Test SS the external moment can be estimated.

4.5 Subjects

Two subjects participated in this study: One neurologically intact subject, 29 years old, male; and one paraplegic subject, 44 years old, male with a complete lesion at level T7/T8, 4 years post injury. He previously participated in the study on unsupported standing reported in the previous chapter and underwent muscle training as reported in Section 3.5.

4.6 Experimental Results with Intact Subject

The results of the identification procedure are similar to those reported in the previous chapter in Section 3.6.

4.6.1 Results of Test M

A test of closed-loop moment control is shown in Figure 4.3 for square wave reference tracking.

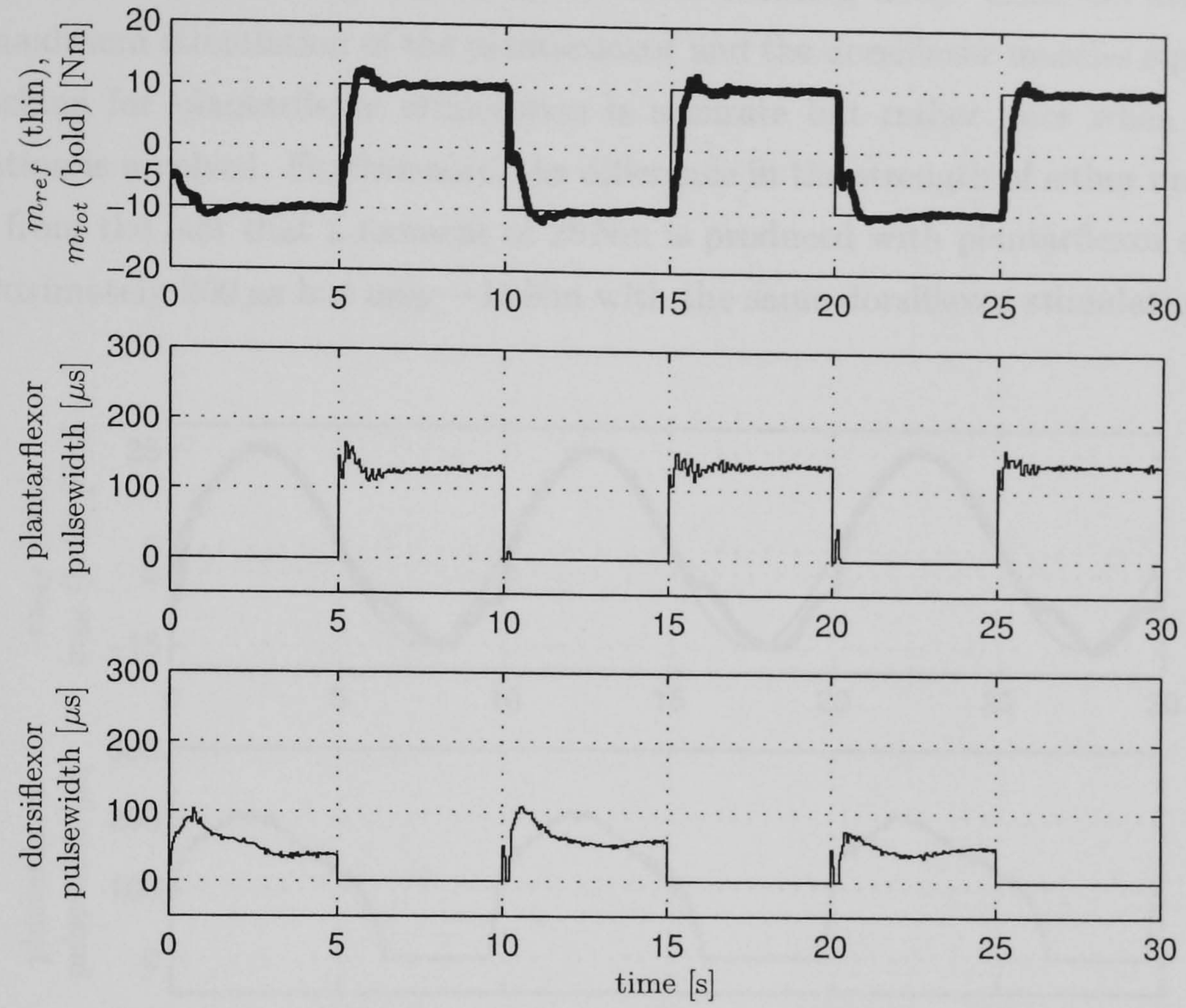

Figure 4.3: Closed-loop moment control with square wave reference tracking around zero with an amplitude of $\pm 10\,\mathrm{Nm}$.

It can be seen that the controller switches between stimulation of the plantarflexor and dorsiflexor muscles to generate either positive or negative moments, as required. Control of plantarflexing moment is fast and accurate. However, when switching from plantarflexing to dorsiflexing, tracking is considerably slower. The reason is that the moment controller is designed based on the plantarflexor model with the highest DC gain to ensure robust stability. The dorsiflexor muscles are, however, much weaker, resulting in a much lower loop gain which then results in poorer tracking performance. Identification results have shown that the DC gain of the dorsiflexor muscles is about a quarter of the DC gain of the plantarflexor muscles.

The fact that a smaller stimulation of the dorsiflexors, although weaker, than of the plantarflexors is required to achieve the same moment is due to the fact that the subject produces a negative moment without stimulation. This can be seen at the beginning of the test at time $t = 0$ where the subject produces a negative moment of approximately $-5\,\mathrm{Nm}$. Moreover, the change in the tracking performance when switching from plantarflexor stimulation to dorsiflexor stimulation occurs at approximately $-5\,\mathrm{Nm}$. We found

it hard to eliminate this phenomenon, due to small movements of the subject, even when held tightly by the safety ropes.

Figure 4.4 shows another test of moment control for sinusoidal reference tracking. This corresponds more closely to the experimental situation of this study and, more importantly, to the situation of standing than a square wave tracking does. Here, we attempted to make maximum stimulation of the plantarflexor and the dorsiflexor muscles equal. Again, the tracking for plantarflexor stimulation is accurate but rather poor when dorsiflexor stimulation is involved. Furthermore, the difference in the strength of either muscle group is seen from the fact that a moment of 25 Nm is produced with plantarflexor stimulation of approximately 200 μs but only -15 Nm with the same dorsiflexor stimulation.

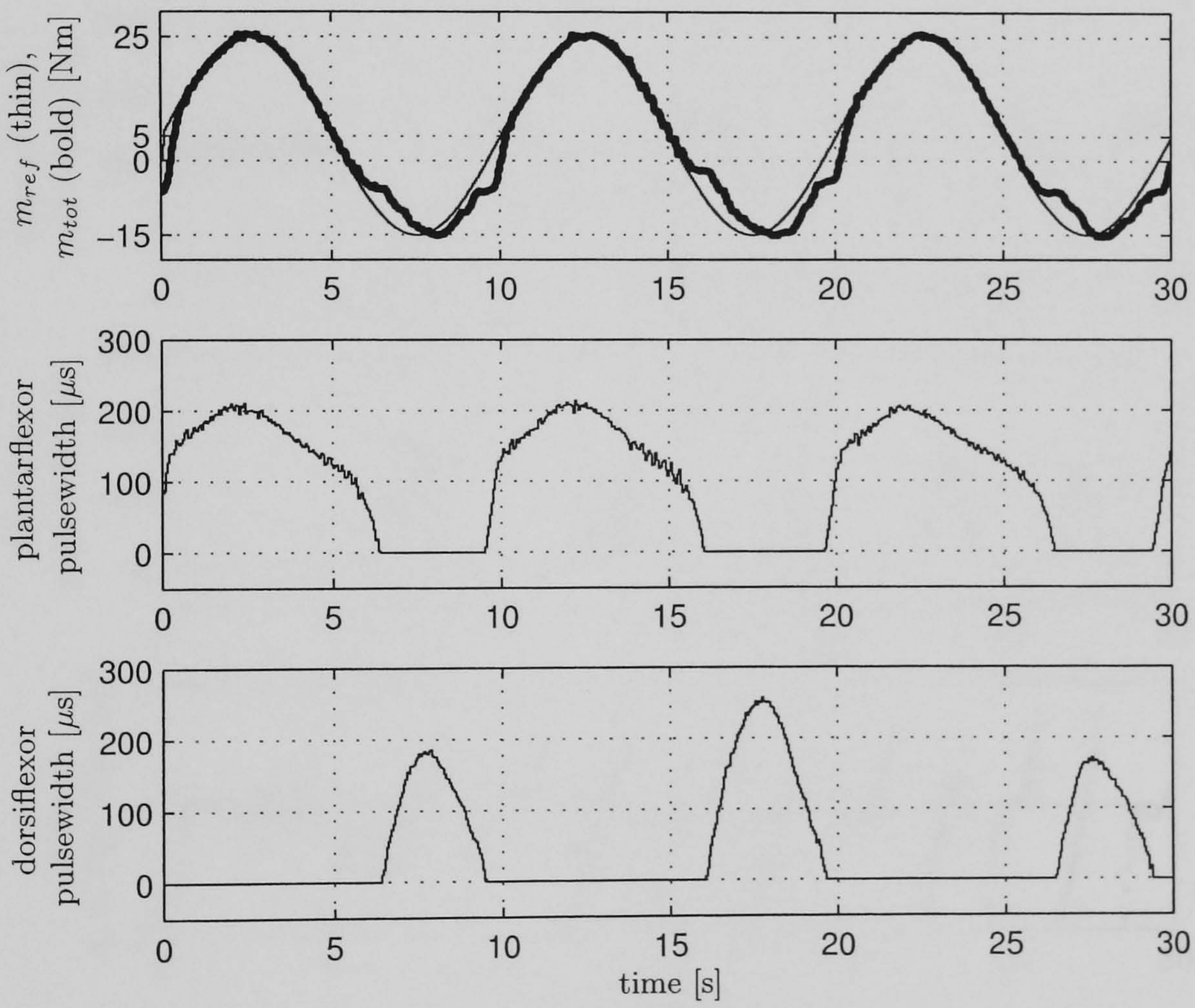

Figure 4.4: Closed-loop moment control with sinusoidal reference tracking with a mean value of 5 Nm and an amplitude of ± 20 Nm.

4.6.2 Results of Test AS

Results from the ankle stiffness control test are shown in Figure 4.5. The body was fixed and the feet were wobbled during this test. The desired stiffness was $K_s = 4\,\mathrm{Nm/deg}$.

The top graph shows the ankle angle θ, measured at the shaft potentiometer. The second graph shows the reference moment $m_{ref} = K_s\theta$ (thin line) and the controlled moment m_{tot} (bold line). The desired stiffness value of 4 Nm/deg is relatively low, and certainly lower than values which would be required for standing. However, this low value

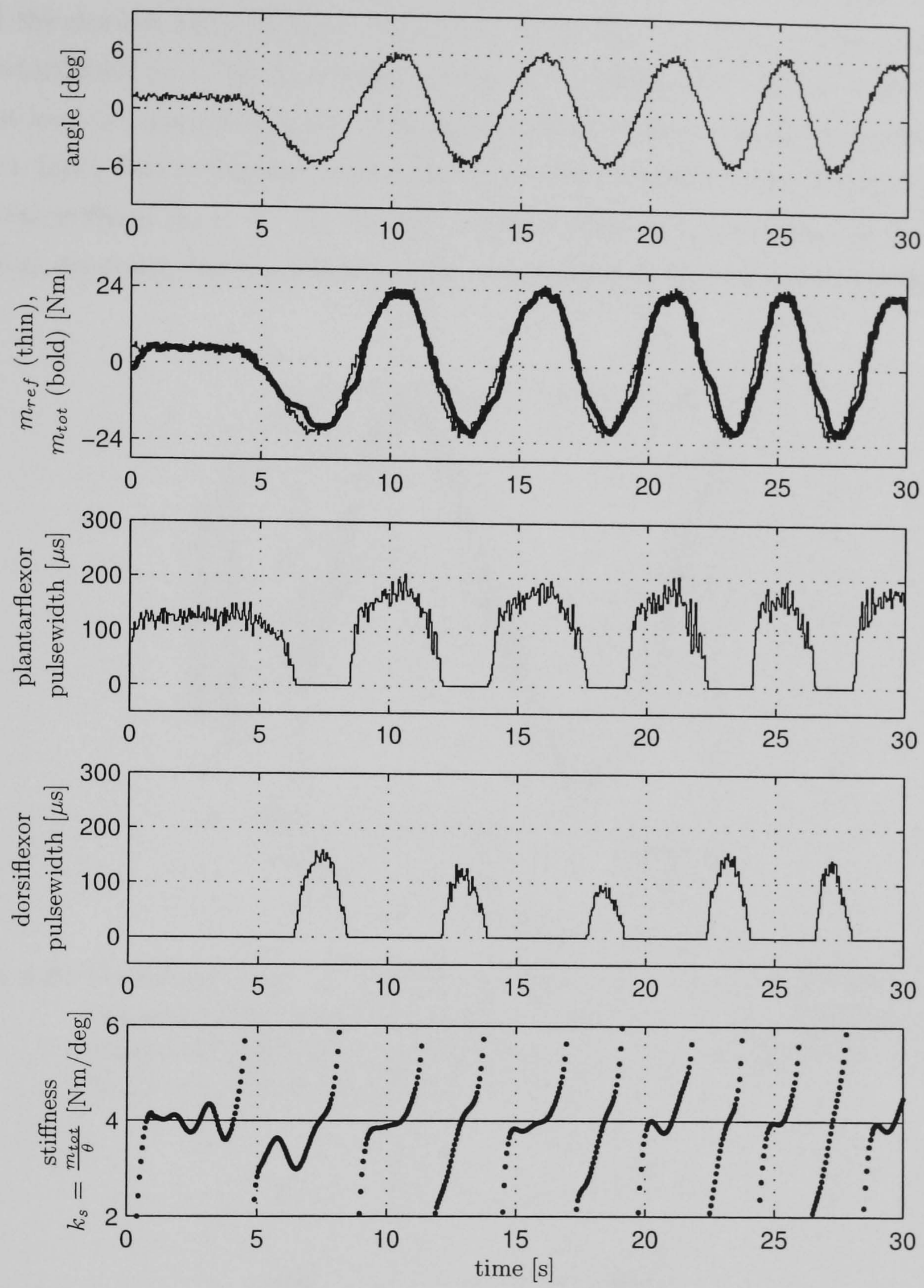

Figure 4.5: Ankle stiffness control (body fixed, feet wobbled) with a desired stiffness of $K_s = 4\,\mathrm{Nm/deg}$.

was selected because of the relatively large amplitude of the ankle angle during this test and the need to constrain the reference moment to within a physically realisable range.

It is seen that the controller switches stimulation between the plantarflexors and dorsiflexors (third and fourth graph of Figure 4.5) to achieve good moment tracking.

The bottom graph shows the actually achieved stiffness at the ankle joints, $k_s = \frac{m_{tot}}{\theta}$. The dots mark the calculated stiffness at the sampled time instants. For this graph, the measured signals of moment and angle were zero-phase-shift digitally filtered (forward and reverse filtered) by a Butterworth filter of order 10 and a cut-off frequency of 1 Hz

in order to eliminate the noise from the data. The actually achieved stiffness centres well around the desired value of $K_s = 4\,\mathrm{Nm/deg}$. Note that the computation of the actually achieved stiffness $k_s = \frac{m_{tot}}{\theta}$ is sensitive to the zero crossing of θ and the bandwidth of the moment loop (cf. equation (4.6)): The angle and the moment signal cross zero at slightly different times due to the limited bandwidth of the moment loop. When $m_{tot} = 0$ and $\theta \neq 0$ the stiffness $k_s = 0$. On the other hand, when $\theta = 0$ and $m_{tot} \neq 0$ the stiffness $k_s \to +\infty$, assuming the bandwidth of the control loop is high compared to the frequency

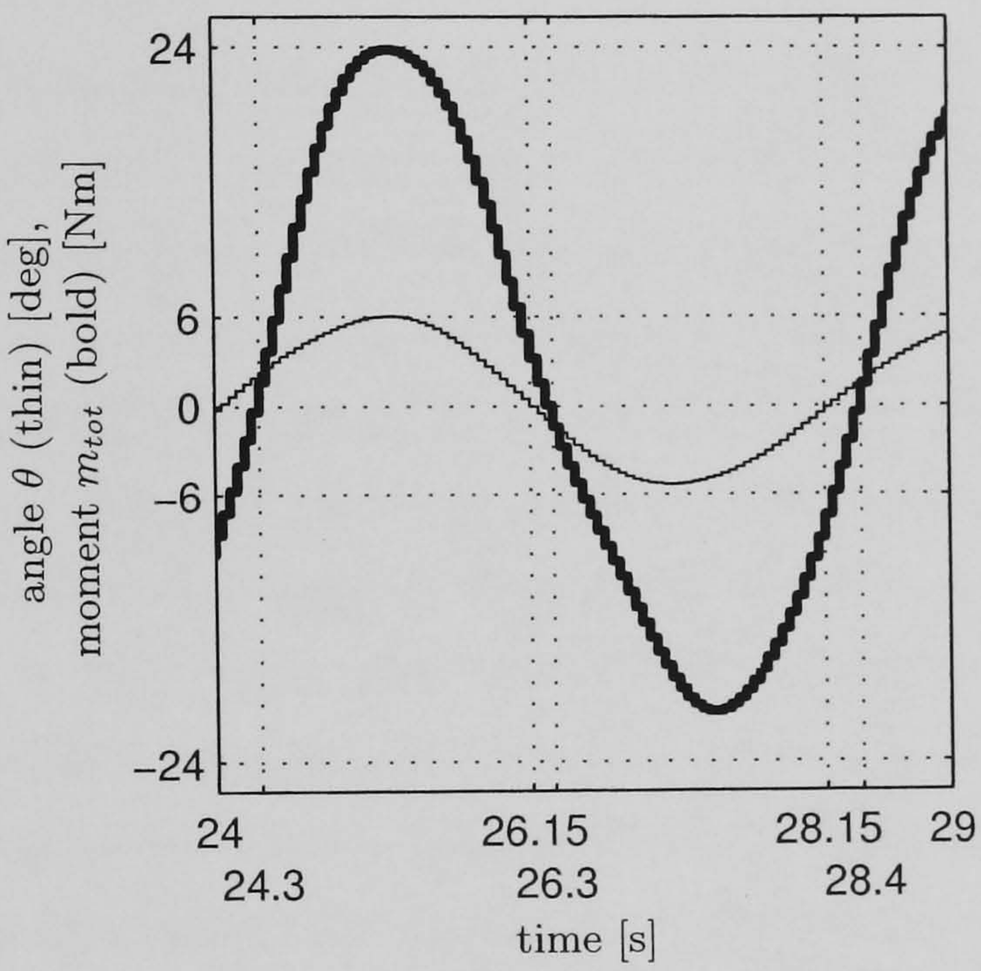

Figure 4.6: Detail of Figure 4.5. Due to the limited bandwidth of moment control loop the controlled moment and the angle cross zero at different times. The computed stiffness is even negative for short intervals ($24 < t < 24.3\,\mathrm{s}$, $26.15 < t < 26.3\,\mathrm{s}$, $28.15 < t < 28.4\,s$).

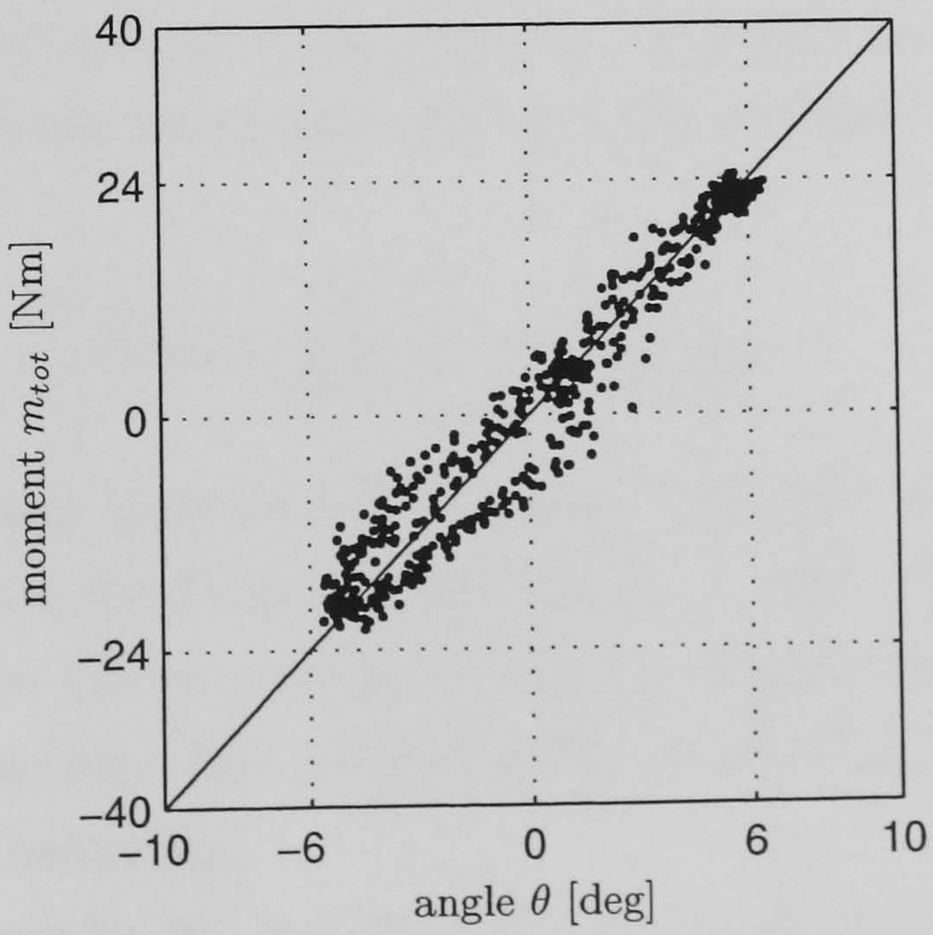

Figure 4.7: Stiffness plot in the phase plane. The straight line represents the desired stiffness of $4\,\mathrm{Nm/deg}$.

of the moment m_{tot} and the angle θ. Figure 4.6 showing a detail of Figure 4.5 clarifies this fact. The calculated stiffness is even negative for short intervals.

A second view of the accuracy of stiffness control during this test is given in Figure 4.7 which is a scatter plot of m_{tot} versus θ. The solid line in this plot represents a "pure" stiffness of 4 Nm/deg. Again, the actually achieved stiffness centres well around the desired value of 4 Nm/deg. The hysteresis is due to the dynamic nature of the controlled stiffness which does not exactly obey a static stiffness.

4.6.3 Results of Test SS

Results from two stiff standing tests (body free to move, feet fixed) are shown in Figure 4.8 and Figure 4.9, respectively. In both cases the desired stiffness was chosen as $K_s = 20\,\mathrm{Nm/deg}$. The top graph shows the body angle θ. The bottom graph shows the estimated external moment (4.2) applied by the experimenter when holding onto the body brace. Results for the subtest SSa are shown in Figure 4.8. Here, the experimenter stands in front of the subject holding onto the body brace and after an initial phase lasting 7 s the body is pulled and held at an angle of approximately $+2\,°$. The experimenter releases the body at time $t \approx 14\,\mathrm{s}$. The high plantarflexor moment of 50 Nm (second graph) pushes the body rapidly back towards the neutral position and at this point ($t \approx 15\,\mathrm{s}$) the experimenter catches the body to prevent it from falling backwards, re-stabilises the subject, and returns the inclination manually to around $2\,°$. This process is repeated at times $t \approx 19\,\mathrm{s}$ and $t \approx 24\,\mathrm{s}$. The fact that the subject is released is reflected in the estimated hand moment (bottom graph) going to zero during the release periods. It was observed during the experiment that if the experimenter does not catch the subject then he falls backwards until caught by the safety ropes. The dorsiflexor muscles will be stimulated due to the required negative moment but these muscles are not strong enough to pull the body forward again. This can be understood by an analysis of the body dynamics. With a stiffness k_s present at the ankle joint, the inverted pendulum model of the body (4.1) becomes

$$G_b(s) = \frac{\Theta(s)}{M(s)} = \frac{\frac{-1}{J}}{s^2 + \frac{k_s - \tilde{m}gl}{J}}\,. \tag{4.8}$$

The poles of the transfer function $G_b(s)$ change from real, one positive one negative, to conjugate complex on the imaginary axis for $k_s > \tilde{m}gl$ (cf. Figure 4.2). For $J = 70\,\mathrm{kgm}^2$, $\tilde{m} = 70\,\mathrm{kg}$, $l = 1\,\mathrm{m}$ as given in section 4.3, this corresponds to a stiffness value of approximately 12 Nm/deg. The specified stiffness, however, was 20 Nm/deg, therefore resulting in oscillatory behaviour.

Figure 4.9 shows results for subtest SSb. Good moment tracking is achieved for forward-leaning posture ($\theta > 0$, for $t < 12\,\mathrm{s}$ and $t > 21.5\,\mathrm{s}$) via plantarflexor stimulation. The actually achieved stiffness k_s (second graph from the bottom) is close to the

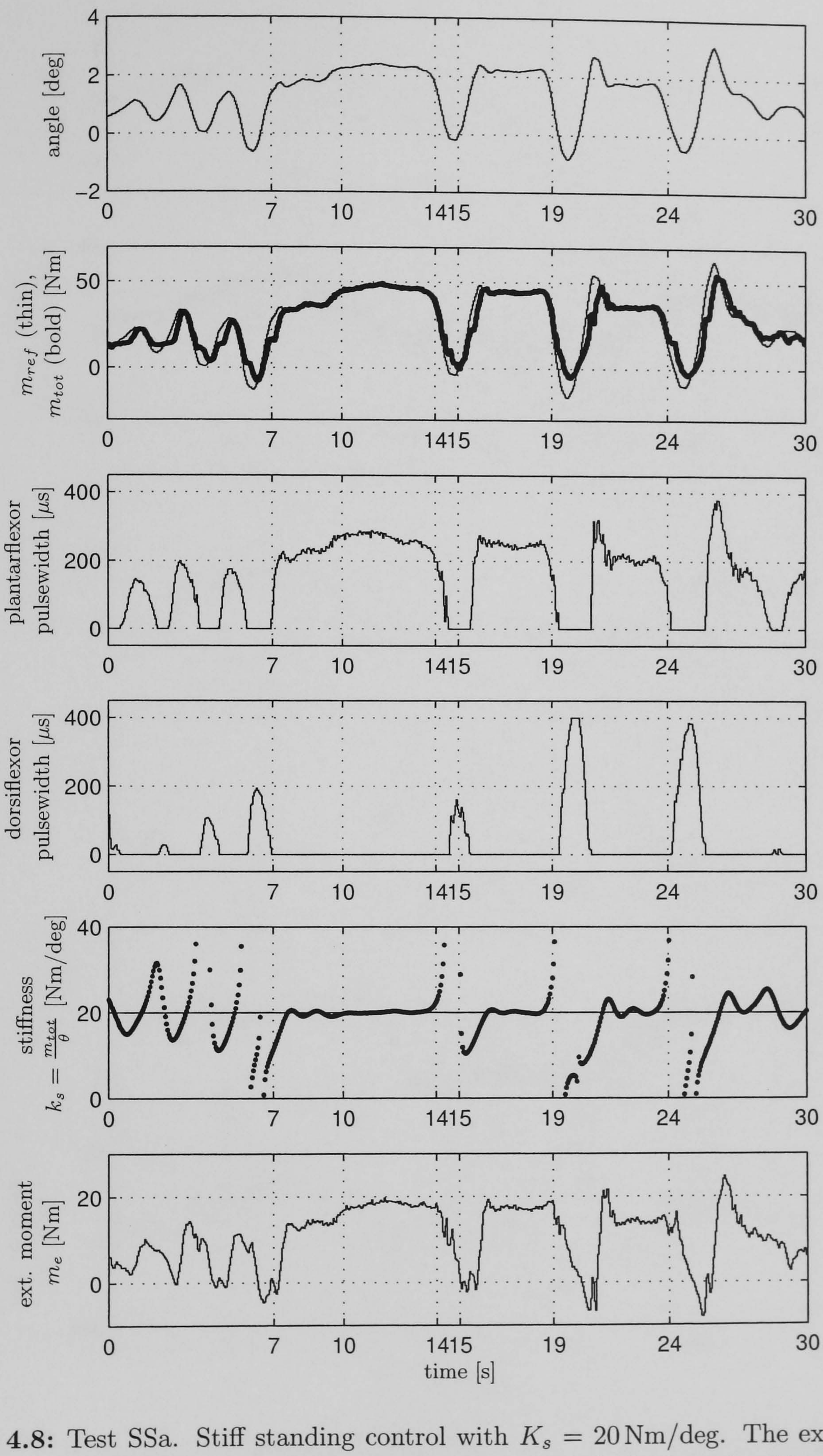

Figure 4.8: Test SSa. Stiff standing control with $K_s = 20\,\mathrm{Nm/deg}$. The experimenter holds the subject at an angle of $+2°$, releases the body at $t \approx 14\,\mathrm{s}$ and catches the body at $t \approx 15\,\mathrm{s}$. This is repeated at $t \approx 19\,\mathrm{s}$ and $t \approx 20\,\mathrm{s}$.

specified value of $K_s = 20\,\mathrm{Nm/deg}$. However, when the subject is held in backward-leaning

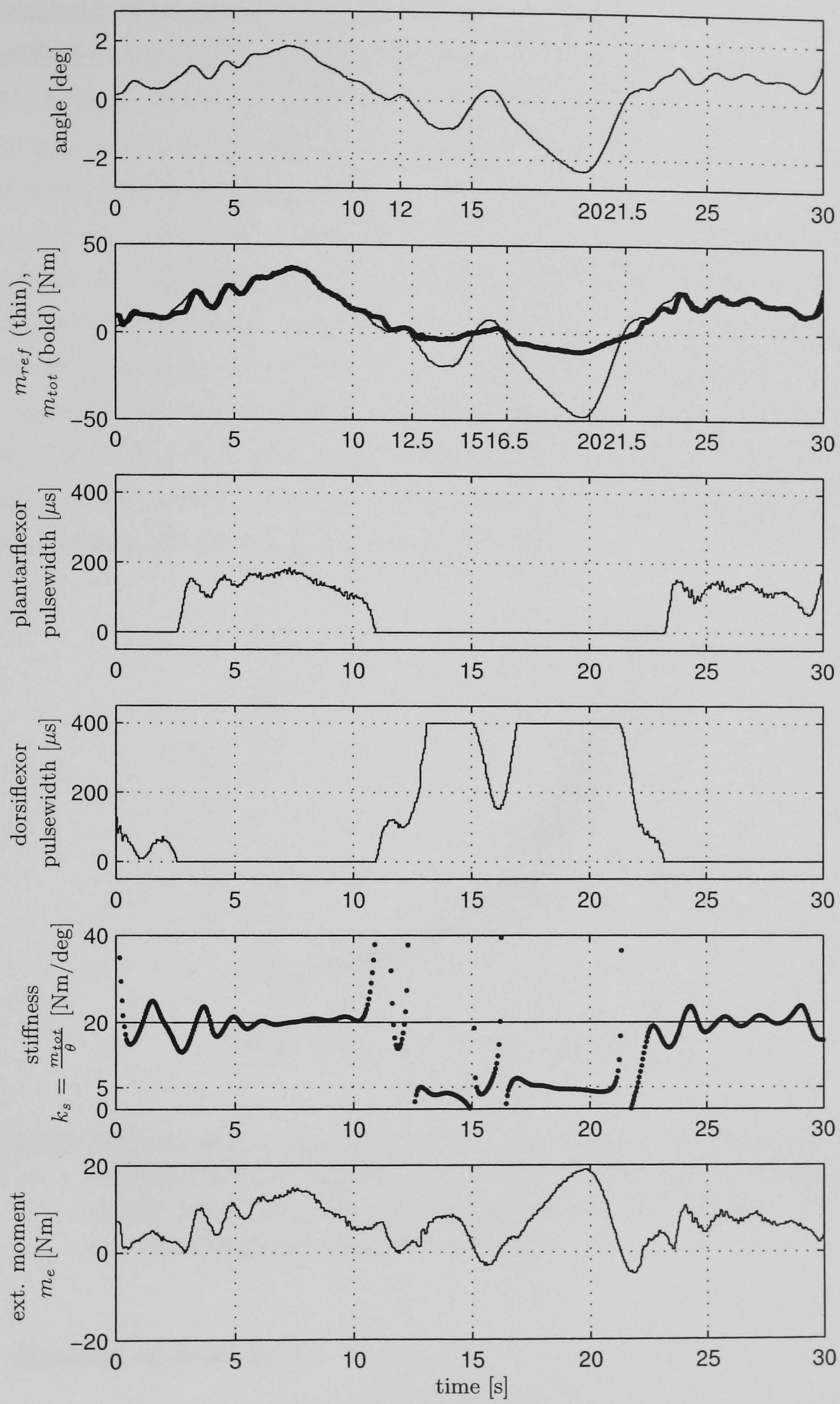

Figure 4.9: Test SSb. Stiff standing control with $K_s = 20\,\mathrm{Nm/deg}$. The experimenter holds the subject and guides it manually through a range of angles.

posture, the weak dorsiflexor muscles are not able to generate the required moment. There is a significant difference between the desired and the requested moment during the time

periods $12.5 < t < 15\,\mathrm{s}$ and $16.5 < t < 21.5\,\mathrm{s}$ (second graph from top) while the dorsiflexor stimulation has reached its maximum value of $400\,\mu\mathrm{s}$. During these periods the desired stiffness level of $20\,\mathrm{Nm/deg}$ cannot be achieved. However, it is interesting to note that with constant, maximal, dorsiflexor stimulation the stiffness achieved settles on an approximately constant level of around $5\,\mathrm{Nm/deg}$. These two stiffness regimes are clearly reflected in the phase plane plot of Figure 4.10.

The external moment is positive for most of the time (Figure 4.9, bottom graph), indicating that the experimenter has to pull the subject forward regardless of whether the subject is inclined forward or backward. When the subject is in forward leaning posture, the plantarflexor muscles tend to push the subject backward (cf. Figure 4.8). To prevent this the experimenter has to apply a positive moment (cf. Figure 4.1). However, when the subject is leaning backwards, the dorsiflexor muscles are not strong enough to pull the subject forward again. Therefore, the experimenter has to apply a positive moment in order to prevent the subject from falling backwards.

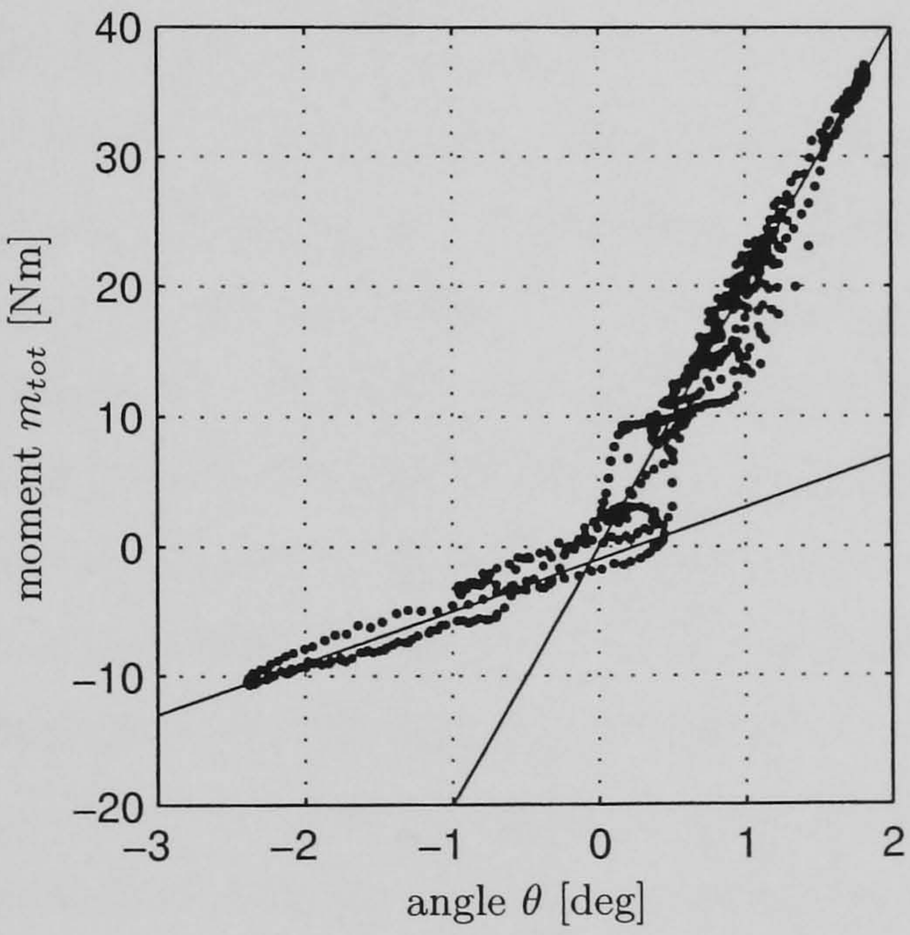

Figure 4.10: Stiffness plot in the phase plane. The straight lines represent the desired stiffness of $20\,\mathrm{Nm/deg}$ and the stiffness of $5\,\mathrm{Nm/deg}$ on which the stiffness settles when dorsiflexor stimulation reaches its maximum value while the requested moment cannot be achieved.

4.6.4 Results of Test EPC

Results for Test EPC are shown in Figure 4.11 and Figure 4.13 for two different value of requested stiffness K_s, $10\,\mathrm{Nm/deg}$ and $30\,\mathrm{Nm/deg}$, respectively. The experimenter tries to follow an online generated sinusoidal reference angle while holding the subject. With a requested stiffness of $K_s = 10\,\mathrm{Nm/deg}$ the experimenter manages to achieve reasonable angle tracking with only modest external hand moments m_e of up to $20\,\mathrm{Nm}$. During forward leaning and associated plantarflexor activity good moment tracking and hence stiffness

control is achieved. On the other hand, the weaker dorsiflexor muscles quickly saturate giving a significant moment tracking error. During periods of dorsiflexor saturation it can be seen that the effective ankle stiffness has a value of around 5 Nm/deg as observed in Test SS. This is also reflected in the stiffness phase plane plot in Figure 4.12.

During periods of backward leaning and associated dorsiflexor saturation, the required external hand moment necessary to follow the reference angle is smaller the larger the subject's own contribution to the total moment (i.e. the moment generated by stimulation), and therefore, the larger the stiffness generated by stimulation. However, the moment the subject is able to produce decreases during the course of the trial due to fatigue resulting in an increased hand moment.

Qualitatively, the experimenter reported that the task was easy to perform at this level of desired stiffness.

Results for Test EPC with a requested stiffness of $K_s = 30\,\mathrm{Nm}$ are shown in Figure 4.13. In this case the increased stiffness generates much higher levels of demanded ankle moment of up to 60 Nm. Good moment tracking is achieved during forward-leaning, with the effective stiffness approximately equal to the desired value of 30 Nm/deg. While backward-leaning, the dorsiflexors again quickly saturate giving large moment tracking errors and a stiffness value around only 5 Nm/deg (cf. Figure 4.14). The time history of the actual ankle stiffness (cf. Figure 4.13, second graph from bottom) shows negative values during periods of dorsiflexor stimulation. However, the moment plot shows the subject does not produce a negative moment while the angle and, hence, the reference moment is negative. An explanation for that can be found again in a shift of the moment offset, which is generated by the weight of the subject, due to small movements of the subject.

The experimenter described this angle tracking task as very difficult, and this is presumably due to the large hand moments required (up to 40 Nm—see the bottom graph in Figure 4.13). The difficulty reported by the experimenter can be supported by the following consideration: With the approximation of the hand moment according to (4.2) and $m_{tot} = k_s\theta$, the hand moment becomes

$$m_e \approx k_s\theta - \tilde{m}gl\theta = (k_s - \tilde{m}gl)\,\theta\,. \tag{4.9}$$

It can be seen that m_e becomes minimal for $k_s = \tilde{m}gl$ which corresponds to a value of $k_s \approx 12\,\mathrm{Nm/deg}$ for the physical parameters of the subject as given above.

Furthermore, it can be seen from Figure 4.1 that if $\theta > 0$ and $m_e < 0$, or if $\theta < 0$ and $m_e > 0$, the hand moment acts "stabilising", moving the body towards the neutral position of $\theta = 0$. On the other hand, if the angle θ and the hand moment m_e have the same sign, the hand moment acts "disturbing", moving the body away from the neutral position.

Defining the *directional hand moment* m_e^d as $m_e^d = m_e\mathrm{sgn}(\theta)$ these conditions can also

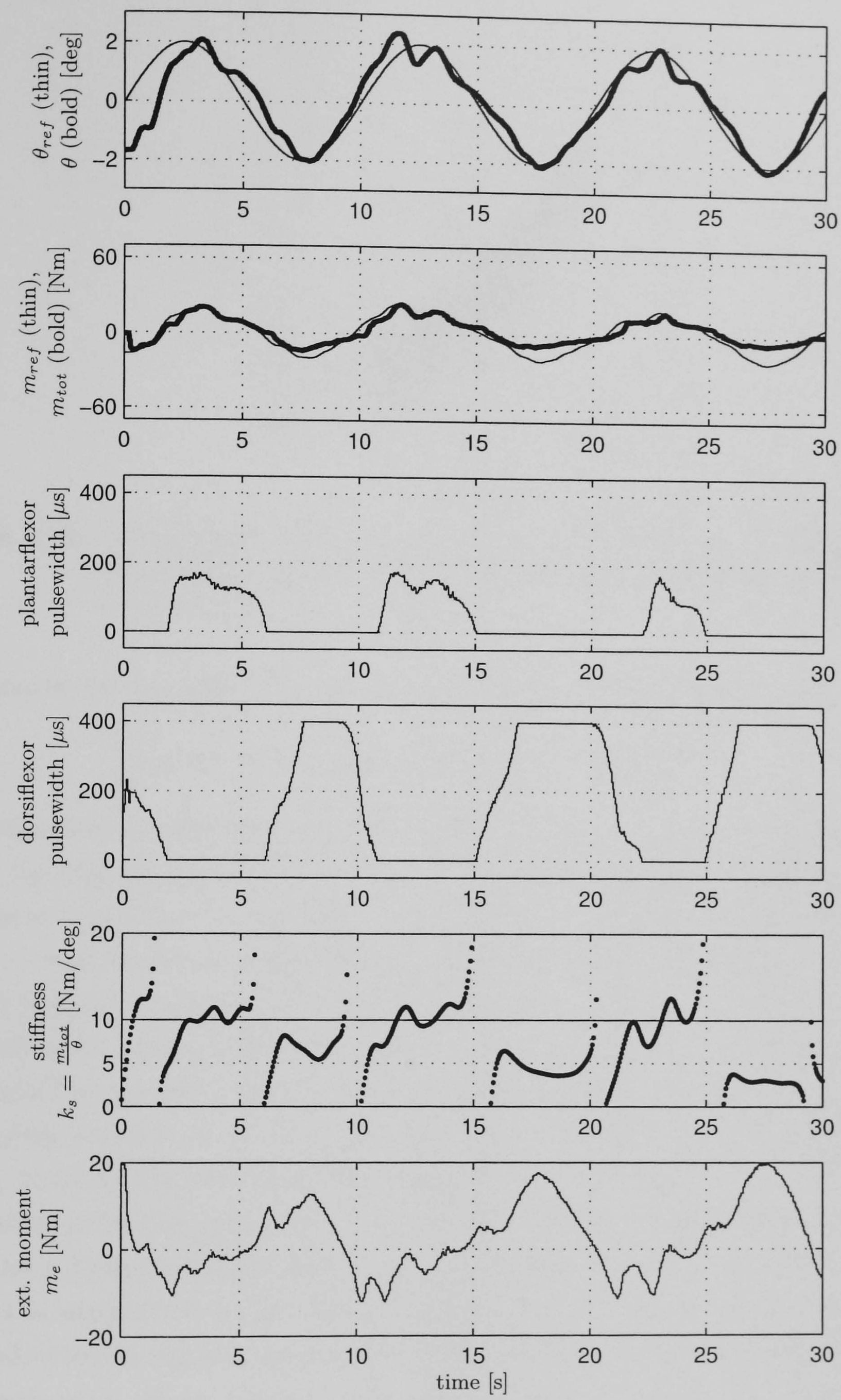

Figure 4.11: Test EPC. The experimenter holds the subject and tries to follow an online generated reference angle. Stiffness specified as $K_s = 10\,\mathrm{Nm/deg}$.

be expressed as

$$m_e \begin{cases} \text{acts stabilising, if } m_e^d < 0 \\ \text{acts disturbing, if } m_e^d > 0 \end{cases} \tag{4.10}$$

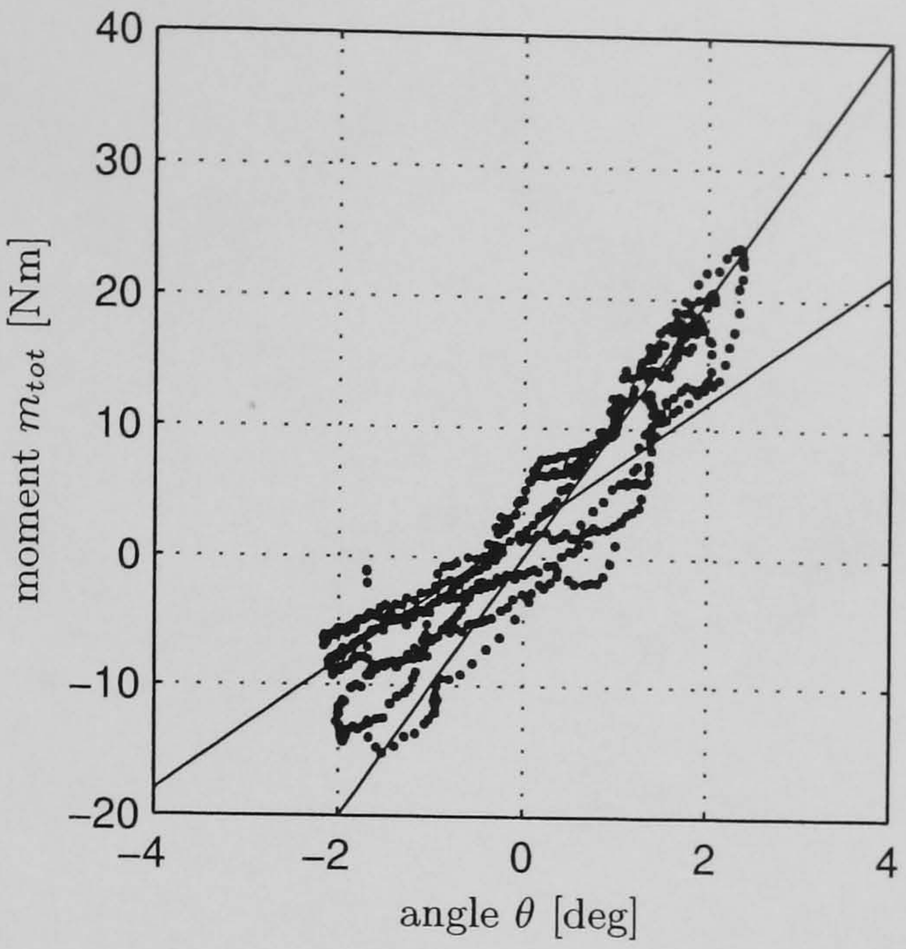

Figure 4.12: Stiffness plot in the phase plane for test EPC with $K_s = 10\,\mathrm{Nm/deg}$. The straight lines represent the desired stiffness of 10 Nm/deg and the stiffness of 5 Nm/deg.

Furthermore, we can define the nominal directional hand moment $m^d_{e,nom}$ as

$$m^d_{e,nom} = (K_s\theta - \tilde{m}gl\theta)\mathrm{sgn}(\theta) = (K_s - \tilde{m}gl)\theta\mathrm{sgn}(\theta)\,, \tag{4.11}$$

which describes the hand moment which would be required to follow the angle trajectory θ_{ref} if the stiffness control were ideal, i.e. the transfer function for moment reference tracking is $G^m_{y/r}(q^{-1}) = 1$. An analysis of (4.11) shows that for a nominal stiffness value of $K_s < \tilde{m}gl$ the nominal directional hand moment $m^d_{e,nom}$ is always negative (since $\theta\mathrm{sgn}(\theta)$ is always positive), indicating that an external moment is required to stabilise the body at all times. Conversely, when $K_s > \tilde{m}gl$, $m^d_{e,nom}$ is always positive, so that (nominally) an external moment is always required to actively move the body away from the neutral position (cf. (4.10)). Figure 4.15 shows a graph of both quantities m^d_e and $m^d_{e,nom}$ in connection with the angle tracking graph. In Figure 4.15(a) the stiffness is specified as 10 Nm/deg and, therefore, below the critical value of 12 Nm/deg. The nominal and actual directional hand moment are always negative which means that the hand moment is required to stabilise the body at all times. In Figure 4.15(b) the stiffness is specified as 30 Nm/deg and, therefore, above the critical value of 12 Nm/deg. The nominal hand moment is always positive which means that, theoretically, the hand moment is required to actively move the body away from the neutral position, or, in other words, to "perturb" the body. However, the actual directional hand moment estimated from the measured moments is only positive for positive angle, i.e. during periods of forward-leaning when the plantarflexor muscles are stimulated. For negative angle, i.e. during periods of backward-leaning when the dorsiflexor muscles are stimulated, the directional hand moment is negative which means that the subject is now being actively stabilised

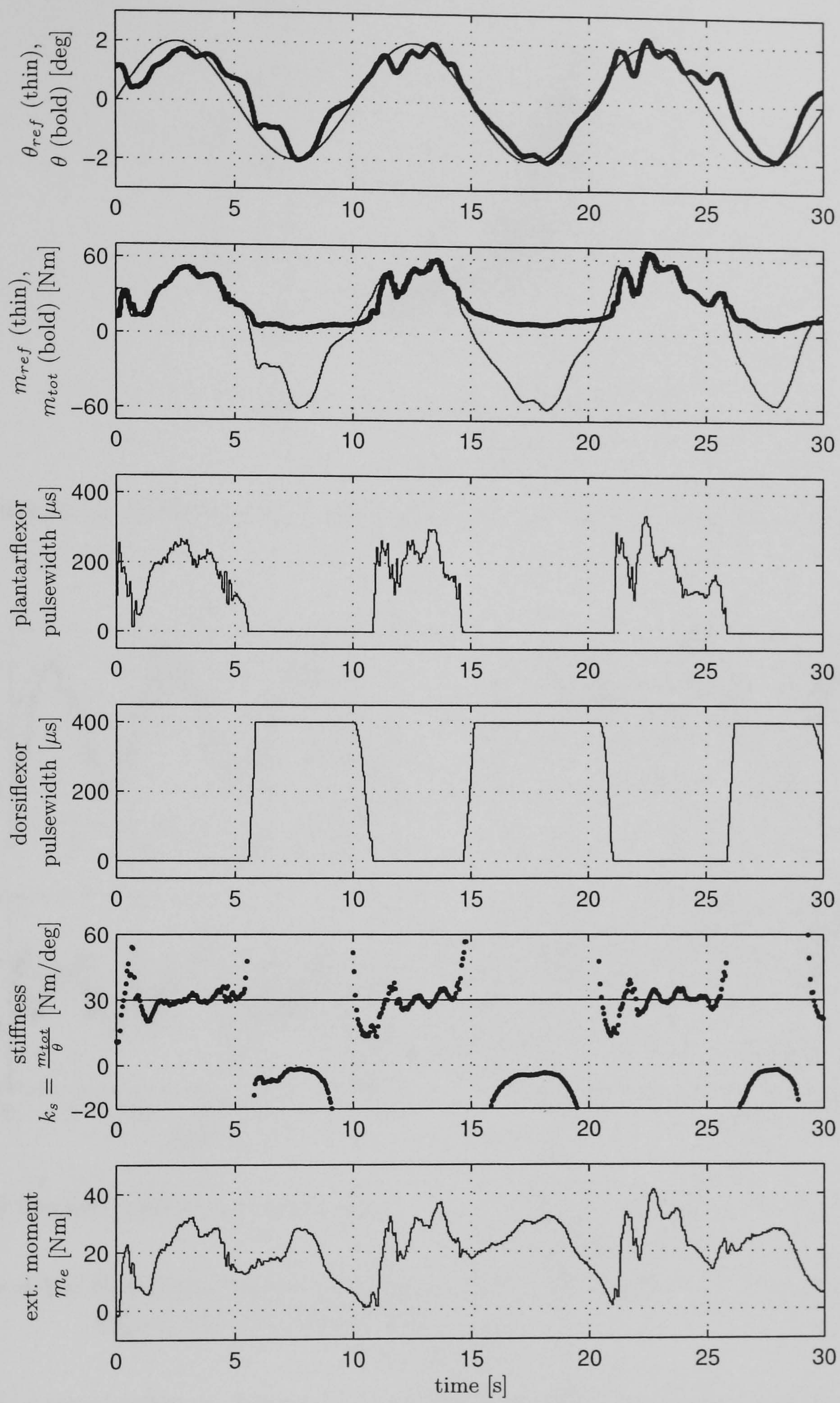

Figure 4.13: Test EPC. As in Figure 4.11 but for $K_s = 30\,\mathrm{Nm/deg}$.

towards the neutral position. Thus, the requirements for application of external moment depend crucially on the ability of the muscles to deliver the nominal moments.

Table 4.1 shows the arithmetic mean value of the directional hand moments $m^d_{e,nom}$

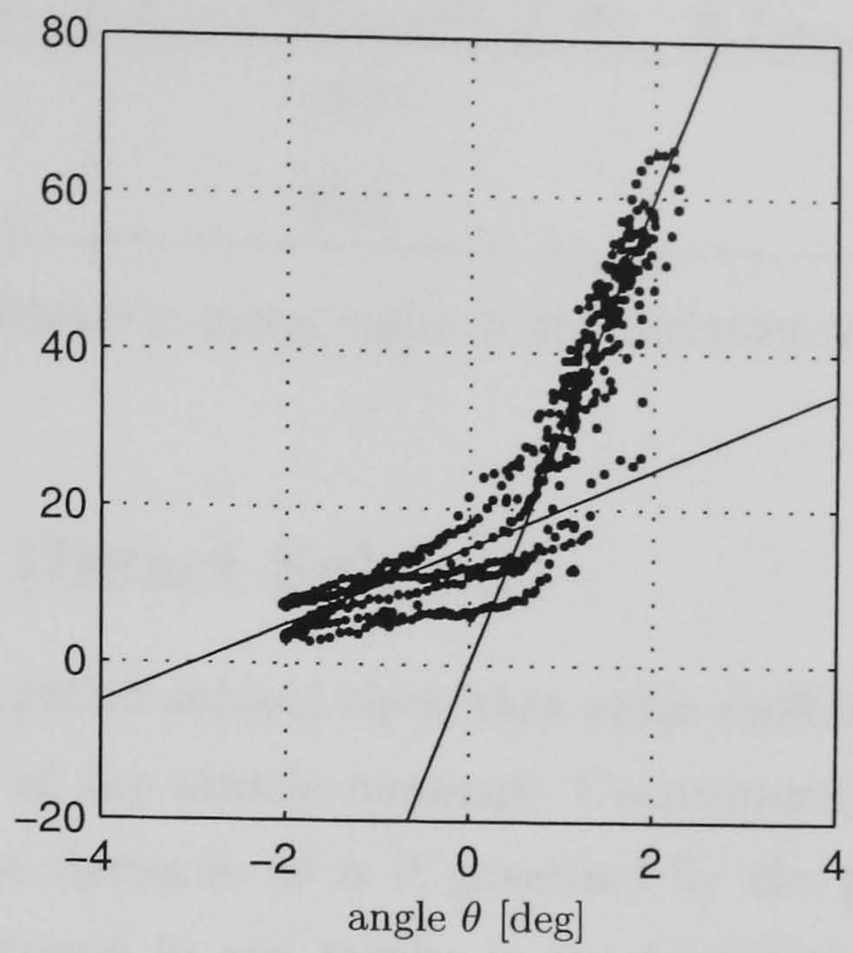

Figure 4.14: Stiffness plot in the phase plane for test EPC with $K_s = 30\,\mathrm{Nm/deg}$.

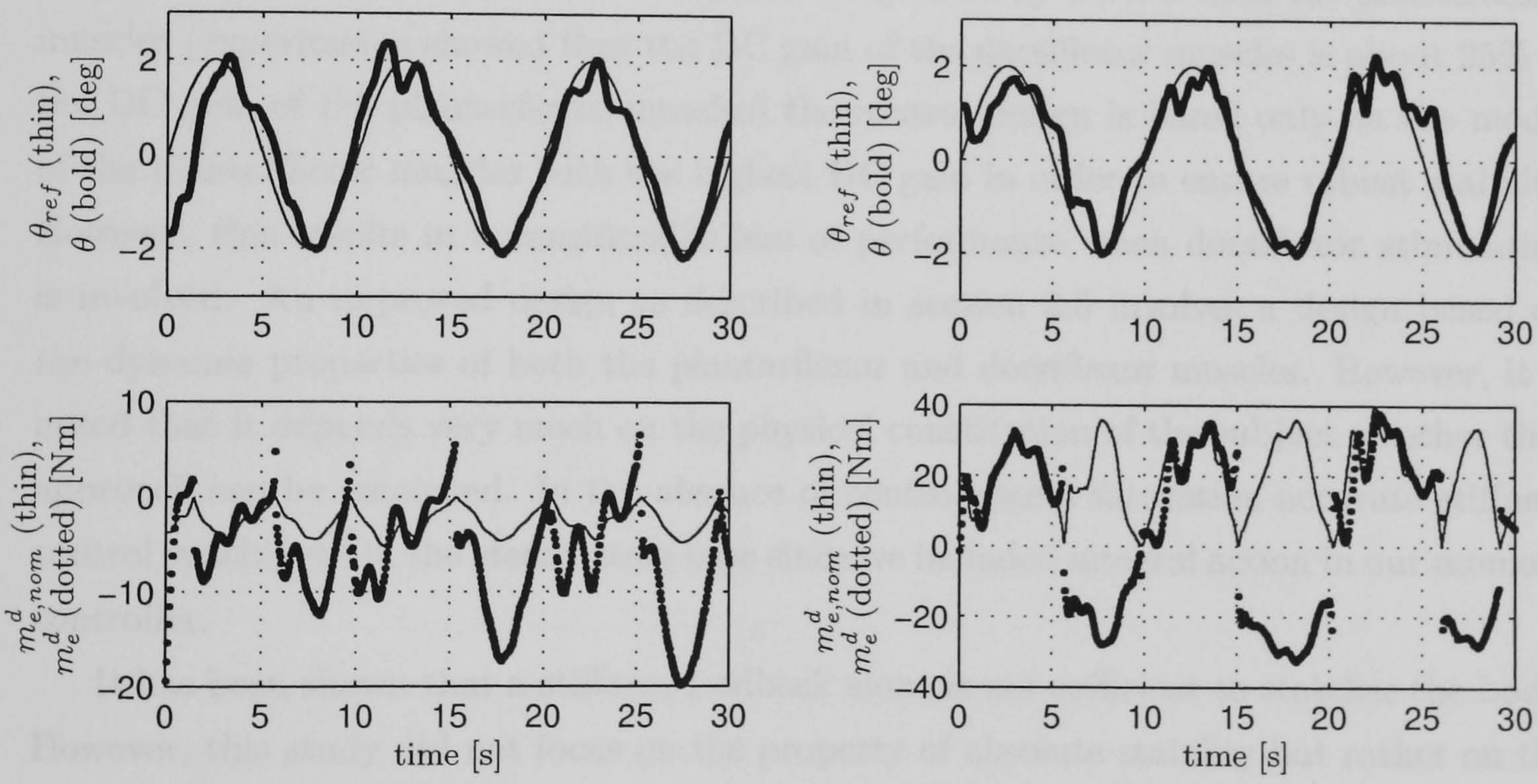

(a) Specified stiffness $K_s = 10\,\mathrm{Nm/deg}$.

(b) Specified stiffness $K_s = 30\,\mathrm{Nm/deg}$.

Figure 4.15: Estimated directional hand moments $m^d_{e,nom}$ and m^d_e during test EPC, cf. Figure 4.11 and Figure 4.13.

and m^d_e corresponding to Figure 4.15. A negative value means that, overall, stabilising action is required while a positive value means that the hand moment acts "perturbing". The difference between the nominal value $\frac{1}{N}\sum_{k=1}^{N} m^d_{e,nom}(k)$ and the actual value $\frac{1}{N}\sum_{k=1}^{N} m^d_e(k)$ is an indication of the overall quality of the stiffness control and is mainly due to the weakness of the dorsiflexor muscles.

K_s [Nm/deg]	$\frac{1}{N}\sum_{k=1}^{N} m^d_{e,nom}(k)$ [Nm]	$\frac{1}{N}\sum_{k=1}^{N} m^d_{e}(k)$ [Nm]
10	−2.61	−6.43
30	20.2	1.76

Table 4.1: Arithmetic mean value of the directional hand moment.

4.7 Conclusions (Intact Subject)

The experiments with the intact subject show that ankle stiffness can be controlled using FES via feedback control of the muscle moment. Consequently, the achievable stiffness is not static in nature but dynamic as is it governed by the properties of the moment control loop. This is expressed in our results in the hysteresis characteristic evident in the angle-moment phase plots. The ankle stiffness control scheme as proposed in this chapter includes stimulation of both the plantarflexor and dorsiflexor muscles. While it is well known that the dorsiflexor muscles are significantly weaker than the plantarflexor muscles (experiments showed that the DC gain of the dorsiflexor muscles is about 25% of the DC gain of the plantarflexor muscles) the control design is based only on the model of the plantarflexor muscles with the highest DC gain in order to ensure robust stability. However, this results in a considerable loss of performance when dorsiflexor stimulation is involved. An improved design as described in section 2.5 involves a design based on the dynamic properties of both the plantarflexor and dorsiflexor muscles. However, it is noted that it depends very much on the physical constitution of the subject whether that approach can be employed. In the absence of control signal saturation accurate stiffness control is achieved in the steady state case since we included integral action in our moment controller.

It has been shown that a stiffness feedback alone is not sufficient to stabilise the body. However, this study did not focus on the property of absolute stability but rather on the degree to which ankle stiffness can facilitate stability by external control of the body. Three key factors have been identified as important to this issue.

1. The value of the actual achieved stiffness k_s. If k_s is greater than the critical value, i.e. $k_s > \tilde{m}gl$, the directional hand moment acts "perturbing", and we therefore suggest that ankle stiffness then eases the task of stabilising the body.

   In fact, the analysis of the root locus showed that at a stiffness of $k_s = \tilde{m}gl$ the poles of the inverted pendulum change from real, one outside the unit circle, to conjugate complex located outside the unit circle, resulting in oscillations of increasing amplitude when excited. This can be interpreted as ankle stiffness making the body "less" unstable.

2. The bandwidth of the ankle moment control loop. How close the actual achieved stiffness k_s follows the requested stiffness K_s mainly depends on the bandwidth of the moment control loop.

3. The muscle strength. The most limiting factor has been found as the ability of the muscle to deliver the requested moments.

Further experiments were carried out with a paraplegic subject to evaluate these findings.

4.8 Experimental Results with Paraplegic Subject

Results are given here for the paraplegic subject for tests M, AS, and EPC. We do not include results from test SS - during sessions with this subject we proceeded directly from test AS to test EPC in order to reduce fatigue effects. In any case, test EPC gives a more systematic way of carrying out sub-test SSb. Again, results of the identification procedure are similar to those reported in the previous chapter as the same subject took part in both studies and are not shown here.

4.8.1 Results of Test M

A result of closed-loop moment control is shown in Figure 4.16.

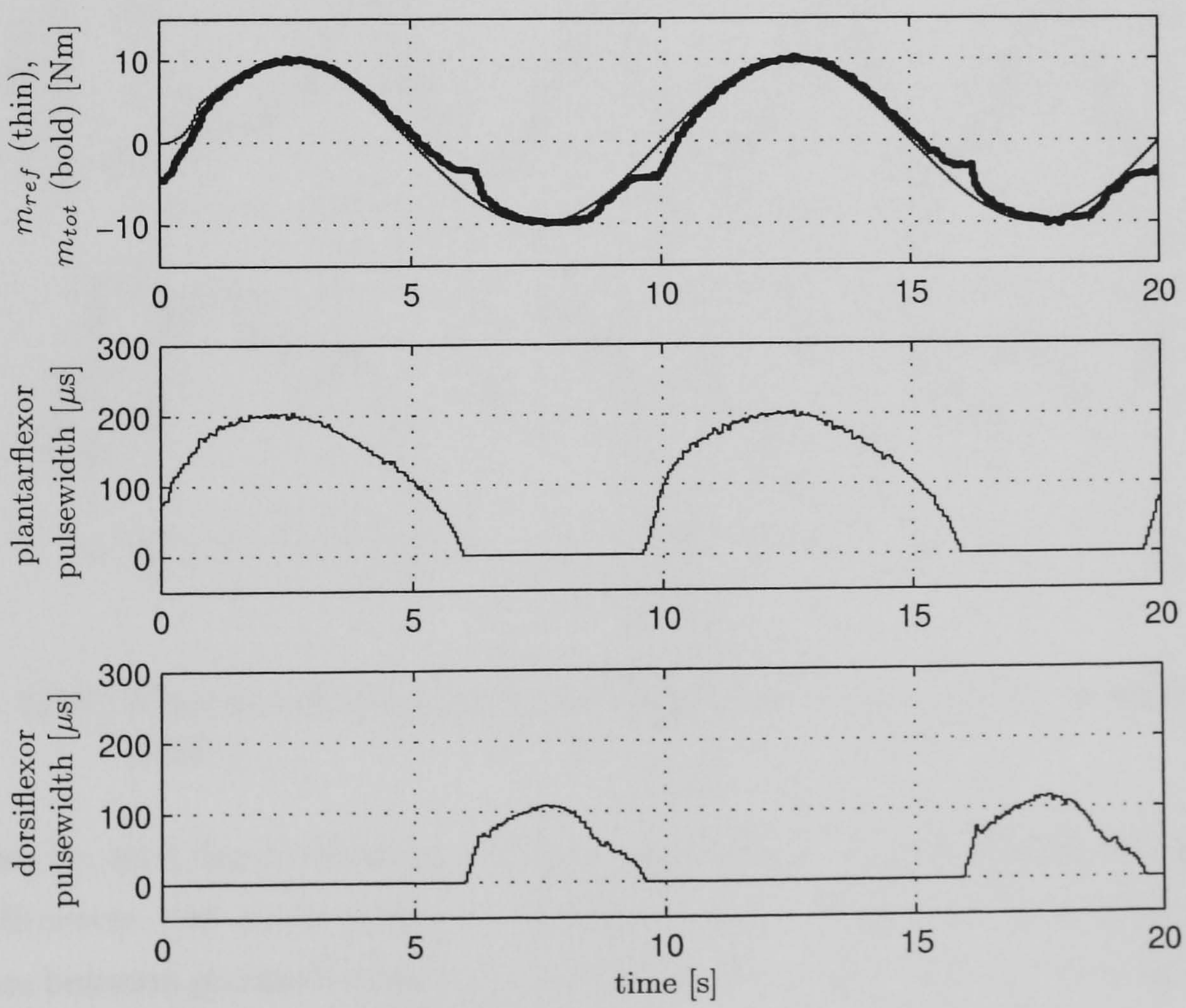

Figure 4.16: Closed-loop moment control (cf. Figure 4.4 for intact subject).

The tracking accuracy is qualitatively similar to that for the intact subject (cf. Figure 4.4). A dead zone can be identified around the switching instants. This is due to the low pulsewidth levels involved which are obviously below the threshold of the muscle. It should be noted that the magnitude of the sinusoidal reference moment is half of that used for the intact subject, and that the stimulation current was set to 120 mA here (for comparison, 60 mA for the intact subject). This is a reflection of the relatively weak paraplegic muscles. It should be noticed again that the neutral moment line (the moment produced without stimulation) is negative (approximately -3 Nm).

4.8.2 Results of Test AS

Test AS was first carried out without stimulation in order to determine the natural ankle stiffness. Thus, the ankles were wobbled and the resulting passive ankle moment measured. Results of this test are shown in Figure 4.17.

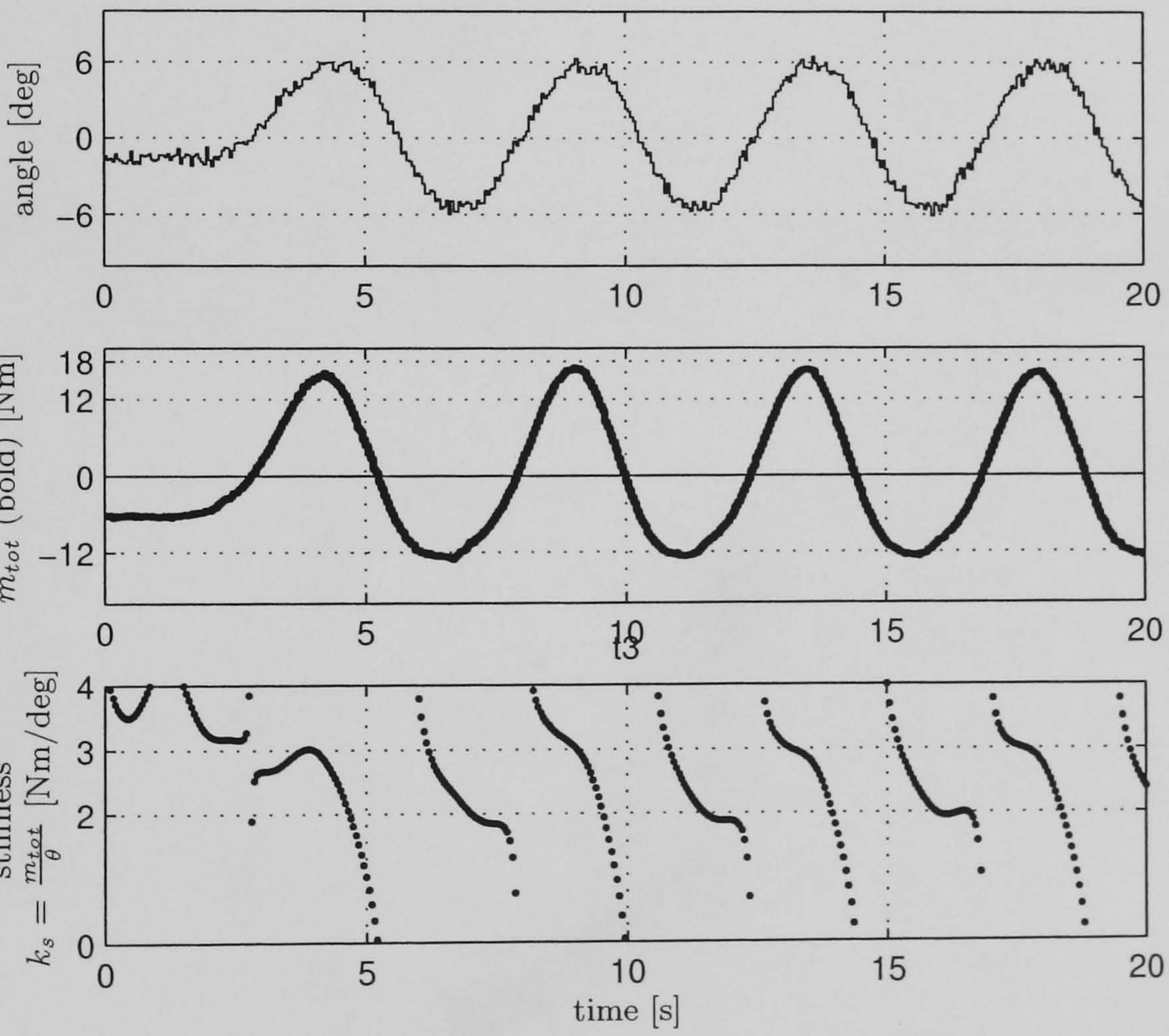

Figure 4.17: Natural ankle stiffness (body fixed, feet wobbled) with no stimulation applied.

It can be seen the produced moment is approximately proportional to the wobbling angle. However, the ankle stiffness calculated from the measured data shows there is a difference between plantarflexion and dorsiflexion. When dorsiflexing (negative angles) the stiffness centers around 2 Nm/deg, while when plantarflexing the stiffness centers around 3 Nm/deg. This is also underlined by the moment plot. The produced moment is higher

for plantflexion than for dorsiflexion. The two stiffness regimes can also be identified in the phase plot in Figure 4.18. Further analysis shows that the natural ankle stiffness fits particularly well into these regimes for a positive angular velocity. Note that it was not possible to accurately determine the natural stiffness in this way for the intact subject due to voluntary interaction from the intact central nervous system.

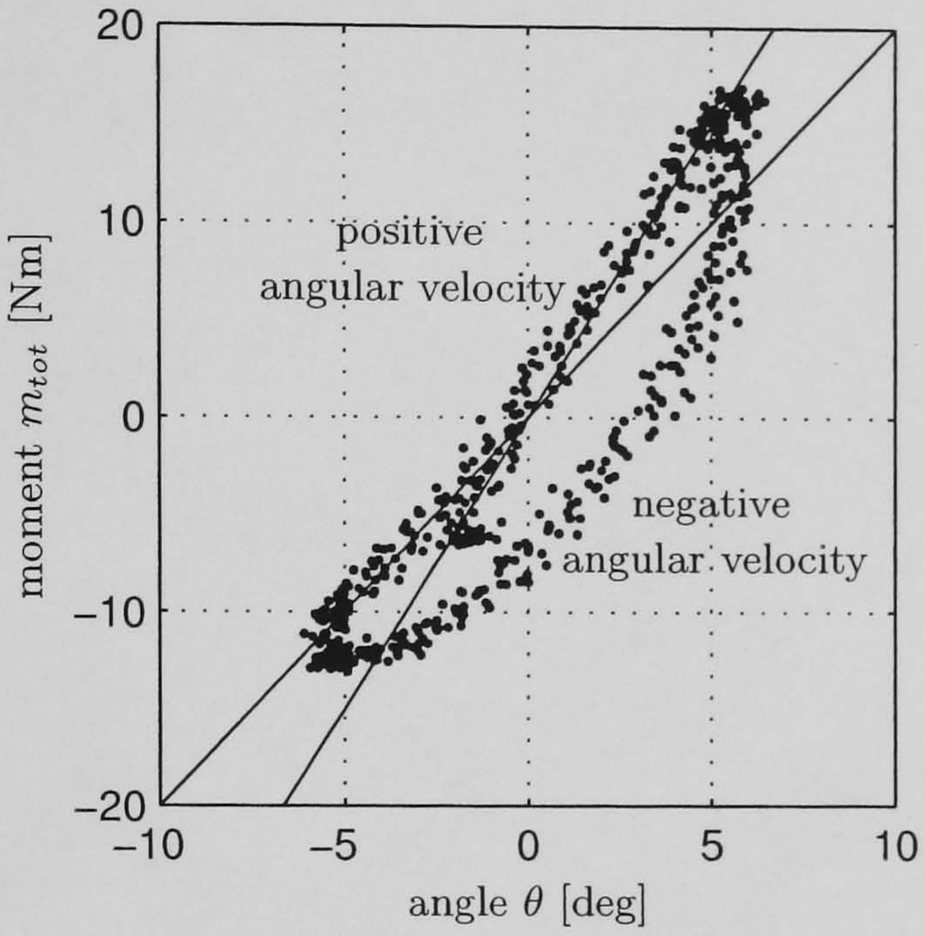

Figure 4.18: Stiffness plot of natural ankle stiffness in the phase plane (with no stimulation applied). The two straight lines represent a constant stiffness of 2 Nm/deg and 3 Nm/deg, respectively.

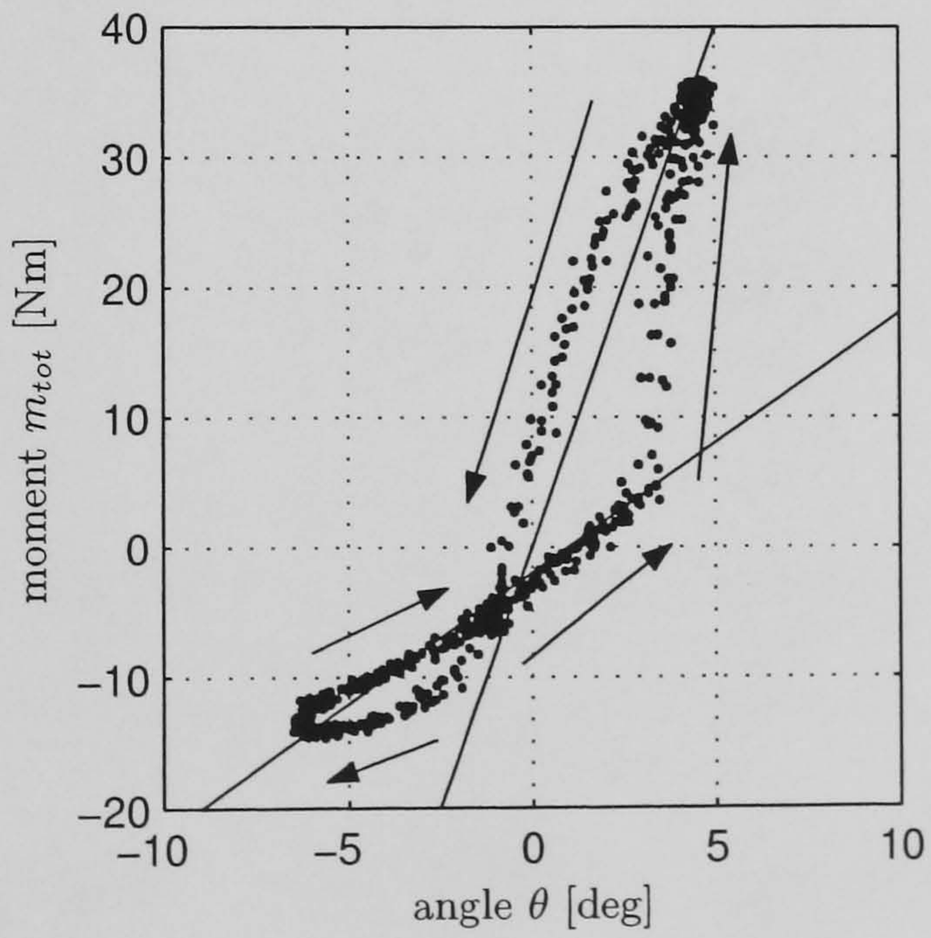

Figure 4.19: Stiffness plot in the phase plane. The straight lines represent the desired stiffness of 8 Nm/deg and the natural value of 2 Nm/deg.

Results from the ankle stiffness control test are shown in Figure 4.20 for a desired stiffness value of $K_s = 8\,\text{Nm/deg}$. The higher value compared to the equivalent test with the intact subject was chosen because 8 Nm/deg is a more realistic value when it comes

to standing [Matjačić and Bajd, 1998a,b]. Good moment tracking is achieved during plantarflexor stimulation. However, the moment plot shows a large tracking error during dorsiflexor stimulation while the stimulation signal saturates due to the weakness of the dorsiflexor muscles. The actually produced stiffness (bottom graph) is close to the desired value of 8 Nm/deg during periods of plantarflexor stimulation. However, during periods of dorsiflexion, when the control signal saturates, the actual stiffness settles at approximately 2 Nm/deg, the inherent natural stiffness during dorsiflexion (cf. Figure 4.17). This suggests that the dorsiflexor stimulation has very little effect.

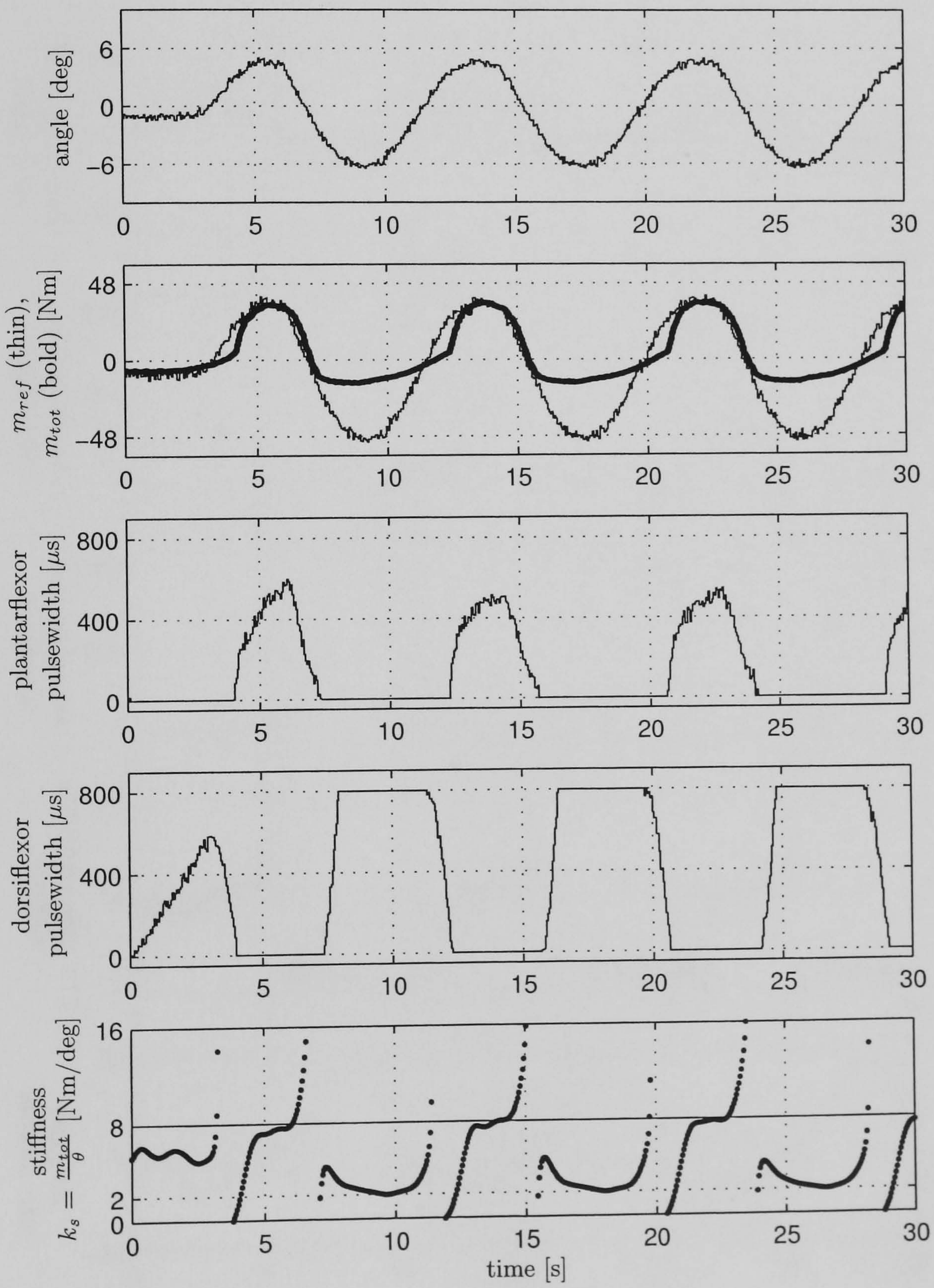

Figure 4.20: Ankle stiffness control (body fixed, feet wobbled) with a desired stiffness of $K_s = 8\,\mathrm{Nm/deg}$.

Figure 4.19 shows the achieved stiffness in the phase plane, revealing a significant hysteresis (cf. Figure 4.18). The hysteresis results from the dynamics of the moment loop as well as from the inherent hysteresis found when stimulation is applied (cf. Figure 4.18).

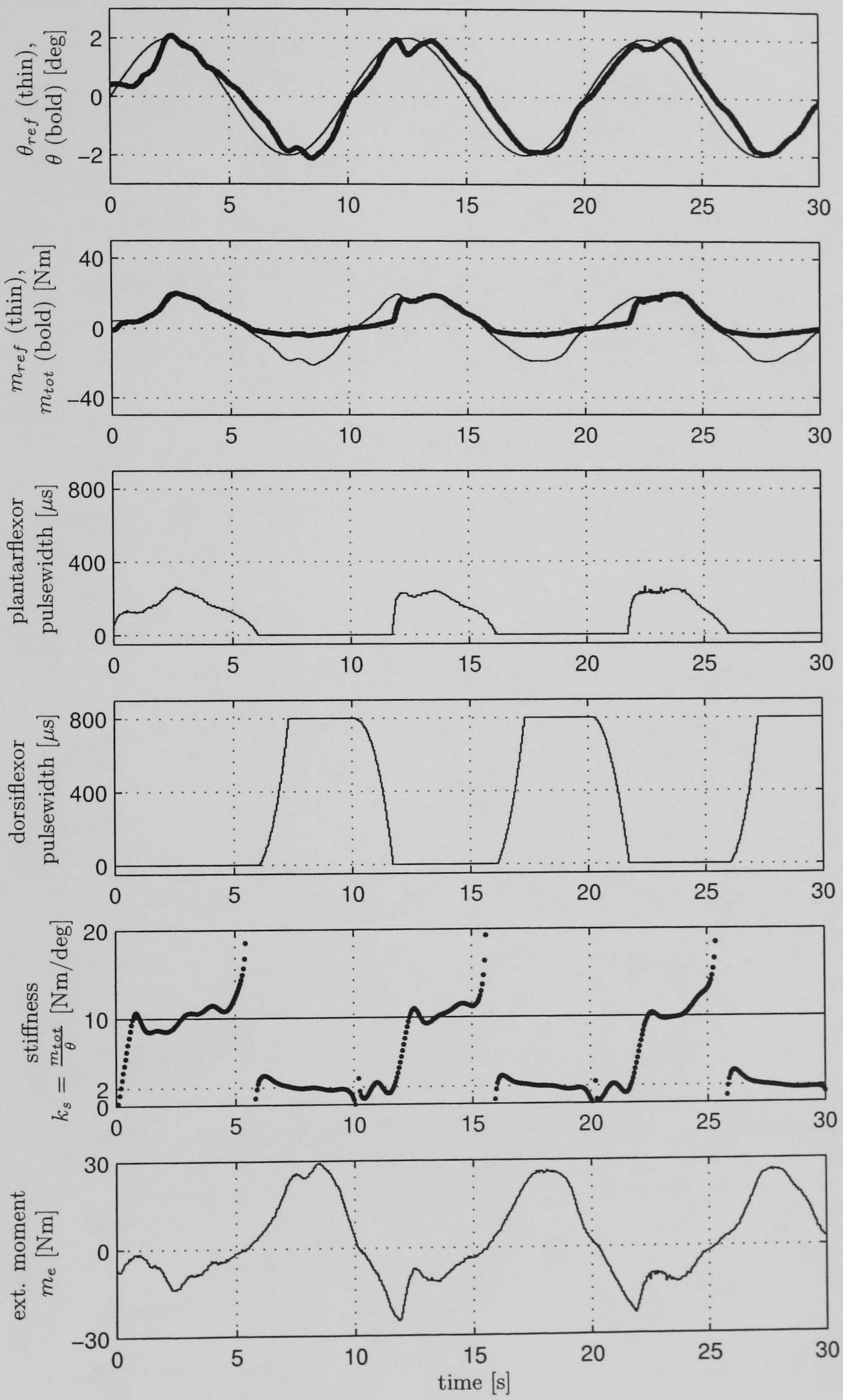

Figure 4.21: Test EPC. The experimenter holds the subject and tries to follow an online generated reference angle. Stiffness specified as $K_s = 10\,\mathrm{Nm/deg}$.

4.8.3 Results of Test EPC

Two tests of external posture control are shown here for two values of desired stiffness. The result in Figure 4.21 is for $K_s = 10\,\mathrm{Nm/deg}$ and the result in Figure 4.22 is for $K_s = 20\,\mathrm{Nm/deg}$. In Figure 4.21 the experimenter achieved very good tracking of the online

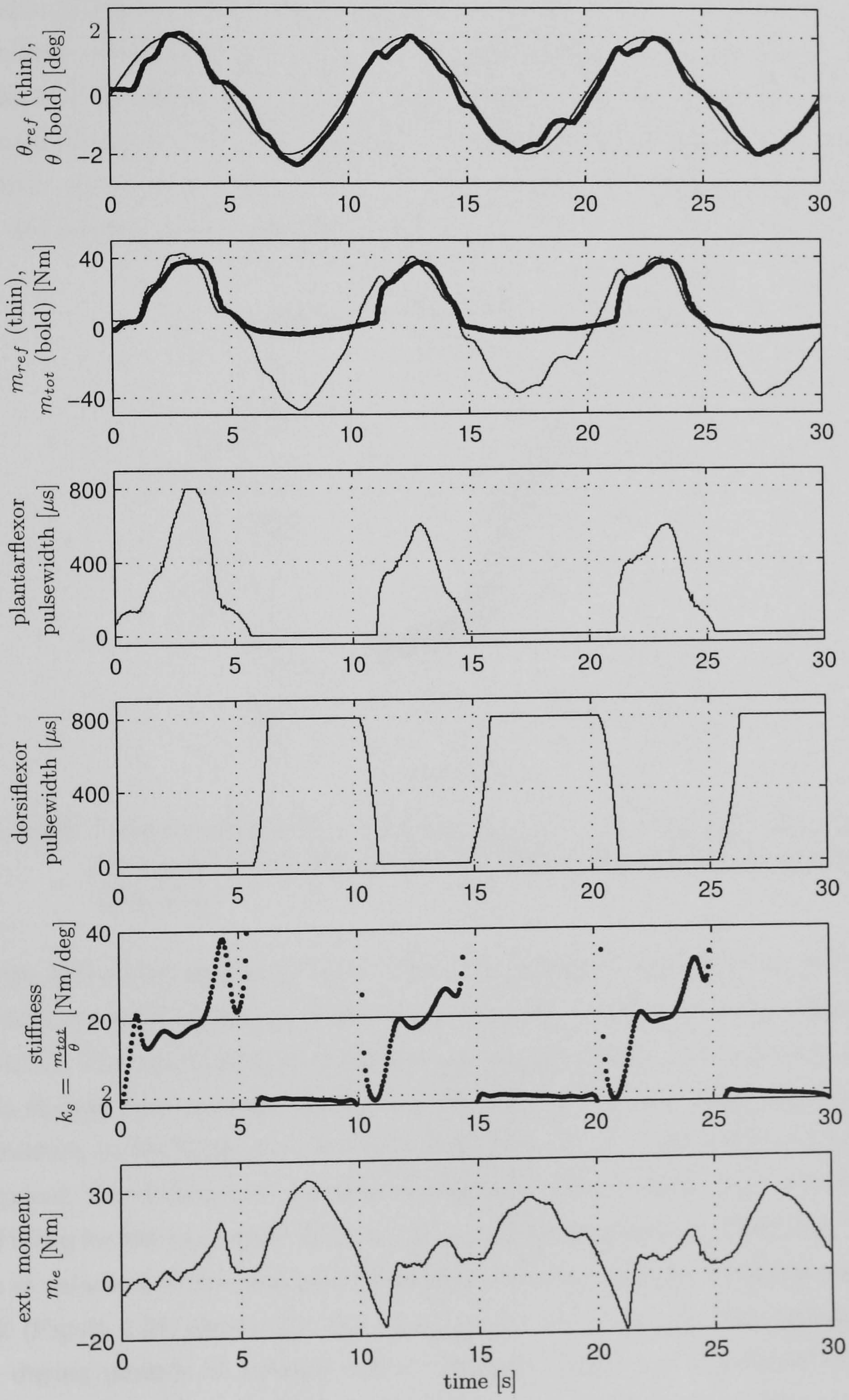

Figure 4.22: Test EPC. As in Figure 4.21 but for $K_s = 20\,\mathrm{Nm/deg}$.

generated reference angle θ_{ref} (top graph). Accurate moment tracking is achieved during periods of plantarflexor stimulation. Dorsiflexor stimulation saturates quickly resulting in a significant moment tracking error. The specified stiffness (second graph from bottom) is achieved during periods of plantarflexor stimulation but settles at around 2 Nm/deg during periods of dorsiflexor stimulation. This corresponds to the inherent ankle stiffness exhibited even when no stimulation is applied at all, suggesting that dorsiflexor stimulation has very little effect (cf. Figure 4.17). These two stiffness regimes are clearly seen in the phase plot of Figure 4.23. Overall, these stiffness control results reflect the behaviour seen during test AS above. The "hand moment" is much higher during periods of dorsiflexor stimulation, up to 30 Nm, illustrating the higher stabilising effort required during these periods due to the weak dorsiflexor muscles.

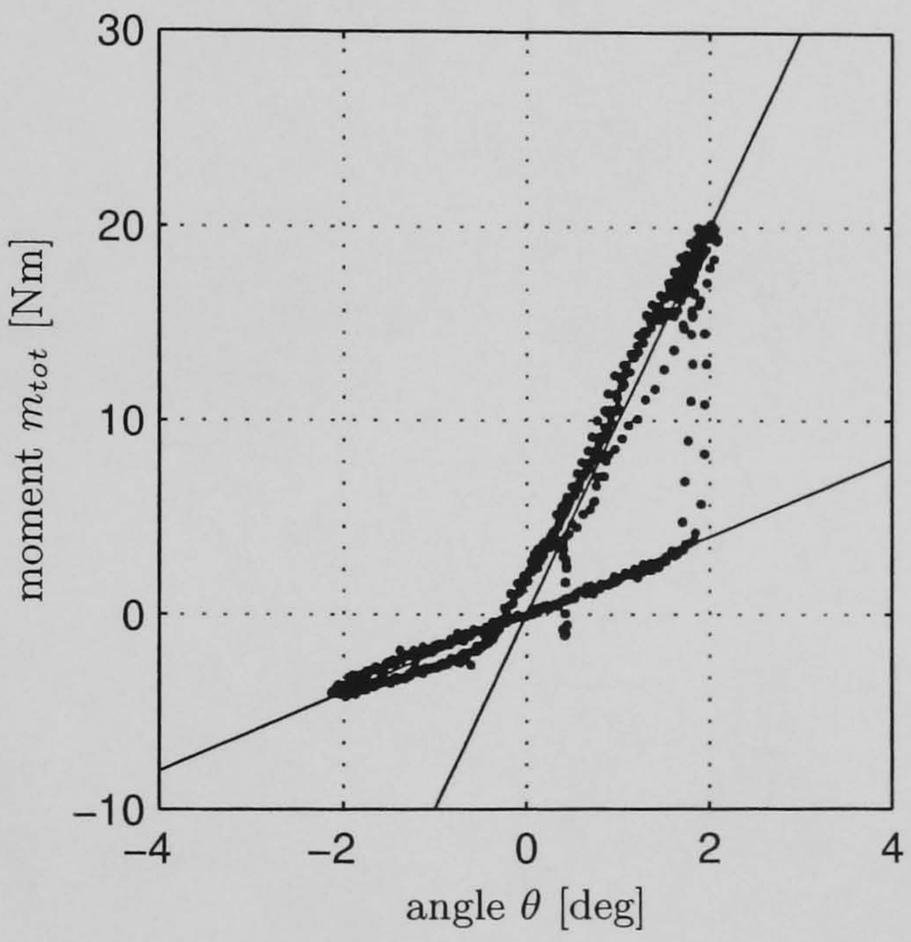

Figure 4.23: Stiffness plot in the phase plane for $K_s = 10\,\text{Nm/deg}$. The straight lines represent the desired stiffness of 10 Nm/deg and the natural stiffness of 2 Nm/deg.

Figure 4.22 shows results for test EPC for a requested stiffness of $K_s = 20\,\text{Nm/deg}$. The results are very similar to those for a requested stiffness of $K_s = 10\,\text{Nm/deg}$ (cf. Figure 4.21). The actual controlled stiffness during periods of a non-saturated stimulation signal is slightly less accurate for $K_s = 20\,\text{Nm/deg}$ due to the larger required moment and, therefore, to the larger error in the moment control (cf. Figure 4.24 and Figure 4.23). The required "hand moments" are also very similar. The reason is that, assuming a body mass of 90 kg for the paraplegic subject, the critical stiffness is ca. 15 Nm/deg. This is the average of values of 10 Nm/deg and 20 Nm/deg. However, the plot of the directional hand moment (Figure 4.25) shows that the "hand moment" acts mostly "perturbing" (positive values) during periods of forward leaning (positive angle) and associated plantarflexor stimulation for a stiffness of 20 Nm/deg while it acts stabilising (negative values) at all times with a stiffness of 10 Nm/deg. Figure 4.25(b) also shows that the nominal directional

"hand moment" is actual "perturbing" at all times but whether this is really the case depends on the ability of the muscles to deliver the requested moment.

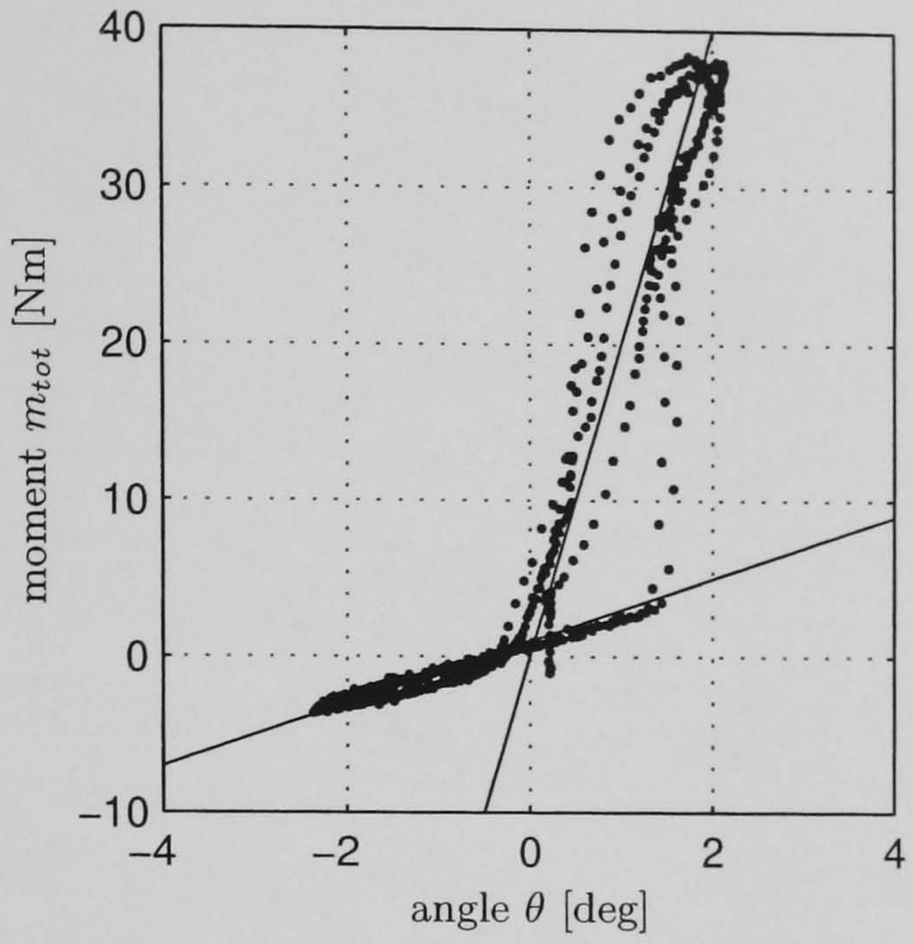

Figure 4.24: Stiffness plot in the phase plane for test EPC with $K_s = 20\,\mathrm{Nm/deg}$. The straight lines represent the desired stiffness of 20 Nm/deg and the natural stiffness of 2 Nm/deg.

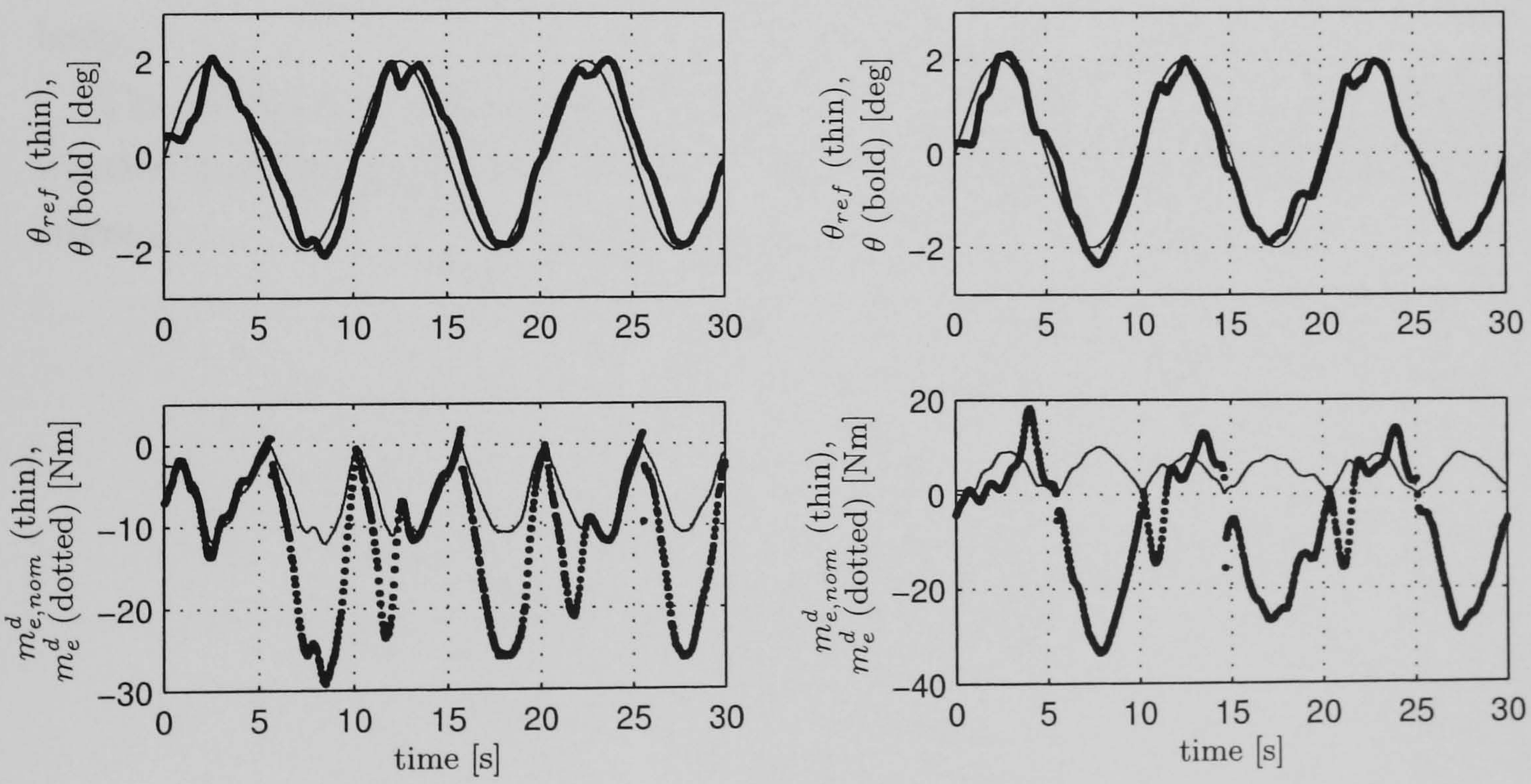

(a) Specified stiffness $K_s = 10\,\mathrm{Nm/deg}$.

(b) Specified stiffness $K_s = 20\,\mathrm{Nm/deg}$.

Figure 4.25: Estimated directional hand moments $m^d_{e,nom}$ and m^d_e during test EPC, cf. Figure 4.21 and Figure 4.22.

4.9 Conclusions (Paraplegic Subject)

The results have shown that ankle stiffness can be controlled by means of FES in paraplegic subjects via feedback control of the muscle moment. However, the major limitation is the ability of the muscle to deliver the requested ankle moment. This is particularly evident in the dorsiflexor muscles. At the beginning of the experimental tests we identified the inherent ankle stiffness when no stimulation is applied as 2 Nm/deg when dorsiflexing and as 3 Nm/deg when plantarflexing. However, throughout the experimental tests, the achieved ankle stiffness with full dorsiflexor stimulation did not significantly increase. This suggest that dorsiflexor stimulation had no effect. The subject's dorsiflexor muscles were far to weak to produce any functional response to the artificial stimulation. Therefore, a more sophisticated control strategy which is based on a model of the dorsiflexor muscles, such as that proposed in section 2.5, is simply not applicable and would not contribute any improvement. However, it should be noted that the study was a proof of feasibility carried out with only one paraplegic subject. Better results might be obtained with a subject in better physical condition regarding his/her paralysed muscles.

Nevertheless, it was shown that accurate stiffness control, limited by the bandwidth of the moment loop, can be achieved for stiffness values with relevance for standing (approximately 10 Nm/deg) as far as the plantarflexor muscles are concerned. Furthermore, we showed that an ankle stiffness above the critical value of $k_s > \tilde{m}gl$ has a stabilising effect. Therefore, we suggest that an increased stiffness generally eases the task of stabilising the body.

The subsequent study presented in the next chapter tries to answer the question of whether a paraplegic subject is able to stand supported only by FES-controlled ankle stiffness.

Chapter 5

Integrated Voluntary Control— Paraplegic Standing supported by FES-controlled Ankle Stiffness

5.1 Summary

Aim: The aim of this study was to investigate the feasibility of paraplegic standing supported by **FES**-controlled ankle stiffness.

Methods: The work was carried out using the "Multipurpose Rehabilitation Frame" as described in section 2.3. The subject was allowed to stand freely and asked to stabilise himself with his upper body, while his ankle stiffness was controlled artificially by FES.

Results: The results show that paraplegic standing can be achieved using FES-controlled ankle stiffness. However, when FES was switched off, standing was no longer possible and the subject lost postural stability.

Conclusion: The paraplegic subject is able to stand and is able to train his balance using FES-controlled ankle stiffness. It was shown that FES-controlled ankle stiffness clearly contributes to the task of stabilising the body. This work has been submitted for publication in IEEE Transactions on Neural Systems and Rehabilitation Engineering [Jaime *et al.*]. A shorter version was presented at the IFESS Conference 2001 [Jaime *et al.*, 2001].

Contribution: This work is the outcome of the author's collaboration with the Center for Sensory-Motor-Interaction at Aalborg University in Denmark. The experimental approach is unique and represents a novel contribution to the literature. The author developed the methods, implemented the experimental software, and ran the experiments. The

work was supported by the European Commission with a Marie Curie Fellowship which allowed the author a 3-month research visit to the Center for Sensory-Motor-Interaction at Aalborg University.

5.2 Motivation

The single-link inverted pendulum approach towards standing described in Chapter 3 provides a useful tool for fundamental studies of unsupported standing, but its practical application is limited. The approach imposes restrictions to the subject's freedom of movement by rigid and rather conservative simplifications. Also, it is only natural to take advantage of the residual sensory-motor faculties of the individual concerned and to integrate them into the control strategy. We call this "integrated voluntary control".

Matjačić and Bajd [1998a,b] proposed a control scheme for standing based on artificially controlled ankle stiffness while utilising voluntary and reflex activity of the paraplegic subject's upper body. The subject stood in an apparatus similar to that described in section 2.3. However, the freedom of movement was restricted to the sagittal plane. The subject's knees were mechanically locked but the subject was free to move his upper body. In this setup the subject was effectively behaving like a double-link inverted pendulum. The ankle stiffness was provided by a hydraulic actuator. Furthermore, they also provided cognitive auditory feedback about the inclination of the lower body. The subject was required to use upper body movement to stabilise himself while standing in the apparatus without any arm support. One neurologically intact and one paraplegic subject with a lesion at level T12 participated in their study. Matjačić and Bajd found that the paraplegic subject was able to maintain balance and even to recover from small disturbances (50 Nm, applied for 100 ms) when an ankle stiffness of 8 Nm/deg was provided. The results were later confirmed and extended to the coronal plane and sagittal plane simultaneously when stiffness was provided around the hips and ankle by hydraulic actuators [Matjačić *et al.*, 2000].

In a further study, Matjačić suggested that the postural response of an intact subject to disturbances could be approximately modelled as a static stiffness in the ankle joints for disturbances in the sagittal plane and in the hips for disturbances in the coronal plane [Matjačić, 2001]. The values of stiffness found were 17 Nm/deg for forward directed disturbances involving plantarflexor activity, 13 Nm/deg for backward directed disturbances involving dorsiflexor activity, and 15 Nm/deg for sideways directed disturbances involving activity of the hip muscles.

Our approach was to substitute the hydraulic actuator by closed-loop FES incorporating stimulation of the plantarflexor and dorsiflexor muscles. A frame controlled by a

hydraulic actuator is a beneficial experimental environment to study the feasibility of a certain principle or control strategy or for balance training purposes. However, it is unwieldy for daily life situations where mobility is required. Compared with that FES provides more flexibility and independence especially when it comes to an implanted system. Furthermore, FES has a greater potential to extend the system towards more functionality. Also, the approach can be widened to a full impedance control of the ankle joint, i.e. controlling not only the stiffness but also the viscosity and inertia of the ankle joint.

Bearing in mind that there are inherent limitations to moment tracking using hydraulic actuators due to the internal feedback of the load velocity (cf. section 2.3.5) the achievable bandwidth of stiffness control is not necessarily higher using hydraulic actuators than when provided by FES (at least for the nominal system). However, as the feasibility study on ankle stiffness control reported in the previous chapter shows, the major limiting factor for controlling ankle stiffness by FES is the ability of the muscles to deliver the requested moment. Furthermore, any FES system is generally affected by fatigue and spasticity, while an "artificial" ankle joint controlled by an hydraulic system is not. Therefore, the following questions arise:

1. Is the quality of ankle stiffness control by FES sufficient to facilitate unsupported standing - without any arm support - in the presence of limited muscle strength and fatigue?

2. Can both control systems, the FES system and the CNS, act in concert to accomplish standing?

5.3 Experimental Setup

The experimental apparatus employed for the study reported in this chapter - called the "Multipurpose Rehabilitation Frame—MRF" is described in section 2.3.

The frame provides two degrees of freedom, i.e. sagittal and coronal planes. It supports the subject around the pelvis and permits motion in a range of $\pm 18°$ around the vertical position in both planes. Two hydraulic actuators can independently control the frame in either of the two planes of motion. The hydraulic actuators can be regarded as artificial ankle and hip joints, respectively.

The subject stood on two force plates allowing independent measurement of the left and right ground reaction forces and moments. The subject's feet can be positioned using cylindrical pegs on two aluminium blocks containing a grid of holes. The subject's knees were mechanically braced by a leather belt. While standing in the frame the subject behaved effectively like a double-link inverted pendulum. The subject in our study was not able to keep his upper body upright without holding on to the frame as shown in Figure 5.1 due to his high level of lesion (T5) and his weak trunk muscles. But since the

frame is moving with the subject's lower body, this does not prevent the subject from falling over and requires active balancing to maintain standing.

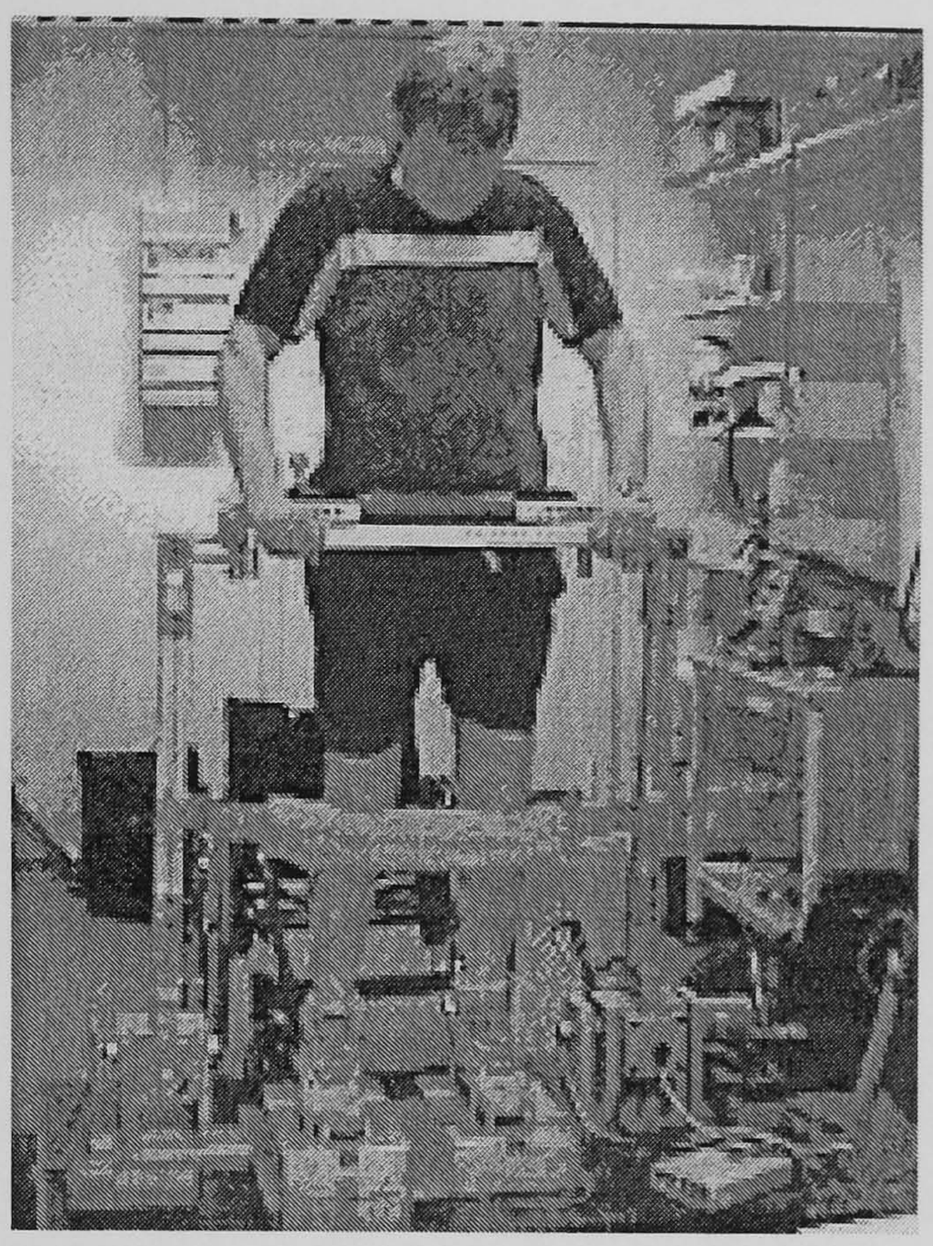

Figure 5.1: Paraplegic subject (T5) balancing while standing in the MRF, with FES at the ankle joints.

The angle of inclination in both the sagittal and coronal planes was measured by a potentiometer. For the experiments presented in this chapter the mobility of the frame was restricted to the sagittal plane by a high value of stiffness in the coronal plane provided by the hydraulic servo system.

The overall standing strategy is shown in Figure 5.2.

While the upper body is still under voluntary control by the CNS, the lower body is supported by FES-controlled ankle stiffness. The inclination angle of the lower body θ is measured by the potentiometer mounted to the frame and multiplied by the desired value of ankle stiffness K_s (typically 10 Nm/deg) which yields the total reference moment $m_{ref,tot}$. The total reference moment is distributed between the left and right ankles following the relative load distribution according to (5.1) and (5.2):

$$m_{ref,l} = \frac{F_{z,l}}{F_{z,l} + F_{z,r}} m_{ref,tot} \tag{5.1}$$

$$m_{ref,r} = \frac{F_{z,r}}{F_{z,l} + F_{z,r}} m_{ref,tot}\,, \tag{5.2}$$

where $F_{z,l}$ and $F_{z,r}$ are the vertical components of the ground reaction force measured by the left and right force plates.

Remark 1 For the experiments reported in this chapter we could also have employed

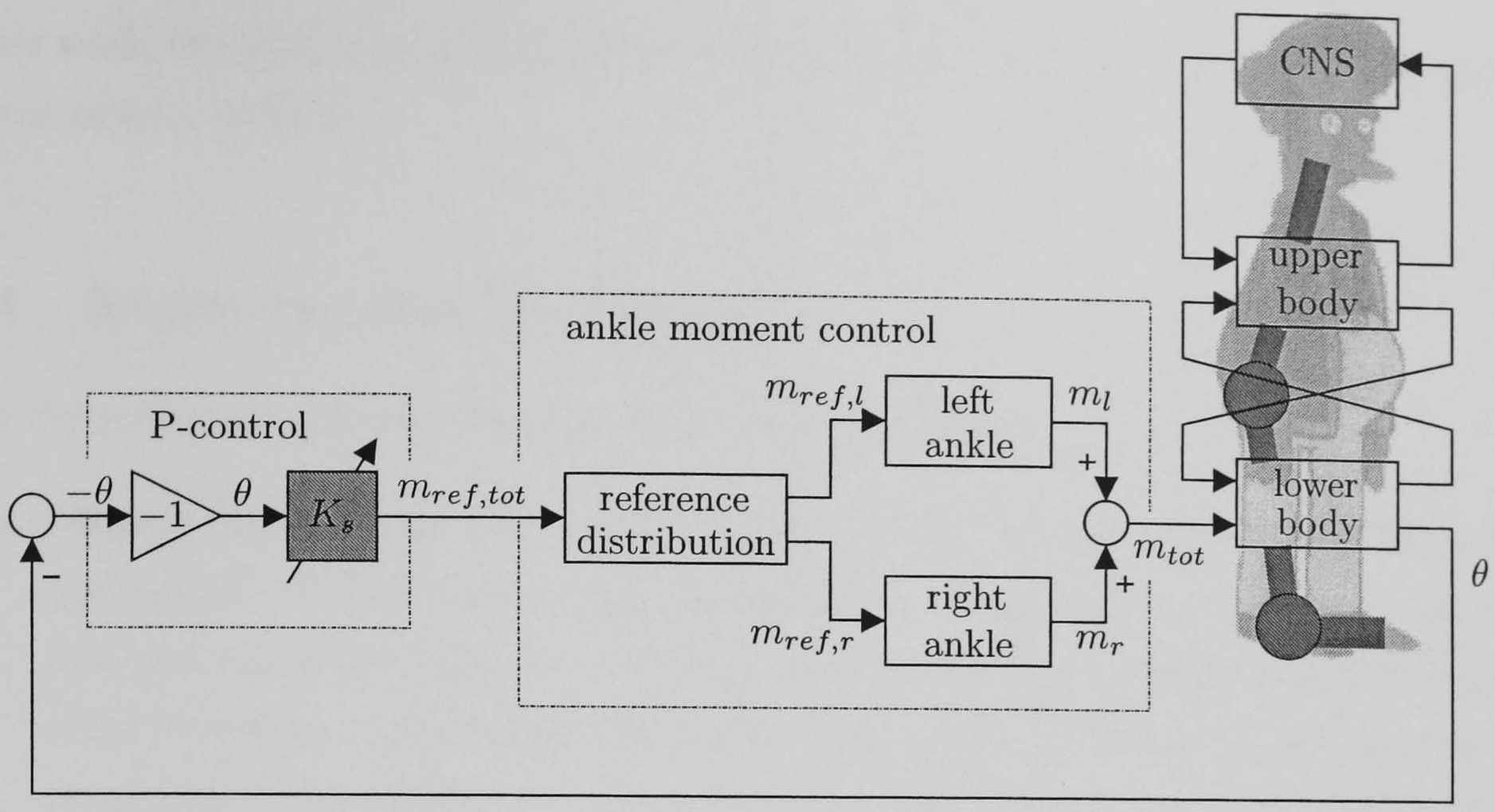

Figure 5.2: Block diagram of ankle stiffness control and standing strategy. The blocks labelled "left ankle" and "right ankle" are **closed-loop** controllers for the left and right ankle moment, respectively (cf. sections 2.4 and 2.5).

the SISO approach for the total ankle moment as utilized for the experiments reported in Chapter 3 and Chapter 4. However, our original intention was also to implement hip stiffness control to facilitate stability in the frontal plane. Then, balancing would involve continuous load shifting from one leg to the other and an equal stimulation of both legs regardless of the contributed moment of either leg would no longer be desirable. However, hip stiffness control had to be abandoned due to the subject's weak muscles. This issue is further discussed in Chapter 6.

The partial ankle moments $m_{ref,l}$ and $m_{ref,r}$ are under closed-loop control. A pole assignment approach is employed separately for the plantarflexor and dorsiflexor muscle groups of each leg with a suitable scheduling strategy (cf. section 2.4 and section 2.5, respectively). Integral action is employed for ankle moment control as we are mainly interested in accurate moment tracking. i.e. $\Delta^m(q^{-1}) = 1 - q^{-1}$ (cf. Figure 2.14).

As mentioned in the previous chapter a stiffness control approach can be regarded as a proportional control for the inclination angle of the lower body. As shown on the single-link inverted pendulum, proportional control is not sufficient for stabilisation. An external moment has to be applied by the experimenter. Here, that "external" moment is implicitly applied via the internal coupling between the two links of the double-link inverted pendulum while the upper link (upper body half) is still under voluntary control by the CNS. For the double-link inverted pendulum configuration, the influence of an ideal ankle joint stiffness, i.e. when the transfer function from $m_{ref,tot}$ to m_{tot} in Figure 5.2 is unity, has been analysed in great detail in [Matjačić and Bajd, 1998a]. The idea behind this setup can be summarised as follows: a certain ankle stiffness makes stable standing

easier while the task of stabilising is left to the paralysed subject, utilizing his/her residual motor-sensory abilities.

5.4 Experimental Procedure

The experimental procedures can be summarised as follows:

1. **Identification.** The paraplegic subject stood on two forceplates, the knees being mechanically locked by a leather belt as shown in Figure 5.1. During the identification procedure the frame was fixed by an aluminium bar mounted on the ceiling in order to ensure static conditions and to gain better results from the identification procedure. The subject was asked to stand still. Test C and Test PRBS (cf. section 3.4) were carried out separately for the plantarflexor and dorsiflexor muscles of both the left and right legs.

The input/output data gained from the PRBS test were used to identify a local linear transfer function at the stimulated operation point for each muscle group. Following the identification procedure and assessment of the quality of the identified models a moment controller was designed for each muscle group. The control design was judged on the basis of the closed-loop frequency responses before testing.

2. **Test M.** This is a test of closed-loop **M**oment tracking. It was carried out to check whether the moment feedback loop was well designed and working properly before a series of standing test would be carried out.

3. **Test B.** This is a test of active **B**alancing. The aluminium bar fixing the frame was removed. The hydraulic circuit of the frame was switched on. The frame provided support in the coronal plane by a stiffness of 10 Nm/deg in order to restrain the movement to the sagittal plane. In the sagittal plane the frame provided a stiffness of 2 Nm/deg in order to compensate the load imposed by the weight of the frame. The frame was held in the upright position by the experimenter. Then the stimulation was switched on and the subject was released while under the influence of closed-loop FES-controlled ankle stiffness. In order to maintain standing the subject was forced to balance actively. The results are presented in chronological order.

5.5 Subject

The experiments reported here were performed with a paraplegic subject with a complete lesion at T5. The subject was male, 38 years of age, 8 years post injury and psychologically and physically in good condition. Prior to the experiments reported here, the subject

underwent the following sessions in the course of this study. However, the subject did not undergo a special muscle training.

- Three sessions of balance training. First, the subject underwent several training sessions where the appropriate level of stiffness around the ankles was maintained by the frame. This enabled the subject to learn how to use the upper body for balancing at a stiffness level of 8 Nm/deg. The subject gained adequate balancing skills after three sessions of balancing that lasted up to half an hour. FES was introduced after the initial three sessions.

- One session of plantarflexor moment control (i.e. "Identification" and "Test M", above).

- Two sessions of standing under FES-controlled ankle stiffness (i.e. "Identification", "Test M", and "Test B", above). The results presented in this chapter are from the second standing session.

5.6 Experimental Results

5.6.1 Results of Test C

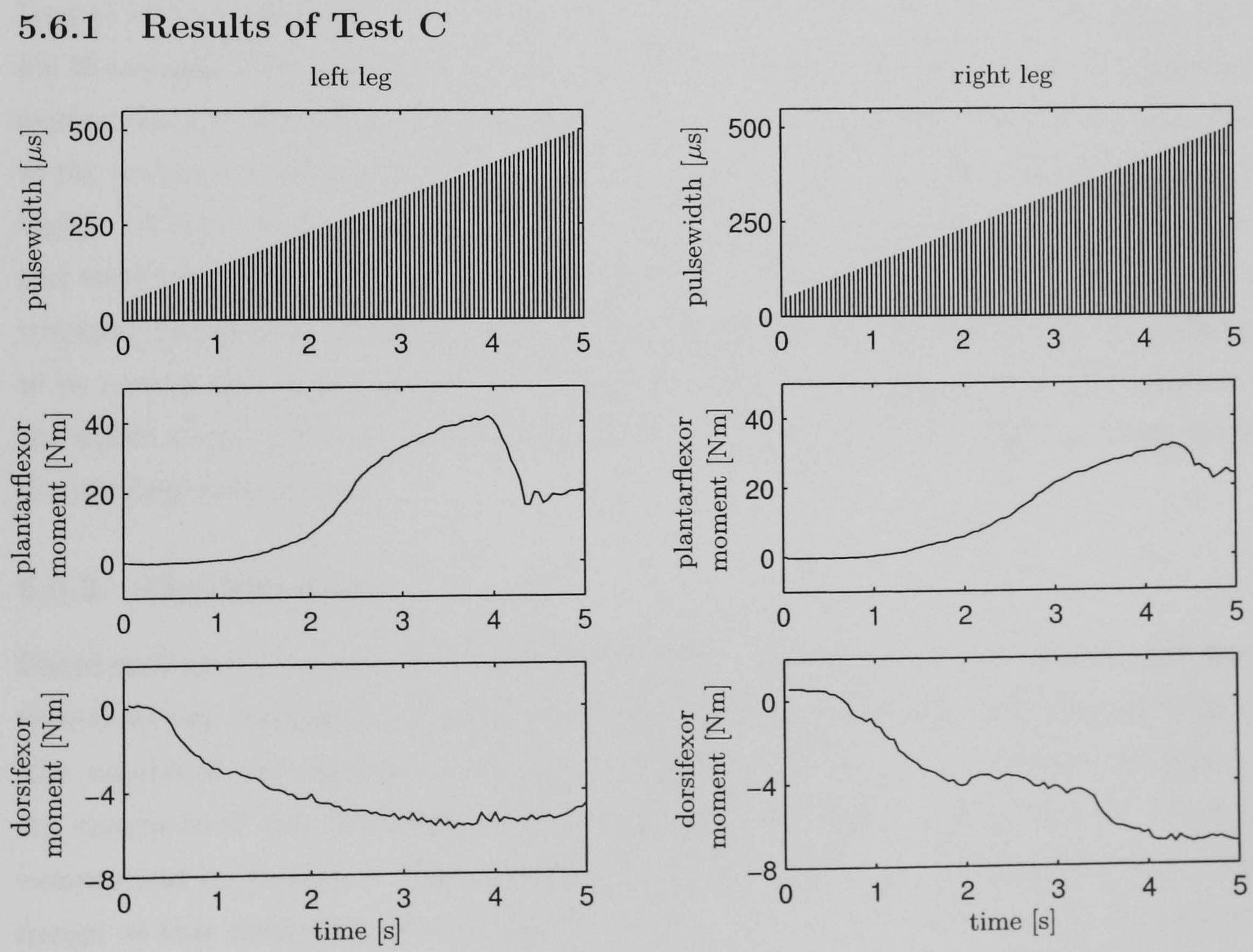

Figure 5.3: Results of Test C with a current of 60 mA. The plantarflexor and dorsiflexor tests were carried out separately. The plantarflexor moment decreases for high stimulation levels due to the lifting of the heels.

The results of Test C can be seen in Figure 5.3. The test was carried out separately for plantarflexor and dorsiflexor muscles, but the data are presented together in Figure 5.3. Test C was carried out with a current amplitude of 60 mA for each muscle group. It can be seen that there is an asymmetry between the left and right legs. Furthermore, the dorsiflexor muscles are considerably weaker than the plantarflexor muscles. It can clearly be seen that the produced moment starts rising once a certain threshold is passed. The plantarflexor moment decreases again at higher stimulation levels. This is due to lifting of the heels that occurred at high stimulation levels since the feet were only held in position for correct forceplate measurements but not mechanically held down. This corresponds to the natural situation of standing. Taking the stimulation threshold, heel lift and the gained moment into account the stimulation amplitude was set to 60 mA for all four muscles during the further course of the experiment. We noted that the lower leg muscles of our patient were quite strong taking into account that he did not undergo any particular muscle training.

5.6.2 Results of Test PRBS

Results of Test PRBS are presented in Figure 5.4. The test was carried out for a mean level of 150 μs (bold) and once repeated for a mean level of 200 μs (thin). Each test lasted for 20 seconds. The stimulation was not further increased because we knew from previous experience that the muscles have a higher DC-gain at low stimulation levels. This is due to the inverse recruitment pattern for artificial stimulation. The identified model with the higher DC-gain would later be used for the controller design. The first 5 seconds of the test were omitted when performing the estimation of the transfer function to exclude the transient response at the beginning of each stimulation cycle. There are also disturbances to be seen in the muscle response. They may be the result of spasticity or the influence of the upper body. This observation emphasises the importance of fixing the frame during the identification process.

5.6.3 Identification

Based on the input/output data from Test PRBS we identified two local second-order linear time-invariant transfer functions for each muscle group using the least squares criterion. The results of the estimation process for both muscle groups are similar in nature to the results from the "Wobbler" experiments shown in Figure 3.30 on page 63. They are summarised in Table 5.1. The model with the highest DC gain was used for the control design as this choice improves robustness against fatigue and variations of the operating point. The model of the right dorsiflexor muscles at 150 μs seems to be inconsistent with the other models and might be affected by modelling errors. Reasons for this have been pointed out above. Nevertheless this model was used for controller design as that error

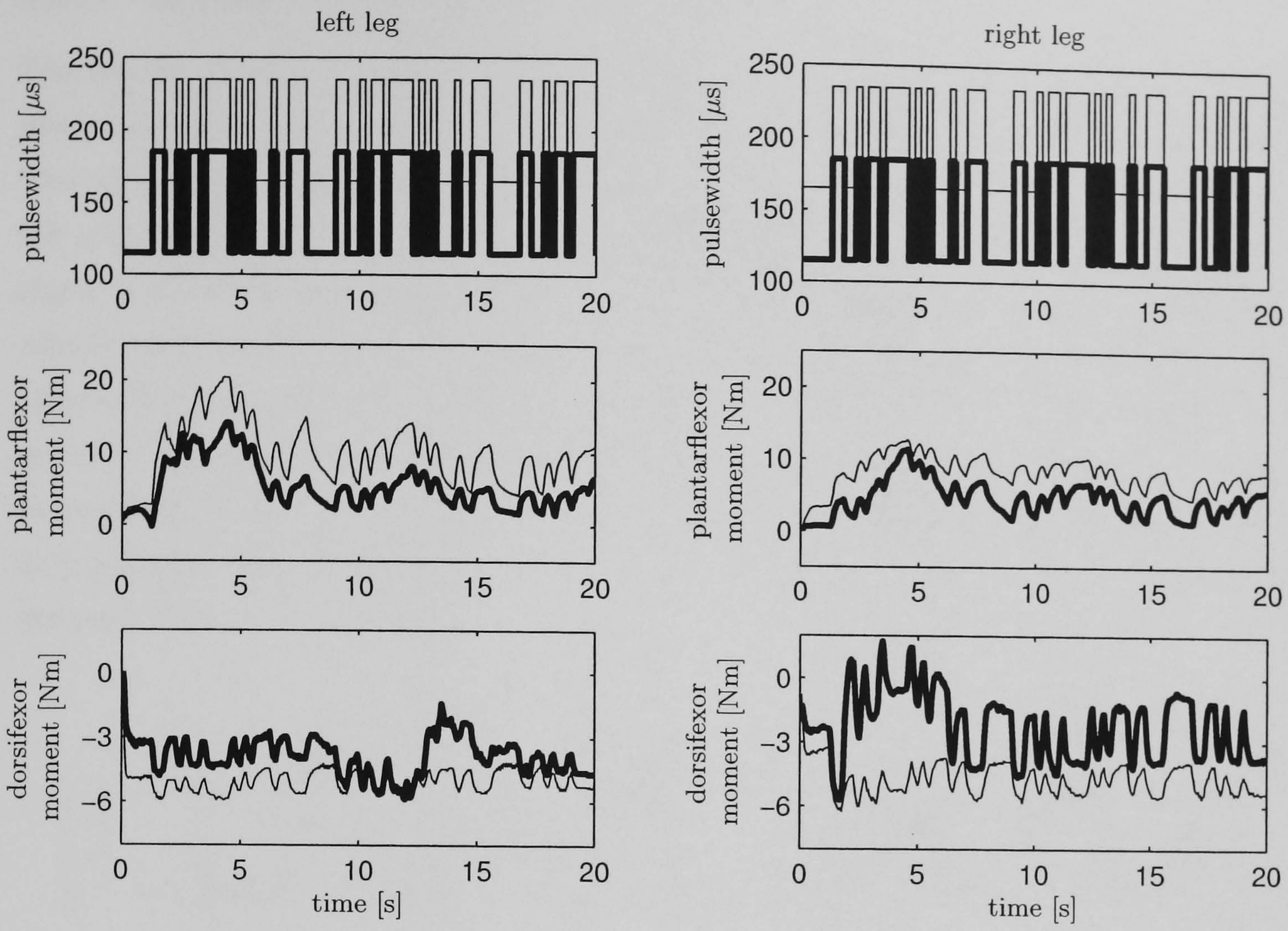

Figure 5.4: Results of Test PRBS. The bold lines in the moment plots correspond to the bold line in the pulsewidth plot. The two PRBS signals for each side were applied to both muscle groups on that side in separate tests, hence four moment plots for each side are shown.

does not endanger robust stability of the moment loop.

muscle group	pulsewidth [μs]	transfer function $G_p(q^{-1})$	rise time [s]	DC gain [Nm/μs]
plantarflexor left	150	$\frac{0.770 \cdot 10^{-2} q^{-1}}{1-1.189q^{-1}+0.272q^{-2}}$	0.87	0.09
	200	$\mathbf{\frac{1.369 \cdot 10^{-2} q^{-1}}{1-1.213q^{-1}+0.327q^{-2}}}$	**0.54**	**0.12**
plantarflexor right	**150**	$\mathbf{\frac{0.717 \cdot 10^{-2} q^{-1}}{1-1.251q^{-1}+0.336q^{-2}}}$	**0.74**	**0.08**
	200	$\frac{0.706 \cdot 10^{-2} q^{-1}}{1-1.166q^{-1}+0.283q^{-2}}$	0.58	0.06
dorsiflexor left	**150**	$\mathbf{\frac{-0.336 \cdot 10^{-2} q^{-1}}{1-1.175q^{-1}+0.272q^{-2}}}$	**0.73**	**-0.04**
	200	$\frac{-0.447 \cdot 10^{-2} q^{-1}}{1-0.689q^{-1}+0.062q^{-2}}$	0.41	-0.02
dorsiflexor right	**150**	$\mathbf{\frac{-0.839 \cdot 10^{-2} q^{-1}}{1-1.221q^{-1}+0.415q^{-2}}}$	**0.22**	**-0.04**
	200	$\frac{-0.441 \cdot 10^{-2} q^{-1}}{1-0.939q^{-1}+0.142q^{-2}}$	0.38	-0.02

Table 5.1: Identification results. The transfer function, rise time and DC gain for each model. The highlighted models were selected for control design.

5.6.4 Results of Test M

The results of typical moment controller tests are shown in Figure 5.5. The plots in the upper row show the reference moment (thin line) and the controlled moment (thick line). The reference moment was a $\pm 5\,\mathrm{Nm}$ square wave signal that was distributed between the left and right legs according to the current load distribution. The plantarflexor stimulation signal is presented in the middle row. The plots in the row below show the dorsiflexor stimulation pulsewidth. It can be seen from the left leg moment plot that switching between plantarflexor and dorsiflexor muscles occurs at a slightly negative moment. Therefore, the moment step required from the plantarflexor muscles is higher than the moment step required from the dorsiflexor muscles due to offsets. This explains why a higher stimulation is required for the plantarflexors than for the dorsiflexors although the plantarflexors are stronger than the dorsiflexors.

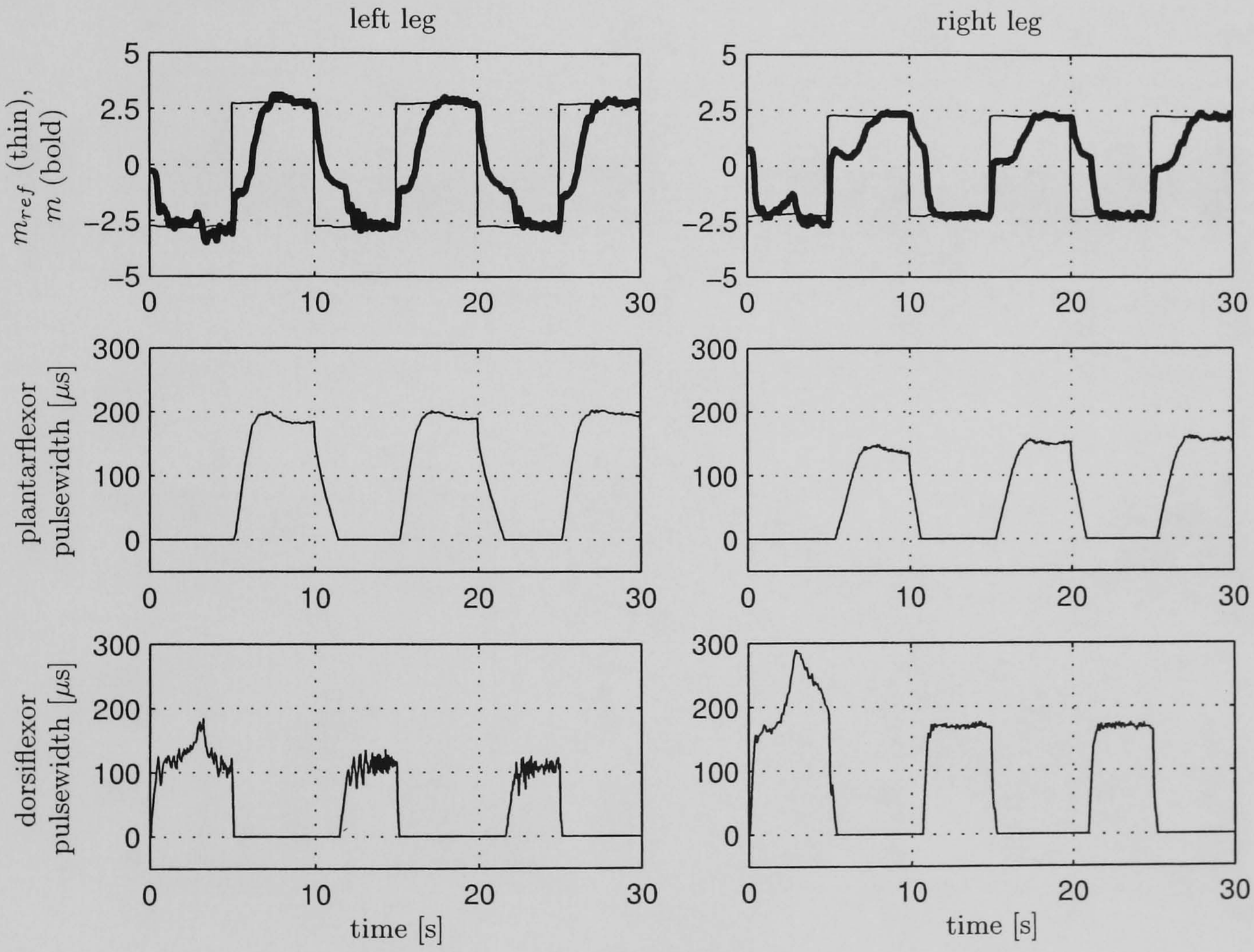

Figure 5.5: Muscle moment control test. Control design parameters are $t^m_{r,c} = 0.5\,\mathrm{s}$ and $t^m_{r,c} = 0.7\,\mathrm{s}$ for the left and right plantarflexor muscle, respectively; $t^m_{r,c} = 0.7\,\mathrm{s}$ and $t^m_{r,c} = 0.3\,\mathrm{s}$ for the left and right dorsiflexor muscle, respectively. All observer rise times were set to $t^m_{r,o} = 0.15\,\mathrm{s}$, all tracking rise times (specified by the pre-filter) were set to $t^m_{r,o} = 0.2\,\mathrm{s}$. All damping factors were set to $\zeta = 0.999$.

5.6.5 Results of Test B

A typical standing trial is shown in Figure 5.6. After the stimulation was switched on the subject was released and was balancing on his own under the influence of the FES controlled ankle stiffness. The stiffness was set at 10 Nm/deg. The frame provided a stiffness of 10 Nm/deg in the frontal plane (restraining movement only to the sagittal plane) and 2 Nm/deg in the sagittal plane in order to compensate the load imposed by the weight of the frame.

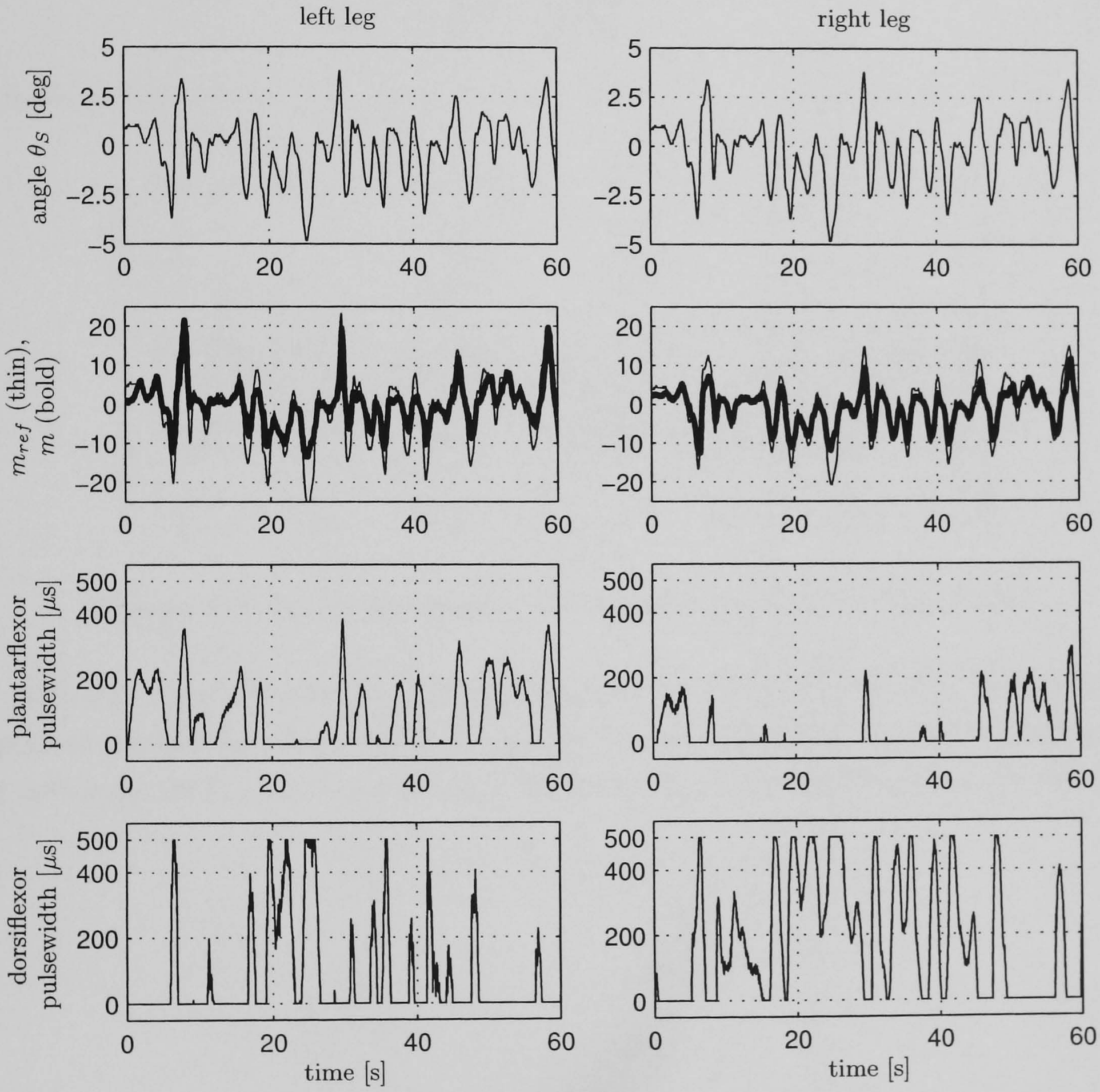

Figure 5.6: First successful standing trial. Specified stiffness $K_s = 10\,\text{Nm/deg}$. The angle plots are the same for the left and right sides.

The graphs on the top show the inclination angle of the frame, i.e. the lower body θ_S in the sagittal plane (cf. Figure 5.2). The plots are identical for the left and right legs. The plots in the second row show the moment tracking control. These plots are different for the left and right leg as the distribution of the reference moment $m_{ref,tot}$ (cf. Figure 5.2) depends on the current load distribution between the two legs (cf. equation (5.1) and (5.2)). The third row shows the associated plantarflexor stimulation while the

bottom graphs show the dorsiflexor stimulation for both the left and right legs. Importantly, in this test the angle of inclination remained bounded to less than $\pm 5°$ over the entire duration of the test, indicating the ability of the subject to successfully balance for the duration of one minute. The moment plots reveal that the dorsiflexor muscles, although weaker than the plantarflexor muscles, are able to produce a moment of 10 Nm on both sides.

The time history of the achieved stiffness $k_s(k)$

$$k_s(k) = \frac{m_{tot}(k)}{\theta_S(k)} \tag{5.3}$$

is shown in Figure 5.7.

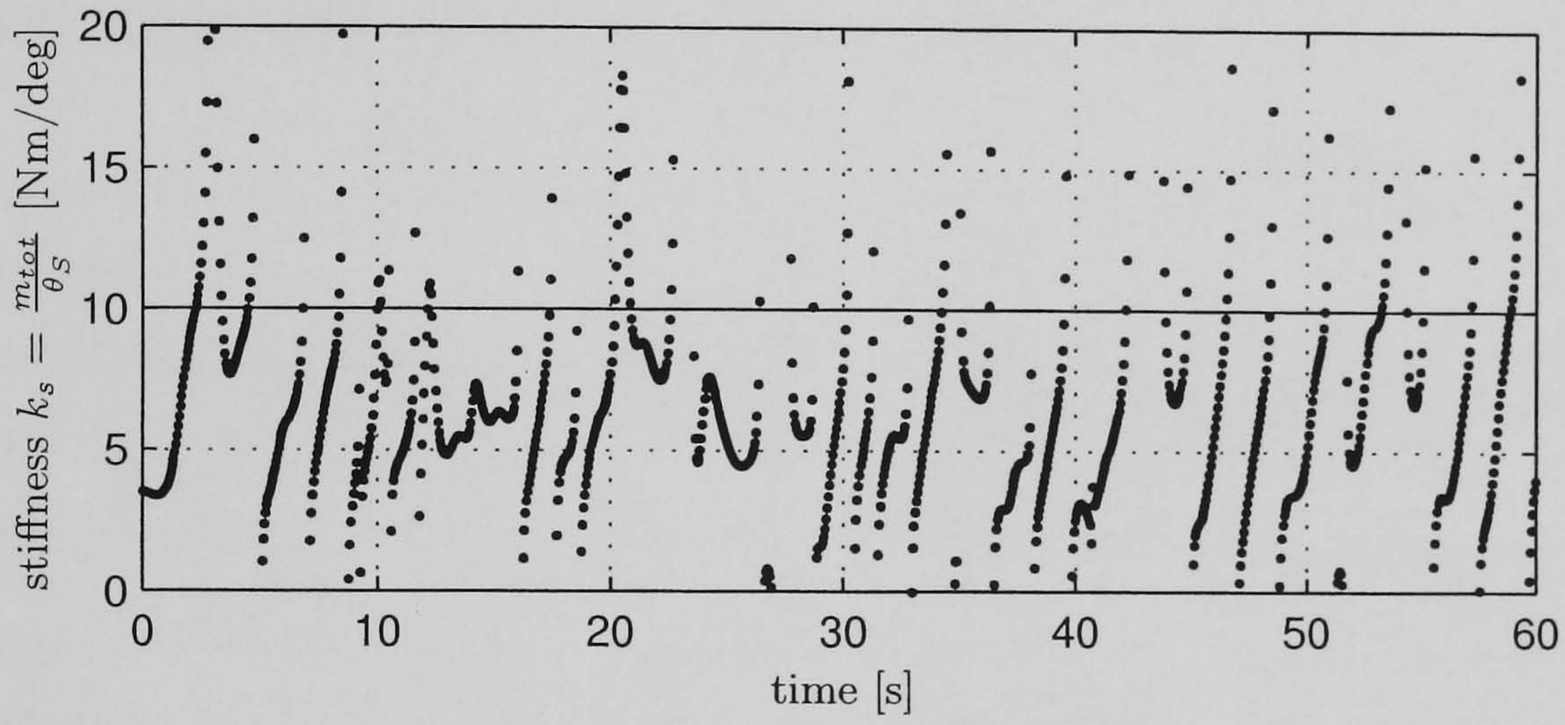

Figure 5.7: Controlled stiffness during standing trial (cf. Figure 5.6).

The dots mark the calculated stiffness at the sampled time instants. The measured signals of moment and angle were zero-phase-shift digitally filtered by a Butterworth filter of 10^{th} order with a cut-frequency of 1 Hz in order to eliminate the noise from the data.

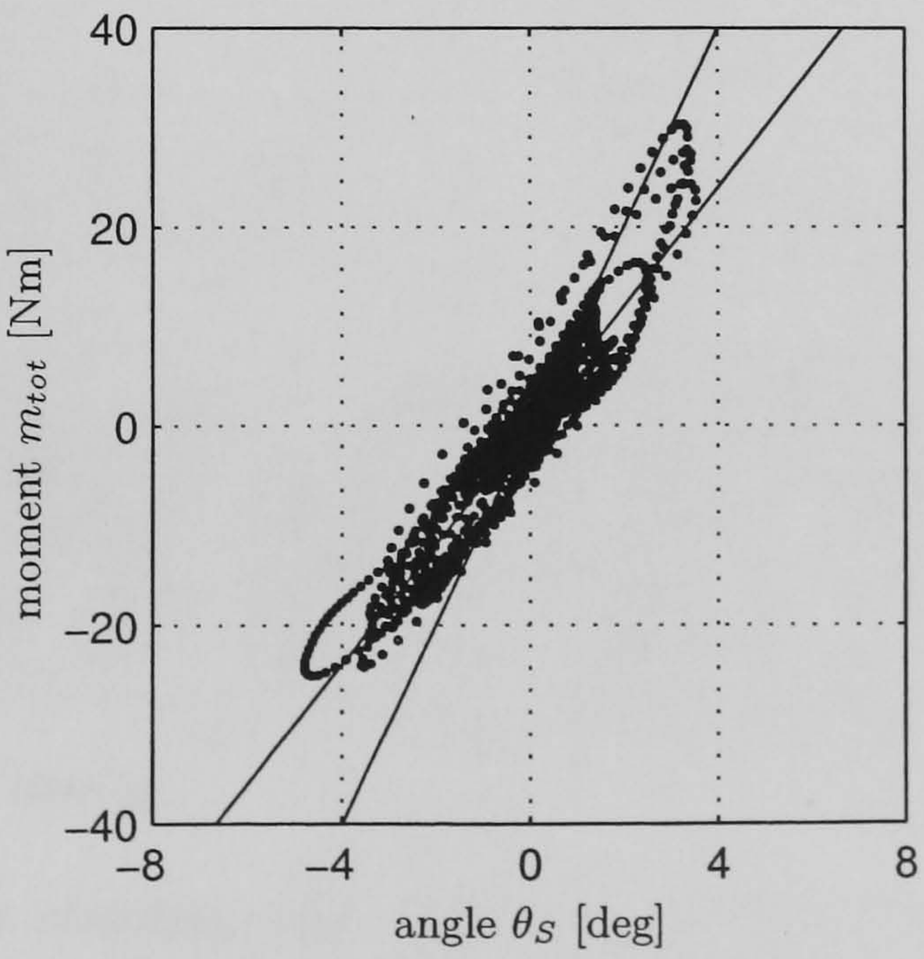

Figure 5.8: Stiffness plot in phase plane. The straight lines indicate a stiffness of 10 Nm/deg (desired value) and 6 Nm/deg.

Due to the highly dynamic characteristics of the standing trial (cf. Figure 5.6), there is a continuing underachievement in stiffness control. The accuracy of stiffness control is limited by the closed-loop bandwidth of the moment control related to the bandwidth of standing. For a general discussion of the appearance of the controlled stiffness refer to section 4.6.2.

Another representation of the achieved stiffness is shown in Figure 5.8 where the stiffness is plotted in the phase plane as moment versus angle. The reference stiffness of 10 Nm/deg as well as a stiffness of 6 Nm/deg, around which the real stiffness approximately centres, are indicated by a straight line.

Another standing trial is shown in Figure 5.9. The dotted lines in the angle plot emphasise the decreasing amplitude of the sway angle θ_S. This suggests that the subject is learning to balance better during the experiment.

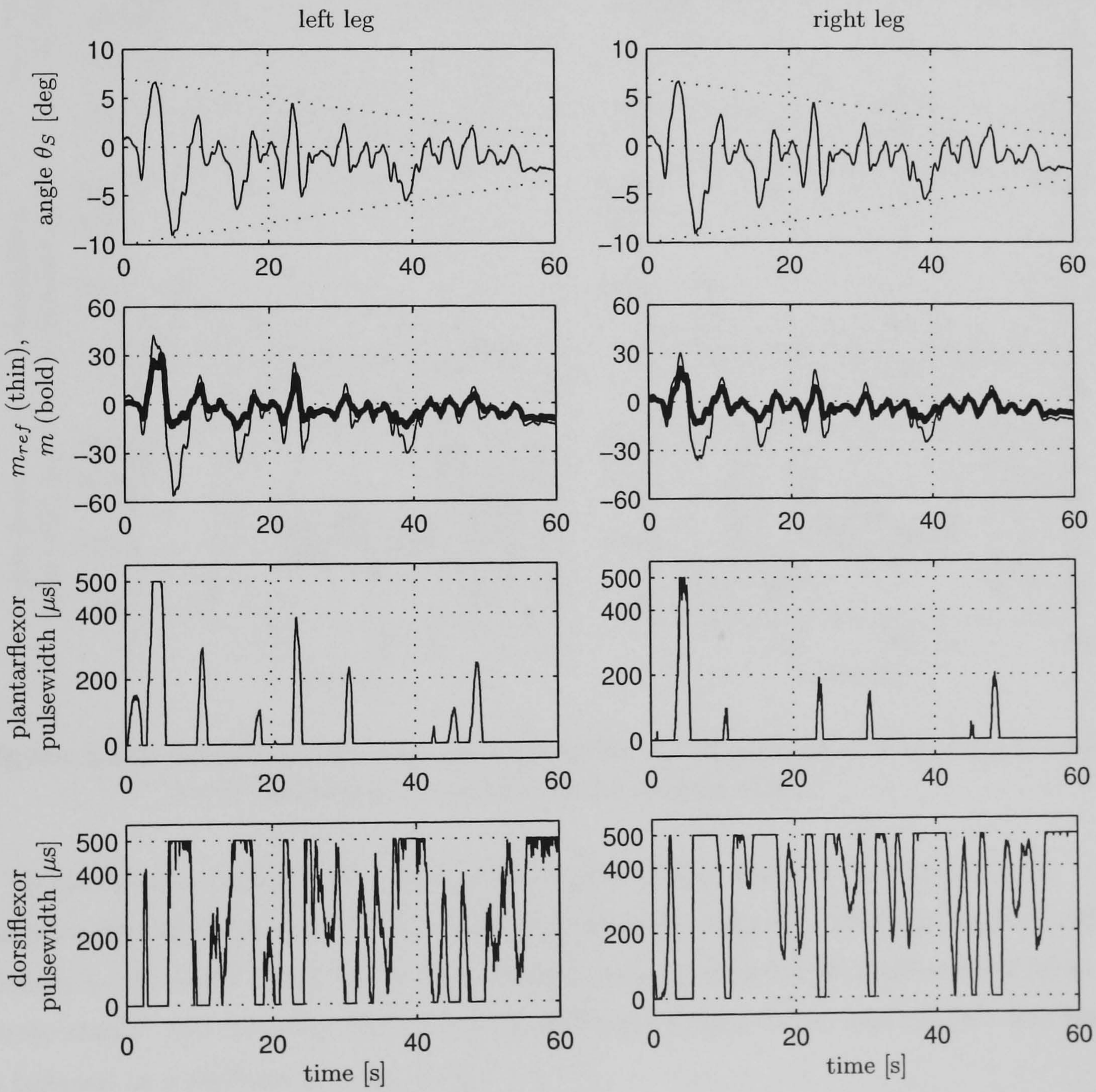

Figure 5.9: Subsequent standing trial. The decreasing amplitude of the sway angle is emphasised by the dotted lines in the angle plots. This indicates a learning effect.

A third standing trial is shown in Figure 5.10. The stiffness was reduced to 8 Nm/deg in order to avoid constant saturation of the dorsiflexor stimulation. A learning process can be observed again in the first 40 seconds of this trial. The subject even stood still for a few seconds between $t = 35 \ldots 42$ s.

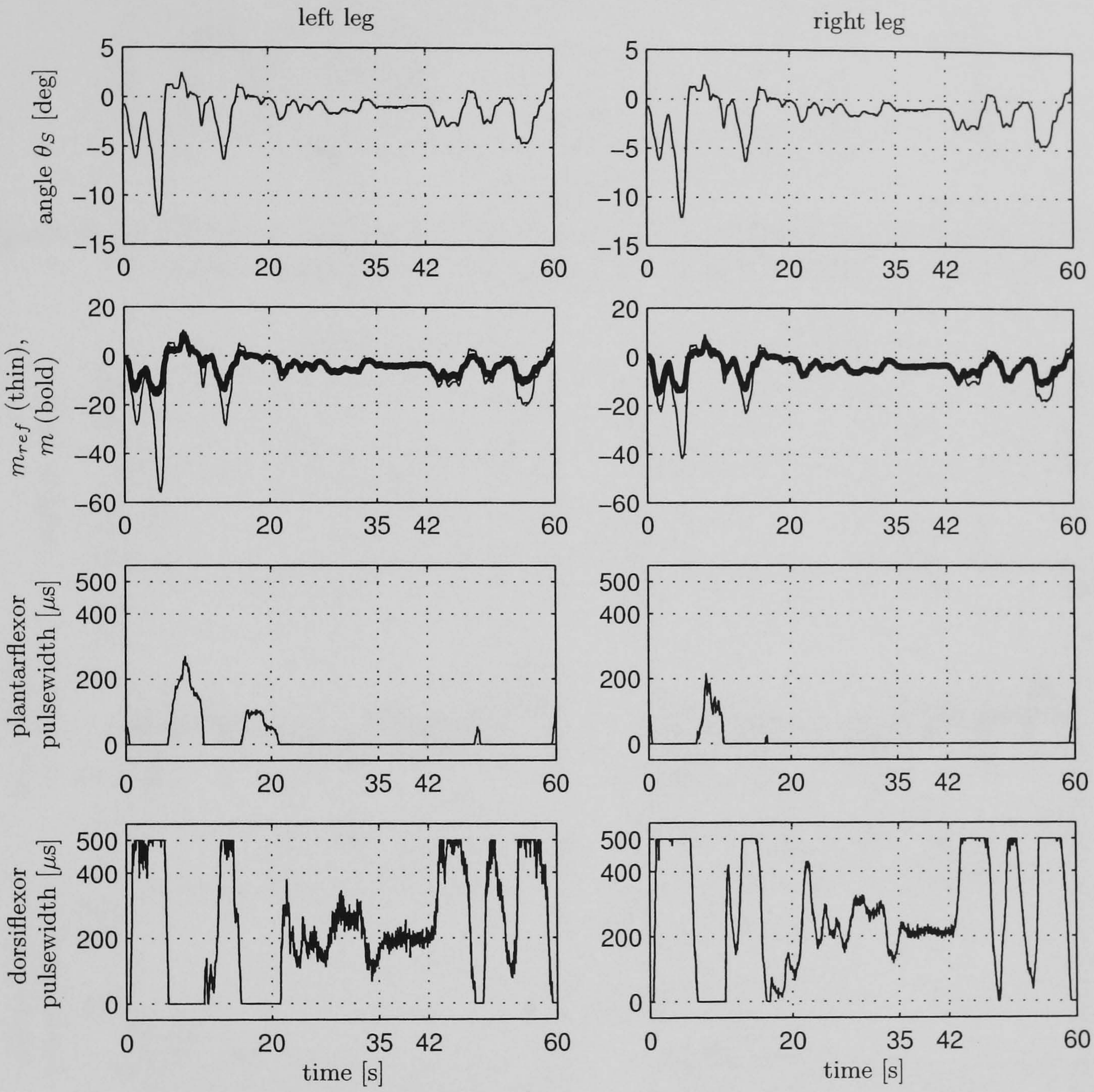

Figure 5.10: Standing trial. The specified stiffness was reduced to 8 Nm/deg in order to avoid permanent saturation of the control signal.

It can be seen from Figure 5.11 that during the period of static standing ($t = 35 \ldots 42$ s) the specified stiffness of $K_s = 8$ Nm/deg is actually achieved, although slightly delayed relative to the angle signal due to the dynamic properties of the moment control loop. The "more static" the standing the better the stiffness control. Note, the subject was trained to balance at a stiffness of 8 Nm/deg.

A final standing trial is shown in Figure 5.12. Here, the stimulation was switched off after 30 s while the subject was balancing. This was done in order to emphasize the stabilising contribution of the FES-controlled ankle stiffness. After the stimulation was switched off the subject immediately lost stability. He was then put back by the

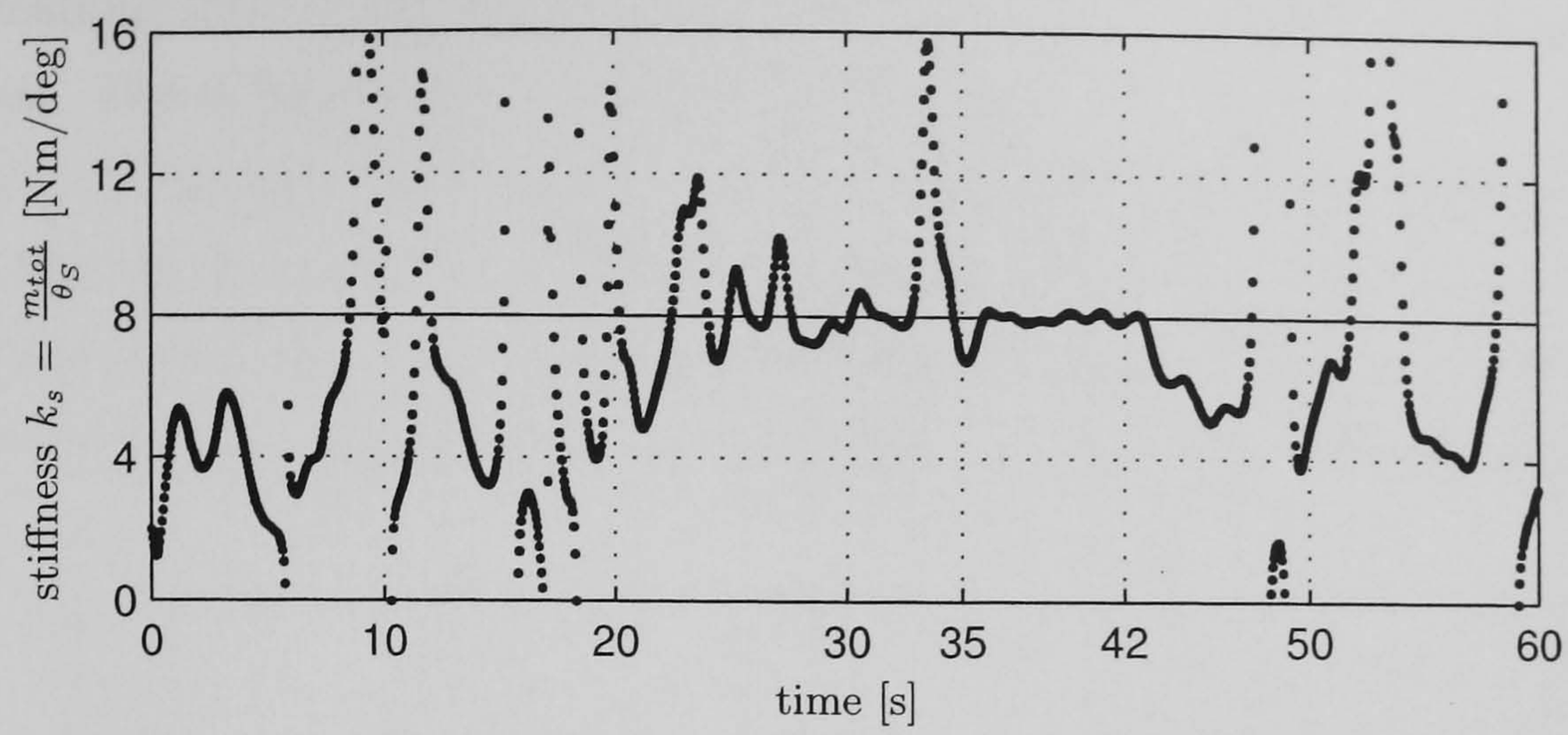

Figure 5.11: Controlled stiffness during standing trial (corresponds to Figure 5.10). For static conditions ($t = 35 \ldots 42\,\mathrm{s}$), the specified stiffness is achieved.

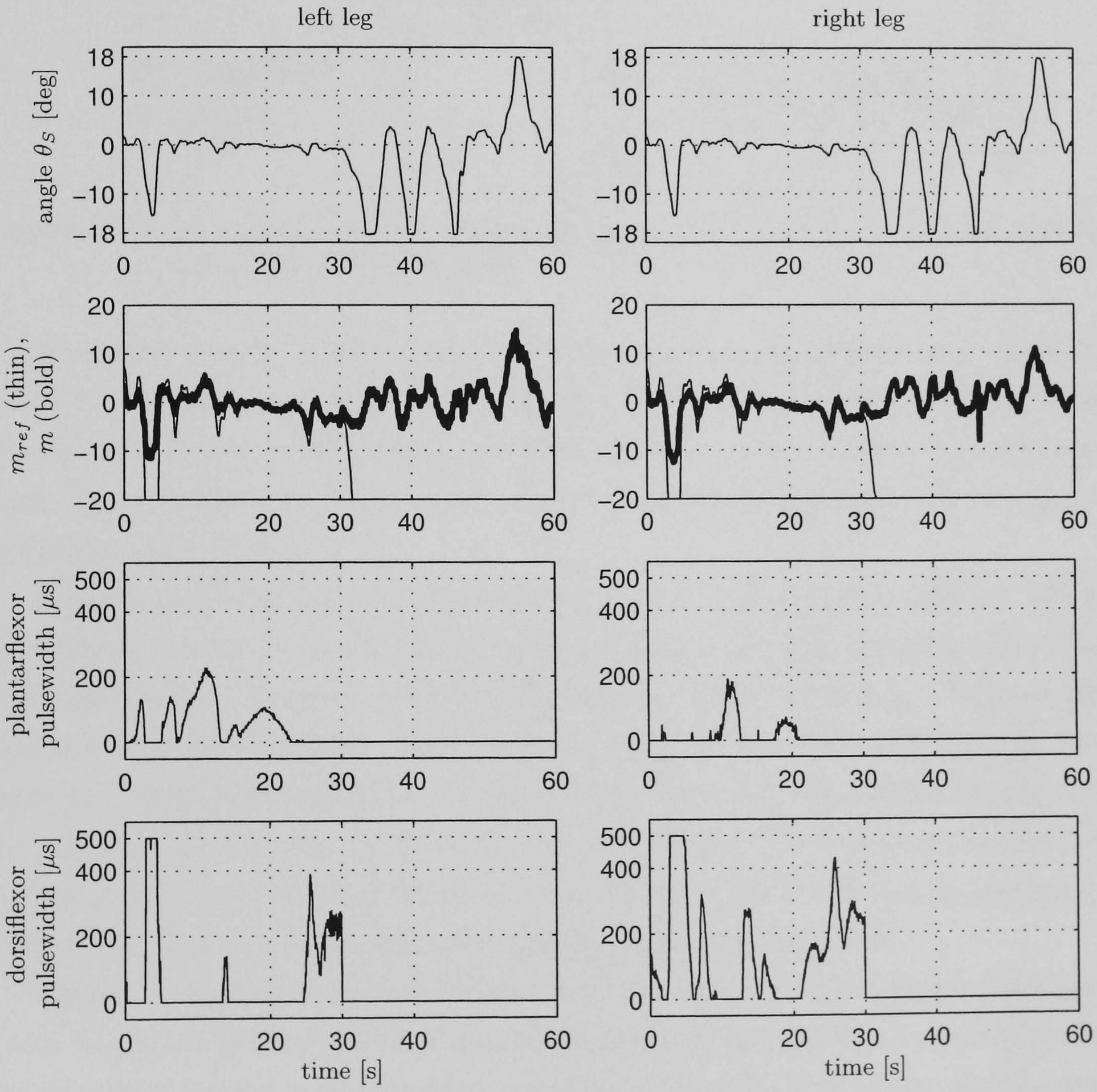

Figure 5.12: Standing trial to emphasise contribution of FES. The stimulation was switched off after 30 s.

experimenter into a nearly vertical position and fell again. This was repeated three times

in the remaining 30 s of this standing trial but the subject was not able to stand without stimulation. The stiffness was specified as 8 Nm/deg.

Figure 5.13 clarifies what happens to the ankle stiffness. Just before the stimulation was switched off the specified stiffness was achieved but after switch off it immediately falls to about 2 Nm/deg. The remaining stiffness seems to be inherent to the ankle joints. Note that the moment produced by the hydraulic actuators was not measured.

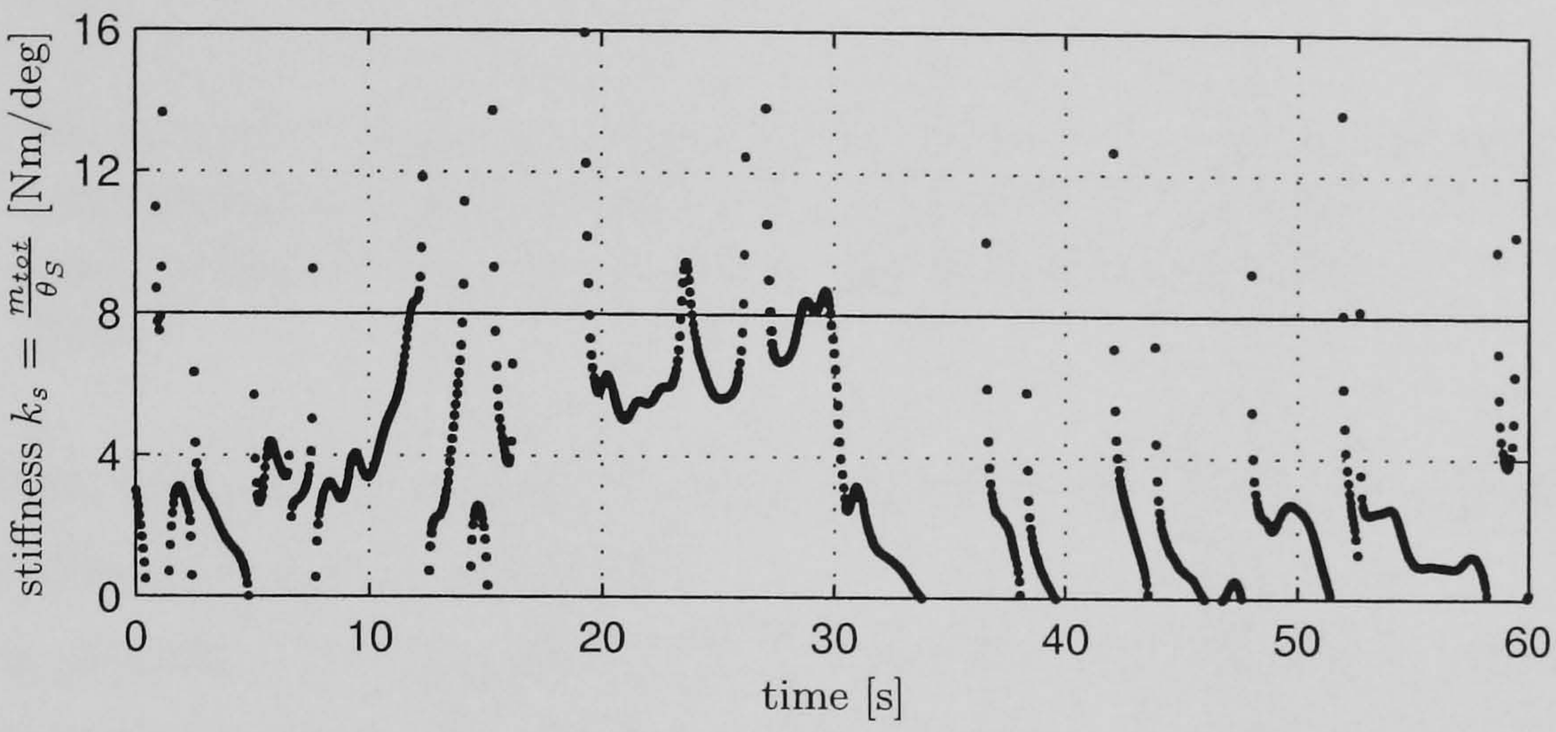

Figure 5.13: Controlled stiffness during standing trial when stimulation was switched off after 30 s (cf. Figure 5.12).

Altogether, a series of five successful standing trials (excluding the trial shown in Figure 5.12) was carried out, each trial lasting 60 s. The results are summarised in Table 5.2. The mean value $\overline{\theta}_S$ as well as the standard deviation $\sigma(\theta_S)$ is given for each standing trial. They represent the angle of inclination of the lower body and the (average) sway amplitude, respectively.

Matjačić and Bajd defined the quantities "posture" and "postural activity" which take the stiffness value into account for a quantitative assessment of the standing trials [Matjačić and Bajd, 1998b]. However, instead of the desired value, the actually achieved stiffness should be considered in order to give these quantities a reasonable meaning. On the other hand, it is difficult to establish a constant value of the present stiffness during standing (cf. Figures 5.7, 5.11 and 5.13). Also, the percentage of time spent in forward leaning posture (referring to the lower body) $t_{+\theta_S}$ as well as in backward leaning posture $t_{+\theta_S}$ is given. Both these values are related to the total duration of the trial.

Trial no. 1 was the first successful trial and the given values are different from the other trials. The main difference is that the subject spent approximately equal time in forward and backward leaning postures which results in a smaller value for the average angle $\overline{\theta}_S$ and the standard deviation $\sigma(\theta_S)$. The difference between the first trial and the others suggest that, during the first trial, the subject was mainly trying to accustom himself to the experimental environment. During the remaining trials the subject clearly preferred a backward leaning posture. This is contrary to results reported with open-loop stimulation,

trial no.	K_s [Nm/deg]	$\overline{\theta}_S$ [deg]	$\sigma(\theta_S)$ [deg]	$t_{+\theta_S}$ [%]	$t_{-\theta_S}$ [%]
1	10	−0.2	1.5	52	48
2	10	−1.2	2.5	26	74
3*	10	−1.2	1.9	30	70
4	8	−1.5	2.1	15	85
5*	8	−1.8	1.9	7	93

Table 5.2: Statistical evaluation of standing trials. Prior to the listed trials the initial two trials failed due to excitation of the knee flexion reflex. The trials marked with a star are not shown here. The trial shown in Figure 5.12 is not listed here.

where the hips were usually hyperextended [Kralj and Bajd, 1989], but coincides with the results from Matjačić and Bajd [1998b].

While the standard deviation does not significantly change during the remaining course of the experimental session, the average inclination angle becomes more negative as the subject relies more and more on the backward posture. The requested stiffness was decreased from 10 to 8 Nm/deg but fatigue may be the major source of this effect.

5.7 Conclusion

The results have shown that paraplegic standing can be achieved by implementing FES-controlled ankle stiffness while the residual sensory-motor abilities of the patient are utilized. The subject in our study had to support his trunk by holding onto the frame due to his rather high level of lesion and his weak trunk muscles. A subject with a lower lesion and adequate trunk muscle strength should be able to perform the balancing task by using his trunk muscles alone, thus leaving the arms to perform a functional task. However, the results demonstrate the feasibility of stable paraplegic standing, when supported by FES-controlled ankle stiffness. FES-controlled ankle stiffness makes an essential contribution to the overall control scheme and enables the subject to stand. This implies that when the subject's residual abilities are adequately trained, quite simple FES control strategies can be sufficient for stable standing. The results of this study can be summarised as follows:

- Paraplegic standing can be achieved by FES-controlled ankle stiffness.
- The subject learned to stand by means of the FES-controlled ankle stiffness. This learning process was observed over the course of the presented series of experiments. Figure 5.6 was the first standing trial during the session on which the results are based. The sway angle is rather restless for the entire duration of the trial. In

the following trials the subjects settled more or less after some initial sways. In Figure 5.9 the sway amplitude steadily decreased and came to rest during the trial shown in Figure 5.10 and Figure 5.12 before the stimulation was switched off. The same observation was made during the trials which are not presented here. These results suggest that the subject would be able to stand quite safely after an initial learning phase.

- The accuracy of stiffness control is fundamentally limited by the bandwidth of the moment controller and the strength of the muscles. Clearly, when the controller saturates and the muscles are not able to produce the requested moment this will result in an underachievement with regard the stiffness control. However, accurate stiffness control can be achieved in static conditions, i.e. when the subject is standing quietly enough.

- Standing is also possible even when the specified stiffness can not be achieved.

- The subject preferred a backward leaning posture with respect to the lower body while the upper body was leaning forward. Consequently, mostly dorsiflexor stimulation was involved. It is therefore desirable to pay attention to the moment tracking properties of dorsiflexor stimulation. Hence, it made sense to have a controller based on the dorsiflexor dynamics as well as the plantarflexor dynamics. However, it has been seen in the previous chapter that it depends on the physical constitution of the subject whether this is possible, although it might be necessary for successful standing.

- Overall the subject was able to stand for a considerable time span. Five successful standing trials were performed during the session, each with a duration of one minute. The initial two trials failed due to excitation of the knee flexion reflex. Additional tests were done to establish the stabilising contribution of the ankle stiffness control as shown in Figure 5.12. At the end of the session a perturbation test (amplitude 20 Nm, duration 200 ms) was carried out (not shown here). However, the subject was not able to recover from the perturbations and fell over. As this test was carried out at the end of the session the subject might already have been too fatigued to successfully deal with perturbations. Matjačić and Bajd also reported in their study that the subject had difficulty to recover from perturbations when no cognitive feedback was provided, as is the case in our study.

- Requirements within the experiment were to be quick during the identification and control design process. This saves muscle power for standing. The identification process has a great potential for automation and the control design method is simple and straightforward. The identification and control design process took approximately $10 - 15$ minutes. The whole experimental session lasted 1 hour.

- Note that no model of the biomechanical structure was required at all. The stiffness value was chosen using the results from Matjačić and Bajd [1998b]. This considerably simplifies the design process of the FES system since an accurate model of the biomechanical structure is difficult to obtain.

- Stiffness is not sufficient to stabilise the body (cf. Chapter 4). The idea was to make the task of stabilising the erect body possible for the subject himself, using his own sensory-motor abilities. However, the FES-controlled ankle stiffness clearly contributes to the task of stabilising the body.

- Without stimulation the subject was not able to stand.

Chapter 6

Conclusions and Recommendations for Future Work

In this thesis, results of a previous experimental study on unsupported standing by Hunt *et al.* [1997] and Munih *et al.* [1997] were verified. This study focussed on the feasibility of paraplegic standing supported only by the subject's paralysed muscles and without any arm support. The control approach was developed further and the achievable periods of standing were prolonged compared to the previous work. The initial approach imposed restriction on the subject's freedom of movement as voluntary inputs by the CNS were minimised by a custom made body shell which confined the subject to a single-link inverted pendulum. This approach was purely experimental and can not be called "functional".

It is only natural to take advantage of the residual sensory-motor faculties of the paralysed subject, rather than to suppress them. We called this "integrated voluntary control". Matjačić and Bajd showed that a paraplegic subject is well able to maintain balance when a sufficient ankle stiffness is provided using his/her residual sensory-motor capacities. They provided ankle stiffness by a hydraulic actuator [Matjačić and Bajd, 1998b]. We therefore aimed to substitute the hydraulic actuator by FES-controlled ankle stiffness. This was a novel approach and unprecedented in the literature.

As a first step we investigated the feasibility of ankle stiffness control accomplished by FES in order to establish the quality of stiffness control which can be expected, what might be the limitations of FES-controlled ankle stiffness and to what extent it might facilitate standing. The main limitation was found to be the strength of the subject's paralysed muscles. This is well known for all FES-supported standing schemes since the paralysed muscles have to support the body weight. However, this could be overcome, to a certain extent, by appropriate muscle training.

In a second study the stiffness control scheme was further developed and transferred into a standing environment. Paraplegic standing was achieved with the proposed strategy. It shows for the first time that **functional** paraplegic standing is possible by means of

FES relying on feedback control and the subject's own capabilities of maintaining balance in order to achieve stability. So far, paraplegic standing is usually achieved by open-loop stimulation of the knee extensor muscles and ankle orthoses while arm support is required to achieve stability, which limits the functional potential of that approach.

The investigated standing strategy and control design can be used by people from a clinical background who have little expertise in control engineering. Moreover, it has great potential to be extended towards more safety and reliability. In fact, standing by FES-controlled ankle stiffness is intended to be only the first step towards a full impedance control, i.e. assigning and controlling favourable values of stiffness, viscosity, inertia and possibly higher order terms. This is expected to minimise the control effort required by the subject.

However, this raises the issue of suitable sensors for feedback. Obtaining angular feedback is straightforward but the values of velocity and acceleration in question are low which would require very sensitive (and probably expensive) sensors. On the other hand, differentiating the angle signal requires filtering which, in turn, can reduce the effect of the derivative feedback.

Another direction which one might be tempted to look is motivated by the observation that the subject was still able to maintain balance even when the stimulation signal saturated. With respect to the underlying moment control loop, this is in fact open-loop control. Therefore, it would be interesting to see whether standing is still possible when the moment control loop is replaced by open-loop stimulation of the plantarflexor and dorsiflexor muscles. Results from Chapter 3 also suggest that accurate moment tracking is less important than a quick reaction to changes in the direction of the inclination angle or inclination velocity. This approach would solve the problem of a practical sensor for the ankle moment. The disadvantage of open-loop stimulation, however, is that usually the full stimulation level is applied, even when this is not necessary. This increases and hastens fatigue and, consequently, shortens the achievable periods of standing.

Furthermore, the current standing strategy can be extended to incorporate hip stiffness control by stimulation of the hip abductor muscles. This could provide stability in the frontal plane. Moreover, it could enable the subject to voluntarily switch his posture in order to rest the leg muscles from time to time and, consequently, prolong the period of standing. Unfortunately, initial experience suggests that this might be beyond the limitations of surface stimulation. Hip abductor muscles are usually quite strong. In intact subjects, they are able to produce moments of around 100 Nm. However, using surface stimulation, we were only able to generate very low moments (> 10 Nm). An explanation is that these muscles are very short. Therefore, the electrodes have to be placed close together and, as a result, the electrical field does not penetrate deeply into the muscle tissue.

The current standing strategy can however, be extended to take the knee extensor

muscles into account. This should be straightforward as this is the current approach to paraplegic standing by FES in clinical therapy. Currently, the knees are braced by a leather belt in front of them in the experimental apparatus.

Finally, the current strategy and any further development should be tested in a larger population of paraplegic subjects in a clinical study in order to assess the full potential and limitations of the approach.

Appendix

Appendix A

Specification of the MRF

Hydraulics

Rotary Actuator

model	Knapp Microfluid DA12 270
maximum torque	120 Nm
maximum work pressure	100 bar
angle of rotation	270°
absorption volume	68 cm^3/a
mass	1.7 kg
friction break-out pressure	10 bar

Servo Valve

model	MOOG E760/100
rated no load flow @ 70 bar	3.85 l/min
maximum work pressure	210 bar
rated current	±15 mA parallel
rise time	ca. 6 ms

Power Unit

model	Knapp Microfluid AKA 5K T2A compact power unit
theoretical flow	5.8 l/min
maximum work pressure	90 bar
motor power	1.1 kW
electrical supply	380 V AC 3-phase

Sensorics

Pressure Transducer

model	MP Filtri TR4002
pressure range	$0 - 100\,\text{bar}$
output	$0 - 10\,\text{V}$ DC
rise time	1 ms
electrical supply	$13 - 30\,\text{V}$ DC

Shaft Encoder

model	Hengstler absolute rotary encoder RA58
resolution	12 bit
output	TTL
interface	parallel, Gray code
electrical supply	5 V DC

Data Acquisition Card

model	Humusoft AD512	
bus system	ISA	
analog input	number	8 SE
	resolution	12 bit
	input range	$0 - 5,\ 0 - 10,\ \pm 5,\ \pm 10\,\text{V}$
	sampling rate	100 kHz
analog output	number	2
	resolution	12 bit
	output range	$0 - 5,\ 0 - 10,\ \pm 5,\ \pm 10\,\text{V}$
	maximum output current	10 mA
digital input	number	8
	level	TTL
digital output	number	8
	level	TTL

model	National Instruments PCI-6503	
bus system	PCI	
digital input/output	number	24, programable
	level	TTL

Force Platform

model	Advanced Mechanical Technology (AMTI) OR6-7	
capacity	$F_x,\ F_y$	500 lb
	F_z	1,000 lb
	M_x	10,000 in lb
	M_y	9,125 in lb
	M_z	5,000 in lb
natural frequency	$F_x,\ F_y$	300 Hz
	F_z	400 Hz
sensitivity	$F_x,\ F_y$	3,000 μV/V/lb
	F_z	750 μV/V/lb
	$M_x,\ M_y$	180 μV/V/(in lb)
	M_z	382 μV/V/(in lb)

Bibliography

Hydraulic Systems

A. G. Alleyne and R. Liu. On the limitations of force tracking control for hydraulic servo systems. *ASME Journal of Dynamic Systems, Measurement, and Control*, 121(2):184–190, June 1999.

A. G. Alleyne and R. Liu. Systematic control of a class of nonlinear systems with application to electrohydraulic cylinder pressure control. *IEEE Transactions on Control Systems Technology*, 8(4):623–633, July 2000.

D. C. Clark. *Technical Bulletin 122: Selection and Performance Criteria for Electrohydraulic Servo Drives*, pages 369–375. In MOOG, Inc.

M. Guillon. *Hydraulic Servo Systems: Analysis and Design.* Butterworths, 1969.

H. E. Merritt. *Hydraulic Control Systems.* John Wiley, 1967.

MOOG, Inc. *Servo and Proportional Systems Catalog.*

T. P. Neal. *Technical Bulletin 126: Performance Estimation for Electrohydraulic Control Systems*, pages 359–368. In MOOG, Inc..

G. A. Sohl and J. E. Bobrow. Experiments and simulations on the nonlinear control of a hydraulic servosystem. *IEEE Transactions on Control Systems Technology*, 7(2):238–247, March 1999.

H. Zoebl. *Fundamentals of Hydraulic Circuitry.* Iliffe Books, 1970.

Control Theory

K. J. Åström and B. Wittenmark. *Computer Controlled Systems.* Prentice Hall, 3rd edition, 1997.

K. J. Åström. *A Paradox in Pole Placement Design*, pages 117–126. In Normand-Cyrot [1998].

R. G. Herrtwich and G. Hommel. *Nebenläufige Programme.* Springer, 2nd edition, 1994.

R. Isermann. *Identification Dynamischer Systeme 1: Grundlegende Methoden.* Springer, 2nd edition, 1992.

V. Kučera. *Discrete Linear Control: The polynomial equation approach.* Wiley, 1979.

D. Liberzon and A. S. Morse. Basic problems in stability and design of switched systems. *IEEE Control Systems Magazine*, 19(5):59–70, October 1999.

L. Ljung. *System Identification: Theory for the user.* Prentice Hall, 2nd edition, 1999.

L. Nashelsky. *Introduction to Digital Computer Technology.* Wiley, 1972.

D. Normand-Cyrot, editor. *Perspectives in Control: Theory and Applications.* Springer, 1998.

W. J. Rugh and J. S. Shamma. Research on gain scheduling. *Automatica*, 36(10):1401–1425, October 2000.

L. Sciavicco and B. Siciliano. *Modelling and Control of Robot Manipulators.* Springer, 2000.

S. Skogestad and I. Postlethwaite. *Multivariable Feedback Control: Analysis and Design.* Wiley, 1996.

H. Unbehauen. *Regelungstechnik I: Klassische Verfahren zur Analyse and Synthese linearer kontinuierlicher Regelsysteme.* Vieweg, 8th edition, 1994.

FES, Standing and Medical Literature

A. Alexandrov, A. Frolov, and J. Massion. *Voluntary Forward Bending Movement in Human: A principal component analysis of axial synergies*, pages 345–3480. In Taguchi *et al.* [1994].

O. Behar, K. Mizunao, S. Neumann, and C. J. Woolf. Putting the spinal cord together again. *Neuron*, 26(2):291–293, May 2000.

Cleveland FES Center, Ohio. Standing and stepping with FES. http://feswww.fes.cwru.edu/standingsystem/index.htm.

G.H. Creasey. Restoration of bladder, bowel and sexual function. *Topics in Spinal Cord Injury Rehabilitation: Special Issue on Functional Electrical Stimulation*, 5(1):21–32, Summer 1999.

J. J. Daly, E. B. Marsolais, L. M Mendell, W. Z. Rymer, A. Stefanovska, J. R. Wolpaw, and C. Kantor. Therapeutic neural effects of electrical stimulation. *IEEE Transactions on Rehabilitation Engineering*, 4(4):218–229, December 1996.

A. Despopoulos and S. Silbernagl. *Color Atlas of Physiology.* Thieme, 4th edition, 1991.

N. Donaldson and C.-H. Yu. FES standing: Control by handle reactions of leg muscle stimulation (CHRELMS). *IEEE Transactions on Rehabilitation Engineering*, 4(4):280–284, December 1996.

N. Donaldson and C.-H. Yu. A strategy by paraplegics to stand up using FES. *IEEE Transactions on Rehabilitation Engineering*, 6(2):162–171, June 1998.

N. Donaldson and C.-H. Yu. Experiments with CHRELMS patient-driven stimulator controller for the restauration of function in paralysed legs. In *Proceedings of the Institute of Mechanical Engineers*, volume 214, pages 1–20, 2000.

N. Donaldson, F. M. D. Barr, G. F. Phillips, and T. A. Perkins. *Unsupported Standing of Paraplegics by Stimulation of the Plantarflexors: Some Results from Wobbler Apparatus*, chapter 3, pages 217–232. In Pedotti et al. Pedotti *et al.* [1996], 1996.

N. Donaldson, M. Munih, G. F. Phillips, and T. A. Perkins. Apparatus and methods for studying artificial feedback control of the plantarflexors in paraplegics without interference from the brain. *Medical Engineering and Physics*, 19(6):525–535, September 1997.

N. Donaldson. Practical ankle controllers for unsupported standing in paraplegia. In *Proceedings of the Ljubljana Conference on Functional Electrical Stimulation*, pages 61–64, Ljubljana, Slovenia, 1993.

E. J. Frey. Central nervous system regeneration: Mission impossible. *Clinical and Experimental Pharmacology and Physiology*, 28(4):253–258, April 2001.

H. Gollee, K. J. Hunt, D. Wood, and C. McFadden. New results in feedback control of unsupported standing in paraplegia. In *Proceedings of the 6th Annual Conference of the International Functional Electrical Stimulation Society*, pages 10–12, Cleveland, Ohio, 2001.

D. Grundy and A. Swain. *ABC of Spinal Cord Injury.* BMJ Publishers, 3 edition, 1996.

K. W. Hammel. *Spinal Cord Injury Rehabilitation*, volume 45 of *Therapy in Practice*. Chapamn & Hall, 1995.

M. Hansen, M. Haugland, Aleksander Kostov, and T. Sinkjær. Machine learning for real time control of foot-drop correction using natural sensors. In *Proceedings of the* 5^{th} *Annual Conference of the International Functional Electrical Stimulation Society*, Aalborg, Denmark, 2000.

M. Haugland, C. Childs, M. Ladouceur, J. Haase, and T. Sinkjær. An implantable foot drop stimulator. In *Proceedings of the* 5^{th} *Annual Conference of the International Functional Electrical Stimulation Society*, Aalborg, Denmark, 2000.

W. Holderbaum and K. J. Hunt. Robust discrete time control design for unsupported paraplegic standing. In *Proceedings of the European Control Conference ECC'01*, Porto, Portugal, 2001.

W. Holderbaum, K. J. Hunt, and H. Gollee. H_∞ robust control design for paraplegic standing. *Control Engineering Practice*, 2001. Submitted for publication.

W. Holderbaum, K. J. Hunt, and H. Gollee. Robust discrete time control design for unsupported paraplegic standing: experimental results. *European Journal of Control*, 2001. Submitted for publication.

W. Holderbaum, K. J. Hunt, and H. Gollee. Application of H_∞ robust control to paraplegic standing. In *Proceedings of IFAC World Congress*, Barcelona, Spain, 2002.

F. B. Horak and J. M. Macpherson. *Postural Orientation and Equilibrium*, pages 255–292. Volume 7 of Rowell and Shepherd Rowell and Shepherd [1995], 1995.

F. B. Horak and L. M. Nashner. Central programming of postural movements: Adaptation to altered support surface configurations. *Journal of Neurophysiology*, 55(6):1369–1381, June 1986.

K. J. Hunt, M. Munih, and N. Donaldson. Feedback control of unsupported standing in paraplegia - part I: Optimal control approach. *IEEE Transactions on Rehabilitation Engineering*, 5(4):331–340, December 1997.

K. J. Hunt, M. Rothe, T. Schauer, A. Ronchi, and N.-O. Negård. Automatic speed control in FES cycling. In *Proceedings of the* 6^{th} *Annual Conference of the International Functional Electrical Stimulation Society*, Cleveland, Ohio, 2001.

A. Inmann and M. Haugland. A flexible, portable FES hand grasp neuroprosthesis incorporating natural sensory feedback. In *Proceedings of the* 5^{th} *Annual Conference of the International Functional Electrical Stimulation Society*, Aalborg, Denmark, 2000.

R. J. Jaeger. Design and simulation of closed-loop electrical stimulation orthoses for restauration of quiet standing in paraplegia. *Journal of Biomechanics*, 19(10):825–835, October 1986.

K. L. Kilgore. *Synthesis of Hand Grasp in Multiple Muscle Systems*, pages 605–616. In Winters and Crago [2000].

R. Kobetic, R. J. Triolo, J. P. Uhlir, C. Bieri, M. Wibowo, G. Polando, E. B. Marsolais, Jr. J. A. Davis, K. A. Ferguson, and M. Sharma. Implanted functional stimulation system for mobility in paraplegia: A follow-up case report. *IEEE Transactions on Rehabilitation Engineering*, 7(4):390–398, December 1999.

A. R. Kralj and T. Bajd. *Functional Electrical Stimulation: Standing and Walking after Spinal Cord Injury.* CRC Press, 1989.

J. Massion, S. Vernazza, and A. Alexandrov. *Feedforward Postural Control during Movement*, chapter 1, pages 3–10. In Pedotti *et al.* [1996].

Z. Matjačić and T. Bajd. Arm-free paraplegic standing—Part I: Control model synthesis and simulation. *IEEE Transactions on Rehabilitation Engineering*, 6(2):125–138, June 1998.

Z. Matjačić and T. Bajd. Arm-free paraplegic standing—Part II: Experimental rsults. *IEEE Transactions on Rehabilitation Engineering*, 6(2):139–150, June 1998.

Z. Matjačić and T. Sinkjær. A mechanical apparatus for arm-free therapeutical paraplegic standing. In *Proceedings of the International Biomechatronics Workshop*, Enschede, The Netherlands, 1999.

Z. Matjačić, I. L. Johannesen, and T. Sinkjær. A multi-purpose rehabilitaion frame: A novel apparatus for balance training during standing of neurologically impaired individuals. *Journal of Rehabilitation Research and Development*, 37(6):681–691, November/December 2000.

Z. Matjačić. A multi-purpose rehabilitaion frame: an apparatus for experimental investigations of human balance and postural control. *Journal of Medical Engineering and Technology*, 24(6):250–254, November 2000.

Z. Matjačić. Control of ankle and hip joint stiffness for arm-free standing in paraplegia. *Neuromodulation*, 4(1):37–46, January 2001.

M. E. Miller and J. T. Mortimer. Interactive showcase of methods and materials for electrical activation of the diaphragm for ventilatory assist. In *Proceedings of the* 16^{th} *Annual Applied Neural Control Research Day, Case Western Reserve University*, Cleveland, Ohio, 2001.

M. Munih, N. Donaldson, K. J. Hunt, and F. M. D. Barr. Feedback control of unsupported standing in paraplegia - part II: Experimental results. *IEEE Transactions on Rehabilitation Engineering*, 5(4):341–352, December 1997.

N. Palastanga, D. Field, and R. Soames. *Anatomy and Human Movement: Structure and Function.* Butterworth-Heinemann, 2nd edition, 1997.

A. Pedotti, M. Ferrarin, J. Quintern, and R. Riener, editors. *Neuroprosthetics from Basic Research to Clinical Application.* Springer, 1996.

T. A. Perkins, N. Donaldson, V. J. Harper, J. Norton, A. M. Thomas, D. E. Wood, and D. H. Rushton. Standing, stepping and cycling for a T9 paraplegic with a lumbo-sacral anterior root stimulator implant. In *Proceedings of the Third Annual Conference of the International Functional Electrical Stimulation Society and INS*, Lucern, Switzerland, 1998.

G. F. Phillips, J. R. Adler, and S. J. G. Taylor. A portable programmable eight-channel surface stimulator. In *Proceedings of the Ljubljana FES Conference*, pages 166–168, Ljubljana, Slovenia, 1993.

D. Popović and T. Sinkjær. *Control of Movement for the Physically Disabled.* Springer, 2000.

M. R. Popović, I. P. I. Pappas, K. Nakazawa, T. Keller, M. Morari, and V. Dietz. Stability criterion for controlling standing in able-bodied subjects. *Journal of Biomechanics*, 33(11):1359–1368, November 2000.

M. S. Ramer, G. H. Harper, and E. J. Bradbury. Progress in spinal cord research: A refined strategy for the International Spinal Research Trust. *Spinal Cord*, 38(8):449–472, August 2000.

R. Riener and T. Fuhr. Patient-driven control of fes-supported standing up: A simulation study. *IEEE Transactions on Rehabilitation Engineering*, 6(2):113–124, June 1998.

L. B. Rowell and J. T. Shepherd, editors. *Handbook of Physiology: Neural Control of Movement*, volume 7. 1995.

Salisbury District Hospital, U.K. Guide for participants on paraplegic muscle retraining and standing programmes. http://www.salisburyfes.com/para.htm.

S. Salmons and J. C. Jarvis. Cardiac assistance from skeletal muscle: A critical appraisal of the various approaches. *British Heart Journal*, 68(3):333–338, September 1992.

A. Stefanovska, L. Vodovnik, N. Gros, S. Reberšek, and R. Ačimović-Janežič. FES and spasticity. *IEEE Transactions on Biomedical Engineering*, 36(7):738–745, July 1989.

K. Taguchi, M. Igarashi, and S. Mori, editors. *Vestibular and Neural Front*, volume 1070 of *International Congress Series*. Elsevier Siences B.V., 1994.

D. Venes, C. L. Thomas, and C. W. Taber, editors. *Taber's Cyclopedic Medical Dictionary*. F. A. Davis, 18th edition, 1997.

S. Vernazza, M. Cincera, J. Massion, and A. Pedotti. *Is the Center of Gravity Controlled during Movement?*, chapter 1, pages 11–14. In Pedotti *et al.* [1996].

D. A. Winter, F. Prince, J. S. Frank, C. Powell, and K. F. Zabjek. Unified theory regarding A/P and M/L balance in quiet stance. *Journal of Neurophysiology*, 76:2334–2343, 1996.

D. A. Winter. *Biomechanics and Motor Control of Human Movement*. John Wiley & Sons, 1990.

J. M. Winters and P. E. Crago, editors. *Biomechanics and Neural Control of Posture and Movement*. Springer, 2000.

D. E. Wood, V. J. Harper, F. M . D. Barr, P. N. Taylor, G. F. Phillips, and D. J. Ewins. Experience in using knee angles as part of a closed-loop algorithm to control FES-assisted paraplegic standing. In *Proceedings of the 6th International Workshop on FES*, Vienna, Austria, 1998.

D. E. Wood, N. Donaldson, C. McFadden, T. A. Perkins, D. N. Rushton, and A. M. Tromans. Is paraplegic standing by root stimulation a practical option?—conclusion from the LARSI project. In *Proceedings of the 6th Annual Conference of the International Functional Electrical Stimulation Society*, Cleveland, Ohio, 2001.